Models and Methods of Cerebrovascular Reactivity Mapping

DPhil Thesis

Genevieve Hayes

Supervisor: Daniel P. Bulte

St. John's College

Institute of Biomedical Engineering

University of Oxford

May 2025

Abstract

Cerebrovascular reactivity (CVR) serves as a critical biomarker for assessing the capacity of cerebral blood vessels to adapt to physiological and pathological challenges. Although numerous methods exist to measure CVR, accurately capturing its full dynamic range remains an ongoing challenge. This thesis presents advances in the underlying principles, measurement techniques, and modelling of CVR, integrating data from transcranial Doppler ultrasound (TCD) and blood-oxygen-level-dependent functional magnetic resonance imaging (BOLD-fMRI).

The thesis begins with a review of the pathophysiological bases of vascular smooth muscle cell dysfunction, showing how impaired vascular regulation can occur before clinical symptoms of neurodegeneration emerge and motivating CVR as a promising tool for assessing brain health. The subsequent chapters develop and utilise different methodologies to map CVR dynamics. First, CVR measured using TCD in combination with a fixed carbon dioxide challenge is compared with the pupillary light response (PLR). Although the PLR reflects certain autonomic responses, it only partially aligns with the broader haemodynamic changes measured by TCD. To investigate whether a probability-driven approach would enhance CVR accuracy, a Bayesian modelling framework is introduced for breath-hold-induced CVR in BOLD-fMRI. By treating both data and parameters as probability distributions, this framework demonstrates greater adaptability and computational speed than general linear modelling while maintaining comparable accuracy. The TCD-based research is then extended using a novel ramp protocol that delivers progressive hypercapnia, enabling fine-grained, non-linear (sigmoidal) characterisation of vascular responses, elucidating inflection points and upper/lower limit plateaus that linear models are unable to identify. Incorporating the Bayesian framework into these TCD ramp analyses further enhances the characterisation of the full CVR response. Applying these non-linear methods to BOLD-fMRI then facilitates side-by-side assessment with TCD, revealing both consistent trends and modality-specific differences. Finally, the thesis validates key physiological assumptions by comparing TCD-derived velocity measures with standard models linking

altered cerebral blood flow to changes in the BOLD signal.

Taken together, these studies contribute to a more nuanced understanding of cerebrovascular function, emphasising the importance of non-linear modelling and multimodal approaches. By advancing experimental protocols, computational frameworks, and preliminary non-invasive metrics (such as the PLR), this thesis opens avenues for earlier detection of vascular involvement in neurodegeneration and for broader clinical adoption of CVR as a routine biomarker of cerebrovascular health.

Acknowledgements

These past years have been some of the best of my life, marked by growth, discovery, and truly unforgettable experiences. Yet, above all, my greatest accomplishment has been the friendships and connections I have made along the way. Firstly, I am incredibly grateful to my supervisor, Daniel Bulte, for giving me the opportunity to come to Oxford and for his unwavering encouragement and support throughout the years. His guidance has been instrumental in shaping both my research and my confidence as a scientist. Furthermore, I am incredibly grateful for the financial support from the Clarendon Fund and St John's College, which made this journey possible.

My time in the Bulte Lab has been enriched by the incredible colleagues I have had the privilege to work with. Joana has been an extraordinary mentor to me - I have learned so much from her, and I am constantly inspired by her passion, hard work, and generosity. I am especially grateful for the way she has always looked out for me. Sierra, sharing this DPhil journey with you has been a privilege. Having a partner to navigate the highs and lows with, to grow alongside, and to enjoy working with every day has made all the difference. I would also like to extend my heartfelt thanks to the rest of the Bulte Lab - Natali, YC, Sherry, Lisa, Bella, and the wider group - who have provided support and inspiration. I am also deeply grateful to the team at OHBA for their invaluable help with fMRI data collection.

The friends I have made at St John's College have become my home away from home, and I am forever grateful for the laughter, support, and memories we have shared. Amin, thank you for the adventures, the grounding presence, the pep talks, and our long philosophical conversations. Becca, I am so lucky to have had you as a confidante, a rain-or-shine running buddy, and a constant source of encouragement. Gabby, thank you for your genuine kindness, your perspective, and for introducing me to so many ice cream flavours. Grace, my Norse pal, thank you for the countless cups of tea, and all the little adventures we've shared. Minying, you have been a great inspiration, bringing poetry into my life in more ways than one, and never shying away from a deep conversation. Cam, thanks for climbing mountains with me and standing up for

me when I needed it most. Martin M., the community builder, thank you for ensuring that I and so many others always felt welcome. Gretchen, our morning coffee walks and your willingness to join me on spontaneous adventures have been a joy. Tianyi, thank you for the crazy adventures, the quiet moments of connection, and for teaching me so much about life. Sammi, you are a wise and wonderful presence in my life, and your support has meant more than I can say. I am also incredibly grateful to the wider college and MCR community for the kindness, the amazing conversations, the laughs, the lessons, and all the encouragement I have received throughout my time at Oxford.

Beyond my academic and college life, I have been fortunate to have friends who helped me find balance and joy in everyday moments. Martin G., thank you for grounding me in Oxford when I first arrived and remaining a friend no matter the distance. Mayur, your nature walks were exactly what I needed at times when my mind was chaotic. Heather, thank you for the road trips, the crafternoon teas, and for giving me the unexpected but wonderful gift of sock knitting.

I am also deeply grateful for the administration, staff, and students at the Basque Centre on Cognition, Brain and Language who made my time in Donosti so special, notably Cesar, Chiara, Cristina, Eneko, Hana, Vicente, Ines, Irene, Maxime. Cesar y los Spins, estoy muy agradecida por su generosidad con su tiempo, energía, y apoyo. Muchas gracias, mila esker.

To my family - Mum, Dad, Eric, and Robert - your unwavering support and love have been my foundation, and I could not have done this without you. Eneko, my partner, best friend, and home, you are the greatest light in my life, thank you for everything maitia.

Finally, to my friends from home, thank you for staying close despite the distance. Hema, your grounding energy and love have been a constant source of strength. Simone, thank you for always rooting for me, no matter what.

This thesis is the culmination of years of work, but it would not have been possible without the people who have supported, challenged, and uplifted me along the way. I am forever grateful.

Research Dissemination

Journal Publications

1. **G. Hayes**, S. Sparks, J. Pinto, and D. P. Bulte, "Transcranial doppler ultrasound validation of BOLD-fMRI cerebral blood flow relationship," *Magn. Reson. Med.*, 2025. doi: 10.1002/mrm.70091.

2. **G. Hayes**, S. Sparks, J. Pinto, and D. P. Bulte, "Models of cerebrovascular reactivity in fMRI and transcranial doppler ultrasound," *J. Appl. Physiol.*, vol. 139, no. 1, pp. 219-230, 2025. doi: 10.1152/japplphysiol.00107.2025

3. **G. Hayes**, S. Sparks, J. Pinto, and D. P. Bulte, "Ramp protocol for non-linear cerebrovascular reactivity with transcranial doppler ultrasound," *J. Neurosci. Methods*, vol. 416, p. 110381, 2025. doi: 10.1016/j.jneumeth.2025.110381.

4. S. Sparks* and **G. Hayes***, J. Pinto, and D. P. Bulte, "Characterising cerebrovascular reactivity and the pupillary light response - a comparative study," *Front. Physiol.*, vol. 15, 2024. doi: 10.3389/fphys.2024.1384113.

5. **G. Hayes**, D. P. Bulte, S. Moia, M. Craig, M. Chappell, E. Uruñuela, S. Sparks, C. Caballero-Gaudes, and J. Pinto, "Bayesian modelling approaches for breath-hold induced cerebrovascular reactivity," *bioRxiv*, 2024. doi: 10.1101/2024.02.06.579134.

6. **G. Hayes**, J. Pinto, S. N. Sparks, C. Wang, S. Suri, and D. P. Bulte, "Vascular smooth muscle cell dysfunction in neurodegeneration," *Front. Neurosci.*, vol. 16, p. 1010164, 2022. doi: 10.3389/fnins.2022.1010164.

7. S. Sparks, J. Pinto, **G. Hayes**, M. Spitschan, and D. P. Bulte, "The impact of Alzheimer's disease risk factors on the pupillary light response," *Front. Neurosci.*, 2023. doi: 10.3389/fnins.2023.1248640.

8. C. Wang, G. Reid, C. E. Mackay, **G. Hayes**, D. P. Bulte, and S. Suri, "A systematic review of the association between dementia risk factors and cerebrovascular reactivity," *Neurosci. Biobehav. Rev.*, vol. 148, p. 105140, 2023. doi: 10.1016/j.neubiorev.2023.105140.

Conference Abstracts

1. **G. Hayes**, S. Sparks, J. Pinto, and D. P. Bulte, "Linear and sigmoidal cerebrovascular reactivity in fMRI and transcranial doppler ultrasound," *Organisation for Human Brain Mapping (OHBM)*, Jun. 2025, Brisbane, Australia.

2. **G. Hayes**, S. Sparks, J. Pinto, and D. P. Bulte, "Transcranial doppler ultrasound validation of BOLD-fMRI cerebral blood flow relationship," *British Neuroscience Association Festival of Neuroscience*, Apr. 2025, Liverpool, UK.

3. **G. Hayes**, S. Sparks, J. Pinto, and D. P. Bulte, "Evaluating the nonlinear dynamics of cerebrovascular reactivity with transcranial doppler ultrasound," *Organisation for Human Brain Mapping (OHBM)*, Jun. 2024, Seoul, South Korea.

4. **G. Hayes**, J. Pinto, S. Moia, M. Craig, M. Chappell, C. Caballero-Gaudes, and D. P. Bulte, "Bayesian and lagged general linear modelling strategies in breathhold induced cerebrovascular reactivity mapping with multi-echo BOLD fMRI," *International Society for Magnetic Resonance in Medicine (ISMRM)*, Jun. 2023, Toronto, Canada.

5. **G. Hayes**, J. Pinto, S. Moia, M. Craig, M. Chappell, C. Caballero-Gaudes, and D. P. Bulte, "Cerebrovascular reactivity mapping with multi-echo BOLD fMRI," *ISMRM Iberian Chapter*, Oct. 2023, Valladolid, Spain.

6. **G. Hayes**, C. Caballero-Gaudes, and D. P. Bulte, "Optimising cerebrovascular reactivity mapping for glioma imaging," *Glioma in Magnetic Resonance COST Action*, Oct. 2022, Kuşadası, Turkey.

7. J. Pinto, S. Suri, S. Sparks, **G. Hayes**, and D. P. Bulte, "Cerebrovascular reactivity in the postpartum period: exploring regional differences using fMRI ," *Organisation for Human Brain Mapping (OHBM)*, Jun. 2025, Brisbane, Australia.

8. J. Pinto, S. Suri, S. Sparks, **G. Hayes**, and D. P. Bulte, "Cerebrovascular reactivity dynamics in the postpartum period: a pilot study," *International Society for Magnetic Resonance in Medicine (ISMRM)*, May 2025, Honolulu, USA.

9. S. Sparks, D. P. Bulte, **G. Hayes**, and J. Pinto, "Investigating the pupillary light response in the postpartum period," *Association for Research in Vision and Ophthalmology (ARVO)*, May 2025, Salt Lake City, USA.

10. S. Sparks, **G. Hayes**, J. Pinto, J. Martin, M. Spitschan, and D. P. Bulte, "Comparing the pupillary light response to white, red, and blue stimuli with cerebrovascular reactivity," *Association for Research in Vision and Ophthalmology (ARVO)*, May 2024, Seattle, USA.

11. S. Sparks, **G. Hayes**, J. Pinto, J. Martin, M. Spitschan, and D. P. Bulte, "Comparing the pupillary light response using two pupillometers with cerebrovascular reactivity," *Oxford Ophthalmological Congress (OCC)*, Jul. 2024, Oxford, UK.

12. J. Pinto, S. Sparks, **G. Hayes**, and D. P. Bulte, "Investigating Alzheimer's disease in women: is pregnancy a risk factor?," *International Society for Magnetic Resonance in Medicine (ISMRM)*, Jun. 2023, Toronto, Canada.

Public Code Repositories

1. `vbayes_lglm_cvr_pipeline`: Variational Bayesian and lagged-General Linear Model CVR analysis code including haemodynamic delay, and statistical analyses using Quantiphyse and accompanying software. Available open-source (MIT License) at Github.com/genhayes/cvr_tcd_steadystate_processing.

2. `cvr_tcd_steadystate_processing`: Scripts and functions used to derive CVR metrics from cerebral blood velocities measured using transcranial Doppler ultrasound during a boxcar CO_2 gas delivery protocol. Available open-source (MIT License) at Github.com/genhayes/vbayes_lglm_cvr_pipeline.

3. `cvr_tcd_ramp_processing`: Preprocessing and analysis pipeline including functions, and statistics for calculating linear and sigmoidal CVR metrics acquired using TCD during a ramp hypercapnic protocol. Available open-source (MIT License) at Github.com/genhayes/cvr_tcd_ramp_processing.

4. `cvr_mri_tcd_ramp_processing`: Analysis scripts and functions for characteris-

ing linear and sigmoidal CVR metrics acquired using BOLD-fMRI and / or TCD and a ramp hypercapnic protocol. Available open-source (Apache License 2.0) at Github.com/genhayes/cvr_mri_tcd_ramp_processing.

Table of Contents

List of Abbreviations

ABP Arterial Blood Pressure

AD Alzheimer's Disease

ALS Amyotrophic Lateral Sclerosis

ASL Arterial Spin Labelling

BOLD Blood-Oxygen-Level-Dependent

bpm Beats Per Minute

CADASIL Cerebral Autosomal Dominant Arteriopathy with Subcortical Infarcts and Leukoencephalopathy

CBF Cerebral Blood Flow

CoV Coefficient of Variation

CO_2 Carbon Dioxide

CSF Cerebrospinal Fluid

CVR Cerebrovascular Reactivity

DS Down's Syndrome

dHb Deoxyhaemoglobin

fMRI Functional Magnetic Resonance Imaging

GLM General Linear Model

ICC Intraclass Correlation Coefficient

LBD Lewy Body Dementia

lGLM Lagged General Linear Model

LMEr Revised Linear Mixed-Effects

LSR Least Squares Regression

MCA Middle Cerebral Artery

MCAv Middle Cerebral Artery Velocity

MNI Montreal Neurological Institute

MMSE Mini-Mental State Examination

MRI Magnetic Resonance Imaging

MS Multiple Sclerosis

$PaCO_2$ Arterial Partial Pressure of Carbon Dioxide

PaO_2 Arterial Partial Pressure of Oxygen

PD Parkinson's Disease

PET Positron Emission Tomography

$PETCO_2$ Partial Pressure of End-Tidal Carbon Dioxide

PLR Pupillary Light Response

ppm Parts Per Million

R^2 Coefficient of Determination

RLM Robust Linear Model

ROI Region of Interest

ROS Reactive Oxygen Species

SNR Signal-to-Noise Ratio

TBI Traumatic Brain Injury

TCD Transcranial Doppler Ultrasound

VSMC Vascular Smooth Muscle Cell

List of Figures

List of Tables

1 | Introduction

1.1 Motivation and Scope

Cerebrovascular disease represents one of the leading contributors to neurological morbidity and economic burden in the developed world [254]. The brain, despite comprising only a small fraction of total body mass, is responsible for approximately 20 % of the body's metabolic consumption and has minimal energy reserves [434]. This high demand for oxygen and glucose renders cerebral function particularly vulnerable to fluctuations in blood supply. Even subtle impairments in cerebral blood flow (CBF) regulation can lead to metabolic dysfunction, oxidative stress, and neuroinflammation, all of which contribute to neurodegeneration [3][90][224]. Understanding how the cerebrovascular system responds to physiological challenges is, therefore, critical in both identifying early disease markers and guiding patient-specific interventions.

Cerebrovascular reactivity (CVR) refers to the ability of blood vessels in the brain to dilate and constrict in response to stimuli - driven by vascular smooth muscle cells (VSMCs) - to ensure optimal perfusion under varying conditions. Dysfunction in CVR has been linked to numerous neurodegenerative conditions, including Alzheimer's disease, dementia, and small vessel disease [61][142][397][323][242]. As mounting evidence suggests that impaired vascular function may precede overt neurodegenerative pathology, CVR has emerged as a promising biomarker for early disease detection and intervention [14][191][360][363]. However, a key challenge in clinically leveraging CVR lies in distinguishing between intrinsic CVR dysfunction - arising from fundamental

smooth muscle impairments - and extrinsic dysfunction, which reflects increased vessel dilation at rest due to systemic or environmental factors such as age, BMI, or smoking. While many extrinsic factors are modifiable through lifestyle changes or pharmacological interventions, intrinsic dysfunction may require different therapeutic approaches.

Assessing CVR accurately and reliably remains a significant challenge in both research and clinical settings. Conventional CVR assessment methods often rely on binary or linear models that fail to capture the full spectrum of cerebrovascular responses. These models assume a proportional relationship between vascular response and stimulus intensity, overlooking the physiological reality that CVR often follows a non-linear, sigmoidal pattern. As a result, they may underestimate vascular saturation effects at high stimulus levels or fail to distinguish between subtle impairments in vasodilation and vasoconstriction. For example, non-linear models could account for multiple parameters in the CVR curve, such as the inflection point between lower and upper plateaus, the range of the response, and an offset in baseline CBF. The limitations in linear modelling are particularly relevant in the context of neurodegenerative diseases, where vascular dysfunction may manifest in different ways depending on disease etiology. The accessibility of CVR imaging also presents a barrier, as many current imaging modalities require specialised equipment and expertise, limiting widespread clinical adoption. Addressing these gaps requires advanced imaging and modelling techniques capable of characterising both linear and non-linear aspects of CVR.

The primary aim of this thesis is to develop robust, accessible, and cost-effective methods to comprehensively map a wide spectrum of the CVR response, enabling multi-parametric characterisation of CVR.

This work integrates transcranial Doppler ultrasound (TCD) and functional MRI (fMRI) to map cerebrovascular responses to controlled vasoactive stimuli. A novel ramp stimulus protocol is introduced to capture both dilation and constriction phases, improving the accuracy of CVR characterisation beyond traditional linear models. Additionally, Bayesian modelling techniques are applied to enhance parameter estimation and capture individual variability in CVR responses.

To facilitate this research, I assisted in establishing a new laboratory in the Institute for Biomedical Engineering at the University of Oxford, setting up the equipment to prototype and validate these methods, ensuring high-quality data acquisition and analysis. This included developing a controlled experimental environment for CVR studies, implementing gas stimulus delivery systems, and training to conduct participant studies. The development of this infrastructure was essential to conducting a comprehensive research study with human participants, the Eye-Brain Study, which allowed for systematic evaluation and refinement of CVR assessment techniques. Furthermore, I employed CVR acquisition and analysis protocols to contribute to an investigation of the relationship between cerebrovascular smooth muscle function and ocular smooth muscle activity via pupillometry. By establishing physiological correlations between cerebral and ocular vasoreactivity, this work aims to uncover novel, non-invasive biomarkers for cerebrovascular dysfunction.

In parallel with the TCD approach, this thesis also explores how the ramp stimulus protocol and sigmoidal modelling can be extended to MRI-based acquisitions for complementary measures of CVR. By leveraging fMRI data, it is possible to capture spatially resolved information on blood oxygenation changes that complement velocity-

based TCD measurements. This multimodal strategy not only improves the sensitivity of CVR assessment but also provides a more comprehensive view of cerebrovascular function, reinforcing the validity and applicability of the proposed methods across different imaging modalities.

The growing interest in advanced imaging and modelling approaches underscores the importance of this research. This thesis contributes methodological approaches and models for more precise characterisation of brain physiology, and seeks to inform early disease detection strategies, optimise pipelines for determining subject-specific risk factors of disease, and ultimately reduce the healthcare burden associated with neurovascular disorders. By improving CVR measurement techniques using non-invasive methods and advancing our understanding of vascular smooth muscle function in neurodegeneration, this thesis contributes to the broader goal of enhancing precision medicine approaches for neurological health.

1.2 Background

Specific methods and background information relevant to each chapter are provided throughout this thesis. This section outlines the essential concepts and methods of the thesis and provides the necessary framework for understanding the approaches employed.

1.2.1 Characterising Blood Flow Changes

Understanding changes in cerebral blood flow is fundamental to assessing cerebrovascular health. Several techniques exist for measuring blood flow dynamics, including transcranial Doppler ultrasound (TCD), magnetic resonance imaging (MRI), positron emission tomography (PET), single-photon emission computed tomography (SPECT), and near-infrared spectroscopy (NIRS). PET and SPECT provide quantitative measures of cerebral blood flow but require exposure to radioactive tracers, making repeated measures less safe and practical. NIRS, while non-invasive and portable, is limited in its spatial resolution and depth penetration. Given these constraints, this thesis employs TCD and fMRI due to their complementary strengths. TCD offers high temporal resolution, allowing for real-time assessment of cerebrovascular responses, while fMRI provides superior spatial resolution to map CVR across the brain.

1.2.1.1 Transcranial Doppler Ultrasound

TCD ultrasonography is a non-invasive, bedside tool for obtaining information about collateral blood flow through various branches of the circle of Willis. In TCD, pulses of sound waves are sent into the centre of a large blood vessel, such as the middle cerebral artery (MCA), and the blood velocity is determined by analysing the Doppler-shifted frequency of the resulting signals [30]. TCD is widely used in cerebrovascular research due to its high temporal resolution, portability, and ability to provide real-time assessment of cerebrovascular responses [55][271].

1.2.1.2 Magnetic Resonance Imaging

MRI methodologies such as arterial spin labeling (ASL) and blood-oxygen-level-dependent (BOLD) imaging enable non-invasive assessment of cerebral perfusion and neural-related activity by measuring blood flow, volume, and oxygenation-related signal changes [96]. Arterial spin labeling (ASL) provides a direct and quantitative measurement of cerebral blood flow (CBF) by using magnetically labeled arterial blood as an endogenous tracer [438]. In contrast, blood-oxygen-level-dependent (BOLD) MRI detects signal changes in T2* relaxation, which are influenced by variations in deoxyhemoglobin (dHb) levels, driven by a combination of physiological factors including CBF, cerebral blood volume, and the cerebral metabolic rate of oxygen [137]. When a hypercapnia challenge is used, it is generally assumed that BOLD signal changes are primarily driven by alterations in CBF [328]. Compared to ASL, BOLD imaging offers a higher signal-to-noise ratio and is less susceptible to motion artifacts [381]. Nevertheless, when compared with TCD, BOLD's accessibility is limited by cost and the need for specialised equipment.

1.2.2 Vasoactive Stimuli and Gas Challenges

To assess CVR, controlled vasoactive stimuli are required to provoke cerebrovascular responses. This thesis employs both hypercapnic (increased CO_2) via breath-hold and gas inhalation, and hypocapnic (decreased CO_2) via deep breathing to induce vasodilation and vasoconstriction, respectively.

1.2.2.1 Inducing Hypercapnia and Hypocapnia

The most common vasoactive challenge used for the assessment of CVR involves the induction of hypercapnia and / or hypocapnia. Hypercapnia refers to an increase in arterial blood partial pressure of CO_2, leading to vasodilation and increased CBF. This occurs due to the direct effect of CO_2 and decreased extracellular pH leading to VSMC relaxation and vasodilation [50]. Conversely, hypocapnia represents a reduction in arterial CO_2 levels, causing vasoconstriction.

One of the most established methods for inducing hypercapnia is the controlled inhalation of air with elevated CO_2 content. Fixed inspired CO_2 techniques and more advanced respiratory gas manipulation methods allow for the regulation of end-tidal CO_2 ($PETCO_2$), a non-invasive surrogate for arterial CO_2 concentration [387][251]. These techniques ensure controlled and reproducible hypercapnic responses, minimising variability across participants. Furthermore, the use of gas inhalation ensures the delivery of O_2 along with CO_2, allowing for much longer acquisition times and higher levels of $PETCO_2$ than breath-holds alone, while ensuring participant safety and protocol tolerance.

Breath-holding is another commonly used method for inducing hypercapnia, as it leads to a natural buildup of arterial CO_2. This approach is simple and requires no external gas delivery equipment, making it particularly useful in settings where controlled gas inhalation is not feasible. However, breath-holds are highly dependent on individual lung capacity and breath control, introducing variability in CO_2 accumulation across participants. Additionally, the duration of hypercapnia induced via breath-holds is

inherently limited, restricting the temporal window available for data acquisition. Despite these challenges, breath-holding remains a practical and widely used method for assessing CVR, especially in studies where accessibility and feasibility are key considerations [328][394][478].

Alternative pharmacological approaches, such as acetazolamide administration, can also induce hypercapnic vasodilation by inhibiting carbonic anhydrase and promoting CO_2 retention. While this method exhibits high reproducibility, inter-subject variability in drug metabolism and cerebrovascular response can limit its precision. Additionally, higher doses may lead to increased side effects and participant discomfort [151]. Hypocapnia, on the other hand, is typically induced via voluntary deep breathing or hyperventilation, which increases the rate of CO_2 elimination from the bloodstream. Deep breathing is a practical and non-invasive method for inducing hypocapnia, allowing for easy implementation in research and clinical settings. However, as arterial CO_2 levels are influenced by multiple physiological factors beyond breathing rate, subject variability must be carefully considered when using this approach. Despite these challenges, deep breathing remains a widely used and accessible strategy for investigating CVR, particularly in settings where gas delivery systems may not be feasible [328].

1.2.3 Existing Models of Cerebrovascular Reactivity

The following section examines the array of modelling approaches used to quantify CVR, ranging from conventional linear methods to advanced non-linear frameworks. This thesis explores both linear and non-linear models.

1.2.3.1 Linear CVR Models

The most standard approach to calculate CVR is using a two-point approach, measuring CBF at baseline and again during hypercapnia. This method assumes a linear relationship between $PaCO_2$ and CBF [52][381][466]. In BOLD-fMRI, the traditional method for characterising CVR employs the general linear model (GLM), which assumes a direct proportionality between CO_2 changes and the BOLD response (often used as a proxy for the CBF response). While straightforward, this approach may not fully capture the complex shape and orientation of cerebrovascular dynamics, limiting its diagnostic and therapeutic utility.

Although they are the most common approach to CVR mapping, linear models rely on a single slope parameter to indicate dysfunction. This simplification overlooks critical features such as shifts in baseline CBF reserve, changes in response amplitude or speed, and inflection points between lower and upper plateaus, which could reveal distinct pathological mechanisms.

1.2.3.2 Non-linear CVR Models

In contrast to linear, non-linear models allow for a richer characterisation of CVR dynamics, incorporating multiple parameters that could provide deeper insights into the nature of vascular dysfunction [31][38][85][117][284]. These models often use four-parameter logistic regression to capture key physiological features, including the minimum and maximum CBF responses, the inflection point of CO_2 sensitivity, and the slope in the linear response region. Alternative approaches, such as biphasic linear fits and circuit analysis models, have also been explored to delineate CVR response types

and vascular bed resistances under progressive CO_2 challenges [126][107].

Moreover, accounting for temporal shifts (haemodynamic delays) between the measured $PETCO_2$ trace and the BOLD signal is also essential for accurate CVR quantification. These delays result from both methodological factors (e.g. the time between CO_2 exhalation and its recording by the gas analyser) and physiological factors (e.g. lung-to-brain transit and local vasodilatory capacity) [288][289][393]. Notably, by shifting the $PETCO_2$ regressor in time to optimise the model fit and accommodating spatial variability in these delays on a regional basis, estimates of CVR amplitude can be substantially improved [393][52][261][289][329].

1.2.4 Bayesian Modelling

Bayesian modelling is a statistical approach that treats variables as probability distributions instead of fixed values and can incorporate prior information into the model fitting. This enables model refinement as new data becomes available and can allow for a more physiological representation of cerebrovascular dynamics, along with a robust estimation process that accounts for uncertainty and individual variability. This is particularly beneficial in CVR mapping, where vascular responses vary across individuals and regions of the brain, introducing significant uncertainty in parameter estimation.

The work presented in this thesis marks the first application of Bayesian inference to CVR modelling. By leveraging prior knowledge about expected cerebrovascular responses - such as baseline reactivity, vascular reserve limits, and response curvature - Bayesian techniques refine parameter estimation, making it more robust to noise and individual variability. Additionally, Bayesian models facilitate multi-parameter

fitting, which is essential for capturing the full sigmoidal CVR response rather than relying solely on single-slope linear approximations. This approach enables a more comprehensive characterisation of cerebrovascular function, potentially improving the sensitivity of CVR mapping for both research and clinical applications.

1.3 Thesis Objectives

The overarching objective of this thesis is to advance CVR mapping by developing and validating acquisition and analysis methods that improve sensitivity, accessibility, and interpretability. CVR is an essential biomarker for cerebrovascular function, with potential applications in evaluating neurovascular health, ageing, and neurodegenerative disorders. However, current methods face limitations in capturing the full dynamic range of CVR responses, integrating multiple imaging modalities, and ensuring widespread clinical applicability. This thesis addresses these challenges by establishing novel CVR assessment protocols, implementing Bayesian and sigmoidal modelling techniques, and evaluating non-invasive methods such as fMRI, TCD and the PLR as potential alternatives or complements to traditional approaches. To achieve these goals, the thesis is structured around three primary objectives:

Objective 1: Develop an acquisition and analysis framework for robust CVR assessment across a wide dynamic range, including non-linear features

1.1 Review CVR physiology and dysfunction

Examine the underlying mechanisms governing CVR, with a focus on how vascular smooth muscle cell dysfunction contributes to cerebrovascular pathology and

neurodegenerative diseases. This review will establish the motivation for CVR as a diagnostic and monitoring tool.

1.2 Develop and implement Bayesian modelling for CVR analysis

Design and test analysis pipelines incorporating Bayesian approaches to improve parameter estimation and sensitivity in CVR modelling.

1.3 Design and validate a ramp $PETCO_2$ CVR protocol

Develop an experimental framework for inducing graded hypercapnia, ensuring accessibility and feasibility in research and clinical settings, using controlled gas delivery with TCD and fMRI.

Objective 2: Collect and analyse CVR data using multimodal imaging techniques

2.1 Conduct Phase 1 of the Eye-Brain Study (TCD-based CVR analysis)

Acquire CVR using TCD and PLR using clinical pupillometer data and analyse CVR data to establish baseline cerebrovascular responsiveness.

2.2 Conduct Phase 2 of the Eye-Brain Study (TCD and fMRI-based CVR analysis)

Expand data collection to include PLR, TCD, and BOLD-fMRI measures, allowing for direct comparisons of the modalities.

2.3 Perform cross-modality comparison of CVR metrics

Analyse the concordance between TCD and fMRI-derived CVR measures to assess their relative strengths and limitations.

2.4 Identify key metrics for CVR characterisation

Establish which physiological and computational features provide the most robust and clinically meaningful assessment of CVR.

Objective 3: Validate accessible and complementary methods for CVR assessment, including TCD and PLR

3.1 Assess the relationship between PLR and CVR

Investigate whether the pupillary light reflex, a non-invasive autonomic response, correlates with CVR measures, potentially serving as an alternative biomarker.

3.2 Compare TCD and BOLD-fMRI CVR measurements under a ramp protocol

Evaluate the reliability and sensitivity of each technique in capturing CVR dynamics under controlled CO_2 modulation in TCD and BOLD-fMRI.

3.3 Examine CBF assumptions in BOLD-fMRI using TCD

Test key physiological assumptions underlying BOLD-fMRI CVR analysis by direct comparison with CBF velocity measurements from TCD.

By achieving these objectives, this thesis aims to enhance the methodological foundation of CVR research, paving the way for more reliable and accessible neurovascular assessments. The findings will contribute to both fundamental neuroscience and clinical applications, potentially informing early diagnostics and monitoring strategies for cerebrovascular and neurodegenerative diseases. Furthermore, the integration of Bayesian modelling and non-invasive physiological measures like PLR could open new avenues for more widespread and cost-effective CVR assessment in both research and clinical

settings.

1.4 Thesis Outline

This thesis is structured to progressively build an understanding of CVR, from physiological mechanisms to methodological advancements in its assessment. The chapters follow a logical progression, beginning with a review of vascular smooth muscle cell dysfunction in neurodegeneration, followed by experimental and computational studies exploring novel approaches for CVR assessment using TCD, PLR, and BOLD-fMRI. The latter chapters introduce and validate innovative modelling techniques, including Bayesian approaches and non-linear response characterisations, to enhance the reliability and interpretability of CVR mapping. The thesis culminates with a discussion of the key findings and their broader implications for research and clinical applications.

Chapter 2 provides an extensive review of vascular smooth muscle cell function and its role in regulating cerebrovascular dynamics. It explores the underlying mechanisms of CVR and its relationship with neurodegenerative disorders such as Alzheimer's disease, Parkinson's disease, and multiple sclerosis. Additionally, the chapter discusses how imaging modalities can be used to study CVR in vivo, providing the physiological and clinical context for the methods developed in later chapters. This review establishes the motivation for improving CVR mapping as a tool for understanding cerebrovascular dysfunction and its implications for neurological health (objective 1.1).

Chapter 3 presents an exploratory study investigating the relationship between CVR and the pupillary light response. Both vascular smooth muscle cell dysfunction and

PLR abnormalities have been linked to neurodegeneration, suggesting that pupil dynamics may serve as a surrogate marker for cerebrovascular health. The study examines whether PLR can provide insight into cerebrovascular function by comparing its response patterns to TCD-derived CVR using a traditional step change gas stimulus protocol. This chapter lays the groundwork for evaluating alternative, non-invasive methods of assessing CVR beyond traditional imaging techniques (objective 3.1).

Chapter 4 explores the application of Bayesian modelling to improve the analysis of breath-hold-induced CVR in BOLD-fMRI (objective 1.2). Conventional general linear models (GLMs) are widely used but can fail to account for inter-individual variability and the non-linearity of vascular responses. The Bayesian approach introduced here enhances parameter estimation by incorporating prior knowledge and uncertainty quantification. The model is validated against a standard GLM approach, demonstrating its advantages in computational efficiency and robustness in handling temporal features of CVR. This chapter contributes to the advancement of modelling frameworks for CVR analysis, providing a more flexible and data-driven approach to interpreting cerebrovascular responses (objective 2.4).

Chapter 5 introduces a novel ramp protocol for assessing non-linear features of CVR using TCD (objective 1.3). Unlike traditional step-based hypercapnia challenges, the ramp protocol provides a gradual increase in $PETCO_2$, allowing for a more precise characterisation of cerebrovascular response dynamics. The study evaluates the feasibility of this protocol in 11 healthy adults and applies custom sigmoid models with both linear regression and Bayesian fitting to characterise the CVR response (objective 1.2 and 2.1). The findings demonstrate the potential for this approach to enhance the

sensitivity of CVR assessment in both research and clinical settings, particularly in resource-limited environments where MRI may not be readily available.

Building on the findings from Chapter 5, **Chapter 6** applies the ramp protocol and advanced modelling techniques to BOLD-fMRI data, leveraging the spatial resolution of MRI to map CVR variations in 25 participants undergoing the same ramp protocol as in TCD (objective 2.2). This chapter presents a direct comparison between TCD and BOLD-fMRI measures of CVR, using both linear and non-linear metrics, and assesses their agreement and limitations (objective 2.3). This work underscores the importance of modality-specific considerations when interpreting CVR data and highlights the complementary strengths of TCD and MRI in cerebrovascular assessment (objective 2.4).

Chapter 7 extends this analysis by examining the physiological relationship between CBF and BOLD-fMRI signal changes using TCD-derived CBF velocity measures. Specifically, this study evaluates whether the Davis model - a widely used framework for linking CBF, cerebral metabolic rate of oxygen consumption, and BOLD signal changes - can reliably describe the dynamic interactions observed during ramp hypercapnia. The Davis model was tested against experimental data using least-squares regression and validated through statistical goodness-of-fit measures. This chapter contributes to the understanding of BOLD as an estimator of CBF and provides a quantitative framework for interpreting fMRI-based cerebrovascular assessments (objective 3.3).

Finally, **Chapter 8** synthesises the key findings from the thesis, discussing their implications for both fundamental neuroscience and clinical applications. The contributions

of the thesis are contextualised within the broader field of CVR research, emphasising the advancements made in acquisition protocols, modelling techniques, and alternative assessment methods. Limitations of the current work are acknowledged, and future research directions are proposed, including the translation of these methods to clinical populations. The thesis concludes with a discussion of how these findings contribute to the evolving landscape of cerebrovascular research and the potential for improved diagnostic and prognostic tools.

2 | Vascular Smooth Muscle Cell Dysfunction in Neurodegeneration

Preface

Building on emerging evidence that vascular smooth muscle cells (VSMCs) are intimately linked to neurovascular health, this chapter examines the pivotal role of VSMCs in both maintaining normal cerebrovascular function and contributing to neurodegenerative processes when dysregulated. By synthesising current literature on how VSMC dysfunction manifests in conditions such as dementia, Alzheimer's disease, and Parkinson's disease, the chapter lays a critical foundation for understanding the mechanistic interplay between vascular and neuronal decline. In doing so, it highlights the potential of techniques like cerebrovascular reactivity to detect VSMC dysfunction in vivo, thereby illuminating new avenues for early intervention and therapeutic strategies.

This chapter was published as:

> **G. Hayes**, J. Pinto, S. N. Sparks, C. Wang, S. Suri, and D. P. Bulte, "Vascular smooth muscle cell dysfunction in neurodegeneration," Front. Neurosci., vol. 16, p. 1010164, 2022. doi: 10.3389/fnins.2022.1010164

The material presented here establishes the rationale for the subsequent experimental investigations in this thesis, underscoring the importance of characterising cerebrovascular dynamics as a window into VSMC pathology and its broader implications for

neurodegeneration.

Author Contribution Statement

G. Hayes, **J. Pinto**, and **D.P. Bulte** contributed to the conception and initial design of the manuscript. **G. Hayes** performed the search and selection of the relevant studies. **G. Hayes** wrote the manuscript. **J. Pinto**, **S. N. Sparks**, **C. Wang**, and **S. Suri** contributed to the manuscript revision and editing. All authors read and approved the final manuscript.

Abstract

Vascular smooth muscle cells (VSMCs) are the key moderators of cerebrovascular dynamics in response to the brain's oxygen and nutrient demands. Crucially, VSMCs may provide a sensitive biomarker for neurodegenerative pathologies where vasculature is compromised. An increasing body of research suggests that VSMCs have remarkable plasticity and their pathophysiology may play a key role in the complex process of neurodegeneration. Furthermore, extrinsic risk factors, including environmental conditions and traumatic events can impact vascular function through changes in VSMC morphology.

VSMC dysfunction can be characterised at the molecular level both preclinically, and clinically ex vivo. However the identification of VSMC dysfunction in living individuals is important to understand changes in vascular function at the onset and progression of neurological disorders such as dementia, Alzheimer's disease, and Parkinson's disease.

A promising technique to identify changes in the state of cerebral smooth muscle is cerebrovascular reactivity (CVR) which reflects the intrinsic dynamic response of blood vessels in the brain to vasoactive stimuli in order to modulate regional cerebral blood flow (CBF).

In this work, we review the role of VSMCs in the most common neurodegenerative disorders and identify physiological systems that may contribute to VSMC dysfunction. The evidence collected here identifies VSMC dysfunction as a strong candidate for novel therapeutics to combat the development and progression of neurodegeneration, and highlights the need for more research on the role of VSMCs and cerebrovascular dynamics in healthy and diseased states.

2.1 Introduction

Cerebrovascular disease is among the leading disease-related causes of societal and economic burden in the developed world [432]. The brain consumes 20 % of the human body's metabolic reserve, but it has a limited capability for energy storage. As a result, small changes in blood supply can lead to severe alterations in metabolic function, which can also lead to the secretion of neurotoxic and inflammatory factors, a reduction in cerebral blood flow (CBF), and hypoxia that might initiate and / or contribute to neuronal degradation [476].

The aim of this review is to identify how vascular smooth muscle cells (VSMCs) participate in these vascular insults, and whether VSMC dysfunction may, in turn, contribute to neuronal degradation. Understanding the role of VSMC dysfunction in neurodegen-

eration is critical as it may inform on the underlying mechanisms behind cerebrovascular impairment that sometimes accompany and precede the onset of various neurological disorders.

In this review, we first summarise how VSMCs normally function to control cerebrovascular dynamics and blood flow, and key mechanisms by which VSMCs grow and communicate. Additionally, we discuss the best candidates for identifying the presence of cerebral VSMC dysfunction. We then present studies on VSMC phenotype, signalling pathways, and general contractility seen in a host of neurodegenerative disorders, presented in order of disorder prevalence. While it is not possible to encompass all neurodegenerative disorders, nor all the mechanisms at play, we review the role of VSMCs in Alzeihmer's disease, Parkinson's disease, amyotrophic lateral sclerosis, multiple sclerosis, Huntington's disease, cerebral small vessel disease, poststroke dementia, Down's syndrome, CADASIL, Lewy body dementia, and Moyamoya disease. In assessing VSMC dysfunction in these disorders, the studies have only considered correlation not causation. Finally, we review how extrinsic influences can affect VSMC function and touch on a few potential therapeutic opportunities in the context of the evidence we have collected on VSMC dysfunction in neurodegeneration.

2.2 VSMCs Control Cerebrovascular Dynamics

The vascular tree supplies the brain with blood flow and spans from the circle of Willis, which is known to be highly variable, down to the capillary network. The circle of Willis interconnects the anterior and posterior cerebral circulation network and gives

rise to pairs of anterior, middle, and posterior cerebral arteries. Each artery divides into progressively smaller arteries and arterioles which run along the brain's surface until they penetrate into the brain tissue [306].

Appropriate CBF is critical for brain function and survival. The regulation of CBF involves a coordinated interplay between different types of cells, including neurons, glia, and vascular cells. The neurons and glia generate signals which are translated into vascular changes by the collaboration of endothelial and mural cells. In particular, the mural cells, which include VSMCs and pericytes, surround the endothelial cell layer and regulate cerebrovascular resistance and blood flow to downstream capillary beds. Surrounding the smooth muscle is the adventitia layer that fuses to the basement membrane of astrocyte end feet, an important mediator of signals from neurons to blood vessels [260]. In recent years, much attention has also been placed on the participation of glial cells, primarily astrocytes signalling pathways for cerebrovascular tone [21][124]. Together, these vascular and perivascular components make up the blood brain barrier (BBB), the selective interface between the blood and central nervous system (CNS). A simplified diagram of the anatomy of a cerebral artery is illustrated in Figure 2.1.

VSMCs are a particular contractile cell type characterised by their expression of contractile proteins such as smooth muscle actin, myosin heavy chain, and myosin light chain [332]. Through contraction and relaxation, VSMCs alter blood vessel diameter and enable the maintenance of appropriate cerebral blood pressure and flow. A cascade of events occurs in response to changing oxygen and nutrient needs, as chemical signals are converted by VSMCs into mechanical constriction or relaxation by inducing changes in calcium ion (Ca^{2+}) concentrations, activating potassium channels, and

altering the contractile state of the light chain of myosin. In response to mechanical forces, such as high circumferential stress, VSMCs undergo mechanical signalling to influence gene expression, regulate cellular function, and alter vascular tone, which occurs even faster than the chemical signal cascade and is known as mechanotransduction [253][296]. VSMCs are coupled by gap junctions which mediate the intramural propagation of vascular signals between cells [185]. The renin-angiotensin system (RAS) is a key mediator of VSMC constriction and the Notch signalling pathway is essential in the coordination of VSMC migration and adhesion [149][386]. Additionally, the free radical, nitric oxide (NO) is a powerful vasodilator, produced most readily through endothelial NO synthesis and is a vital component of the signalling cascade [471]. Notably, changes in these pathways may play a role in pathological states and are discussed in more detail below.

Some studies have reported that capillary pericyte contractility affects CBF as well, though at a much slower time-scale than VSMCs due to their lack of smooth muscle actin [159][164][461]. While there are still unresolved controversies regarding pericyte contractility, it remains that in arteries and arterioles in the brain, VSMCs are likely to be the primary regulators of cerebrovascular dynamics and blood flow changes in response to the brain's oxygen and nutrient demands [165].

2.2.1 VSMC Phenotypic Plasticity

VSMCs and endothelial cells exhibit a spectrum of genetically distinct phenotypes along the arteriovenous pathway, known as zonation [421]. Within arterial zones, VSMCs can also express different phenotypes that change their properties, assuring

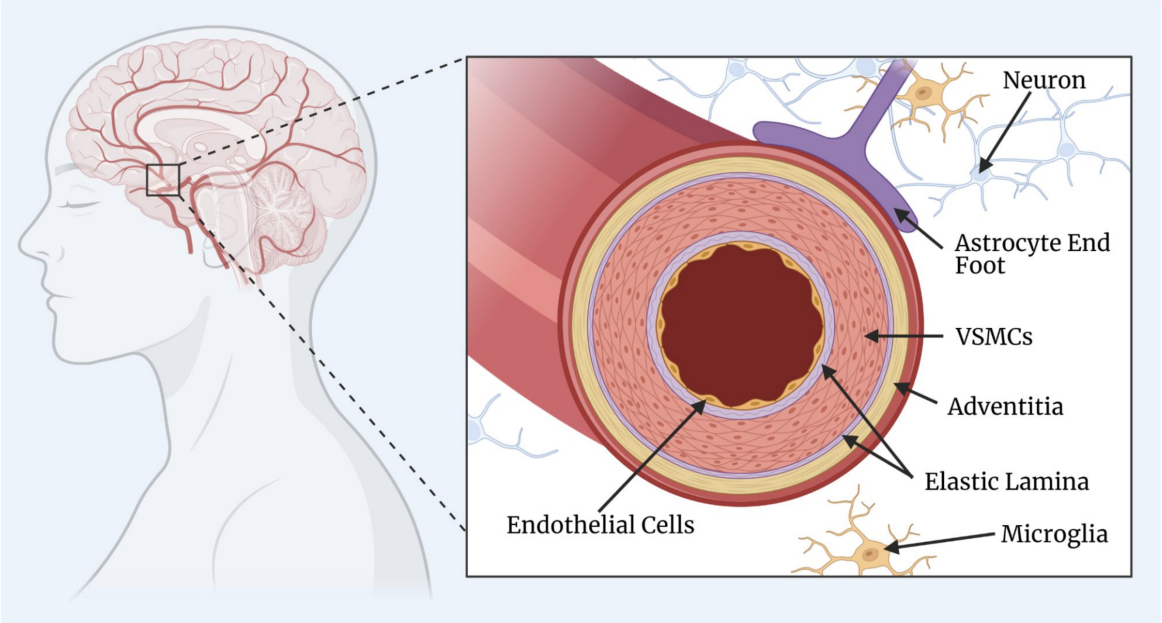

Figure 2.1: Simplified diagram of a cerebral artery. The key components of the cerebral artery include the endothelial cells, elastic lamina (one internal and one external), vascular smooth muscle cells (VSMCs), and the adventitia layer. The surrounding and supporting cells include the astrocytes, microglia, and neurons. This figure was created by GH rendering using BioRender.com.

that each vessel can adapt to changes in the local conditions. VSMC phenotype modulation is affected by innate genetic programmes and environmental cues. Contractile and synthetic VSMCs represent the two ends of a spectrum of intermediate phenotypes that have clearly different morphologies. While many different phenotypes exist, the contractile and synthetic VSMCs are by far the most abundant and better researched than the others.

Contractile VSMCs are long, spindly, and contain lots of contractile filaments, while synthetic VSMCs are wider, with large extracellular matrices [346]. Contractile VSMCs are more abundant in healthy vessels than the synthetic VSMC phenotype. Furthermore, synthetic VSMCs tend to exhibit higher proliferative and migratory activity than contractile VSMCs, and increase local inflammation [412]. The VSMC phenotype

and function can change in response to cell-signalling proteins, cell-to-cell contact, extracellular matrix interactions, injury stimuli, and mechanical forces. For example, immediately after an insult, VSMCs dedifferentiate, becoming more synthetic-like to promote the repair of the vessel. Then, once the injury is resolved, healthy VSMCs return to a non-proliferative, contractile phenotype [93]. In rare cases, VSMCs may also become hypercontractile due to excess contractile filaments which can increase the speed and amplitude of shortening (contraction) in response to stimulation and impair vasorelaxation [257].

These transitions between the different phenotypes can be transmitted and regulated at multiple levels, including gene transcription, epigenetic modification, signal generation, and transduction [131]. It has been suggested that the switch to and from differentiated/contractile and dedifferentiated/synthetic phenotypes is a key element of disease progression and imbalanced VSMC plasticity might lead to progression of VSMC-driven vascular disorders [131]. An illustration of contractile and synthetic phenotypes is presented in Figure 2.2 along with their key attributes.

2.2.2 Renin-Angiotensin System in VSMC Function

The renin-angiotensin system (RAS) is an important mediator of VSMC contractility [149]. When RAS is stimulated, the level of renin in the blood increases and promotes the production of angiotensin II (Ang II). Ang II is essential for the function and proliferation of healthy VSMCs but also plays a role in diseased states due to its growth-promoting effects on dysfunctional cells. The two major isoforms of the Ang II receptors, type-1 (AT1) and type-2 (AT2), appear to have opposing effects. Most of the

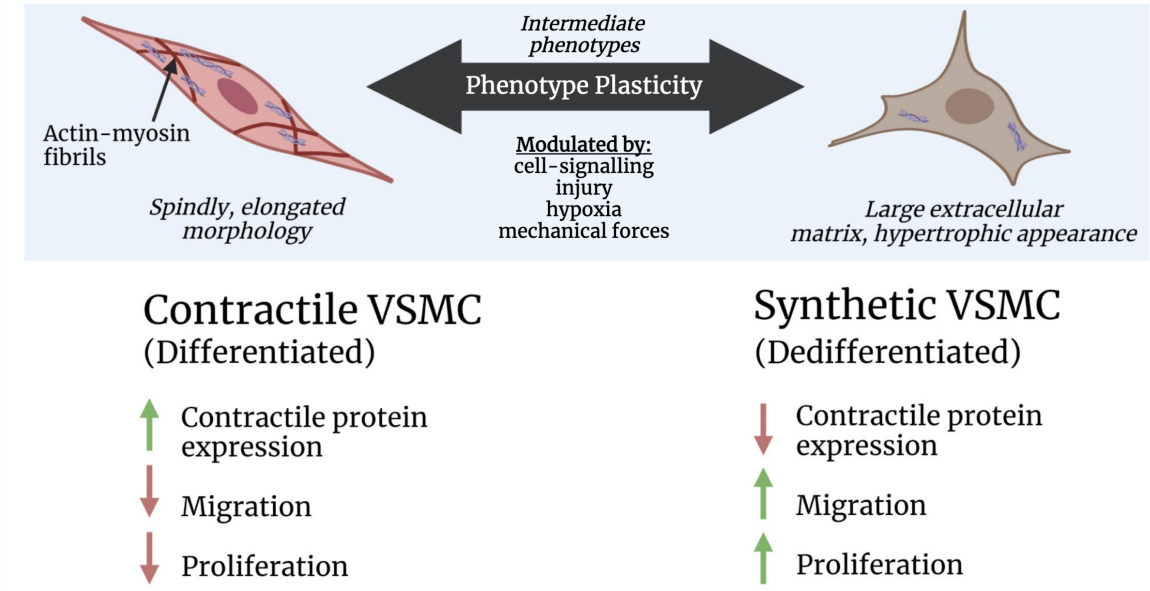

Figure 2.2: Simplified illustration of contractile and synthetic vascular smooth muscle cell (VSMC) phenotype plasticity. The key attributes for each phenotype are presented relative to each other, including their expression of contractile protein genes, migration, and proliferation. Higher levels are indicated by green, upward-facing arrows, and lower levels are indicated by red, downward-facing arrows. This figure was created by GH rendering using BioRender.com.

known effects of Ang II are attributed to the AT1 receptors, which have a hypertensive effect, while AT2 receptors tend to produce hypotension [391].

The response of VSMCs to Ang II is multiphasic, first involving the mobilisation of Ca^{2+} and phospholipase C [450]. Phospholipase C mediates two distinct pathways which commonly result in VSMC contraction by activating several protein kinases, including myosin light chain kinase and Rho-kinase [179]. The removal of Ca^{2+} from the cytosol and the increase in myosin phosphatase initiate VSMC relaxation.

The prolonged effect of Ang II binded to AT1 receptors is the activation of NADH/-NADPH oxidase which stimulates the intracellular formation of reactive oxygen species (ROS) such as superoxide anions [149]. While their precise mechanisms remain unexplored, ROS appear to play an important role in VSMC proliferation, DNA synthesis,

and apoptosis [342][414].

2.2.3 Notch Signalling in VSMCs

Notch receptors in VSMCs appear to promote the phenotypic transition towards a contractile, differentiated state and promote VSMC survival [23][24]. The Notch signalling pathway is one the prominent communication routes between vascular cells and has been found to be upregulated in VSMCs after vessel injury, particularly in VSMC regions close to endothelial cells in the regenerating endothelium [245]. Notch signalling is reiteratively used in VSMCs to positively regulate differentiation, arterial specification, and maturation. The connection between notch signalling and vasculature was first recognised when dominant mutations in the Notch3 receptor were found to be responsible for CADASIL [203].

2.3 Characterising VSMC Dysfunction In Vivo

A pure representation of VSMC dysfunction can be identified at the molecular level both preclinically, and clinically ex vivo, however in vivo methods are necessary for the identification of VSMC dysfunction in patients when interventions may still be possible. Characterising VSMC dysfunction can be difficult in vivo due to the high number of physiological and environmental parameters affecting in vivo measurements. Here, we will discuss the most promising parameters and techniques for identifying the presence of cerebral VSMC dysfunction.

2.3.1 Cerebral Blood Flow and Cerebrovascular Reactivity

VSMCs directly participate in the regulation of CBF and due to their contractile properties, they largely mediate vascular contraction and relaxation, [180]. Decreased baseline CBF correlates with the severity of cognitive symptoms of dementia, showing the potential contribution of CBF alteration to cognitive decline [46].

Cerebrovascular reactivity (CVR) is an indicator of the intrinsic ability of brain vessels to contract or dilate in response to vasoactive stimuli and therefore characterises the brain's ability to support neuronal function under stress. Changes in vessel calibre occur in response to a stimulus, such as alterations in the brain's oxygen/nutrient requirements, or changes in the partial pressure of carbon dioxide (CO_2). As a result, CVR might provide additional and more sensitive information on brain health compared with baseline CBF. For example, in a comparison of MRI-derived CVR and CBF using arterial spin labelling in healthy adults and adults with mild cognitive impairment, whole-brain CVR in both grey and white matter was positively associated with cognitive performance in response to hypercapnia, even in the absence of a statistical relationship between baseline CBF and cognitive performance [217].

Furthermore, because the dilation of cerebral blood vessels, known as vasodilation, is induced during CVR measurements, CVR may also be more representative of VSMC function and morphology than baseline CBF.

2.3.2 Imaging Cerebral Blood Flow and Cerebrovascular Reactivity

Whole brain CBF and CVR mapping can be acquired using positron emission tomography (PET) and single-photon emission computed tomography (SPECT), however, they require the administration of radiotracers, limiting their ease of use and appropriateness in many studies. Non-invasively, CBF and CVR can be measured using MRI methodologies such as arterial spin labelling (ASL) and blood-oxygen-level-dependent (BOLD) imaging [328]. ASL allows direct and quantitative measurement of CBF, while the BOLD signal results from a combination of several physiological parameters (CBF, cerebral blood volume, and cerebral metabolic rate of oxygen). When using a challenge that increases the arterial blood partial pressure of CO_2, it is assumed that the BOLD signal changes predominantly result from changes in CBF. It should also be noted that the BOLD signal has a better signal-to-noise ratio, higher temporal resolution, and is more widely available in conventional MRI scanners than ASL [64]. Nevertheless, CVR and CBF quantification obtained using MRI techniques have been shown to have similar accuracy and precision to 15O H2O PET, which is considered to be the gold-standard measurement of CBF [166][172]. Hauser and colleagues found that CO_2-triggerent BOLD MRI correlates strongly with 15O H2O PET acetazolamide challenge [166]. Heijtel and colleagues compared ASL MRI and PET in both baseline and CO_2-induced hypercapnia, and found intra- and inter-session measurements to be highly comparable with similar precision [172].

Transcranial Doppler (TCD) ultrasound, near infrared spectroscopy (NIRS) can also

be used as non-invasive and indirect measures of CBF regulation and CVR [5][12]. TCD measures blood velocities within an artery, often the middle cerebral artery, as a proxy for CBF. Although it is inexpensive, portable, and relatively easy to use, TCD has low spatial resolution and cannot be used for regional analysis. NIRS provides a real-time assessment of fluctuations in cerebral blood haemoglobin differences in large blood vessels, which is highly correlated with CBF [415]. It should be noted that localised pathologies may not manifest as global changes in cerebrovascular dynamics, and therefore CVR measured using TCD and NIRS might not show changes, while regional CVR measured using PET, SPECT, or MRI may. Other imaging techniques exist for the quantification of CBF in preclinical models including two-photon fluorescence microscopy and laser Doppler flowmetry which can both image the motion of red blood cells in microvasculature and at the subcellular level in the cortex in vivo [98][219].

2.3.3 Methods for Inducing Hypercapnia and Hypocapnia

The most common vasoactive challenge used for CVR assessment involves inducting hypercapnia and / or hypocapnia. In hypercapnia, the arterial blood partial pressure of CO_2 is increased leading to vasodilation and increased CBF. This is achieved by the direct effect of CO_2 and its conversion to carbonic acid (H_2CO_3) via the enzyme carbonic anhydrase. Carbonic acid rapidly dissociates into bicarbonate (HCO_3^-) and hydrogen ions (H^+), thereby decreasing extracellular pH. This lowered pH acts on VSMCs to open their potassium channels, resulting in hyperpolarisation [48]. This decreases the activity of voltage-dependent Ca^{2+} channels, thus decreasing intracellular

Ca^{2+} and leading to VSMC relaxation and vasodilation [323]. Hypocapnia represents the inverse, whereby the arterial blood partial pressure of CO_2 is decreased leading to vasoconstriction. Cerebral vasodilation and vasoconstriction requires the orchestration of the whole neurovascular unit including endothelial cells, astrocytes, parenchymal neurons, and perivascular nerves, in addition to VSMCs [158][186][228]. Therefore, VSMC dysfunction cannot be completely isolated under hypocapnic and hypercapnic conditions, however their functionality may still be well characterised under these conditions as they change and maintain vascular tone [50][83].

One well-known method of inducing hypercapnia in subjects is the inhalation of air with increased CO_2 content. Different techniques have been developed in order to more precisely control CO_2 concentrations, including those based on fixed inspired CO_2 [251]. Some more complex respiratory gas manipulation techniques allow for the precise targeting and maintenance of end-tidal CO_2 ($PETCO_2$), a non-invasive surrogate for the corresponding arterial gas concentration [387]. Since room air has very low concentrations of CO_2, hypocapnia is usually achieved through hyperventilation to increase CO_2 removal from the blood. $PETCO_2$ is derived from air expelled from the lungs during hypocapnia or hypercapnia. $PETCO_2$ and CVR exhibit a sigmoidal relationship which is best modelled using progressively applied levels of hypo-/hypercapnia [38].

Vasodilation can also be induced with exogenous chemicals such as acetazolamide, which can be done in a single dose with a high reproducibility. Acetazolamide is a carbonic anhydrase inhibitor which prevents the conversion of CO_2 to bicarbonate and H^+, thereby promoting vasodilation. In most cases, the administration of CO_2 is still preferred over intravenous acetazolamide because the final serum concentration

for a given dose of acetazolamide and the cerebrovascular responses to that serum level can vary considerably between subjects. These variations are reduced at higher concentrations of acetazolamide, but higher concentrations also increase the severity and frequency of side-effects and subject discomfort [151].

Strategies based on breathing tasks have also been used, such as breath holding or paced deep breathing that can readily induce changes in arterial pressure of blood gases and consequently drive hypercapnia (vasodilation) and hypocapnia (vasoconstriction), respectively. Breathing tasks are often simple and inexpensive to implement, therefore they may offer an accessible option for CVR mapping. However due to the many factors that affect arterial blood CO_2 other than the breathing rate, subject variability must be considered to make this a reliable stimulus to identify cerebrovascular pathology [123].

2.4 Vascular Smooth Muscle Cell Dysfunction and Neurodegenerative Disorders

Many neurological disorders share a common pathological triad of vascular damage, neuronal degeneration, and neuroinflammation. This vasculo-neuronal-inflammatory triad was termed by Zlokovic and colleagues, and involved not just neurons, but brain endothelium, VSMCs, pericytes, astrocytes, and activated microglia [476]. Specifically, many brain disorders share VSMC dysfunction as a mechanism for the progression of neurodegenerative pathology. Although there may be overlap between many of these pathologies, here we discuss and summarise existing research on the role of VSMCs in

prevalent neurodegenerative disorders.

2.4.1 Alzheimer's Disease

Alzheimer's disease (AD) is characterised by progressively impaired memory, cognition, and behavioural changes, and it is the most common cause of dementia. Of the three polymorphic alleles of the human apolipoprotein E (APOE) gene, $\epsilon 2$, $\epsilon 3$, and $\epsilon 4$, the presence of APOE $\epsilon 4$ has been identified as the most prominent genetic risk factor for late-onset AD [35]. Notably, increasing evidence indicates that APOE genotypes differentially modulate cerebrovascular function, and that APOE $\epsilon 4$ induces detrimental cerebrovascular effects including reduced CBF, increased BBB leakiness, and disrupted transport of nutrients and toxins [10][161][467].

Decreased VSMC density was identified in the blood vessels of the arachnoid, grey matter, and white matter of patients with AD compared with age-matched, healthy controls [114]. Patients with AD expressing the APOE$\epsilon 4$ gene also have less smooth muscle actin immunoreactivity, associated with more severe AD, than patients with AD expressing APOE $\epsilon 3$ [114]. Furthermore, APOE $\epsilon 4$ is associated with impaired intramural periarterial drainage (IPAD) in mice [167].

Studies have reported that in patients with AD and mouse models of AD, the overexpression of molecules that control the rate of cell transcript in cerebral VSMCs generates a hypercontractile VSMC phenotype with reduced clearance receptors for the notorious amyloid-beta (Aβ) peptides [32][80]. Autoimmune response mechanisms may also be involved in the degeneration of VSMCs during the development of AD. For example, an increase in anti-smooth muscle antibodies was found to be strongly

correlated with brain atrophy in patients with early AD [141].

Furthermore, specific genes have been associated with changes in VSMC in AD. An upregulation of synthetic-VSMC genes has been found in patients with AD, while the expression of VSMC contractile-genes is significantly reduced in AD cerebral pathology compared to healthy brains [131][259][307]. Notably, changes in the gene encoding for the sarco-endoplasmic reticulum calcium ATPase isoform 2 (SERCA2), a gatekeeper of normal VSMC function, have been associated with AD [53]. The overexpression of SERCA2b was shown to lead to elevated Aβ production, while the knockdown of SERCA2b caused a drastic decline in Aβ [147]. Gallego and colleagues further support the importance of maintaining SERCA activity and show that dysfunctional SERCA can have damaging effects on VSMC Ca^{2+} homeostasis causing AD-associated neuronal cell death [135].

Growing evidence shows that cerebrovascular contractility may be impaired in AD as well as in mild cognitive impairment (MCI), a stage of cognitive decline more severe than what is expected through normal ageing, but less serious than the decline seen in AD. People with MCI are significantly more likely to progress to AD and dementia than healthy adults and are therefore a group of interest for better understanding the development and progression of AD [127]. Several studies have shown that neurocognitive decline in MCI and AD is paralleled by reduced CVR and deficits in vascular contractility, identified using hypercapnic challenge in CO_2 BOLD MRI, TCD, and PET imaging [61][349][422][462]. A recent investigation using ASL MRI showed that impaired CVR in grey matter regions and the whole brain white matter may be an early imaging biomarker revealing the relationship between cerebrovascular function

and cognitive decline [217]. However, other studies have shown that baseline CBF and global CVR are preserved in AD [142][192][353]. Rodell and colleagues found that after factoring out the effects of CO_2 on blood flow, people with AD no longer showed significant inter-subject global CBF variability, though reduced water and oxygen clearance was reduced in specific regions of the brain. While clinical studies are not yet conclusive, there is a substantial body of research that highlights that CVR may be a prospective means to detect early vascular dysfunction in subjects at risk [143]. However, it is also clear that the way in which CVR is measured must be standardised to make it clinically useful.

A common pathological feature associated with AD is cerebral amyloid angiopathy (CAA). CAA results from the build-up of Aβ in the basement membrane of VSMCs in cerebral arteries and the basement membrane of cortical capillaries. Studies have demonstrated that VSMCs can undergo dramatic phenotypic transitions in CAA-like neuroinflammatory conditions, adopting synthetic and proliferative phenotypes [3]. Additionally, these phenotypic transitions often occur in conjunction with tau protein hyperphosphorylation and accumulation in the brain [3].

Aldea and colleagues have studied the impact of vasomotion, a rhythmic relaxations and contractions of cerebral vasculature of 0.1 Hz, on the IPAD mechanism in CAA, and propose that the failure of the vasomotion-driven IPAD mechanisms are responsible for the progression of CAA [8][343]. Their mathematical models showed that the contractile VSMCs of cerebral arteries act as the drivers of IPAD in the brain by inducing basement membrane deformation in the direction of the vasomotion, contributing to the drainage of fluid and soluble metabolites from the brain. It has been suggested that

the force of contractile VSMCs in arteries and arterioles contribute to drainage along the IPAD pathway all the way down to the capillary level, and that impaired VSMCs could result in the accumulation of Aβ in the walls of macro- and microvasculature, contributing to CAA pathology [8]. In CAA, Aβ peptides may also contribute to the transition of VSMCs from contractile to synthetic phenotypes. One study showed that VSMCs exposed to Aβ1-40-peptide, the main amyloid peptide found to accumulate in the vessel wall in sporadic forms of CAA before the addition of proinflammatory cytokines, was greatly intensified compared to those only exposed to the cytokines [428]. Additionally, changes in transcription factors were suggested as a possible path leading to VSMC phenotypic changes and vascular dysfunction in CAA.

Further research into VSMC function and signalling in AD and CAA pathologies is required to better understand the mechanisms underlying vascular and neuronal degradation. However, the cumulation of these findings support that VSMC dysfunction may be a potential biomarker for characterisation or treatment during the development and progression of disease.

2.4.2 Parkinson's Disease and Lewy Body Dementia

Parkinson's disease (PD) is characterised by the presence of intracellular Lewy bodies containing alpha-synuclein (aSyn) fibrils, which are thought to lead to the cell death of dopaminergic neurons in the substantia nigra, affecting motor control, tremors, and gait [458]. The mechanism by which aSyn causes neurodegeneration is unclear, however these fibrils are linked to mural cell function because VSMCs and pericytes appear to be able to take up, secrete, and transfer aSyn [121][402]. A loss in BBB integrity has

been observed post-mortem and it has been suggested that aSyn may be responsible for the breakdown of mural and endothelial cells in the BBB [99].

The specific role of VSMC dysfunction is not yet clear in PD pathologies. One study showed that the global response of CBF and CVR did not differ significantly between patients with PD and healthy controls, though a correlation was identified between increased CBF in posterior regions of the brain and severity of cognitive impairment in the PD group [7]. Another study also did not find any significant difference between the whole-brain CBF and CVR measurements between patients with PD and health controls [318]. However, similar to Al-Bachari and colleagues, Pelizzari's group found that regional increases in CBF correlated with the severity of PD motor symptoms, most significantly in the postcentral gyrus. Furthermore, significant negative correlations were found between CVR and PD severity, corrected for age, in specific regions of the brain, such as the corpus striatum, which is involved in the generation and inhibition of movement.

Genetics also play a role in PD pathogenesis, such as protein deglycase Dj-1 and NDUFV2 [243][359]. Dj-1 is a gene accountable for the autosomal recessive early-onset form of PD and is multifunctional [27][86]. Mutations in Dj-1 result in neurodegeneration, leading to an early onset familial form of PD [44]. Dj-1 also responds to oxidative stress in VSMCs, inhibits hyperplasia, and maintains vasorelaxation by participating in endothelial NO synthesis, though the effects of Dj-1 in VSMC phenotype switching remain unclear [444]. The NDUFV2 gene, also involved in AD pathogenesis, contributes to VSMC communication and may play a role in phenotypic switching to synthetic, pro-inflammatory phenotypes [136]. Furthermore, like with AD, changes in the gene

encoding for SERCA2 have recently been associated with aSyn and PD pathology. The investigators proposed that abnormal accumulation of aSyn could lead to intracellular Ca^{2+} dyshomeostasis due to the downregulation of SERCA2 activity in preclinical models [416].

Lewy body dementia (LBD) is a type of dementia in which the same aSyn Lewy bodies found in PD clump in the cytoplasm of neurons, which disrupts the production of dopamine and causes cognitive decline often as well as motor symptoms such as muscle weakness and rigidity. The role of VSMCs in LBD has been very minimally studied and is largely based on evidence of changes to general cerebrovascular function. Reductions in CBF and microvessel density associated with deficient vascular endothelial growth factor have been described in the occipital cortex of LBD patients compared with controls, though it was unclear whether this was secondary to the accumulation of aSyn [283]. The contribution of hypoxia and hemodynamic changes has been hypothesised based on the high levels of cortical microinfarcts in LBD which is also found in CAA and vascular dementia [348]. LBD patients appear to experience a significant inflammatory response and vascular abnormalities, which exacerbate Lewy body-induced neuropathology, though specific research on VSMCs in LBD has not yet been explored [344]. Changes in CVR and CBF mechanisms have yet to be investigated in patients with LBD.

2.4.3 Amyotrophic Lateral Sclerosis

Amyotrophic lateral sclerosis (ALS) is a progressive neurodegenerative disease of the motor system characterised by focal to generalised weakness leading to paralysis and

respiratory failure [321].

Patients with ALS can exhibit more than a 50 % reduction in pericyte numbers in the spinal cord and a significant increase in platelet-derived growth factor (PDGF) expression, a potent protein, which enhances the rate of cell division and is involved in VSMC recruitment, differentiation, and homeostasis [441]. PDGF also induces VSMC phenotypic switching from a contractile to proliferative and proinflammatory state, and it has been suggested that this plays an important role in atherosclerosis [222][470].

There have been very few studies that have investigated the role of VSMC dysfunction in ALS pathology, however it has been speculated that VSMCs could be involved in ALS due to upregulation of Ang II in the CNS [386]. This is accompanied by a significant reduction in Ang II found in cerebrospinal fluid (CSF) from patients with ALS, which has been associated with disease severity and progression rates [211]. This indicates that changes to RAS and Ang II levels may induce VSMC dysfunction and ALS pathology, but more research is required to better understand the mechanisms and integrity of VSMCs and cerebrovascular dynamics in ALS.

2.4.4 Multiple Sclerosis

Multiple sclerosis (MS) is a complex inflammatory autoimmune disease, largely affecting the white matter of the CNS characterised by demyelination, axonal loss, and the formation of focal and diffuse lesions [175].

Compared with other neurodegenerative diseases, the role of VSMCs in MS progression is not very well understood, though it's clear that Ang II plays a role in the pathogenesis

of MS. Enhanced levels of Ang II in the CNS are culprits of vascular disease and inflammation, and are also seen in MS along with decreased CSF Ang II and increased serum angiotensin-converting enzyme [156][269]. Increased CNS Ang II was also found in a mouse model of MS accompanied by an up-regulation of AT1 receptors in MS brain lesions [331]. In VSMCs, up-regulated AT1 can promote hypertensive effects and increase ROS activity.

A significant decrease in grey matter CVR has been shown in patients with MS compared to healthy controls [265]. The same study found that impaired CVR was significantly correlated with increased lesion volume and grey matter atrophy, suggesting that impaired vasodilation may be an underlying cause of neurodegeneration in MS. More research is needed to properly understand the role and mechanisms of VSMC dysfunction and altered vascular dynamics in MS.

2.4.5 Huntington's Disease

Huntington's disease (HD) is an autosomal-dominant neurodegenerative disorder affecting the CNS, which can lead to involuntary choreiform movements, personality changes, and dementia [313].

The role of VSMCs in HD is not yet conclusive and is largely based on preclinical studies. Models using mice expressing the huntingtin gene indicate that vascular dysfunction might develop earlier in life in the HD mice than in wild-type mice [341]. The HD mice presented with reduced contractility in arteries of varying vascular beds, attributed to altered Ca^{2+} fluctuations in the arterial VSMCs. However, in a different HD mouse model, the response to potassium chloride was tested as a global measure

of vascular smooth muscle structure, mass, and function, and no difference was found compared to wild-type mice [205].

Studies have also investigated the role of myosin phosphatase target subunit 1 and Rho kinase in HD [297]. Myosin phosphatase target subunit 1 is essential for VSMC relaxation through the regulation of myosin light chain phosphatase, and Rho kinase contributes to Ca^{2+} sensitisation in VSMC contraction. Both the myosin phosphatase target subunit 1 and Rho kinase were significantly increased in patients with HD and were found to lead to increased apoptotic cell death [297]. More research is required to better understand the implications of VSMC dysfunction and their molecular pathways in HD.

2.4.6 Down's Syndrome

Down's syndrome (DS) is caused by complete or partial trisomy of chromosome 21, frequently causing intellectual disability and reduced lifespan [312]. People with DS are at a high risk of developing AD at an early age, but are much less likely to develop cardiovascular disease than those without, despite DS being associated with premature ageing, the early onset of AD, and a higher prevalence of risk factors for cardiovascular disease such as obesity, dyslipidemia, and sedentarism [293][312][384].

Structural MRI studies have shown notable increases in cerebrovascular pathology in people with DS, including lobar microbleeds, infarcts, and WMHs, not strongly associated with Aβ pathology [97]. CBF is significantly lower among adults with DS with probable AD compared with controls and participants with DS without dementia when measured using pulsed ASL [406]. The implications of VSMCs on these changes have

not yet been explored.

Two genes are found on chromosome 21 in DS that appear to play a role in vascular health, neural development, and the onset of AD: DYRK1A and RCAN1 [357]. DYRK1A has recently been shown to decrease neprilysin enzyme levels in subjects with DS [212]. Neprilysin degrades natriuretic peptides and vasodilators, which are negatively correlated with VSMC migration and proliferation, and the inhibition of neprilysin is related to the accumulation of Aβ peptides and the development of AD in adults with DS [138][209][282]. Interestingly, it has the opposite effect in cardiovascular disease where its inhibition has been shown as an effective treatment for heart failure and hypertension [255][427]. The effect of RCAN1 on VSMC phenotype is unclear, though it appears to play a role in VSMC migration. The genetic ablation of RCAN1 in mice led to decreased VSMC migration and resistance to Ang II induced aneurysm and restenosis [116]. In contrast, endogenous RCAN1 knockout was found to increase migration in cancer cells in vitro, whereas the expression of exogenous RCAN1 reduced migration [115]. RCAN1 thus appears to have different effects on cell migration depending on the setting.

2.5 Vascular Smooth Muscle Cell Dysfunction and Cerebrovascular Pathology

Here we review the existing research on the role of VSMCs in pathologies that are well known to present a clear vascular component: cerebral small vessel disease, CADASIL, stroke, post-stroke dementia, and Moyamoya disease.

2.5.1 Cerebral Small Vessel Disease and CADASIL

Cerebral small vessel disease (CSVD) is composed of several diseases affecting the small arteries, arterioles, capillaries, venules, and small veins, which may include genetic, idiopathic, infectious, and immune-related pathologies [60]. While the manifestation and progression of CSVD is broad reaching, VSMC migration and hypertrophy due to the upregulation of Ang II and leading to increased ROS may be a common link to vascular remodelling and dysfunction [425]. In preclinical and in vitro studies of Ang II-induced CSVD, ROS have been shown to alter blood pressure, vascular structure, and collagen deposition [148][425].

Beyond investigating the role of Ang II and ROS in VSMC function in CSVD, much of the research on VSMCs in CSVD has been based on CVR and CBF studies. It has recently been demonstrated that patients with advanced hypertensive CSVD have impaired CVR in the basal ganglia, temporal lobe, and frontal lobe, determined using ASL MRI with an intravenous vasoactive stimulus [231]. The same study found that the reduced vasoconstriction was significantly associated with conventional MRI markers of CSVD, including cerebral microbleeds, white matter hyperintensities (WMHs), and deep lacunar infarcts. Furthermore, lower CVR determined using BOLD MRI under hypercapnic challenge was found to be indicative of WMHs and perivascular spaces associated with CSVD when controlling for patient characteristics [40]. Another BOLD MRI study showed that areas of reduced CVR precede the progression of normal-appearing white matter to WMHs suggesting that impairment of vascular contractility may contribute to the pathogenesis and progression of CSVD [363]. A

systematic review of CSVD and ischaemia associations showed that baseline CBF was also negatively related to WMH severity linked to CSVD, and Shi and colleagues noted that investigating CVR in patients with CSVD may provide new insights [374].

Cerebral autosomal dominant arteriopathy with subcortical infarcts and leukoencephalopathy (CADASIL) is a rare, hereditary CSVD characterised by VSMC degradation and the accumulation of Notch3 receptors on the VSMCs of small and middle-sized arteries [201][202]. A common pathological feature of CADASIL is the dramatic reduction of VSMCs in cerebral arterioles walls, which may be attributed to irregular mitochondrial proliferation and function in CADASIL VSMCs [423].

In a study comparing proteomic expression of cultured CADASIL and control VSMCs isolated from human umbilical cord, it was found that CADASIL is likely caused by misfolded Notch3 molecules [188]. This impairs the Notch3 signalling cascade, increases ROS, inhibits cell proliferation, and degrades VSMCs. Ihalainen and colleagues found that this also induces the overproduction of collagen type I, leading to fibrosis, vascular stenosis, and ischaemic lesions as seen in patients with CADASIL. Similarly, cultured CADASIL VSMCs have been shown to have a lower proliferation rate compared to control VSMCs and also showed an increased gene expression of transforming growth factor-beta that, when neutralised, corrected the proliferation rate [309].

The CVR and mean CBF in the middle cerebral artery, measured using TCD and MRI, have been shown to be reduced in CADASIL compared with controls, attributed to VSMC dysfunction [22][242][291][323]. Pfefferkorn and colleagues also found reduced CO_2 reactivity in patients with CADASIL before they became disabled, suggesting

that CVR plays an early role in the evolution of the disease. In an MRI analysis using an intravenous acetazolamide vasoconstrictive challenge, CVR was significantly reduced in CADASIL and was identified as an important determinant of development of WMHs [242]. Furthermore, an overall decrease in relative CBF and cerebral blood volume, before and after an acetazolamide challenge, were detected in patients with CADASIL when measured using MRI [66].

There have also been studies that found that CVR was not impaired in patients with CADASIL when measuring large arterial flow using MRI and TCD [45][379]. Both of these studies found that baseline CBF was lower in subjects with CADASIL than in controls. As a result, Van den Boom and colleagues suggested that flow impairment may give rise to the development of WMHs and lacunar infarcts in patients with CADASIL [45].

More research specifically on the contribution of VSMCs to vascular changes in CSVD and CADASIL is essential to better understand the underlying mechanisms of these disorders.

2.5.2 Stroke and Post-Stroke Dementia

Ischaemic strokes are caused by a sudden blockage of blood flow to an area of the CNS. Having a stroke doubles the risk of dementia and the prevalence of post-stroke dementia (PSD) has been predicted to increase in the future because of better survival after stroke and ageing of the population [237]. VSMCs appear to play an important role in the early development of ischaemic stroke and PSD due to their role in stabilising BBB integrity and perfusion, and maintaining healthy vasculature [274].

Phenotypic switching of VSMCs to a synthetic state has been shown to induce BBB disruption after ischaemic stroke in mice [274]. Meng and colleagues found that a deficiency in myosin phosphatase target subunit 1 stimulated the phenotypic switching to a synthetic, pro-inflammatory state in human brain VSMCs and after ischaemic stroke in mice. It was also found that modifications in VSMC phenotype after stroke in vivo can impact the incidence, severity, pattern, and outcome of ischaemic stroke [332].

Furthermore, stroke-induced hypoxia can lead to the overexpression of amyloid precursor protein (APP) in VSMCs, which could exacerbate or expedite the development and progression of CAA, worsen stroke outcome, and lead to PSD [347]. Notably, before the deposition of Aβ in the brain and blood vessels, mice with APP mutations show reduced hypercapnic CVR and altered neurovascular coupling [300]. Zlokovic proposed a model to explain how cerebrovascular diseases, such as stroke, can lead to AD and dementia [475]. He proposed that stroke-induced hypoxia compromises the BBB and the overexpression of APP alters the balance between Aβ production and clearance in favour of production, which induces neuroinflammation. As a result, this may lead to synaptic dysfunction, and the accelerated onset of CAA and PSD.

Atherosclerotic plaque stability, a leading cause of ischaemic stroke, also appears to be highly dependent on the VSMC phenotype, which may either undergo apoptosis or activate the production of inflammatory mediators that can trigger plaque rupture and thrombosis [134][176]. In an experimental focal cerebral ischaemia model, simvastatin promoted arteriogenesis through increased Notch receptor expression in the ischaemic cerebral arteries and peri-infarct area and it was suggested that the regulation of VSMC

function through Notch signalling may be a determinant of the outcome of cerebral ischaemic disease [465].

Further assessment of the role of VSMCs in ischaemic brain disease and PSD may offer a new avenue for understanding the development and severity of stroke, and its progression to AD and dementia.

2.5.3 Moyamoya Disease

Moyamoya disease (MMD) is a rare cerebrovascular disease characterised by progressive stenosis or occlusion of the terminal portion of the internal carotid arteries [225].

VSMCs in patients with MMD have shown specific differentially expressed contractile protein genes such as increased expression of smooth muscle actin and myosin heavy chain, compared with healthy control volunteers [206]. Notably, these mutations are related to VSMC adhesion, cell migration, immune response, and vascular development. The increased expression of α-smooth muscle actin may be involved in the increased proliferation of VSMCs, contributing to MMD stenosis [154]. Post-mortem analysis of patients with MMD has shown degeneration in the cerebral VSMCs, and migration and morphological changes of VSMCs in the thickened intima [244].

It has also been suggested that endothelial cell dysfunction contributes to the early development of MMD and that VSMCs may require additional factors to contribute to the pathophysiology of MMD. In the analysis of VSMCs from neural crest stem cells, MMD patients and healthy control subjects were observed to have similar VSMCs proliferation, migration and contractile abilities, in contrast to the endothelial cells,

which displayed distinct transcriptome profiles [409].

Studies have shown a significant CVR impairment in patients with MMD, based on ASL MRI and PET measurements following the injection of vasodilator acetazolamide [468][94]. These studies showed that the CBF of patients with MMD did not increase after the injection of acetazolamide, suggesting that the cerebral vessels were already at maximal vasodilation to compensate for CBF reduction. Heyn and colleagues also identified decreased regional CVR in patients with MMD using CO_2 BOLD MRI [177]. Interestingly, unilateral surgical revascularisation, a widely used preventative treatment for MMD, was found to improve PET-derived CVR in MMD patients not only in the hemisphere ipsilateral to the flow restoration, but also in the non-intervened hemisphere [94][364]. It remains that more research is required to better understand how and at what stage VSMC dysfunction may contribute to MMD development and progression.

2.6 Extrinsic Influences on VSMC Dysfunction

Extrinsic influences such as lifestyle choices, environmental effects, and traumatic events can impact the function, migration, and proliferation of VSMCs, and are likely to be factors in the onset and progression of neurodegenerative disorders. Many of these have been identified as risk factors for cerebrovascular and cardiovascular disorders as well as neurodegenerative disorders [254]. Understanding how extrinsic factors may influence VSMCs may inform novel interventions and therapies for preventing and arresting neurodegeneration.

2.6.1 Toxins

Toxins such as those introduced to the body through cigarette smoking, alcohol or drug consumption, or air pollution are major risk factors for the early-onset of neurodegenerative disorders [63][195][268][362]. Exposure to toxins can also lead to profound remodelling and apoptosis of cerebral VSMCs.

Exposing cultured cerebral VSMCs to cigarette smoke extract was found to induce phenotypic switching to a pro-inflammatory, synthetic state, and suggested an avenue for the major risk that cigarette smoking causes for cerebral vascular injury such as atherosclerosis and stroke [392]. In a preclinical study, nicotine exposure has been shown to stimulate abnormal growth of VSMCs and fibroblasts due to an enhanced Ang II type 1 receptor-mediated functional response [238]. The same study showed that nicotine can also cause phenotypic changes of contractile VSMCs to synthetic VSMCs. The effects of nicotine on VSMCs in humans is not yet conclusive, but it has been proposed that nicotine can induce imbalances in RAS, which can cause VSMC dysfunction [301].

High concentrations of ethanol have been shown to increase neuronal apoptosis due to increased ROS and induced apoptosis of cerebral VSMCs [240]. Similarly, exposure to even small doses of cocaine induces rapid apoptosis in cerebral VSMCs, contributing to the development of stroke and neurodegeneration [395]. Exposure to smaller concentrations of ethanol has been found to inhibit Notch signalling and, therefore, decrease proliferation and migration in VSMCs in vitro and during vessel remodelling in response to flow reduction in vivo in mice [173][292]. In these studies, VSMC pro-

liferation was found to increase when Notch pathways were artificially turned back on. Morrow and colleagues suggest that the inhibitory effect of moderate alcohol on VSMC growth may prevent vessel thickening associated with atherosclerosis and stroke [292]. However, recent studies suggest that no level of alcohol consumption is safe in humans. These studies show that even moderate alcohol consumption has been associated with ROS generation, hypertension, stroke, vascular alterations in the peripheral and central nervous systems, cognitive decline, and more [78][140][304][354][411].

Exposure to air pollutants and ambient particulate matter has been shown to induce the transitioning of VSMCs from contractile to synthetic phenotypes, increasing cell migration and expression of proinflammatory cytokines [181]. Furthermore, organic matter from ambient particulates and polycyclic aromatic hydrocarbons induce VSMC migration through ROS generation leading to vascular pathology [204]. NO is a common free radical which is both present in the environment and can be produced in the body as a vital signalling molecule. In the blood vessels, NO decreases the intracellular concentration of Ca^{2+} and causes VSMC relaxation, and is thus a potent vasodilator [471]. In the environment, NO can react with other gases in the atmosphere to form nitrogen dioxide (NO_2) and nitrous oxide (N2O). Notably, evidence is emerging that air pollution, including high ambient particulate matter, NO, and carbon monoxide, is also associated with increased risk of dementia and vascular damage [65][322]. More research on the effect of poor air quality on cerebral VSMCs and in neurodegenerative pathology is required to better understand the neurotoxic effect of air pollution.

2.6.2 Pulsatility

Pulsatility is generated by oscillations in arterial blood flow and pressure that occur with each heartbeat. Normal haemodynamic pulsatility can be affected by age, hypertension, diabetes mellitus, hyperlipidaemia, and haematocrit levels [197]. Pulsatility factors such as blood flow-induced vessel wall shear stress, cyclic strain, and hydrostatic pressure can affect the function and phenotype of VSMCs, which has been attributed to vascular disorders [375]. A recent review by Thorin and colleagues suggests that age-related increased arterial stiffness may promote high pulse pressure in cerebrovasculature that leads to functional and structural alterations that could promote neuronal dysfunction and cognitive decline [408]. Notably, a chronic increase in pulse pressure has been associated with cognitive decline and dementia [314][371].

VSMCs have multiple sensing mechanisms to perceive mechanical stimuli generated from pulsatile stretch and transduce signals resulting in the modulation of gene expression, and cellular functions such as proliferation, apoptosis, migration, and remodelling [157][339]. A recent review found that high pulsatile shear stress induces VSMC apoptosis due to the increased release of NO from endothelial cells and low shear stress increases VSMC proliferation and migration through endothelial-released platelet-derived growth factor [339]. Other studies have shown that both the pressure amplitude and frequency of pulsatile flow can affect VSMC morphology and alterations in the cyclic oscillations modulated VSMC function and tissue stiffness [273][299].

While more research is needed to understand the vascular changes that occur in response to pulsatile load, the effects of pulsatility on blood vessel contractility and

VSMC function are notable and warrant further investigation in healthy and pathological states.

2.6.3 Traumatic Brain Injury

Traumatic brain injury (TBI) leads to an increased risk of progressive neurodegeneration and dementia [146]. While the mechanisms for this are not yet clearly understood, it has been shown that TBI results in a loss in cerebrovascular tone and changes in the function of VSMCs and the neurovascular unit, which may contribute to the increased risk of neurodegenerative disease.

TBI has been reported to increase concentrations of endothelial-released NO, severely blunting pressure-induced vasoconstriction [424]. This was found in conjunction with a decrease in VSMC Ca^{2+} levels, which collectively led to VSMC apoptosis and profound cerebral artery dilation after TBI.

In preclinical studies, it has been demonstrated that TBI reduces gap junction coupling in VSMCs through mechanisms related to increased ROS [464]. Substantial increases in hydrogen peroxide were found in VSMCs of cerebral arteries after TBI leading to decreased pressure-induced constriction of cerebral arteries in rats [399]. The impaired VSMC contractility was restored after the VSMCs were treated with a mitochondria-targeted antioxidant that blocked specific ion signalling channels in VSMCs.

A study of patients with blast-induced TBI found an overexpression of mRNA markers in contractile VSMCs and suggested that TBI leads to phenotype switching mechanisms in VSMCs of cerebral arteries, as well as prolonged hypercontraction and vasospasm

[9]. Alford and colleagues proposed that trauma causing small perturbations in tissue tension results in contractile-dominant VSMC phenotypes, while larger perturbations shift VSMCs towards a synthetic phenotype, causing large-scale remodelling.

2.7 Therapeutic Opportunities

The key to developing novel therapeutic treatments for neurodegenerative disorders depends on the understanding and investigation of the underlying molecular mechanisms. Some of these are genetic, such as in Huntington's disease, Down's syndrome, and CADASIL, however others such as Alzheimer's disease, Parkinson's disease, ALS, and multiple sclerosis, can occur sporadically, and their mechanisms have been harder to establish.

Despite their variability in symptoms and progression, VSMC dysfunction appears to be a common link between these disorders and could prove to be a promising target for intervention. Studies have shown that targeting the vascular tissue with drugs may be effective at modulating and / or preventing neurodegenerative disorders such as AD and PD [4][390]. It has also been suggested that intervening during the differentiation, proliferation, and / or migration mechanisms of VSMCs could be a therapeutic strategy to reduce pathological VSMC functions while maintaining their stabilising roles in CBF [447]. Here, we will review recent insights on VSMC-based therapeutics in vascular pathology and discuss how VSMCs could be targeted to intervene in the development and progression of neurodegenerative disorders.

2.7.1 Signalling Pathways

It has been proposed that targeting VSMC signalling mechanisms could be protective against the onset of neurodegeneration [243][264]. Notably, increased VSMC proliferation and migration exhibited in AD, ALS, and Moyamoya disease can be harmful to cerebrovascular function and may contribute to the accumulation of toxic plaques in the central nervous system [3][154][222]. In other pathologies, such as CADASIL, a dramatic reduction in VSMC proliferation can lead to vessel thinning and reduced CVR amplitude [242][309]. VSMCs have several signalling pathways to control cell function and proliferation, however a few players have been identified as key contributors in VSMC proliferation.

VSMC proliferation and migration can be manipulated by inhibiting the degradation of cyclin-dependent kinase (CDK) with pharmaceuticals like thiazolidinediones, which have been developed for treating type II diabetes [429]. These drugs are also peroxisome proliferator-activated receptor γ (PPARγ) agonists and the activation of PPARγ in VSMCs has been shown to inhibit synthetic VSMC proliferation and migration, which may have vascular-protective effects [229][456]. The CDK pathway is also involved in telomere activity, which stabilises chromosomes. Telomerase reverse transcriptase (TERT) phosphorylation, which is upregulated during and following hypoxia, has been shown to increase VSMC proliferation [281]. Some evidence has shown that inhibiting TERT in vivo, such as via the CDK pathway, may reduce vascular disease [133].

The transient receptor potential vanilloid (TRPV) family is expressed abundantly in cerebral artery VSMCs and has been shown to be an important mediator of vascular

tone [153]. The overexpression of TRPV1 has been found to inhibit Ang II induced VSMC migration and phenotype transitions from a contractile to secretory state [433]. Another study found that activated TRPV1 inbited VSMC proliferation, migration, and ROS production by upregulating the expression of PPARγ [473]. Additionally, TRPV4 channel activity has been found to increase vasoconstriction and elevate resting blood pressure in mice and patients with hypertension [76].

RhoA/Rho-kinase have been shown to modulate VSMC phenotype switching including affecting proliferation, dedifferentiation, apoptosis, and migration in VSMCs, which is discussed extensively in the review paper by Sawma and colleagues [367]. Notably, the inhibition of Rho signalling using fasudil hydrochloride is currently used clinically for the treatment of vasospasm [290]. It has been suggested that it may also reduce inflammation and lesion volume in multiple sclerosis [6].

Interestingly, berberine has been increasingly found to have vascular- and neuro-protective effects against neurodegenerative pathology, which could be attributed to its effects on signalling pathways [223][459]. Berberine is an organic compound in classical natural medicine, proven by modern research to have various pharmacological effects, including antiviral, anti-inflammatory, and lipid regulation [460]. Preclinically, berberine was found to affect smooth muscle contractility by regulating the VSMC handling of intracellular Ca^{2+} [258]. In vitro, berberine inhibited early signalling pathways induced by VSMC injury, reducing the contraction and proliferation of dysfunctional VSMCs [241]. Other studies have shown that berberine inhibits induced VSMC proliferation via the PPARγ signalling pathway by stimulating a beneficial increase in NO [58][338].

Notch signalling has gained significant attention in the context of vascular biology and has been identified as a possible culprit for VSMC and pericyte reduction seen in some neurodegenerative disorders [243]. As mentioned earlier, Notch3 is a gene involved in the pathogenesis of CADASIL, though it is currently not known if the mutations in Notch3 are causative [188]. One study showed that Notch3 is necessary for pericyte proliferation in zebrafish [435]. In contrast, another study found that while Notch3 mutations disrupt and compromise the BBB, the mutations have no direct effect on mural cells [174]. While very minimal research has been conducted on Notch-based therapeutics in neurodegeneration, targeting Notch receptors in mice models of inflammatory disorders that share features with human MS has shown very minimal side effects while safely preventing and reversing inflammation [285][365].

The renin-angiotensin system may also be a potential target for therapeutic intervention for VSMC dysfunction. Angiotensin-converting enzyme inhibitors and angiotensin receptor blockers have been shown as effective modulators of AD in preclinical models [233]. In a mouse model, angiotensin receptor blockers alone were not found to restore Aβ-related cognitive and cerebrovascular deficits [358]. However, captopril (another angiotensin converting enzyme inhibitor) alone was found to reduce Aβ deposition in vitro and in vivo, and improve cognition in animal models [2][19].

Another major signalling molecule, adenosine, is synthesised by VSMCs and endothelial cells via multiple pathways, and may be useful for controlling VSMC growth in vascular disease [316]. Studies have shown that adenosine inhibits VSMC growth and that a reduction in local adenosine levels may initiate VSMC growth and contribute to the vascular remodelling in hypertension and atherosclerosis [105]. Additionally, abnormal

adenosine homeostasis has been observed in Parkinson's disease, Huntington's disease, and ALS [15][232][463]. The review by Chang and colleagues summarises this topic more extensively and highlights the therapeutic opportunities for targeting adenosine homeostasis in neurodegenerative disorders [67].

VSMCs are crucial in hypertension progression and the response of VSMCs to statins, most commonly used to treat and prevent hypertension, has therefore been more extensively researched, though only more recently in the context of neurodegeneration [366]. Statins can affect several components of RAS pathways in conjunction with lowering low-density lipoprotein cholesterol. Notably, statins can inhibit the harmful overexpression of Ang II and AT1 receptors, and support healthy VSMC contraction [216]. It has been shown that statins can inhibit VSMC proliferation and reduce vascular inflammation, likely by decreasing the sensitivity of VSMCs to Ca^{2+} leading to structural remodelling, and reduced vascular constriction [138][207]. As a result, statins may have vasodilatory and antithrombotic properties, which could enhance collateral circulation and improve CVR, notably in cases where VSMCs are hypercontractile [139]. It appears that statins may also reduce the accumulation of Aβ in the brain and have protective effects against cognitive decline, however it is unclear which mechanisms drive these outcomes [369].

Here we have identified signalling pathways such as PPARγ, CDK, Notch, Rho, TRPV, adenosine, and RAS, which may be potential targets for intervening in VSMC dysfunction. Further research is critical to clearly understand the effect of these signalling pathways on VSMC physiology in both healthy and diseased states.

2.7.2 Inhibiting Reactive Oxygen Species

Another method of inhibiting VSMC phenotype transitions could be through the inhibition of ROS. In VSMCs, ROS are known to mediate many physiological processes such as phenotypic switching and signalling pathways, as well as pathophysiological processes, including migration, proliferation, apoptosis, and inflammatory cytokine secretion [149][342][414].

In mice, the inhibition of ROS via the oral administration of the antioxidant drug apocynin suppresses proinflammatory and proliferative synthetic VSMCs associated with vascular disorders [324]. While the precise mechanisms underlying the effect of ROS remain unclear, the same study suggested that ROS induces VSMC phenotype switching through the upregulation of toll-like receptor 4 (TLR4) in endothelial cells, which can be modulated using drugs such as apocynin. Shimokawa and colleagues showed that the growth factor cyclophilin A contributes to ROS effects in VSMC by promoting growth and, as a result, the effect of ROS on VSMC function may be possible by blocking the cyclophilin A signalling or binding pathways [377].

It has been demonstrated that ROS mediates vascular contraction and remodelling by activating Rho-signalling [199]. For example, the long-term blockage of the Rho-kinase pathway was shown to inhibit induced vascular remodelling in mice by blocking the synthesis of ROS, such as NO [189]. As a result, the Rho pathways may be a target for inhibiting ROS.

These findings suggest that novel pharmacological strategies aimed at mediating the effect of VSMC phenotype switching through the inhibition of ROS may have thera-

peutic potentials in treating VSMC dysfunction.

2.7.3 Gene Therapy

Gene therapy is an emerging therapeutic tool by which functional genetic material is delivered to specific cells to correct a defective gene. Several clinical studies have tested gene therapy for treating neurodegenerative disorders, including Parkinson's disease and Alzheimer's disease, though the efficacy of these approaches has yet to be determined [29][308][419].

Among the most promising of potential gene therapy targets for VSMC dysfunction is SERCA2a, the SERCA isoform present in the nervous system, which has been approved as a human gene therapy target to treat heart failure [198]. This has been attributed to the normalisation of Ca^{2+} cycling in VSMCs and inhibiting Ca^{2+}-dependent transcription factors [275]. This could be used to target VSMC dysfunction as forced expression of SERCA2a in contractile VSMCs has been shown to prevent injury-induced dedifferentiation towards a synthetic, inflammatory phenotype, whereas forced expression in synthetic VSMCs reduces their proliferation and migration, but has no effect on their phenotype [43].

The review papers by Martier and colleagues, and Piguet and colleagues explore the past, current, and future perspectives of gene therapy for neurodegenerative disorders [266][325]. Importantly, it has been noted that delivering therapies administered before the onset of neurodegeneration is essential to improve the efficacy of gene therapies [266]. Therefore, the discovery of biomarkers for early detection of neurodegenerative disorders and a better understanding of factors leading to these disorders is essential

to improve clinical applications of gene therapy.

2.8 Concluding Remarks

In this work, we reviewed the role of VSMCs in the most common neurodegenerative disorders and identified mechanisms by which VSMC dysfunction may contribute to neurodegeneration. In particular, changes in VSMC phenotype, signalling pathways, and interactions with ROS are seen in a host of neurodegenerative disorders and could serve as targets for novel therapeutic interventions. We identified CVR and CBF measurements as promising techniques by which VSMC dysfunction could be characterised in vivo, but further research is required to understand how to isolate VSMC contributions. Note that correlations between VSMC dysfunction and some of the disorders were more extensively studied than others, and methodologies varied greatly between them. Furthermore, inferences drawn from some of the studies analysed in this review should be taken with caution as not all of them were specifically assessing VSMC dysfunction in this context, and it remains unclear whether VSMC dysfunction is a cause or a consequence of these disorders. In conclusion, the evidence collected here highlights the critical role of VSMC dysfunction in the development and progression of neurodegeneration, and the need for more investigation into VSMCs and cerebrovascular dynamics in neurodegenerative disease.

Funding Acknowledgments

This work was supported by Engineering and Physical Sciences Research Council UK through grant EP/S021507/1. GH was supported by Clarendon, SNS by the Rhodes Trust, and SS by the Alzheimer's Society.

Declaration of Competing Interests

The authors declare that this research was conducted in the absence of any commercial or financial relationships that could be construed as a potential conflict of interest.

3 | Characterising Cerebrovascular Reactivity and the Pupillary Light Response – A Comparative Study

Preface

Based on the role of smooth muscle in both cerebral and ocular physiology, this chapter presents a novel investigation into the relationship between cerebrovascular reactivity (CVR) and the pupillary light response (PLR). By measuring the middle cerebral artery's blood flow response to controlled CO_2 and the eye's reaction to flashes of light and dark, the study explores whether shared underlying vascular smooth muscle mechanisms might manifest across these two distinct physiological pathways. The analysis reveals a significant negative correlation between CVR and PLR latency in a dark flash protocol, suggesting that smooth muscle dysfunction could influence both cerebral blood flow regulation and pupil dynamics. These findings provide an important starting point for future research aimed at developing non-invasive biomarkers of vascular and autonomic function.

This chapter was published as:

> S. Sparks* and **G. Hayes***, J. Pinto, and D. P. Bulte, "Characterising cerebrovascular reactivity and the pupillary light response - a comparative study," Front. Physiol., vol. 15, 2024. doi: 10.3389/fphys.2024.1384113

A subset of these results was presented at the following conferences:

S. Sparks, **G. Hayes**, J. Pinto, J. Martin, M. Spitschan, and D. P. Bulte, "Comparing the pupillary light response to white, red, and blue stimuli with cerebrovascular reactivity," *Association for Research in Vision and Ophthalmology (ARVO)*, May 2024, Seattle, USA.

S. Sparks, **G. Hayes**, J. Pinto, J. Martin, M. Spitschan, and D. P. Bulte, "Comparing the pupillary light response using two pupillometers with cerebrovascular reactivity," *Oxford Ophthalmological Congress*, S. Sparks, **G. Hayes**, J. Pinto, J. Martin, M. Spitschan, and D. P. Bulte, "Comparing the pupillary light response to white, red, and blue stimuli with cerebrovascular reactivity," *Association for Research in Vision and Ophthalmology (ARVO)*, Jul. 2024, Oxford, UK.

Drawing parallels between brain and ocular dynamics, this work underscores the broader relevance of smooth muscle function in maintaining both cerebral perfusion and pupil regulation. It lays the groundwork for subsequent chapters focused on refining methodologies for CVR assessment and further exploring their clinical implications.

Author Contribution Statement

S. Sparks contributed to the pupillometry study concept and design, acquisition, analysis and interpretation, writing of the manuscript. **G. Hayes** contributed to the CVR study concept and design, acquisition, analysis and interpretation, writing of the manuscript. **J. Pinto** contributed to ethics approvals, data acquisition, and critical revision of the manuscript. **D. P. Bulte** developed the original study concept and

design, critical revision of the manuscript, and study supervision. All authors read and approved the final manuscript.

Abstract

Introduction: Smooth muscle is integral to multiple autonomic systems, including cerebrovascular dynamics through vascular smooth muscle cells and in ocular muscle dynamics, by regulating pupil size. In the brain, smooth muscle function plays a role in cerebrovascular reactivity (CVR) that describes changes in blood vessel calibre in response to vasoactive stimuli. Similarly, pupil size regulation can be measured using the pupillary light response (PLR), the pupil's reaction to changes in light levels. The primary aim of this study was to explore the interplay between cerebral blood flow and pupil dynamics, evaluated using CVR and PLR, respectively.

Methods: A total of 20 healthy adults took part in a CVR gas stimulus protocol and a light and dark flash PLR protocol. CVR was calculated as the blood flow velocity change in the middle cerebral artery, measured using transcranial Doppler ultrasound in response to a 5 % increase in CO_2. Multiple PLR metrics were evaluated with a clinical pupillometer.

Results: CVR and PLR metrics were all within the expected physiological ranges for healthy adults. Nine different PLR metrics, assessed through the light and dark flash protocols, were compared against CVR. A significant negative relationship was observed between the latency of the PLR in the dark flash protocol and CVR. No statistically significant relationships were found between CVR and other PLR metrics.

Conclusion: This is the first study to investigate the relationship between cerebral blood flow and pupil dynamics. A significant relationship between dark flash latency and CVR was observed. Future work includes evaluating these relationships using more robust CVR and PLR measurement techniques in a larger, more diverse cohort. Notably, more research is warranted into the PLR using a dark flash protocol and its connection to cerebrovascular function.

3.1 Introduction

Cerebrovascular dynamics are crucial for the maintenance of adequate cerebral blood flow (CBF) to the brain and can be quantified using a metric known as cerebrovascular reactivity (CVR). CVR describes the intrinsic ability for cerebral blood vessels to dilate and constrict in response to vasoactive stimuli, a phenomenon that is largely mediated by vascular smooth muscle cells (VSMCs) that surround arteries and arterioles [165][168].

CVR can be measured by varying the arterial partial pressure of CO_2 ($PaCO_2$), inducing either hypercapnia (increased $PaCO_2$) or hypocapnia (decreased $PaCO_2$) through stimuli such as voluntary breathing tasks or gas protocols [252][328][351]. Alternatively, cerebral vasodilation can be induced pharmacologically using acetazolamide, which increases hydrogen ion concentration via inhibition of carbonic anhydrase, rather than by increasing $PaCO_2$ directly. The concomitant CBF changes can be measured non-invasively using an appropriate imaging modality such as magnetic resonance (MR) imaging or transcranial Doppler ultrasound (TCD). While MR provides CVR mea-

sures with relatively high spatial resolution including brain micro-vasculature [381], TCD is a simpler, more widely available and cost-effective alternative that measures blood velocity in single major arteries [55][271]. Measurements of CVR are emerging in clinical use to assess cerebrovascular function including in Alzheimer's disease and dementia [11][118][355][397][431], carotid artery stenosis [278][350], stroke [372], congestive heart failure [451], hypertension [28][248].

Smooth muscle can also be found outside of the brain, such as in the iris in the form of sphincter and dilator muscles to control the size of the pupil [190]. These muscles can be easily assessed using the pupillary light response (PLR, also called the pupil flash reflex). The PLR characterises pupillary size changes to different light conditions [235]. These changes are mainly controlled by opposing branches of the autonomic nervous system: whilst the parasympathetic nervous system controls the constriction facilitated by the sphincter muscles of the iris, the sympathetic nervous system controls the dilation facilitated by the dilator muscles of the iris [434][442][449]. In response to a light stimulus, the PLR can be categorised into four dynamic phases: response latency, maximum constriction, pupil escape, and recovery [160]. Various parameters of the PLR can be extracted from these four phases for further assessment, depending on the application.

The PLR has been used in clinical and research settings as a diagnostic tool for several mental and physical health problems, including acute and traumatic brain injury [305][311][413], depression [34][129][276][279], diabetes [39][208][227][457], and increased intracranial pressure and intracranial hypertension [75][193][310][356][404]. Changes in the PLR have also been reported in both preclinical and clinical Alzheimer's

disease cases [79][128][132][449], as well as in those identified to have increased risk of developing neurodegenerative disorders [389].

Given that both of these measures appear to be related to a variety of factors including smooth muscle dynamics and function, and additionally show overlapping changes in several pathologies, it is important to investigate their association to better understand pathological mechanisms and their identification. Therefore, this pilot study aims to explore the relationship between the PLR and CVR in healthy adults with no history of cerebrovascular or eye disorders as a means of assessing the interplay between dynamics in the brain and in the pupil.

3.2 Materials and Methods

3.2.1 Subjects

We acquired data from twenty healthy subjects with no record of neurological disorders (9F, age range 23-68 years, with a mean of 33.5 $\pm$ 11.5 years at the time of acquisition). Inclusion criteria consisted of having no diagnosed cognitive impairment, psychiatric conditions, diabetes, high blood pressure, respiratory, or cardiac health issues. Participants with corrective prescription glasses did take part in the study, but none who had known vision loss and none who had undergone eye or brain surgery. They were also instructed to refrain from consuming caffeinated drinks for two hours before the session. All participants provided informed written consent before each session, and the study was approved by the Medical Sciences Interdivisional Research Ethics Committee (MS IDREC) of the University of Oxford's Central University Research Ethics

Committee (CUREC).

3.2.2 Data Acquisition

Data acquired in this study included cerebral blood velocities using TCD and a respiratory gas stimulus, and pupil dynamics using pupillometry with light stimuli. For all participants, the sequence of protocols involved the completion of the TCD and gas stimulus first, followed by the dark adaptation and pupillometry protocols, with at least 10 minutes between protocols to change equipment and transfer setups.

3.2.2.1 Transcranial Doppler Ultrasound and Gas Stimulus

A 2 MHz pulsed transcranial Doppler ultrasound system (7760EN Doppler-BoxX Digital, Compumedics DWL) was used to measure cerebral blood velocities in the middle cerebral artery (MCA). A transmission gel was applied to the transtemporal window of the volunteer and the TCD probe was placed over the gel and secured using an adjustable headset. The location and angle of the probe was changed until a steady blood flow velocity with good signal-to-noise ratio was achieved.

CO_2 and O_2 levels in respired air were sampled using a thin nasal cannula placed into both nostrils and an infrared gas analyser (ML206, ADInstruments). The CO_2, O_2, and TCD signals were recorded using a PowerLab 8/35, 8 Channel recorder (PL3508 ADInstruments) and accompanying LabChart Software.

For the gas stimuli, a custom gas delivery system was used to carry out the procedure and accurately monitor physiological parameters throughout it. This system was built in-house at the University of Oxford [398]. It consisted of a disposable non-rebreathing

anaesthetic face mask with a Laerdal bag placed over the participant's nose and mouth, secured using a head strap. Holes on either side of the mask were covered by unidirectional silicon membranes to allow exhaled air to escape the mask while being sealed during inhalation. A medical-grade respiratory filter was placed at the junction of the disposable circuit and the permanent fixtures to prevent cross-contamination. On the permanent side of the filter, a short length of tubing led to a parallel Y-pieces where respiratory gas mixtures could be delivered one at a time.

Two different levels of inspired gases (medical air and air with 5 % CO_2) were delivered to the face mask at a rate of 15 L/min through unidirectional tubing. The gas cylinders, each fitted with a pressure regulator and flow metres, were operated by hand, following a predefined protocol.

The gas stimulus protocol consisted of a period of baseline measurements of blood flow velocity while the subject breathed normally on medical air for 3 minutes. After this period, the gas was switched from synthetic medical air (21 % O_2 / 79 % N_2) to a mixture of 5 % CO_2 balance air (BOC Group, Linde, Surrey, UK) for another 3 minutes and the subject was instructed to continue breathing normally. Finally, the gas was switched back to medical air and another baseline measurement was taken for 2 minutes.

3.2.2.2 Pupillometry and Light Stimuli

The NeurOptics PLR-3000 hand-held pupillometer was used to measure the pupillary light response (NeurOptics, Irvine, CA). This hand-held pupillometer uses an infrared camera to capture and measure the pupil size, is automated and monocular, and is

widely used in clinical practice and research settings.

There were two protocols used to assess the pupillary light response. Before both protocols, subjects had 2 minutes of adaptation in a dark, quiet testing room, and throughout the pupillometry testing the subject was sat in a chair. Each protocol was done using the NeurOptics PLR-3000 device on one eye at a time.

For each subject, six measurements were performed on each eye, alternating eyes between each trial, starting with the right eye. The first three measurements on each eye, the light flash protocol, were with the positive step-input stimulus, which had a 1-second baseline measurement, a 1-second flash of 50 uW white light, and 7 seconds of post-stimulus measurement, with a 1-minute interstimulus interval. The last three measurements on each eye, the dark flash protocol, were with the negative step-input stimulus, which had a 1-second baseline measurement with the 50 uW light on, a 1-second dark flash with the light off, and a 7-second measurement with the light back on, also with a 1-minute interstimulus interval. These two protocols were matched to be the opposites of each other for comparison of the positive and negative pulses and the responses they evoked in subjects.

During the measurements, subjects were instructed to keep their eyes wide open and to avoid blinking, and to hold a constant gaze position. The pupillometer was held at a right angle to the subject's line of sight. All measurements were taken between 09:00 and 16:00 to avoid interference from circadian rhythms. While this time window avoids the extremes of diurnal variation typically seen in early morning and late evening, we acknowledge that some residual circadian effects may persist across this

interval. However, measurement times were distributed evenly across participants, and no systematic bias was introduced by time of day.

3.2.3 Data Analysis

3.2.3.1 Cerebrovascular Reactivity Analysis

The CO_2, O_2, and TCD, and time courses were exported at a time resolution of 200 Hz and processed using custom scripts in Python 3.10.8. The CO_2 and O_2 signals were converted from percent to mmHg using a conversion factor based on the midday pressure reading on the day of each acquisition in Oxford, UK [113]. The raw Doppler-BoxX TCD outputs were converted to cm/s using a calibration factor of 202.1 cm/s/V based on the DWL application software and values below 14 cm/s were removed since they corresponded to the bottoming out of the signal.

Two minutes of near-steady state data were extracted from each of the baseline and 5 % CO_2 periods, starting at least 30 seconds after a transition. The end-tidal CO_2 ($PETCO_2$) peaks were automatically segmented using tools from the SciPy package [426] to be used as a surrogate for arterial $PaCO_2$ [387]. The mean $PETCO_2$, $PETCO_2$, and TCD blood flow velocity were taken within each segment. The CVR was calculated by dividing the relative change in measured blood flow velocity by the change in the mean $PETCO_2$ between the segments as shown in Equation (3.1), where $\mathrm{MCA}v_{\mathrm{5CO2}}$ and $\mathrm{MCA}v_{\mathrm{baseline}}$ are the mean blood flow velocities during the 5 % CO_2 gas and baseline medical air segments respectively, and the $\mathrm{PETCO_2}_{\mathrm{5CO2}}$ and $\mathrm{PETCO_2}_{\mathrm{baseline}}$

are the mean end-tidal CO_2 values within each segment.

$$\mathrm{CVR(percent/mmHg)} = \frac{\frac{\mathrm{MCA}_{\overline{v}5CO_2} - \mathrm{MCA}_{\overline{v}baseline}}{\mathrm{MCA}_{\overline{v}baseline}}}{\mathrm{PETCO}_{2_{5CO2}} - \mathrm{PETCO}_{2_{baseline}}} \cdot 100 \tag{3.1}$$

3.2.3.2 Pupillometry Analysis

The time course data from the pupillometry experiments were extracted directly from the NeurOptics PLR-3000 pupillometer in a CSV file format and processed using custom scripts in MATLAB.

The NeurOptics pupillometer automatically calculates several metrics: initial and end pupil diameters, latency, average and maximum constriction velocity, dilation velocity, and time to 75 % recovery for each 9-second measurement. All values were averaged across all trials for each participant.

Due to the nature of the PLR protocols, constriction parameters, dominated by the sphincter muscles and parasympathetic nervous system, were only assessed in the light flash protocol, as the dark flash protocol's constriction amplitude was significantly smaller than that of the light flash protocol where the pupil starts at a larger, dark-adjusted diameter. Dilation parameters, however, were assessed in both the light and dark flash protocols, and have contributions from the dilator muscles and sympathetic nervous system as well as the sphincter muscles and parasympathetic nervous system.

For the light flash protocol, the key parameters that were assessed were (a) the average constriction velocity, (b) the maximum constriction velocity, (c) the constriction amplitude, (d) the dilation velocity, (e) the time to 75 % recovery, and (f) the latency

of the response. For the dark flash protocol, the key parameters assessed were (g) the dilation velocity, (h) the dilation amplitude, and (i) the latency of the response. All these parameters are visually depicted in Figure 3.1.

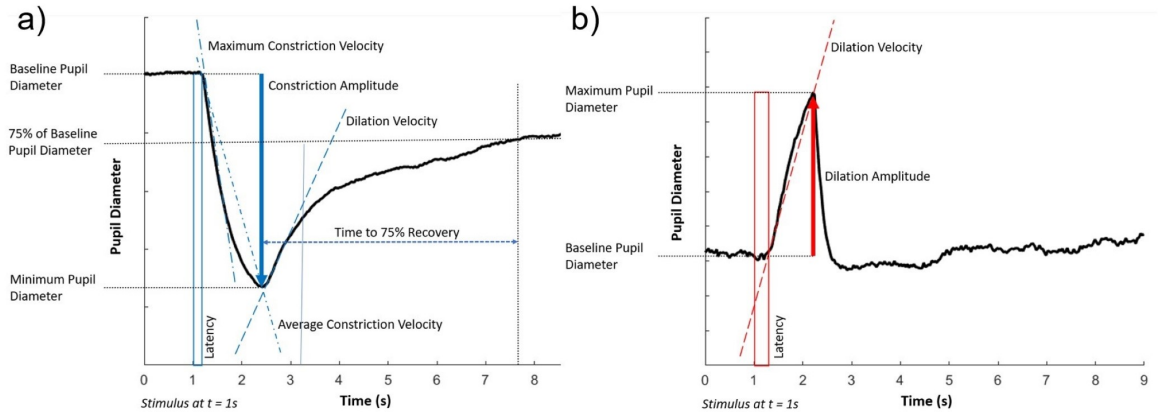

Figure 3.1: Key components of the pupillary light response to a) the light flash protocol (positive stimulus) and b) the dark flash protocol (negative stimulus). Each stimulus starts at 1 s and lasts for 1 s. Note that the latency in the dark flash protocol (shown in a red box) is longer than in the light flash protocol (shown in a blue box).

3.2.3.3 Comparative Analysis

To identify the strength and direction of any linear relationships between the PLR and CVR, we performed a linear correlation analysis for each PLR parameter (significance level $p < 0.05$, uncorrected for multiple comparisons).

3.3 Results

Data from 18 of the 20 subjects were included for analysis. One of the subjects was excluded due to a noisy TCD signal which was likely the result of the probe moving out of alignment with the MCA during the gas protocol. The other participant was excluded due to recent history of smoking, as this could have been a confounding factor to the results.

3.3.1 Cerebrovascular Reactivity Results

The TCD-derived blood flow velocity, CO_2, and O_2 traces for a representative subject during the protocol are shown in Figure 3.2 where the baseline and 5 % CO_2 gas stimulus periods are both highlighted.

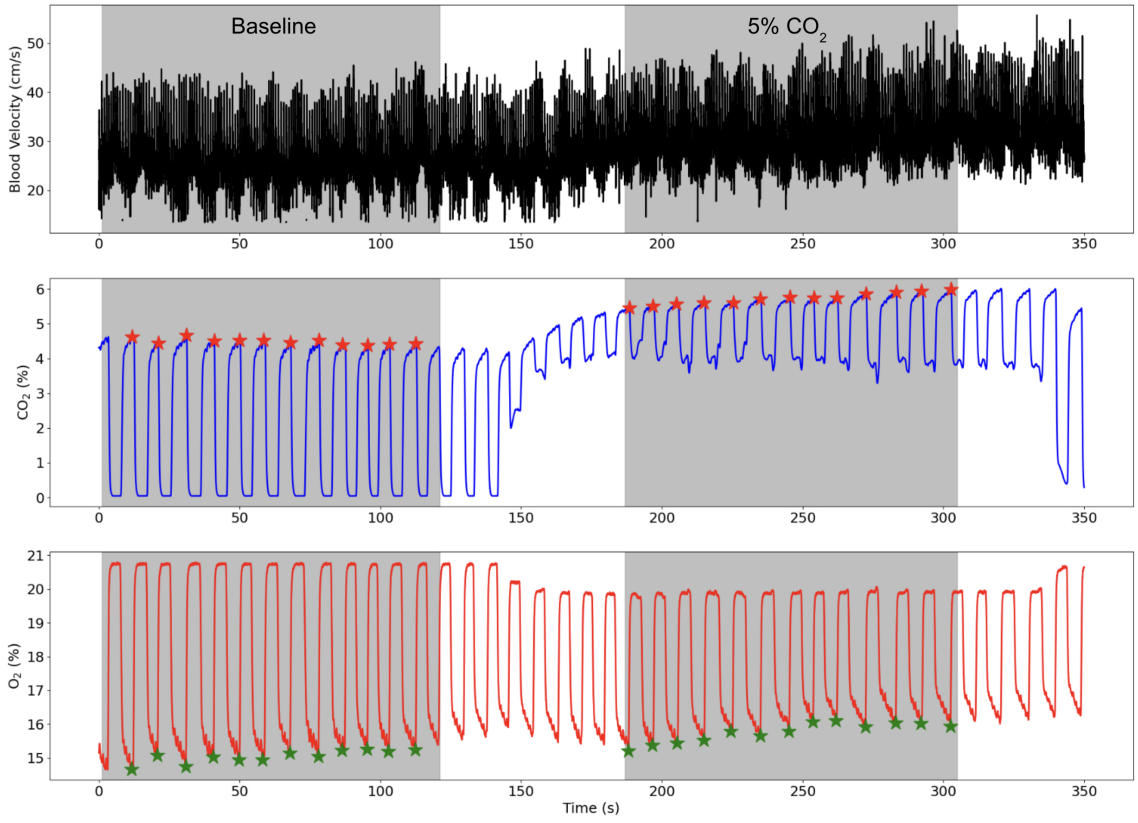

Figure 3.2: TCD blood flow velocity (cm/s), CO_2 (%), and O_2 (%) traces for a representative subject while the subject breathed medical air (baseline) and air with 5 % CO_2 gas. The baseline and 5 % CO_2 periods are shaded in grey and the end-tidal points for the CO_2 and O_2 traces are illustrated by red and green stars respectively.

$PETCO_2$ increased significantly from baseline with a mean $PETCO_2$ difference between the 5 % CO_2 hypercapnia period and baseline periods across subjects of 10.01 $\pm$ 2.05 mmHg (t-statistic = 9.17, p « 0.01). Similarly, MCA blood flow velocity increased with hypercapnia from baseline with a mean difference across subjects of 9.43 $\pm$ 3.24

cm/s (t-statistic = 3.83, p « 0.01). Breathing rates, end tidal points, mean blood flow velocities varied between subjects, but all were within normal and expected ranges [55][218][317][451]. CVR was calculated using Equation (3.1) (relative change in MCA velocity compared to the change in $PETCO_2$), yielding an average CVR value of 2.90 ± 0.56 %/mmHg, across all subjects.

Minimal differences in breathing rate and heart rate were observed between the baseline period and the 5 % CO_2 period. The mean and standard deviation of the breathing rate and heart rate for each period across all 18 subjects are presented in Table 3.1.

Table 3.1: Mean and standard deviation of the breathing rate in breaths per minute ($b_r$pm) and heart rate in beats per minute (bpm) of the participants during the baseline period and during the 5% CO_2 period.

Parameter	Mean ± Standard Deviation
Baseline Breathing Rate ($b_r$pm)	11.9 ± 5.5
5 % CO_2 Breathing Rate ($b_r$pm)	12.0 ± 5.0
Baseline Heart Rate (bpm)	69.1 ± 10.3
5 % CO_2 Heart Rate (bpm)	71.9 ± 6.7

3.3.2 Pupillometry Results

The pupillary light and dark responses for the same representative subject in their right eye are shown in Figure 3.3, where the mean response across the three trials in the right eye is highlighted.

Data from both eyes were collected to ensure that any inconsistencies among subject eyes were noted. However, for the analysis, only the right eye was included for further analysis due to the more complete data among all included subjects. This was also to ensure that the average across both eyes did not introduce any artefacts.

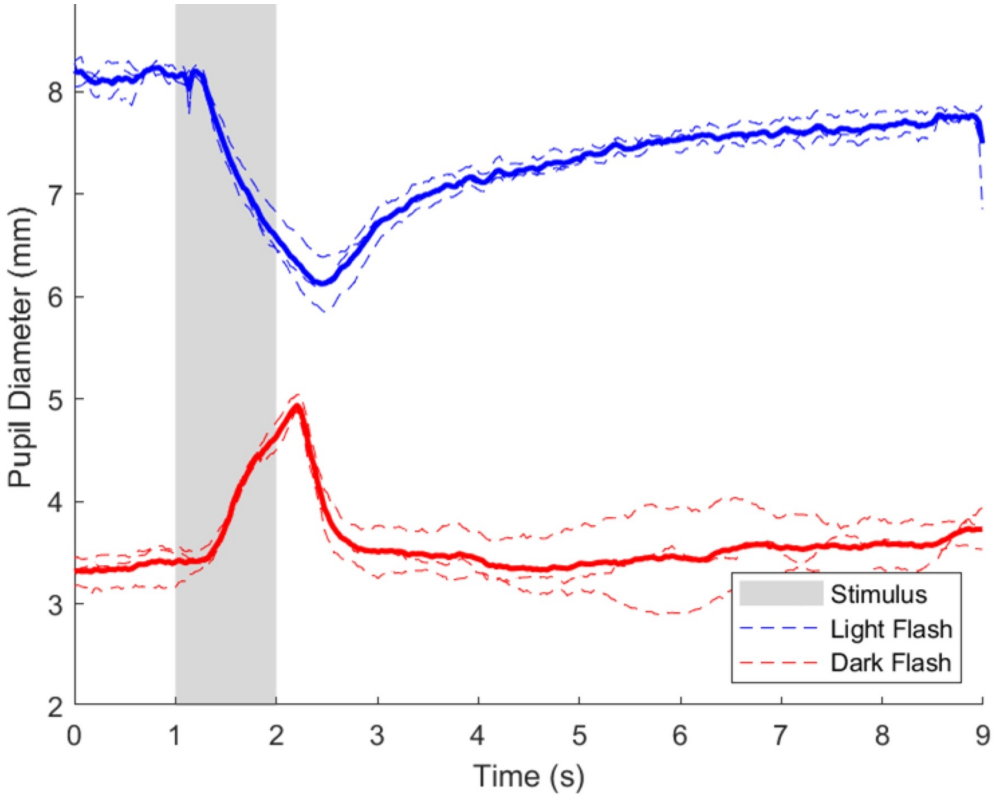

Figure 3.3: Pupillary light and dark flash response for the right eye of a representative subject. Three trials were performed in the right eye for both the light and dark flash protocols, which are shown on the plot in dashed blue and red lines, respectively. The average response of the light and dark flash protocols in the right eye across trials is shown in a thicker blue and red line, respectively. The stimulus for both protocols started at t = 1 s and ended at t = 2 s, and is shown in a shaded area on the plot.

Figure 3.3 shows minor differences among individual trials, but the overall pupillary light response characteristics in the right eye were as expected and were comparable to previous studies [47][267]. The selected interstimulus interval was sufficient for the pupil diameter to return to baseline before subsequent trials. Data from all three trials were averaged to account for minor variations due to hippus and other minor physiological variations that can be expected in assessing pupillary dynamics [417].

3.3.3 Comparison Results

The constriction parameters of the light flash protocol compared to CVR are shown in Figure 3.4. The dilation parameters of both the light and dark flash protocol compared to CVR are shown in Figure 3.5. Finally, the latency in both the light and dark flash protocol compared to CVR is shown in Figure 3.6.

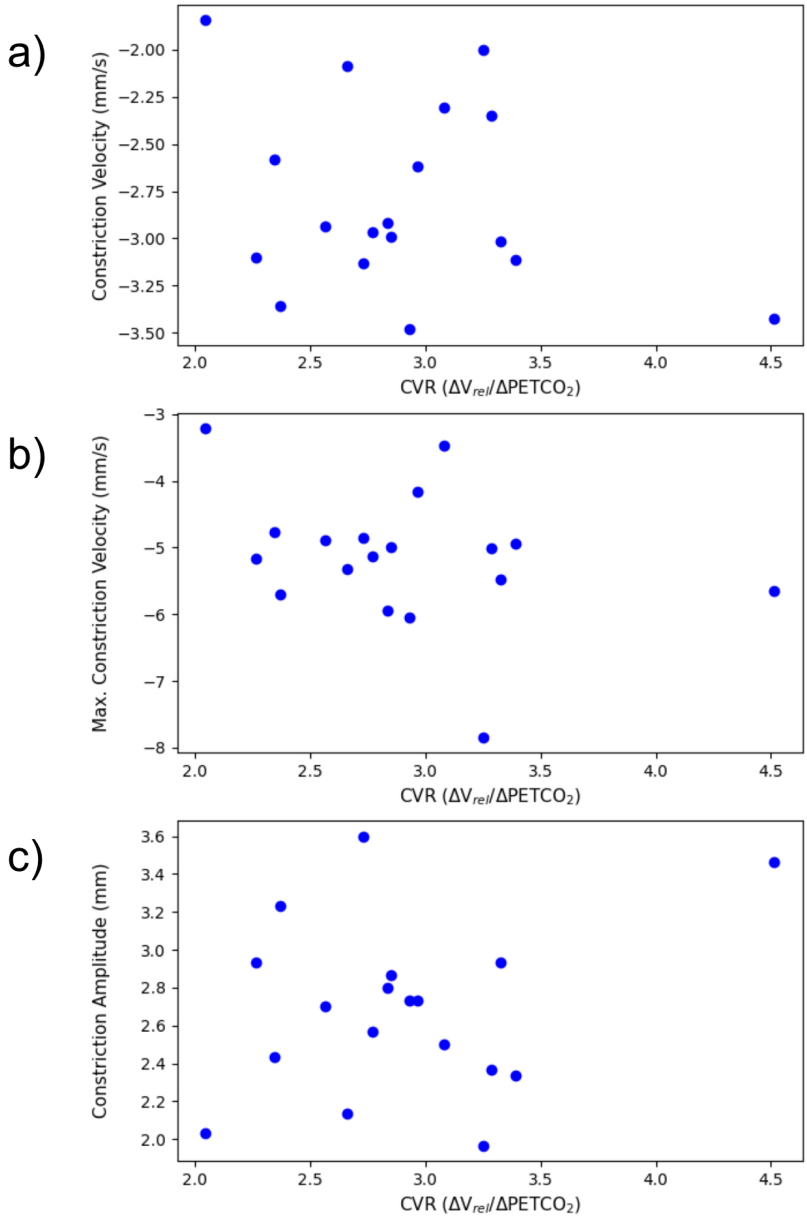

Figure 3.4: Constriction parameters of the light flash protocol, plotted against CVR. This includes a) the average constriction velocity ($p = 0.307$), b) the maximum constriction velocity ($p = 0.201$), and c) the constriction amplitude ($p = 0.349$), all from the light flash protocol compared to the CVR.

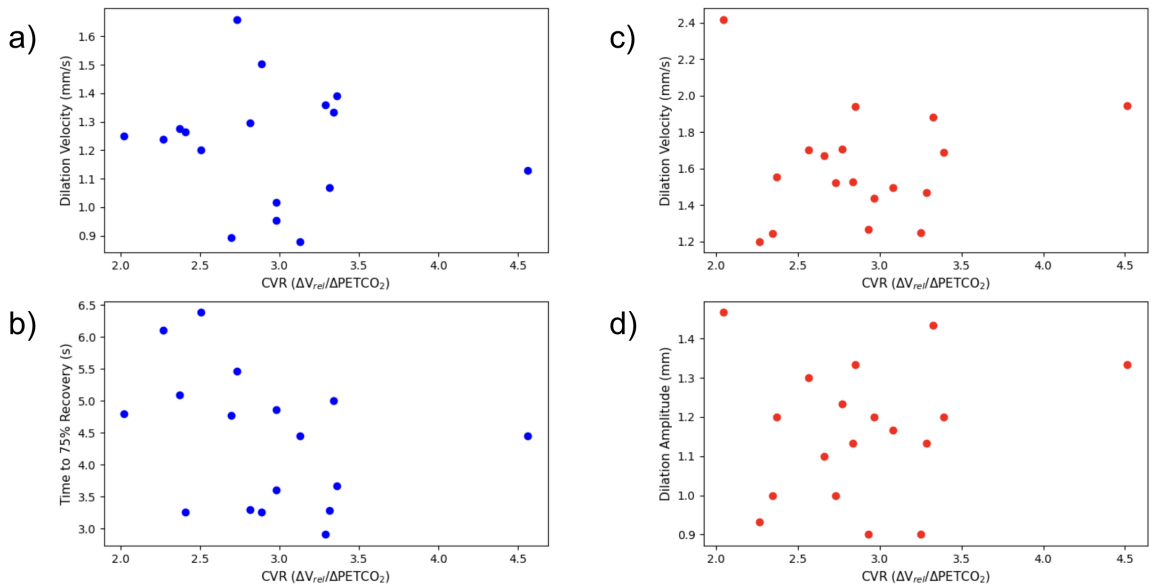

Figure 3.5: Dilation parameters of the light and dark flash protocols, plotted against CVR. The light protocol a) dilation velocity ($p = 0.668$) and b) time to 75 % recovery ($p = 0.237$) are shown on the left in blue. The dark protocol c) dilation velocity ($p = 0.764$) and d) dilation amplitude ($p = 0.561$) are shown on the right in red. Note that one subject is not included in the light flash plots as they did not have a complete dataset for their right eye in the light dilation parameters, due to blinking and other artefacts.

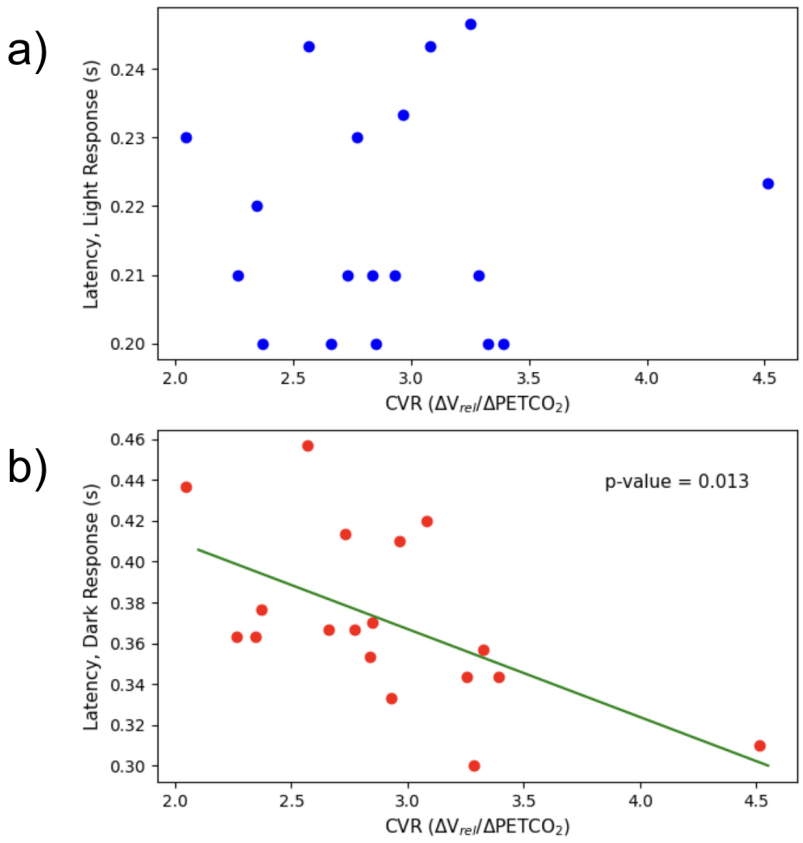

Figure 3.6: Latency plotted against CVR. This includes the latency in both a) the light flash protocol (p = 0.902) and b) the dark flash protocol (p = 0.0127) compared to the CVR. It should be noted that the correlation between the dark flash latency and CVR (b) is still on the cusp of significance even if the data point in the bottom right of the plot is removed (p = 0.0501).

There were no statistically significant linear relationships between the constriction or dilation parameters of the PLR and CVR. There was, however, a statistically significant negative trend (p = 0.0127) with the latency in the dark flash protocol and CVR. It should be noted that the correlation between the dark flash latency and CVR (Figure 3.6b) is still on the cusp of significance even if the data point in the bottom right of the plot is removed (p = 0.0501). There was no trend between the latency in the light flash protocol and CVR.

3.4 Discussion

To the authors' knowledge, this is the first study to provide an analysis of CVR and PLR measurements taken together.

CVR was calculated based on mean MCA blood velocity at baseline and during the inhalation of air with 5 % CO_2 gas. The relative as opposed to absolute change in mean blood velocity between baseline and 5 % CO_2 was used as the measure of interest for the CVR calculation, as this approach mitigates differences in probe location and angle that inherently occurs when collecting TCD data from different subjects. Participants were told to relax and breathe normally throughout the gas stimulus procedure and minimal differences were observed in the breathing rate and heart rate between the baseline and 5 % CO_2 gas periods.

It should be noted that the cerebrovascular response is entangled with physiological mechanisms that affect cerebrovascular function including ventilatory sensitivity, chemoreflexes, and nitric oxide (NO). NO bioavailability has been shown to be a key contributor to cerebral shear-mediated dilation [420], however some studies have shown that NO synthase inhibition does not influence CVR based on a steady-state CO_2 stimulus [183][187].

The CVR response to the inhalation of air with 5 % CO_2 can also be impacted by the sensitivity of chemoreflexes including central and peripheral chemoreceptors, central nervous system, and ventilatory response to $PaCO_2$ [5][62]. Notably, the sensitivity of central chemoreflexes in response to changes in $PaCO_2$ can differ between subjects and

alter their ventilatory response [452]. An increase in the ventilatory response to CO_2 is especially pronounced when CBF is reduced such as in subjects with congestive heart failure and sleep apnea [453] and changes in breathing could significantly alter CBF and $PaCO_2$ measures. As a result, despite relatively constant breathing rate and heart rate in our study, the CVR response is likely in-part also representative of chemoreceptor and ventilatory sensitivity [5].

As a result of the complex interplay between these mechanisms, vascular smooth muscle function is unlikely to be the only contributor to the CVR response. CVR may still be a good method for characterising vascular smooth muscle cell function *in-vivo* [168], however the involvement of numerous mechanisms is still poorly understood in humans due to the experimental limitations of isolating independent involvement.

For the PLR analysis, we investigated several parameters relating to both constriction and dilation of the pupil, as there are opposing systems working in both the constriction and dilation phases. Pupillary constriction and dilation are controlled by a variety of physiological mechanisms and neural pathways, including opposing muscles and different branches of the autonomic nervous system. In particular, the parasympathetic/sphincter system dominates the constriction phase with negligible contribution from the sympathetic/dilator system, while both systems contribute to the beginning of the dilation phase [434]. This means that it is difficult to isolate the specific contributions of smooth muscle alone on various parameters of the PLR, as the smooth muscle dynamics relate strongly to contributions from the sympathetic and parasympathetic nervous systems. Despite the complexities associated with disentangling these relative contributions, assessing specific parameters of the PLR in relation to CVR can

potentially provide a valuable insight into the relationship between the eye and the brain.

The average dilation velocity in the light flash protocol (1.22 ± 0.21 mm/s) was consistently smaller than the average dilation velocity in the dark flash protocol (1.61 ± 0.31 mm/s) and this difference was statistically significant ($p \ll 0.001$). This could be due to the nature of the protocols. In the light flash protocol, the stimulus first elicits a greater contribution from the sphincter/parasympathetic system to cause constriction, which is likely still active to a certain extent when the dilator/sympathetic system works to dilate the pupil post-stimulus. In the dark flash protocol, however, the stimulus first elicits a contribution from the dilator/sympathetic system, which would explain the larger magnitude of dilation velocity. Additionally, the pupil is only moderately constricted during the light flash protocol when it first begins to dilate, compared to the highly constricted pupil in the dark flash protocol, which would also support a smaller dilation velocity.

The latency of the dark flash protocol (mean = 0.37 ± 0.04 s) was consistently larger than that of the light flash protocol (mean = 0.22 ± 0.02 s). Conversely, the time to change response directions after the end of the second stimulus, was consistently larger in the light flash protocol than in the dark flash protocol - this demonstrates that the latency in response to a loss of light was larger than that in response to the onset of light.

When comparing the PLR to CVR measurements, most constriction and dilation PLR parameters did not yield statistically significant results. The maximum constriction

velocity and the time to 75 % recovery showed negative trends associated with CVR, but these were not statistically significant.

Interestingly, there was a significant negative trend relating the latency in the dark flash protocol to CVR ($p = 0.00918$). In contrast, no statistically significant trend was observed with the latency in the light flash protocol and CVR. However, the range of values in latency for the light flash protocol, was significantly smaller than that of the dark flash protocol, which might partially explain the lack of trend. In the dark flash protocol, this statistically significant negative relationship between the pupillary latency and CVR, implies that with a higher CVR, the latency, or time to react to a stimulus change, is smaller. However, if accounting for multiple comparisons, the dark latency falls just outside of statically significant, therefore additional data and tests are necessary to confirm any significance of the results. Further research is warranted into pupillary parameters of the dark flash protocol, as this protocol has been less studied than the standard light flash protocol.

3.4.1 Limitations and Future Work

For CVR assessment, we used a 2-point CVR measure as this is the most common method for deriving CVR using TCD [252][286][466]. This strategy assumes a linear relationship between CVR and changes in $PETCO_2$. Although, it is known that CVR response is in fact sigmoidal in shape [38][350], given our small dynamic range in CVR and $PETCO_2$ measurements, we expect that our results fall within the linear range of the sigmoidal curve [144][271]. Nevertheless, future research is warranted to further explore more descriptive models of the response of cerebral VSMCs to vasoactive

stimuli.

It was also assumed that a steady state was achieved after 30 seconds of breathing the 5 % CO_2 gas. While we know that $PETCO_2$ can continue to increase over even a 10-minute period [336], minimal change occurs after the 1^{st} minute and a long period of breathing air with increased levels of CO_2 can be challenging for participants. Therefore, to maintain a clinically viable vasoactive stimulus, 3 minutes was agreed upon as a reasonable upper limit for most volunteers to comfortably breathe 5 % CO_2.

Another possible limitation of the gas protocol was leakage of room air into the face mask during the gas stimulus which was an issue for some participants since the standardised mask did not create a tight seal with all face shapes. Minimal leakage of the 5 % CO_2 gas mixture is visible in Figure 3.2 by the drops in the CO_2 trace during the inhales (troughs). Worse leakage was mitigated by using only one ventilation valve which was often one site of room air entry and refitting the mask to ensure no gaps were left around the participant's nose and mouth.

While a baseline blood pressure measurement was taken for all subjects using an arm cuff to rule out hypertension, continuous arterial blood pressure (ABP) measurements were not acquired in this study. Some studies have shown that changes in ABP, both spontaneous or induced by the inhalation of air with increased CO_2, can impact CBF velocity in response to vasoactive stimuli and therefore CVR in some adults adults [184][345][440]. However, other studies have shown that even when using air with up to 7 % inspired CO_2, the increase in ABP has minimal effects on MCAv and CVR [445]. Notably, Dumville et al. also reported that in healthy adults with no

vascular disease and intact cerebral autoregulation, the CVR assessment as determined by the relative changes in velocity and $PETCO_2$ are independent of ABP provided that the pressure change is contained within the autoregulatory plateau [108]. This was echoed by Battisti-Charbonney et al., who showed that the MCAv response to CO_2 was unchanged by ABP considerations up to a threshold of approximately 50 mmHg, above which both MCAv and ABP appeared to increase linearly with CO_2 tension [31]. However, in patients with pathophysiology such as carotid artery disease, ABP has been shown to significantly alter CVR index calculations in response to inhalation of air with 5 % CO_2 [108]. In our study, assessing only healthy adults below that threshold (maximum $PETCO_2$ of 46.5 mmHg) when undergoing the gas stimulus, the effects of ABP on our CVR calculations are assumed to be negligible. None-the-less, future studies may benefit from including continuous ABP monitoring (such as by using finger photoplethysmography or more accurately using an arterial catheter) during gas stimulus protocols, especially when investigating pathology.

Furthermore, regional differences in CVR are likely to exist throughout the brain [51][234][329], therefore CVR values based on the blood velocity measures in the MCA alone may only be representative of the brain regions supplied by the artery and may not illustrate cerebrovascular function in other regions of the brain.

Lasting cerebrovascular responses triggered during hypercapnic challenges can take additional time to return to baseline post-stimulus, and although the pupillometry was done at least 10 minutes after the gas stimulus for each participant, there is a small chance that there were still residual hypercapnic effects while the beginning of the pupillometry protocols were being performed. In the future, the PLR data could be

collected prior to the gas stimulus. Alternatively, in a larger study cohort, the sequence of protocols could be swapped in half of the study cohort to clarify the PLR without the potential contamination of the after-effects of hypercapnia.

There are also some technical limitations that might have impacted the PLR data collected. Firstly, the frame rate of the NeurOptics pupillometer is low, with only 30 frames per second (i.e., 0.033 seconds per measurement). When comparing this to the entire range of average latency values in the light flash protocol, which is 0.043 seconds, this shows that the range of values is comparable to the sampling period of the device. The latency in the dark flash protocol avoids this problem due to the larger magnitude and range of values. With a smaller sampling period, there is potential that a trend could be identified in the light flash latency - this could not be investigated with the limitation of the current equipment. In future experiments, equipment with a higher frame rate should be used to thoroughly investigate any trends between the light flash latency and CVR.

An additional limitation was the assessment of the time to 75 % recovery in the light flash protocol. The protocol only included 7 seconds of recovery time post-stimulus, as it was important to ensure that the entire protocol was short enough so that participants could withstand not blinking for the duration of each trial. In some cases, however, 7 seconds was not enough time for subjects to recover to 75 % of their baseline, initial pupil diameter. When the pupil did not recover to 75 % of its initial diameter, no value was reported for this parameter, reducing the number of trials to be included in the average. Additionally, if the subject blinked, the time to 75 % recovery and dilation velocity parameters were also not calculated - this also reduced the number of

trials included in the analysis for some subjects. In the future, using equipment that can remove blinking artefacts in the data, which would enable a longer recovery time to be included in the analysis, would enable a more confident assessment of dilation parameters in the light flash protocol - especially with the time to 75 % recovery, where we would expect to see some higher values recorded.

Although CVR and certain PLR metrics are known to be dependent on age [112][119][319] and sex [210][380][401], we did not observe significant differences between ages and sexes. This is likely explained by our small sample size of groups, and as a result statistics could not be confidently performed on the influences of sex and age.

In the future, we plan to increase the dynamic range in vasoactive stimuli, vary the light stimuli for the eye, and improve the imaging resolution for both the blood flow measures and pupil measures. Notably, independently repeating the experiment of the dark flash protocol is necessary to confirm any significance in latency correlating with CVR. This analysis will take place in a larger participant group with a wide range of ages, lifestyle factors, and demographics for a more robust statistical analysis of the interplay between cerebral blood flow and pupil dynamics.

3.5 Conclusion

In this work, we compared the pupillary light response in light and dark flash protocols, to cerebrovascular reactivity assessed using transcranial Doppler ultrasound, to investigate the relationship between dynamics in the eye and brain. We found a significant negative relationship between the latency of the PLR in the dark flash protocol

and CVR. No statistically significant relationships were found between CVR and other PLR metrics. This is the first study that has investigated the relationship between cerebral blood flow and pupil dynamics. Future work will incorporate other protocols and equipment, in both pupillometry and in CVR assessment, that might retrieve additional information of interest and further control for confounding factors. Furthermore, a broader range of subjects across age, health, and lifestyle factors will be considered to investigate the validity of these relationships when subject to a larger dynamic range of subjects.

Data Availability

The data that support the findings of this study are available from the corresponding author upon reasonable request.

Acknowledgements

The authors would like to thank all the volunteers who participated in this study. We would also like to thank Dr. Manuel Spitschan for his expert advice on pupillometry and Dr. Johannes Klein for training the team on transcranial Doppler ultrasound.

Funding Acknowledgments

This work was supported by Engineering and Physical Sciences Research Council UK through grant EP/S021507/1. GH was supported by Clarendon, and SS by the Rhodes Trust.

Declaration of Competing Interests

The authors declare that the research was conducted in the absence of any commercial or financial relationships that could be construed as a potential conflict of interest.

4 | Bayesian Modelling Approaches for Breath-Hold Induced Cerebrovascular Reactivity

Preface

This chapter advances the methodological toolkit for cerebrovascular reactivity (CVR) mapping by introducing a variational Bayesian framework to analyse breath-hold BOLD-fMRI data. Building on conventional time-shifted general linear model approaches, the chapter demonstrates how Bayesian methods can more efficiently estimate CVR amplitude and delay, particularly in low-signal regions. Through multiple sessions in a cohort of healthy participants, the results reveal strong repeatability of CVR maps and highlight the potential for future extensions that integrate physiologically informed priors or more complex noise models.

This chapter was published as:

> **G. Hayes**, D. P. Bulte, S. Moia, M. Craig, M. Chappell, E. Uruñuela, S. Sparks, C. Caballero-Gaudes, and J. Pinto, "Bayesian modelling approaches for breath-hold induced cerebrovascular reactivity," 2024. doi: 10.1101/2024.02.06.579134

A subset of these results was presented at the following conferences:

> **G. Hayes**, J. Pinto, S. Moia, M. Craig, M. Chappell, C. Caballero-Gaudes, and D. P. Bulte, “Bayesian and lagged general linear modelling strategies in breath-hold induced cerebrovascular reactivity mapping with multi-echo BOLD fMRI,”

International Society for Magnetic Resonance in Medicine (ISMRM), Jun. 2023, Toronto, Canada.

G. Hayes, J. Pinto, S. Moia, M. Craig, M. Chappell, C. Caballero-Gaudes, and D. P. Bulte, "Cerebrovascular reactivity mapping with multi-echo BOLD fMRI," *ISMRM Iberian Chapter*, Oct. 2023, Valladolid, Spain.

G. Hayes, C. Caballero-Gaudes, and D. P. Bulte, "Optimising cerebrovascular reactivity mapping for glioma imaging," *Glioma in Magnetic Resonance COST Action*, Oct. 2022, Kuşadası, Turkey.

By emphasising computational efficiency and robust parameter estimation, this work sets the stage for the wider application of Bayesian modelling in CVR research and underscores the importance of capturing nuanced vascular dynamics for both basic neuroscience and clinical applications.

Author Contribution Statement

G. Hayes contributed to the conceptualisation, methodology, software, formal analysis, writing the original manuscript, manuscript revising and editing, visualisation, and funding acquisition. **D. P. Bulte** contributed to the methodology, resources, investigation, and manuscript revising and editing. **S. Moia** contributed to the data curation, software, formal analysis, investigation, manuscript revising and editing, and visualisation. **M. Craig** contributed to the software, methodology, resources, and manuscript revising and editing. **M. Chappell** contributed to the software, methodology, resources, and manuscript revising and editing. **E. Uruñuela** contributed to the

software, investigation, data curation, and manuscript revising and editing. **S. Sparks** contributed to the investigation and manuscript revising and editing. **C. Caballero-Gaudes** contributed to the conceptualisation, methodology, data curation, resources, investigation, manuscript revising and editing, supervision, project administration, and funding acquisition. **J. Pinto** contributed to the conceptualisation, methodology, resources, investigation, manuscript revising and editing, supervision, project administration, and funding acquisition.

Abstract

Cerebrovascular reactivity (CVR) reflects the ability of blood vessels to dilate and constrict in response to a vasoactive stimulus and is an important indicator of cerebrovascular health. CVR can be mapped non-invasively with functional magnetic resonance imaging (fMRI) based on blood oxygen level-dependent (BOLD) contrast in combination with a breath-hold (BH) task. There are several ways to analyse this type of data and retrieve individual CVR amplitude and timing information. The most common approach involves employing a time-shifted general linear model with the measured end-tidal carbon dioxide signal as a regressor of interest. In this work, we introduce a novel method for CVR mapping based on a variational Bayesian approach which is compared against the general linear modelling strategy. We analysed BOLD-fMRI data from six participants who performed a BH task in ten different sessions each, and computed the corresponding CVR amplitude and delay maps for each session/subject. No statistically significant differences were observed between the modelling approaches in the CVR delay and amplitude maps in grey matter. Notably, the

largest difference between methods was apparent in the case of low CVR amplitude, attributed to how each method addressed noisy voxels, particularly in white matter and cerebral spinal fluid. Both approaches showed highly repeatable CVR amplitude maps where between-subject variability was significantly larger than between-session variability. Furthermore, our results illustrated that the Bayesian approach is more computationally efficient, and future implementations could incorporate more complex noise models, non-linear fitting, and physiologically meaningful information into the model in the form of priors. This work demonstrates the utility of variational Bayesian modelling for CVR mapping and highlights its potential for characterising BOLD-fMRI dynamics in the study of cerebrovascular health and its application to clinical settings.

4.1 Introduction

The maintenance of appropriate cerebral blood flow (CBF) is critical for brain function and survival, and is closely regulated by the contraction and dilation of cerebral blood vessels. Cerebrovascular reactivity (CVR) reflects this intrinsic mechanism of blood vessels to alter their calibre in response to vasoactive stimuli. Notably, CVR has been identified as an imaging biomarker of cerebrovascular health in a number of diseases including stroke [221][263], brain tumours [122][327], carotid occlusion [68][102][437], Alzheimer's disease [61][142][397], Parkinson's disease [59], multiple sclerosis [265], and traumatic brain injury [81][89][295], among others. Vascular smooth muscle cell dysfunction attributed to vascular and neurodegenerative pathologies may also be identified by changes in CVR [168][215].

Non-invasive magnetic resonance imaging (MRI) has emerged as a promising tool for characterising anatomical and haemodynamic changes in the brain. In particular, functional magnetic resonance imaging (fMRI) based on blood oxygen level-dependent (BOLD) contrast acquired during a breath-hold (BH) task is a robust method to derive CVR maps in response to vasoactive stimuli [328][394][478]. The BOLD signal arises from differences in the magnetic properties of oxyhaemoglobin and deoxyhaemoglobin, providing an indirect measure of neural activity through changes in blood oxygenation. During a BH task, the partial pressure of CO_2 ($PaCO_2$) in the blood increases, triggering vasodilation and an elevation in CBF. While BOLD-fMRI is sensitive to these haemodynamic changes, it is important to note that BOLD is only a proxy for CBF, as it is influenced by multiple factors, including cerebral blood volume, oxygen extraction fraction, and the metabolic rate of oxygen consumption [249][57][130]. The end-tidal CO_2 ($PETCO_2$), measured at the end of exhalation, serves as a non-invasive surrogate of arterial $PaCO_2$ [272][385][400]. Consequently, CVR can be determined by quantifying the ratio between the change in the BOLD signal and the change in $PETCO_2$, as depicted in Equation (4.1).

$$\text{CVR}(\text{percent/mmHg}) = \frac{\Delta\text{BOLD}}{\Delta\text{CO}_2} \cdot 100 \tag{4.1}$$

The CVR metric defined in Equation (4.1), assumes that the CVR response occurs at the same time across the different brain regions. However, there are known differences in CVR delays across the brain, due to a variety of factors including different blood arrival times and tissue reactivity to $PaCO_2$ along the vascular tree [261]. These temporal features need to be taken into account to accurately characterise CVR amplitude

across the brain [329].

The most common way to model CVR amplitude and delay is through the application of time-shifted regressors in a general linear model (GLM) approach [288][381]. In this work, we compare this method with a novel variational Bayesian (VB) approach for CVR mapping which allows for the incorporation of prior information and simultaneous fitting of CVR amplitude and delay [69]. In this study, we evaluate the performance of these two methods on multi-echo BOLD-fMRI data, acquired in ten subjects performing a BH task during ten repeated sessions each [289], to obtain subject-specific CVR and haemodynamic delay estimates, and their corresponding repeatability metrics.

As this is an initial proof-of-concept study, we employ wide, non-informative priors in the VB approach. These broad priors allow for flexibility in parameter estimation but do not yet incorporate physiologically informed constraints. Future work will aim to refine these priors by incorporating known characteristics of CVR responses, which could further enhance the robustness and interpretability of the Bayesian framework.

4.1.1 Lagged General Linear Modelling

The conventional approach to derive CVR from the BOLD-fMRI time series is to use a general linear model (GLM), in which the acquired signal is separated into pertinent parameters of interest. In the GLM approach, the measured BOLD-fMRI signal from each voxel, Y, is expressed as the sum of experimental design variables in a scaled design matrix comprised of regressors of interest (in this case the corresponding $PETCO_2$ time course), and a weighted combination of nuisance regressors where β_i denotes the fitted coefficients for each regressor. The regressors included the motion parameters

and their temporal derivatives (denoted Mot), Legendre polynomials of up to the fourth order (denoted $Poly$) which accounts for low-frequency signal drift, and rejected independent components (denoted IC_{rej}) that have been orthogonalised with respect to the PETCO_2 trace and the accepted components (denoted IC_{acc}), and residual random noise (denoted E) as show in Equation (4.2).

$$Y = \beta_1 PETCO_2 + \beta_2 Mot + \beta_3 Poly + \beta_4 [IC_{rej} \perp (PETCO_2, Mot, Poly, IC_{acc})] + E \tag{4.2}$$

GLM is a univariate approach by which each voxel is treated as independent from one another, and it is assumed that the errors are random and follow a Gaussian distribution with a mean of zero.

To achieve accurate estimates of CVR amplitude using a GLM, it is important to also consider spatially variable haemodynamic delays (lags) between the PETCO_2 regressor and the measured BOLD signal. To account for this, several GLMs are performed, each using a time-shifted PETCO_2 regressor, and a single delay is selected for each voxel by selecting the shift that yielded the highest CVR amplitude [289][393][478].

4.1.2 Variational Bayesian Modelling

In Bayesian modelling, variables are treated as probability distributions as opposed to fixed values. Based on the Bayes theorem, the series of measurements, y, are used to determine the parameters, w, using the chosen model, M. The posterior probability of the parameters given the data and the model, i.e. $P(w|y, M)$, is then a product of the likelihood of the data given M and w, i.e., $P(y|w, M)$, the prior probability of the

parameters given the model, i.e., $P(w|M)$, and the evidence for the measurements in the chosen model, i.e. $P(y|M)$, as shown in Equation (4.3).

$$P(w|y,M) = \frac{P(y,w|M)}{P(y|M)} = \frac{P(y|w,M)P(w,M)}{P(y|M)} \tag{4.3}$$

In most cases, it is not feasible to evaluate the posterior probability distribution analytically. Alternatively, a variational Bayesian (VB) approach implements this solution as derived by [69]. In this case, an approximate posterior distribution $q(w)$ can be computed and parameterised to define the form of the distribution on the parameters of interest, w. Then, the true posterior distribution can be inferred by minimising an error measure that quantifies the deviation of the approximate distribution $q(w)$ from the exact Bayes' posterior. The fit of the approximate distribution to the true distribution can be calculated using the variational free energy, F (which encodes the divergence between the approximate and true probability distributions) as shown in Equation (4.4).

$$F = \int q(w) log \left[\frac{P(y|w)P(w)}{q(w)} \right] dw \tag{4.4}$$

The correct estimation of $P(w|y)$ is achieved by maximising free energy over $q(w)$, which is equivalent to minimising the statistical dissimilarity, between $q(w)$ and the true posterior distribution [20].

A common form for the prior distributions is a Gaussian distribution with a defined mean and variance as shown in Equation (4.5) and Equation (4.6). $P(\theta)$ has a normal distribution with mean m_θ and variance σ_θ^2 for the parameter of interest, θ, and $P(t)$ is the temporal prior with mean m_t and variance σ_t^2.

$$P(\theta) \sim \mathrm{N}(m_\theta, \sigma_\theta^2) \tag{4.5}$$

$$P(t) \sim \mathrm{N}(m_t, \sigma_t^2) \tag{4.6}$$

The mean and variance of the posterior distribution are commonly estimated using the priors and the data. In the context of deriving CVR maps from BOLD data, the VB approach replaces multiple GLMs with time-shifted regressors (lGLM) to a single model fit, where CVR delay is a parameter obtained simultaneously with CVR amplitude. Notably, VB inference also provides useful regularisation to deal with noisy imaging data and is far less computationally intensive than other Bayesian methods [69].

4.2 Materials and Methods

4.2.1 Data Collection

Multi-echo BOLD-fMRI data was previously acquired in ten subjects with no history of psychiatric or neurological disorders (5 females, range of 24-40 years of age). Each subject performed a BH protocol which was repeated for ten sessions over ten weeks (one each week), on a 3T Siemens PrismaFit scanner with a 64-channel head coil (340 scans, TR=1.5 s, TEs=10.6/28.69/46.78/64.87/82.96 ms, FA=70°, multiband=4, GRAPPA=2 with gradient echo reference scan, 52 slices with interleaved acquisition, Partial Fourier=6/8, voxel size=2.4x2.4x3 mm^3) [289]. The protocol consisted of eight

repetitions of a BH task composed of four paced breaths of 6 s each, a 20 s BH, an exhalation of 3 s, followed by a recovery period of 11 s without pacing. Subjects were instructed prior to scanning about the importance of the exhalations preceding and following the apnoea to accurately characterise the $PETCO_2$ [328]. During the fMRI acquisitions, exhaled CO_2 and O_2 levels were measured using a nasal cannula (Intersurgical) with an ADInstruments ML206 gas analyser unit. Informed consent was obtained from all participants for being included in the study, and the study was approved by the local ethics committee. A complete detailed description of the participants and acquisition protocol are described in [289].

4.2.2 Data Preprocessing

The end-tidal CO_2 peaks across the CO_2 time courses were automatically and manually identified using custom scripts in Python 3.6.7 [262][289] after high-pass filtering and downsampling. Linear interpolation between the end-tidal peaks was used and a cross-correlation bulk shift was applied to the time series to match $PETCO_2$ values with the optimally-combined BOLD images. The $PETCO_2$ signal was not convolved with a haemodynamic response function (HRF) as the time-scale of the effect is assumed to be negligible during the gradual increase in $PaCO_2$ that occurs throughout a BH [100].

Preprocessing of the MRI data was done in AFNI [91], FSL [196], and ANTs [418] using custom scripts [289][287]. The T2-weighted images were skull-stripped and the obtained brain map was coregistered to the T1-weighted space. The latter was tissue-segmented in grey matter (GM), white matter (WM), and cerebral spinal fluid (CSF), and normalised to the MNI template (FSL 2mm). The MNI atlas was chosen for robust

region and inter-subject comparisons while maintaining a balance between anatomical specificity and statistical power, reducing the risk of overfitting in highly granular analyses. The first 10 volumes of the MRI data were discarded to remove the rest portion of the task data, and ensure that a steady state of magnetisation was achieved. After motion realignment, the multiple echo time series were optimally combined voxelwise by weighting each time series by its T2* value, providing a weighted average of the time series across echoes. Multi-echo independent component analysis decomposition was then performed on the optimally combined data using tedana [109], and manual classification of the independent components was conducted by experts based on temporal, spatial, and spectral features. The output of the multi-echo independent component analysis included a cleaned, denoised fMRI time series in which non-BOLD artefacts had been regressed out. Contrarily to [289], voxelwise denoising was applied via nuisance regression before subsequent data analysis. The set of nuisance regressors included: the motion realignment parameters and their temporal derivatives, Legendre polynomials up to fourth order, and the rejected independent components from ME-ICA which were previously orthogonalised with the accepted independent components and the $PETCO_2$ signal at delay time zero. This approach was chosen so that both the VB and lGLM could be compared with the same denoising and preprocessing steps. It should be noted that simultaneous fitting of the nuisance regressors and the regressor of interest is preferable, but is expected to be very similar to the sequential modelling approach [246][288].

4.2.3 Data Analysis

Data analysis was performed using Quantiphyse, an open source analysis and visualisation platform for medical imaging data, particularly well suited for quantitative and physiological imaging methods [340]. The CVR toolbox in Quantiphyse was used for the VB and lGLM analyses to estimate the CVR amplitude and delay maps for each subject and session. To account for measurement delay, Quantiphyse applied a bulk time-shift to individual $PETCO_2$ traces, where at the time of the bulk shift corresponds to a delay of 0 s. This time-shift was obtained by selecting the shift that yielded the highest cross-correlation between $PETCO_2$ trace and the corresponding average whole-brain fMRI signal. For the lGLM approach, we established a window for the candidate CVR delays of ± 8 s from the bulk time-shift with a 0.25 s timestep. This temporal range was based on previous literature, which rarely reports haemodynamic delays over ± 8 s in healthy individuals, with spurious large delays most often caused by noise or poor model fits [51][289][101]. The lGLM calculation was repeated at a higher time resolution (with a time step of 0.025 s from -8 s to 8 s) for a representative case to see how it impacted the lGLM delay map. The VB analysis was done with the BOLD timeseries modelled as a scaled difference between the $PETCO_2$ timeseries with a time delay t_{delay} relative to the minimum $PETCO_2$ with error ϵ, as shown in Equation (4.7).

$$BOLD(t) = \frac{\epsilon}{100} \cdot \Big(1 + \theta_{CVR}(P_{ET}CO_2(t - t_{delay}) - \min(P_{ET}CO_2(t))\Big) \tag{4.7}$$

The VB analysis used 10 iterations, starting with wide non-informative priors. The prior distribution for the CVR was $P(\theta) \sim N(1, 2000)$, and the prior for the delay was

$P(t) \sim N(0, 100)$.

4.2.4 Statistical Analysis and Repeatability

All CVR and delay maps were co-registered to the MNI152 template using the ANTs tool and nearest neighbour interpolation [145]. A revised linear mixed effects (LMEr) model was then applied voxelwise, taking into account variability within and across subjects [70]. The LMEr model was formulated as presented in Equation (4.8) where Var represents the variable CVR or delay of each voxel.

$$Var \sim model + (1|subject) + (1|session) \tag{4.8}$$

Z-scores produced by the LMEr calculation were thresholded to investigate statistical significance, defined as cluster-corrected p-value < 0.01. Cluster correction was applied to control for multiple comparisons and reduce the likelihood of false positives, ensuring that significant findings reflect spatially coherent effects rather than isolated statistical noise.

Additionally, to directly compare the outputs of the two methods, we fit a voxelwise linear model to the comparison plots of methods for the CVR and delay values respectively. This model assessed the correspondence between the methods and quantified the degree of agreement.

The repeatability of the CVR and delay maps for each method was assessed by computing the intraclass correlation coefficient (ICC) considering two-way random effects, absolute agreement, and a single measurement (ICC(2,1)) with AFNI's tool 3dICC

[72][220]. The ICC(2,1) is calculated as shown in Equation (4.9) where MS_{sub} is the mean square for subjects, MS_{ses} is the mean square for sessions, MS_n is the mean square for residuals, k is the number of sessions, and n is the number of subjects [378].

$$ICC(2,1) = \frac{MS_{sub} - MS_n}{MS_{sub} + (k-1)MS_n + \frac{k}{n}(MS_{ses} - MS_n)} \tag{4.9}$$

Note that a high ICC score (up to 1) indicates high repeatability, where intrasubject variability is lower than intrasession variability. For fMRI studies, an ICC score below 0.40 is considered poor, 0.40-0.59 is considered fair, above 0.60-0.74 is good, and above 0.75 is excellent [16][82][111].

The ICC analysis was first conducted voxelwise across the lGLM and VB maps for both methods. A regional analysis was also performed using the MNI-maxprob-thr25 brain atlas at 2.5 mm in FSL [88], [270], applied to the standardised CVR and delay maps. The ICC scores were calculated from the mean and median values within each region across all subjects and sessions.

4.3 Results

Four subjects were excluded due to incomplete $PETCO_2$ traces in one or more of the 10 sessions. Excluded traces were most often the result of inadequate execution of the exhalations preceding and following the BH which prevented accurate determination of the $PETCO_2$ traces.

4.3.1 Cerebrovascular Reactivity and Delay Maps

The CVR amplitude and delay maps derived for a representative subject and session are presented in Figure 4.1 and Figure 4.2, respectively, for each method. Figures showing the CVR and delay maps for the same subject across all sessions with both methods are available in Figure A.1 and Figure A.2 of Appendix A.

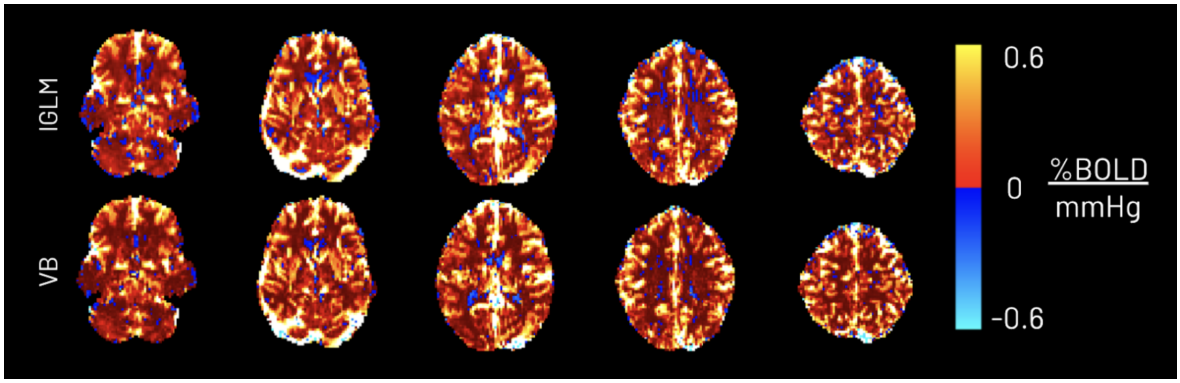

Figure 4.1: CVR amplitude maps obtained using the lagged-GLM (lGLM) and variational Bayesian (VB) analyses for representative subject 002 and session 04.

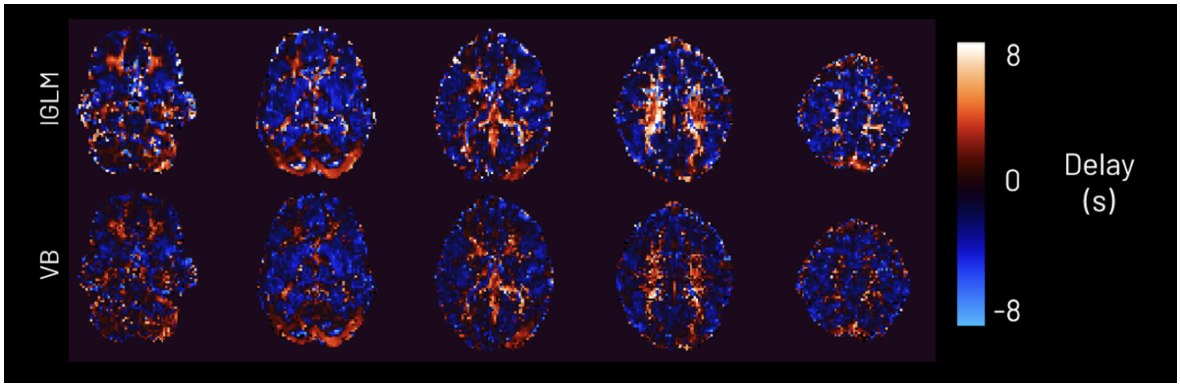

Figure 4.2: CVR haemodynamic delay maps obtained using the lagged-GLM (lGLM) and variational Bayesian (VB) analyses for representative subject 002 and session 04.

Scatter plots comparing the CVR values derived by both methods of a representative session are presented in Figure 4.3 along with the best fit line corresponding to $y = 0.93x - 0.0002$ and a Pearson R of 0.98. The same comparison for the delay maps

are presented in the top plot of Figure 4.4. The lGLM delay map calculation was repeated at a higher time resolution (with a time step of 0.025 s from -8 s to 8 s) for the representative case and the scatter plot comparison is presented in the bottom plot of Figure 4.4. The best fit line for both delay value comparisons corresponds to the equation $y = 0.36x - 0.35$ and a Pearson R of 0.34. The least sum of absolutes fit for the CVR, and both delay maps correspond to Spearman rho constants of 0.94 and 0.65 respectively.

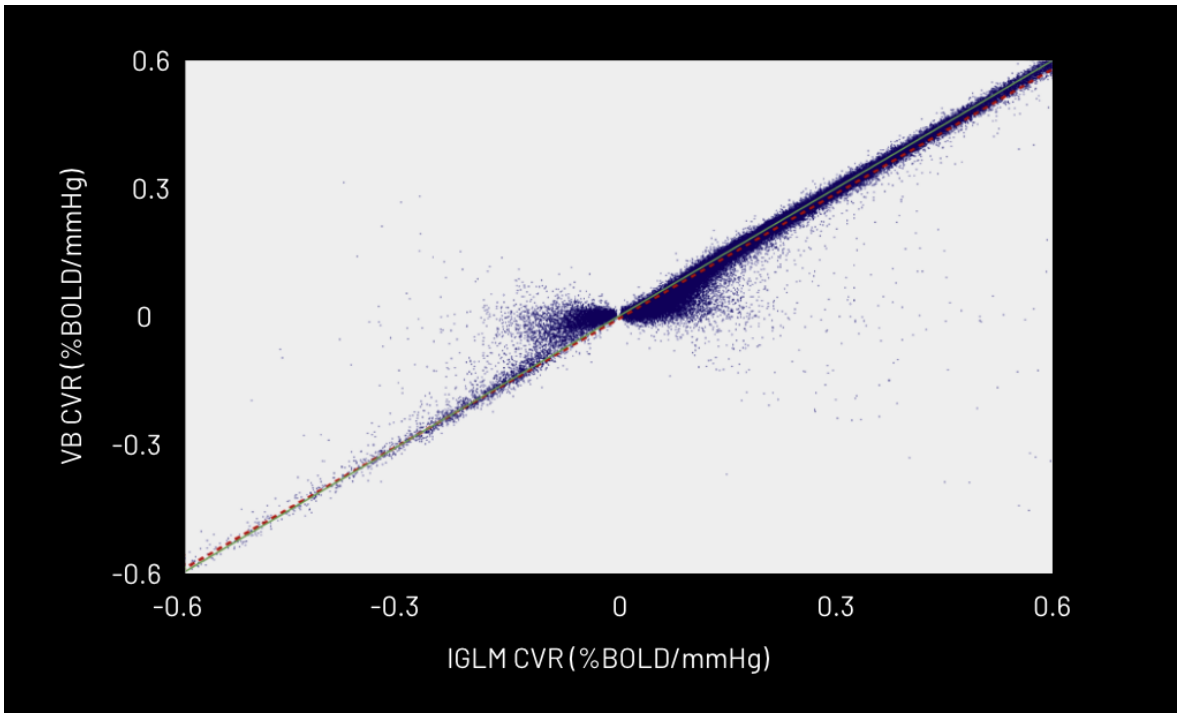

Figure 4.3: Scatter plot of CVR amplitude values obtained using the variational Bayesian (VB) method as a function of those obtained using the lagged general linear model (lGLM) approach for representative subject 002 and session 04. The least squares fit line is plotted in red which corresponds to the equation $y = 0.93x - 0.0002$ and a Pearson R of 0.98. The least sum of absolutes fit of this data corresponds to a Spearman rho constant of 0.94. The $y = x$ line is plotted in green.

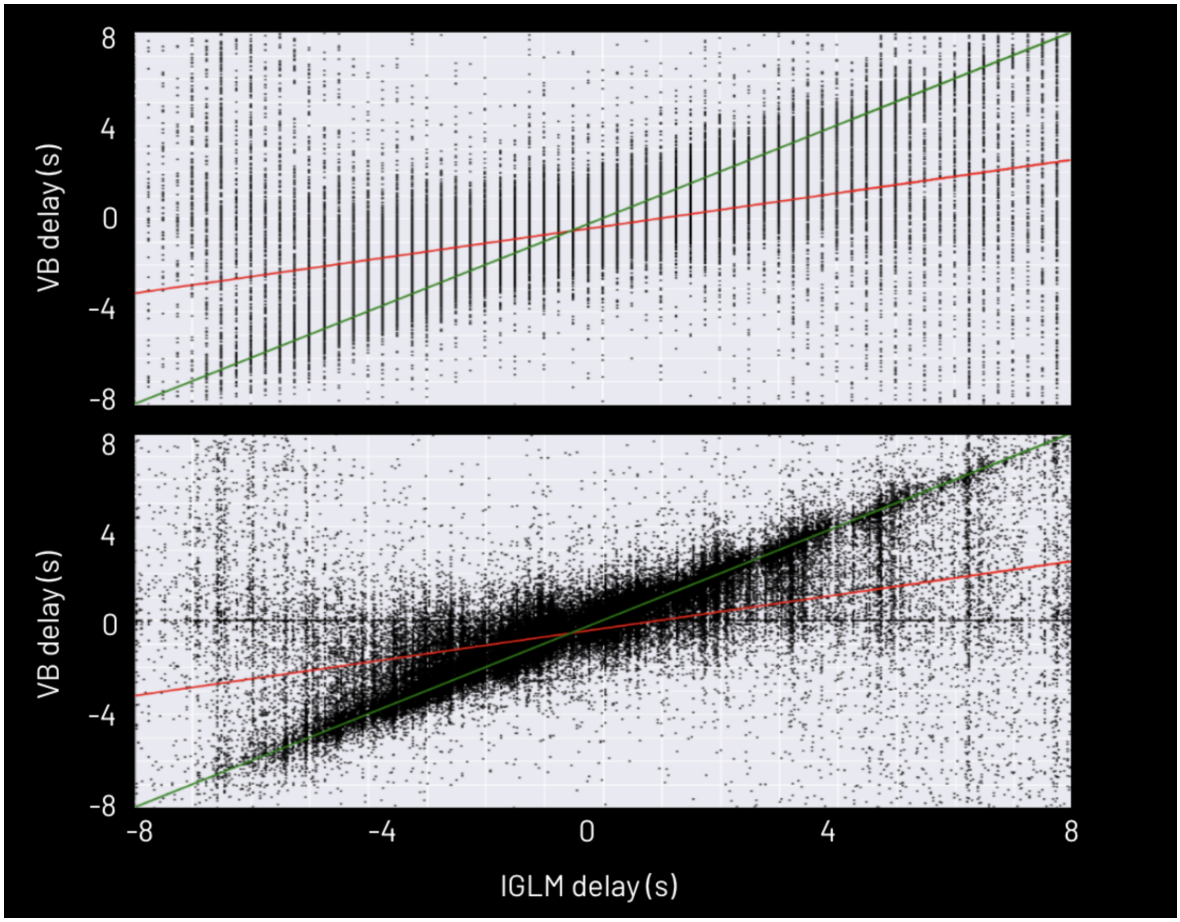

Figure 4.4: Scatter plots of haemodynamic delay values obtained using the variational Bayesian (VB) method as a function of those obtained using the lagged-GLM (lGLM) approach for representative subject 002 and session 04. The scatter plots show the lGLM delay values calculated using a 0.25 s timestep (top) and a 0.025 s timestep (bottom). The least squares fit line is plotted in red which corresponds to the equation $y = 0.36x - 0.35$ and a Pearson R of 0.34 for both timesteps. The least sum of absolute fits of these comparisons both correspond to a Spearman rho constant of 0.65.

To test the time-efficiency of each method, the analysis of a subset of the data was timed on a shared high-performance computer with an Intel Xeon CPU with 32 cores and 132 GB of RAM. For 10 sessions, the VB method took 69 mins and the lGLM method took 130 mins. We expect the computation cost to scale with the number of sessions because no parallelisation was implemented.

4.3.2 Statistical Analysis

The results of the revised linear mixed effects (LMEr) analysis are presented in Figure 4.5. Notably, the CVR difference range (-0.03 to 0.03 percent/mmHg) is much smaller than the full CVR value range (-0.6 to 0.6 percent/mmHg). The LMEr delay difference range (-1 to 1 s) is similarly small compared to the full delay range (-8 to 8 s). There are no statistically significant differences between the CVR values of the lGLM and VB methods in grey matter (using $p < 0.01$, FDR corrected). Statistically significant differences between the methods ($p < 0.01$, FDR corrected) are apparent in white matter and CSF, especially around the ventricles. P-values were adjusted for control of false discovery rate (FDR) [33], and then compared against an alpha of 0.01 to determine significance. The thresholded z-score maps for the CVR and delay LMEr comparison are available in Figure A.3 of Appendix A.

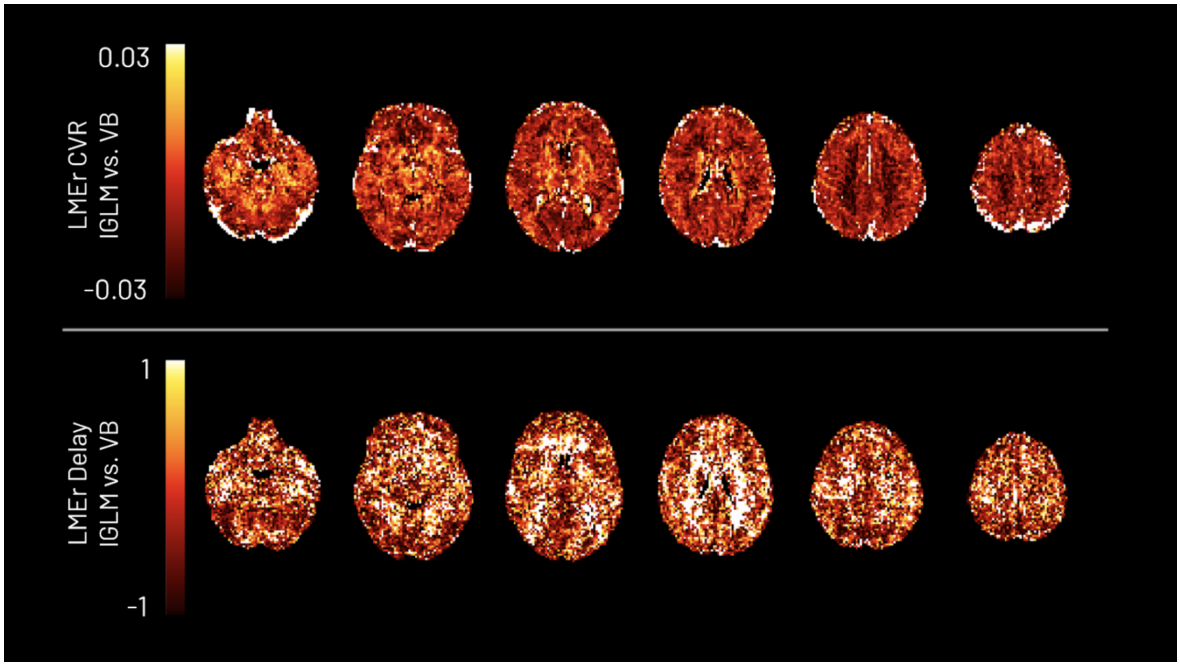

Figure 4.5: Revised linear mixed effects (LMEr) pairwise comparison between the lagged-GLM (lGLM) and variational Bayesian (VB) analyses. Note that the CVR difference range (-0.03 to 0.03 percent/mmHg) is much smaller than the overall CVR value range (-0.6 to 0.6 percent/mmHg). Similarly, the LMEr delay difference range (-1 to 1 s) is much smaller than the full delay value range (-8 to 8 s).

4.3.3 Repeatability

4.3.3.1 Voxelwise Repeatability

The ICC scores in the CVR amplitude maps are presented in Fig. 6 and indicate a high repeatability with higher inter-subject variability than intrasubject variability in both methods. Poor repeatability (< 0.4) is illustrated for the delay maps for both methods, attributed to high variability in fitting this parameter and differences in bulk shifts between sessions.

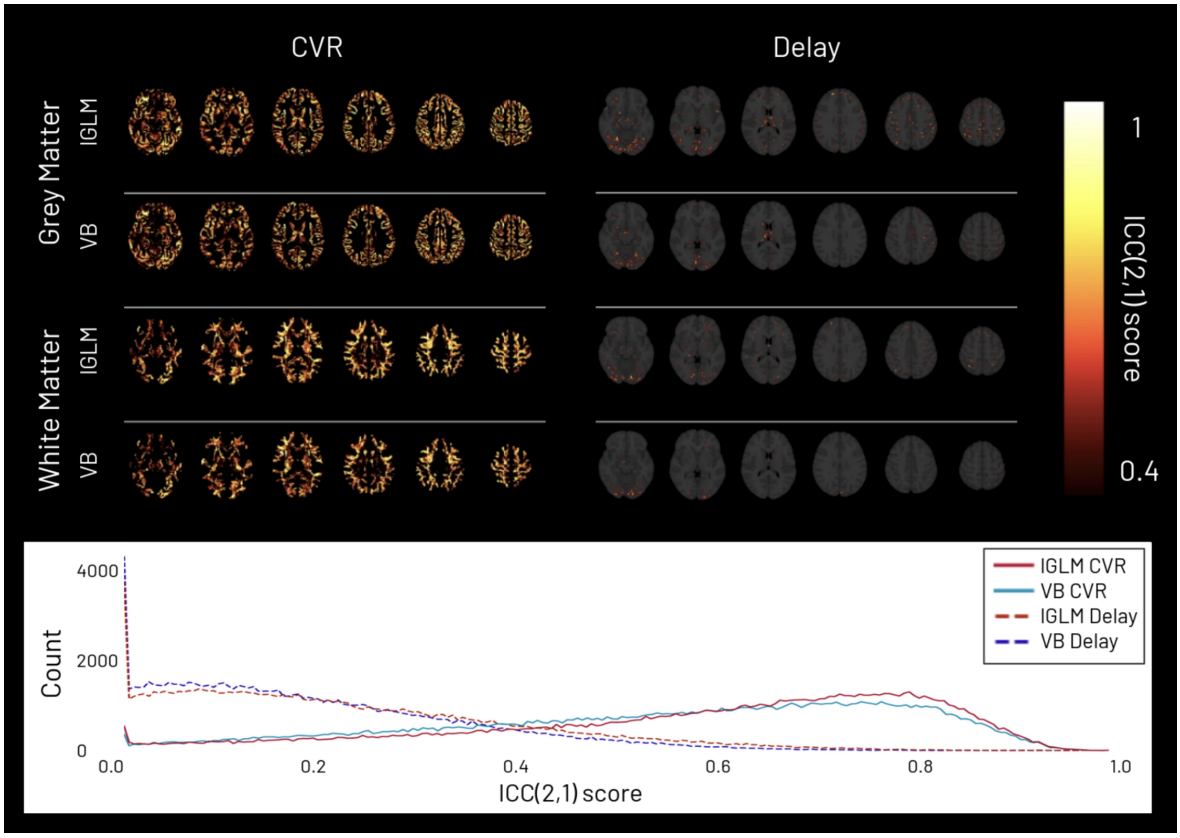

Figure 4.6: Intraclass correlation coefficient ICC(2,1) maps of CVR amplitude (left) and delay maps (right) for the lagged-GLM (lGLM) and variational Bayesian (VB) methods in grey matter and white matter. The maps are thresholded at 0.4 since scores lower than it indicate poor repeatability. The bottom row depicts the whole brain distributions of ICC scores across voxels for CVR amplitude (solid lines) and delay (dashed lines) for the lGLM (red) and VB (blue) methods.

4.3.3.2 Regional Repeatability

The regional ICC scores for both methods are presented in Table 4.1 using the mean and median values within each region. Notably, a handful of outliers using the lGLM method skewed the mean value in some regions, significantly reducing the ICC score (denoted by * in Table 4.1). The median was used to remove the effect of outliers. The group-level mean and median CVR and delay values for both methods in each region are available in Table A.1 of Appendix A.

Table 4.1: Regional intraclass correlation coefficient ICC(2,1) values of the CVR amplitude and delay maps for lGLM and VB methods in 8 MNI-atlas regions of the brain. *denotes regions containing significant outlier values in the mean calculation.

	ICC(2,1) CVR				ICC(2,1) Delay			
	lGLM		VB		lGLM		VB	
Regions	**Mean**	**Median**	**Mean**	**Median**	**Mean**	**Median**	**Mean**	**Median**
Caudate	0.71	0.73	0.67	0.61	0.31	0.24	0.51	0.41
Frontal Lobe	0.58	0.76	0.70	0.70	0.22	0.20	0.13	0.27
Insula	0.76	0.74	0.74	0.70	0.12	0.15	0.32	0.43
Occipital Lobe	0.50	0.69	0.51	0.62	0.41	0.44	0.47	0.58
Parietal Lobe*	0.10	0.78	0.70	0.74	0.38	0.39	0.12	0.31
Putamen	0.73	0.66	0.69	0.56	0.28	0.24	0.56	0.61
Temporal Lobe*	0.20	0.61	0.57	0.47	0.20	0.26	0.44	0.58
Thalamus	0.57	0.58	0.55	0.53	0.10	0.13	0.38	0.50

4.4 Discussion

In this study, we compared two modelling approaches, lagged-GLM (lGLM) and variational Bayes (VB), to estimate CVR amplitude and delay maps based on BOLD-fMRI data acquired during a BH protocol. To the authors' knowledge, this is the first time these approaches have been compared in the context of CVR and delay mapping using multi-echo BOLD-fMRI.

Regarding our BOLD-fMRI data preprocessing, multi-echo independent-component analysis denoising was used to remove components exhibiting noise-like signal decay patterns across echos [109]. An optimal combination of the echos was used as it has been shown to improve BH-induced CVR mapping sensitivity, specificity, repeatability, and reliability [87]. For both modelling approaches, a conservative nuisance regression approach was used prior to the CVR fitting to preserve the BOLD variance associated with local CVR responses while still adequately removing noise-related effects from the

time series [289]. The $PETCO_2$ signal was not convolved with an HRF in the CVR mapping presented here as this was assumed to play a negligible role at the time-scale of a 20 s BH. A recent study showed that when computing CVR amplitude and delay maps, using a $PETCO_2$ regressor without an HRF convolution performed very similarly to a single-gamma HRF convolution and performed better than convolving with a canonical (double-gamma) HRF [100]. However, a previous study showed that convolution with a canonical (double-gamma) HRF explained significantly more variance in CVR than without convolution, although haemodynamic delay was not considered [294].

The main difference between the lGLM and VB modelling strategies is that the VB method treats the inputs and outputs as probability distributions, and simultaneously fits the CVR amplitude and temporal delay parameters. Visually comparing the maps derived using the lGLM and VB methods indicates that the output CVR maps are very similar between methods. The LMEr analysis confirms that the CVR amplitude maps do not show statistically significant differences between methods in grey matter (using $p < 0.01$, FDR corrected). Within these grey matter regions, the CVR values are highly comparable to results from previous studies that also take regional haemodynamic delays into account [247][289][329]. White matter and CSF show statistically significant differences between methods ($p < 0.01$, FDR corrected), likely illustrating that the VB and lGLM methods treat low SNR voxels differently. This is also seen in the scatter plot comparison where low signal voxels result in low CVR amplitude values in the lGLM method, but are close or equal to zero in the VB method.

The LMEr of the delay maps shows a variation of $\pm$ 1 s of the mean whole-brain delay

time between methods. The scatter plot comparison of the delay maps showcases how the discrete time step in lGLM approach forces all estimates into bins as opposed to allowing for a continuous distribution. At the expense of computational resources, this was improved by increasing the time step in one representative subject (illustrated in Figure 4.4). Notably, in comparing the delay values for both methods, the VB method forces more voxels towards a delay of 0 s, attributed to the prior distribution reverting low SNR voxels to the prior distributions. Consistent with previous studies, we find considerable variations in the delay across the brain with both methods, supporting the use of modelling strategies that include temporal aspects of the CVR response [13][51][234].

The voxelwise and regional CVR ICC scores in this analysis are similar to previous work and illustrate high repeatability for both methods [52][261][289][329]. The regional ICC values of the CVR amplitude for the VB method (Mean: 0.51-0.74; Median: 0.47-0.74) are all above 0.4, considered the acceptable minimum in fMRI studies [16][82][111]. The regional ICC values for the lGLM method (Mean: 0.10-0.76; Median: 0.58-0.78) highlighted large outliers that skewed the mean and resulting ICC scores in the parietal and temporal lobes, while all other regions are above 0.4. This issue was overcome by using the median CVR values within each region, which brought all ICC values above 0.4 (fair) and most above 0.6 (good). The ICC values are comparable to previously reported regional CVR ICC, notably showing higher repeatability in the frontal and parietal lobes, and lower repeatability in the parietal and temporal lobes (Bright and Murphy, 2013).

The voxelwise ICC scores of the delay map are lower than previously reported [289].

Fewer subjects were included in our analysis compared to [289], which is expected to have altered the results of the repeatability assessment. Furthermore, we are using a different ICC test model since in [289], the t-statistic maps associated with the estimation of the CVR using the lGLM method were attributed to the delay values and were included in their ICC calculation [71][289]. The t-statistics were excluded from the repeatability comparison for fairness to both methods since t-statistic maps are not currently calculated during the VB implementation in Quantiphyse. Without the t-statistic, both the lGLM and VB methods show good repeatability in CVR maps, but poor repeatability in the delay maps, likely due to high-variance estimates between sessions from the ICC calculation itself as a result of session-specific temporal shifts.

The regional delay ICC results for the VB method (Mean: 0.12-0.56; Median: 0.27-0.61) and lGLM method (Mean: 0.10-0.41; Median: 0.13-0.44) range from fair (ICC > 0.4) to poor ICC levels (ICC < 0.4). Notably, the regional delay repeatability is higher than the voxelwise repeatability as it averages over noisy voxels. Fair delay repeatability was found in the caudate, insula, occipital lobe, putamen, temporal lobe, and thalamus when using the median VB-derived values. Only the occipital lobe showed fair repeatability when using the lGLM-derived delay values.

Both methods reported primarily positive CVR amplitude values in GM; however, negative CVR values are visible in WM and CSF. This negative CVR might originate from inaccurate modelling in noisy voxels with reduced CVR-related changes and / or other flow and volume changes (e.g., CSF). The vascular steal effect has also been reported as an underlying physiological cause of negative CVR, which may be used as a biomarker of pathology [333]. The vascular steal phenomenon occurs when a

stimulus results in redistribution of blood flow from regions of exhausted vasodilatory capacity to areas with preserved cerebrovascular reserve. However, vascular steal does not appear to be an expected physiological event in the absence of pathology [17], and due to the consistent pattern of negative CVR values in the WM and CSF in all healthy subjects, the negative CVR voxels are likely not caused by this effect. However, the mechanisms behind negative CVR in specific brain tissues in healthy subjects are not yet explained; hence, further work is still required to validate this observation.

Practically speaking, the VB method can be more time-efficient at scale as it fits the CVR and delay simultaneously, while the lGLM approach requires several GLMs to assess both parameters. Additionally, the lGLM approach uses a step-fit and requires the user to select the delay range and step size a priori. To illustrate this, the analysis of a subset of the data was timed on a shared high-performance computer and demonstrated a more than 80 % increase in performance of the VB method compared to the lGLM method. We expect the computation cost to scale with the number of sessions since no parallelisation was implemented. To approach the continuous distribution of delay values generated by the VB modelling, the lGLM method will take exponentially more time, as the model recomputes a GLM for each voxel at each specified delay value in a discreet manner.

Another approach to estimating CVR delays is the Rapidtide package, which applies a phase optimisation algorithm to determine voxelwise haemodynamic delays in a continuous manner [410]. Unlike the lGLM method, which assesses delays at predefined intervals, Rapidtide estimates delays without requiring a priori step sizes, potentially improving sensitivity to fine-scale variations in vascular response timing. Integrating

such methods could offer an alternative means of accounting for CVR delays alongside the Bayesian approach.

When using Quantiphyse, the denoising and voxelwise response estimation could not take place simultaneously since multiple regressors are not yet implemented. Simultaneous regression has previously been shown to improve output precision as it ensures that the degrees of freedom and the interactions between regressors are accounted for [200][246]. This is a difference from [288] and [289] which showed that simultaneous modelling is more appropriate to account for potential correlations between modelling regressors in BOLD-fMRI. Future implementations of Quantiphyse could address this by allowing for multiple regressors.

4.4.1 Limitations

Despite the advantages of the VB approach, several limitations should be acknowledged in this study. First, while the Bayesian framework allows for incorporating prior information, we employed wide, non-informative priors, making this work an initial proof of concept rather than a fully optimised implementation. The primary motivation behind this was to allow the priors to be generalisable to participants with a wide range of demographics and ages, and not to bias the CVR fitting. However, future studies should explore the integration of physiologically informed priors, which could help constrain parameter estimates and improve the accuracy of CVR amplitude and delay mapping. Furthermore, while the VB method improves computational efficiency compared to the lGLM approach, it does not yet account for more complex noise models, which could impact CVR estimation, particularly in regions with lower SNR such as white matter

and CSF [69]. Incorporating noise priors could be a valuable next step to enhance the robustness of the model. This may be particularly useful for analysing task-based functional MRI data, where changes in stimuli and tasks may introduce different levels of noise throughout an acquisition. In the case of noisy data, variance maps can be calculated during the VB method and may be useful to assess the confidence in the VB model fit, however minimal trends were found to distinguish between tissue types or SNR in the CVR or delay maps and were not used in this analysis (see Figure A.4 of Appendix A). More research on confidence metrics on both the VB and lGLM methods is warranted, as it would benefit their clinical and research utility.

As in the case of both VB and lGLM approaches, linear models are the most common form for generating CVR maps [381]. However, CVR has a sigmoidal non-linear relation to $PETCO_2$, and BH-induced hypercapnia can also have a complex shape in terms of temporal and amplitude responses through the brain due to multiple physiological factors [38][261]. Accounting for these non-linear components is an important next step to improve the full characterisation of the CVR response, and demonstrates a potential benefit of the VB approach which can be expanded to allow for non-linear modelling.

Additionally, when comparing the VB and lGLM estimates, we used the sum of squared differences to quantify voxelwise disagreement. While commonly used, this metric assumes all variance lies in the dependent variable (the VB method in our case), treating the lGLM as the reference method ("ground truth") and did not account for error in both estimates. Since both VB and lGLM outputs contain uncertainty, this may underestimate total variance.

Finally, our study analysed a limited number of participants (N = 6), and while repeated measures were used to assess repeatability, future work should validate these findings in larger cohorts, including patients with cerebrovascular disease, to assess the generalisability of the VB method to clinical populations.

4.4.2 Implications for Clinical Practice

The ability to accurately map CVR is increasingly recognised as a valuable tool in clinical diagnostics and treatment planning, particularly for conditions affecting cerebrovascular health such as stroke [221][263], neurodegenerative diseases [142][397][59], and traumatic brain injury [81][89][295]. The findings of this study suggest that the VB approach offers a computationally efficient alternative to traditional GLM-based methods, providing simultaneous estimation of CVR amplitude and delay without requiring multiple GLM iterations. By improving CVR quantification and reducing computational burden, this method has the potential to facilitate the integration of CVR mapping into routine clinical MRI protocols.

In addition, accounting for haemodynamic delays is critical in clinical settings where delayed vascular responses may indicate cerebrovascular pathology, such as in patients with carotid artery stenosis or small vessel disease. The Bayesian framework provides a flexible modelling approach that could be further extended to incorporate non-linear effects and patient-specific priors, potentially improving diagnostic precision and treatment monitoring in cerebrovascular disorders. Future work will aim to validate this method in clinical populations and explore its utility in detecting early cerebrovascular impairment.

4.5 Conclusion

Both lGLM and VB modelling strategies provide robust CVR amplitude and delay maps for breath-hold BOLD-fMRI data, with no statistically significant differences observed between them in grey matter. Noteworthy distinctions are apparent for low CVR amplitude, attributed to how each method addressed noisy voxels, particularly in white matter and cerebral spinal fluid. The CVR mapping was found to be highly repeatable for both methods. Despite higher variability in the haemodynamic delay maps between sessions for both methods, the VB method exhibited fair repeatability in more regions than the lGLM method. Furthermore, the VB method estimated a continuous delay map, which is discrete for the lGLM method, and with a delay timestep of 0.25 s, the VB estimation performed 80 % faster than the lGLM. More research is still required to identify goodness-of-fit and confidence metrics for both approaches, as well as to discriminate against low SNR voxels. Future work will include implementing different physiologically relevant priors and incorporating non-linear modelling into Bayesian CVR modelling. This study underscores the utility of variational Bayesian modelling for CVR mapping, emphasising its potential to interpret BOLD-fMRI dynamics in cerebrovascular health studies and clinical applications.

Data Availability

The methods pipeline for this analysis is available at https://github.com/genhayes/vbayes_lglm_cvr_pipeline, and all MRI images, physiological data, and manual classification used in this study are available on OpenNeuro [288]. Original preprocess-

ing and analysis scripts are available at https://github.com/smoia/EuskalIBUR_dataproc. Additional tutorials explaining how to use Quantiphyse are available at https://github.com/physimals/quantiphyse.

Funding Acknowledgements

This research was funded by the Clarendon Fund, the Engineering and Physical Sciences Research Council UK (EP/S021507/1 and EP/P012361/2) the Spanish Ministry of Economy and Competitiveness (RYC-2017-415 21845), the Basque Government (BERC 2018-2021, PIB_2019_104), the Spanish Ministry of Science, Innovation and Universities (PID2019-105520GB-100), the GliMR 2.0 COST Action (CA18206), the European Union's Horizon 2020 research and innovation program (Marie Skłodowska-Curie grant agreement No.713673), and a fellowship from La Caixa Foundation (ID 100010434, fellowship code LCF/BQ/IN17/11620063). The authors would like to thank the Basque Centre on Cognition, Brain and Language for its support.

Declaration of Competing Interests

Michael Chappell is employed by and holds equity in Quantified Imaging Ltd. Martin Craig provides consultancy for Quantified Imaging Ltd.

5 | Ramp Protocol for Non-linear Cerebrovascular Reactivity with Transcranial Doppler Ultrasound

Preface

This chapter introduces a novel ramp-based approach for capturing the non-linear aspects of cerebrovascular reactivity (CVR) using transcranial Doppler ultrasound. By systematically driving end-tidal CO_2 levels from hypocapnia to hypercapnia, the study reveals sigmoidal vascular responses that are poorly captured by conventional linear models. Leveraging both least squares regression and Bayesian methods, the chapter demonstrates that non-linear modelling offers a more physiologically faithful quantification of cerebral blood flow dynamics. These findings underscore the feasibility of a low-cost, accessible protocol with significant potential for clinical translation.

This chapter was published as:

> **G. Hayes**, S. Sparks, J. Pinto, and D. P. Bulte, "Ramp protocol for non-linear cerebrovascular reactivity with transcranial doppler ultrasound," J. Neurosci. Methods, vol. 416, p. 110381, 2025. doi: 10.1016/j.jneumeth.2025.110381

A subset of these results was presented at the following conference:

> **G. Hayes**, S. Sparks, J. Pinto, and D. P. Bulte, "Evaluating the nonlinear dynamics of cerebrovascular reactivity with transcranial doppler ultrasound," *Organisation for Human Brain Mapping (OHBM)*, Jun. 2024, Seoul, South Korea.

By highlighting the limitations of traditional linear CVR assessments and showcasing a scalable, cost-effective alternative, this work opens new avenues for detailed investigation of cerebrovascular function in both research and clinical settings.

Author Contribution Statement

G. Hayes contributed to the study concept and design, recruitment, and led the data acquisition, analysis and interpretation, and writing of the manuscript. **S. Sparks** contributed to data acquisition, recruitment, and critical revision of the manuscript. **J. Pinto** contributed to ethics approvals, study design, data acquisition, and critical revision of the manuscript. **D. P. Bulte** developed the original study concept and design, and contributed to critical revision of the manuscript, and study supervision. All authors read and approved the final manuscript.

Abstract

Cerebrovascular dynamics are vital for maintaining brain health and can be evaluated using cerebrovascular reactivity (CVR), the ability of blood vessels to adjust their diameter in response to vasoactive stimuli. CVR is commonly assessed using a two-point measurement that assumes a linear relationship between cerebral blood flow and arterial CO_2, however this neglects plateaus at the extremes of the CO_2 spectrum. This study introduces a cost-effective end-tidal CO_2 ($PETCO_2$) ramp protocol to assess the non-linear aspect of CVR by monitoring blood velocity responses to increasing levels of arterial CO_2 using transcranial Doppler ultrasound. All eleven participants completed

the protocol with an average $PETCO_2$ of 26 ± 4 mmHg from hypocapnia to hypercapnia and blood velocity range of -29 % to +50 % relative to baseline. Non-linear CVR characteristics were observed across all subjects. Sigmoid models provided significantly better fits than linear models and Bayesian approaches appeared to follow expected physiological ranges more accurately than least squares regression strategies. This study demonstrates the effectiveness of the ramp $PETCO_2$ protocol and non-linear CVR modelling. Given the high completion rate, simple implementation, and low equipment cost, these methods and models hold promise for more accurate quantification of CBF dynamics with significant potential for clinical application.

5.1 Introduction

Cerebrovascular reactivity (CVR) describes the capacity for blood vessels in the brain to constrict and dilate in response to vasoactive factors. This metric can be measured by applying a vasoactive stimulus, such as voluntary breathing tasks, gas inhalation protocols, or an acetazolamide injection [252][328][351], and measuring the concomitant blood flow changes with a non-invasive imaging modality such as magnetic resonance imaging (MRI) or transcranial Doppler ultrasound (TCD).

MRI-based techniques, such as blood-oxygen-level-dependent (BOLD) and arterial spin labelling (ASL) imaging, offer high spatial resolution to non-invasively map CVR [328][381]. However, TCD provides a simpler, widely available, and cost-effective alternative, enabling the measurement of blood velocity in major cerebral arteries [55][271].

Hypercapnia induced by inhaling gas mixtures with elevated CO_2 content is a common

method to elicit CVR. This increases the partial pressure of arterial CO_2 ($PaCO_2$), typically estimated via end-tidal CO_2 ($PETCO_2$) measurements. While many studies calculate CVR using a two-point approach, one measure at baseline and another during hypercapnia, this method assumes a linear relationship between $PaCO_2$ and cerebral blood flow (CBF) [52][381][466]. However, at the end ranges of $PaCO_2$ levels, both hypo- and hypercapnia, the relationship between CO_2 and CBF exhibits non-linear characteristics, often plateauing due to maximal vasoconstriction or vasodilation. This plateau effect indicates that beyond certain CO_2 thresholds, further changes in CO_2 do not elicit corresponding changes in CBF resulting in a non-linear relationship between $PaCO_2$ and blood flow. Progressive changes in CO_2 have indeed demonstrated the sigmoidal nature of CVR in healthy subjects [31][38][85][350].

Existing methods for eliciting and measuring non-linear CVR responses have primarily relied on rebreathing protocols, computerised targeted end-tidal forcing systems, and sequential gas delivery methods. These approaches often involve progressive CO_2 challenges to map CBF responses, leveraging techniques such as TCD or MRI for assessment [31][38][85][117][126][350][383]. While effective, these protocols often require specialized equipment and complex methodologies, limiting their accessibility for broader clinical and research applications. Current non-linear models of CVR commonly utilize a 4-parameter logistic regression to capture physiologically relevant features, such as maximum and minimum CBF responses, the inflection point of CO_2 sensitivity, and the slope in the linear response region [31][38][85][117]. Alternative approaches, such as biphasic linear fits or circuit analysis models, have also been applied to delineate CVR response types or vascular bed resistances under progressive CO_2 challenges [126][107].

Despite these advances, asymmetric sigmoid models, which may account for differential mechanisms governing cerebral blood vessel dynamics at their smallest and widest calibres, remain unexplored in CVR research.

Motivating our research is the need for more clinically relevant and broadly applicable measures of CVR. The two-point measure, a common surrogate for CVR, fails to capture the complex shape and orientation of the full CVR response, which may limit its diagnostic and therapeutic utility. For example, a shift in baseline CBF reserve or a change in the amplitude or speed of the CVR response could signify distinct pathological mechanisms, yet these nuances remain indistinguishable with a simplified measure. Linear models, while useful, are inherently limited as they rely on a single parameter, slope, to indicate dysfunction. In contrast, non-linear models can account for multiple parameters, such as the inflection point between lower and upper plateaus, the range of the response, and the baseline offset, which may provide deeper insights into the nature of dysfunction and improve our understanding of vascular responses in different pathologies. Given the association of altered CVR with conditions such as stroke, cognitive decline, and traumatic brain injury, advancing our ability to assess these dynamics comprehensively is critical [81][89][221][263][295][18]. While further research is needed to validate these applications, capturing the full spectrum of CVR dynamics without the need for complex protocols or equipment could ultimately enhance diagnostic precision and support the development of tailored therapeutic strategies.

In our study, we aim to address these limitations by presenting a cost-effective and widely accessible protocol for eliciting non-linear CVR responses using a combination of voluntary breathing techniques and gas stimuli. We measure the resulting CBF

changes in the middle cerebral artery (MCA) using TCD, providing a robust and practical approach to characterizing cerebrovascular dynamics. In addition, we evaluate and compare multiple modelling strategies, including 4-parameter (symmetric) and 5-parameter (asymmetric) sigmoidal models, to capture the full spectrum of CVR responses. By incorporating least-squares regression and Bayesian methods, we aim to identify an accurate and clinically relevant approach to modelling CVR.

5.2 Materials and Methods

5.2.1 Ethical Approval

All experimental procedures and protocols were approved by the Medical Sciences Interdivisional Research Ethics Committee (MS IDREC) of the University of Oxford's Central University Research Ethics Committee (CUREC), all of which conformed with the Declaration of Helsinki. Written informed consent was obtained for all participants before taking part in the study.

5.2.2 Data Acquisition

A total of 11 healthy participants (5 female, 33 $\pm$ 9 years of age) were included in this study. All participants were non-smokers with no history of psychiatric or brain disorders, hypertension, diabetes, or cardiovascular disease. The sample size of 11 subjects was chosen based on precedent set by similar studies employing non-linear CVR methods, which have typically used sample sizes ranging from 8 to 18 subjects [31][38][85][37][126].

To characterise the dynamics of the cerebral blood flow response to the novel CVR protocol, blood flow velocity in the left MCA was measured continuously using a 2 MHz probe and clinical TCD (7760EN Doppler-BoxX Digital, Compumedics DWL). Along with transmission gel, the TCD probe was placed on the transtemporal window and was secured using an adjustable headset. The location and angle of the probe was changed until a consistent blood flow velocity was achieved with a high signal-to-noise ratio. All TCD data were acquired by a single trained operator to ensure consistency and minimize operator-dependent variability. Signal quality was confirmed qualitatively by the trained operator, ensuring stable, pulsatile waveforms with clear spectral delineation of systole and diastole, and high peak-to-background amplitude.

A thin nasal cannula placed into both nostrils was used to sample CO_2 and O_2 levels in respired air and an infrared gas analyser (ML206, ADInstruments). The CO_2, O_2, and TCD signals were recorded using a PowerLab 8/35, 8 Channel recorder (PL3508 ADInstruments) and accompanying LabChart Software.

Inspired gases were delivered using a custom gas delivery system built in-house at the University of Oxford [388]. The setup consisted of a disposable non-rebreathing anaesthetic face mask (Model 1181015, Intersurgical EcoLite Oxygen Mask) placed over the participant's nose and mouth, secured using a head strap. Unidirectional silicon membranes on either side of the mask allowed exhaled air to escape the mask while being sealed during inhalation and a medical-grade respiratory filter (Model 1644007, Clear-Guard Midi Low Volume Breathing Filter) was placed at the junction of the disposable circuit and the permanent fixtures to prevent cross-contamination. On the permanent side of the filter, a short length of tubing attached to two interconnected

Y-pieces where respiratory gas mixtures could be delivered one at a time at 15 L/min. The gas cylinders, each fitted with a pressure regulator and flow meters, were operated by hand, following a predefined ramp protocol.

The ramp protocol consisted of 3 repetitions of 5 deep breaths, followed by 30 s of regular breathing on synthetic medical air (21 % O_2 / 79 % N_2), 40 s breathing a 5 % CO_2 balanced gas mixture (BOC Group, Linde, Surrey, UK), and 40 s breathing a 10 % CO_2 balanced gas mixture (BOC Group, Linde, Surrey, UK). A diagram of the protocol is illustrated in Figure 5.1. The deep breathing instructions were given verbally and the participants were notified when the gases were changed and for the last 10 s of breathing the 10 % CO_2 gas mixture. Participants were trained prior to starting the ramp protocol to take full deep breaths without pauses and were allowed to test breathing the different gases. This testing time was also used to check for leaks at the mask-face interface identified via the capnometry trace which were plugged with additional rubber fittings if needed.

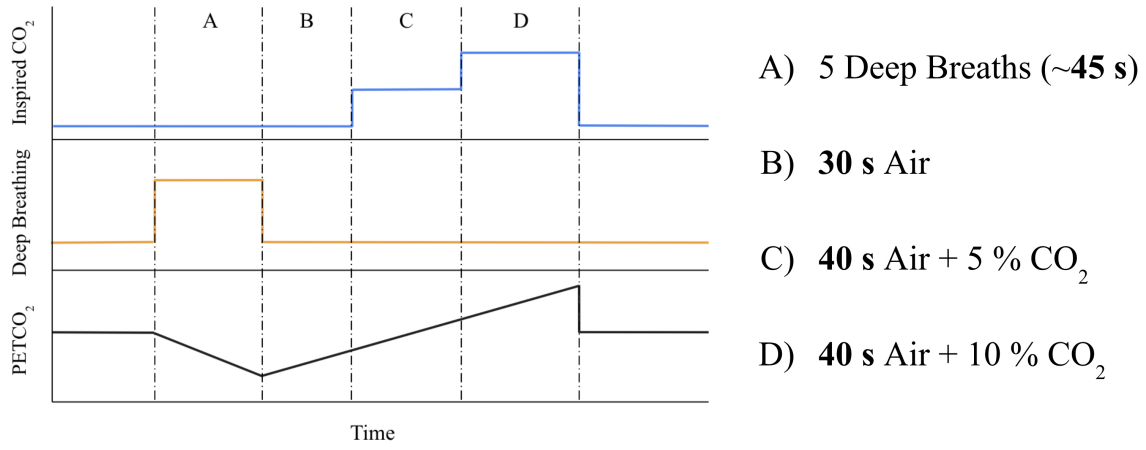

Figure 5.1: Ramp paradigm diagram consisting of A) 5 deep breaths, B) 30 s of air, C) 40 s of air with 5 % CO_2, and D) 40 s of air with 10 % CO_2. The full ramp protocol consisted of 3 repeats of this sequence.

5.2.3 Data Analysis

5.2.4 Preprocessing

The CO_2, O_2, and TCD data were acquired at 200 Hz. Data processing and analysis was performed using custom scripts in Python 3.10.8. The raw TCD outputs were converted to cm/s using a calibration factor of 202.07 cm/s/V based on the DWL software, where V denotes the voltage output between 0 and 1. Values below 14 cm/s were removed as they corresponded with bottoming out of the TCD signal. The gas signals were converted from percent to mmHg using a conversion factor derived from the acquisition-day 12.00 PM atmospheric pressure in Oxford, UK [113].

A rolling mean of the MCA velocity (MCA$\overline{v}$) was applied across the pulsatile signal. The end-tidal peaks in the CO_2 and O_2 time-courses were selected automatically. To account for measurement delay, a bulk shift was applied to each $PETCO_2$ trace to maximise its cross-correlation with the mean MCA$\overline{v}$ signal. To account for equipment and physiological delays, a manual shift (mean across subjects of -16 $\pm$ 8 s) was applied to align each participant's $PETCO_2$ trace with their MCA$\overline{v}$ trace. A low-pass filter was applied to the MCA$\overline{v}$ and $PETCO_2$ time courses with a window size of 50 samples, corresponding to a time window of 0.25 s at the sampling rate of 200 Hz, corresponding to an effective cutoff frequency of 2 MHz. The filter was implemented using the rolling mean method in Python's Pandas library, which calculated the rolling average over the specified window size [405]. This approach smoothed high-frequency noise while preserving the physiological signal's key characteristics. MCA$\overline{v}$ was normalised relative to the mean MCAv during the baseline period (breathing air) to account for any

variations in probe angle relative to the MCA. Only the 3 ramp-up, blood vessel dilation components of the protocol were isolated for further analysis since the dynamics for dilation and constriction may not be the same [472]. This approach was chosen to prioritize consistency in the modelling process and reduce potential variability.

5.2.5 Model Fitting

CVR was characterised by fitting 4-parameter and 5-parameter sigmoid models to the MCA$\overline{v}$ vs. $PETCO_2$ data for each subject as shown in Equation (5.1) and Equation (5.2) respectively. In these equations, 'a' represents the minimum blood velocity (bounded between 0<a<1 a.u.), 'b' represents the slope of the linear region (0<b<20 mmHg/a.u.), 'c' describes the $PETCO_2$ value for the inflection point (0<c<60 mmHg), and 'd' is the span of the blood velocity (0<d<4 a.u.) [38][85]. It should be noted that the inflection point in the sigmoid model represents the CO_2 level corresponding to the steepest slope of the curve, marking the transition between lower and upper plateaus, irrespective of the specific CO_2 inhalation conditions. The 5th parameter in Equation (5.2), 's', is an asymmetry parameter that allows the lower and upper plateaus to occur at different rates (0.1<s<10 a.u.).

$$y = a \ + \frac{d}{1 + e^{\frac{(c-x)}{b}}} \tag{5.1}$$

$$y = a \ + (\frac{d}{1 + e^{\frac{(c-x)}{b}}})^s \tag{5.2}$$

Fitting of these models was done using a least-squares regression (LSR) method with SciPy [426] and a Bayesian nested sampler method with the python package Bayesic-

Fitting [213]. Gaussian priors were used for the parameters in the Bayesian fitting approach, defined by a mean and standard deviation with 'a' ∼N(0.3 ± 0.15 a.u.), 'b' ∼N(10 ± 5 mmHg/a.u.), 'c' ∼N(35 ± 4 mmHg), 'd' ∼N(2.5 ± 0.5 a.u.), 's' ∼N(1 ± 0.5 a.u.).

5.2.6 Statistical Analysis

To compare the goodness of fit of the models to the data, the Bayesian information criterion (BIC) was calculated for all the models based on Equation (5.3) [370].

$$BIC = n \cdot log(\frac{RSS}{n}) + K \cdot log(n) \tag{5.3}$$

In the calculation of the BIC, n is the number of data points, RSS is the residual sum of squares error, and K is the number of model parameters. Here a lower BIC value indicates a closer fit to the true model and favours model simplicity (fewer parameters) to avoid overfitting.

5.3 Results

All 11 participants completed the full protocol. A few participants reported noticing a slight difference in smell/taste and feelings of breathlessness during the protocol, notably especially during the 40 s of 10 % CO_2 gas mixture. None-the-less, all participants responded that they would still be comfortable to repeat the study.

The TCD blood velocity measure and CO_2 trace for a representative subject is shown in Figure 5.2. The rolling mean blood velocity signal, MCA$\overline{v}$, is overlaid on the TCD

signal, and the $PETCO_2$ points and interpolation are overlaid on the CO_2 signal.

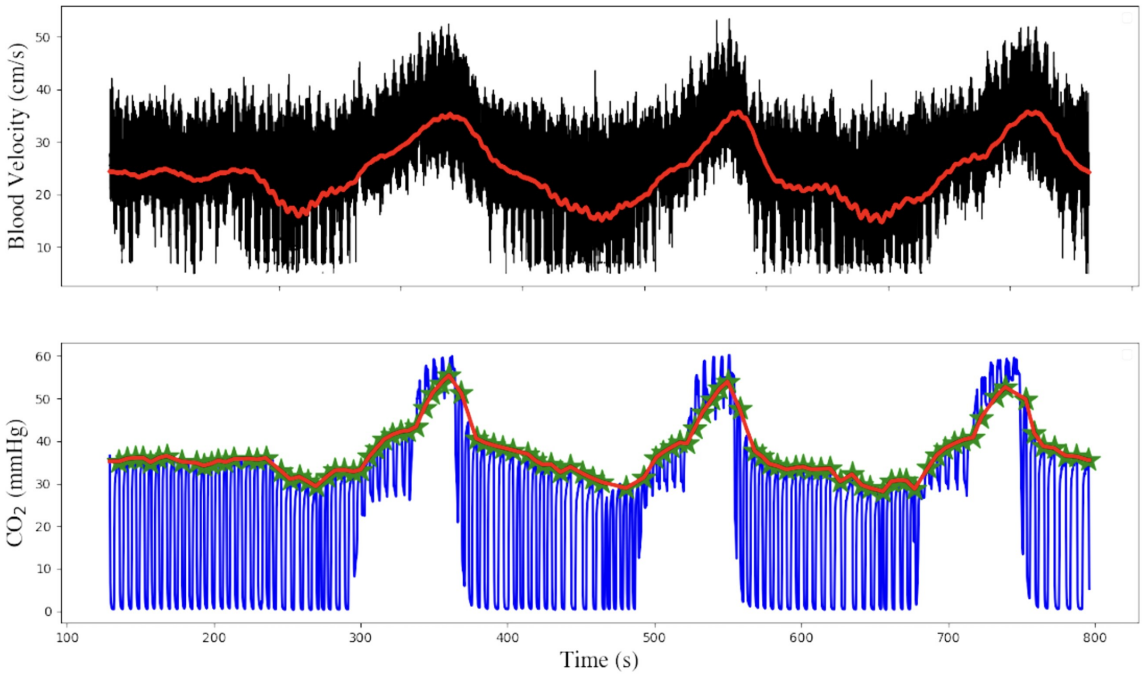

Figure 5.2: TCD blood velocity (black, top) and CO_2 trace (blue, bottom) during the ramp protocol for a representative subject. The rolling mean of the blood flow velocity is overlaid in red (top). The end-tidal CO_2 points are represented by green stars and the interpolation between those points is shown in red (bottom). Sub-007.

The range in $PETCO_2$ throughout the ramp protocol varied somewhat between subjects due to differences in the seal of the mask, breathing rate and depth as well as individual metabolism. On average, the maximum and minimum $PETCO_2$ values reached were 52 ± 2 mmHg and 27 ± 4 mmHg respectively, with a mean $PETCO_2$ span of 26 ± 4 mmHg. The average baseline $PETCO_2$ was 34 ± 2 mmHg. The average baseline MCA$\overline{v}$ was 32 ± 7 cm/s, and across all participants, the average MCA$\overline{v}$ reduction during hypocapnia was 71 ± 15 % of baseline and the subsequent increase during hypercapnia was 150 ± 23 % relative to baseline.

The MCA$\overline{v}$ is plotted as a function of the $PETCO_2$ for each participant, presented

in Figure 5.3, including the linear regression lines, and the 4-parameter (4p) and 5-parameter (5p) models both fit with the LSR and Bayesian methods. It should be noted that subject 8 illustrated a highly variable $PETCO_2$ trace, attributed to shallow breathing.

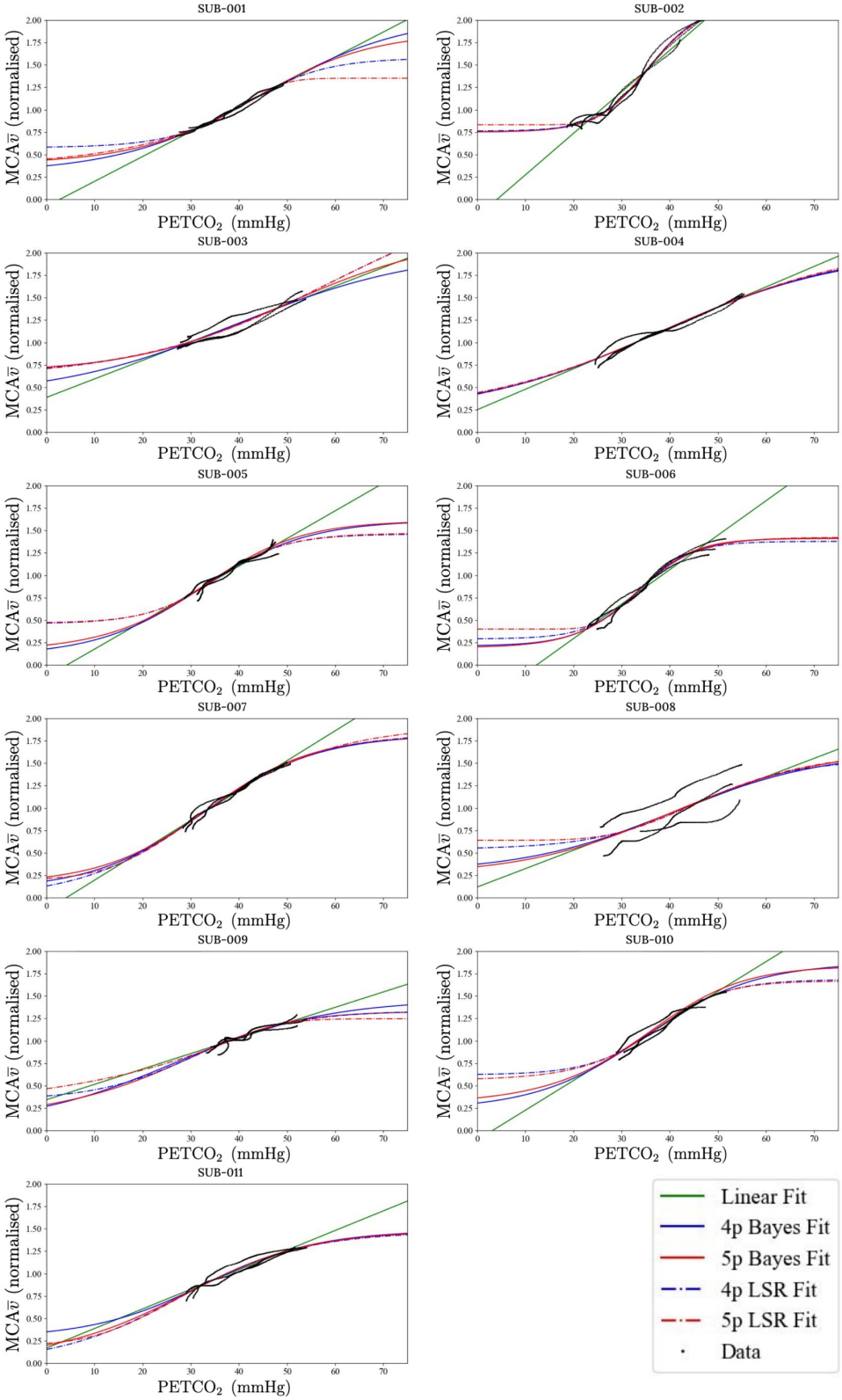

Figure 5.3: MCA rolling-mean blood velocity as a function of $PETCO_2$ (black dots) for all subjects. Each dataset is fit with 2 models each with 2 fits: 4p LSR (blue, dashed line), 4p Bayes (blue, solid line), 5p LSR (red, dashed line), and 5p Bayes (red, solid line). Sub-008 was excluded due to noise and high variability.

Bar graphs of the parameter values for each subject for the 4p and 5p models are presented in Figure 5.4 and Figure 5.5 respectively. The values derived using the LSR and Bayes methods are presented for both models.

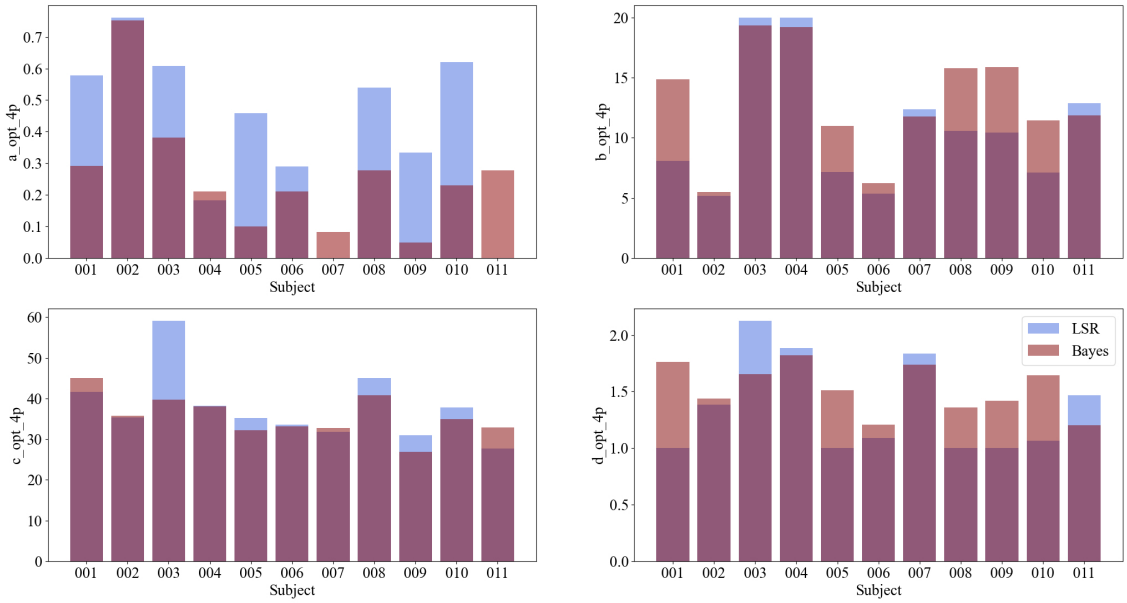

Figure 5.4: 4-parameter model bar graphs for parameters a (lower plateau, top left), b (upper plateau, top right), c (inflection point, bottom left), and d (steepness, bottom right) for each subject fit with the LSR (blue) and Bayes (red) methods.

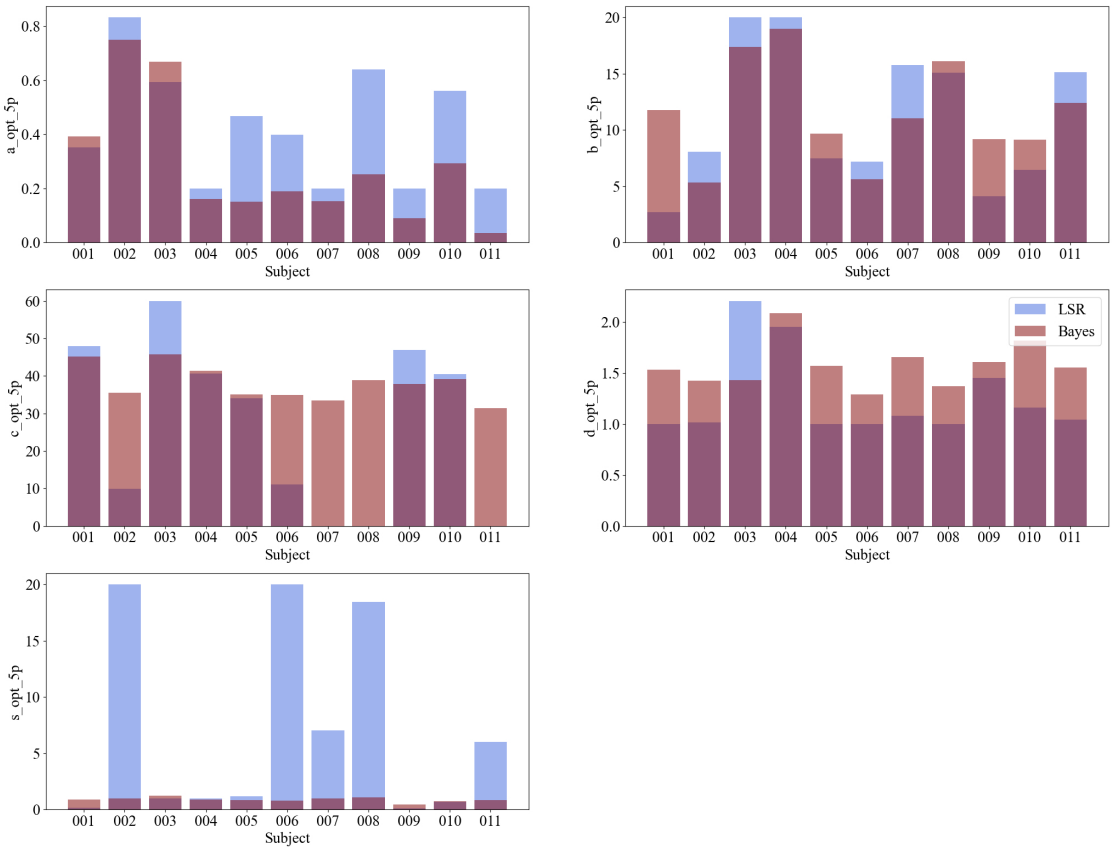

Figure 5.5: 5-parameter model bar graphs for parameters a (lower plateau, top left), b (upper plateau, top right), c (inflection point, middle left), d (steepness, middle right), and s (symmetry, bottom left) for each subject fit with the LSR (blue) and Bayes (red) methods.

The BIC values of the linear, 4p LSR, 4p Bayes, 5p LSR, and 5p Bayes models are presented for each subject in Table 5.1. The subject mean and standard deviations (with and without sub-008) are also shown. Note that a more negative BIC value corresponds to a closer fit to the data, while accounting for the number of parameters in the model.

Table 5.1: Bayesian information criterion error for linear regression, 4p LSR, 4p Bayes, 5p LSR, and 5p Bayes for all subjects including the mean and standard deviation for each model across subjects, with (red) and without (black) sub-008.

Subject	Linear	LSR 4p	LSR 5p	Bayes 4p	Bayes 5p
Sub-001	-4536	-4673	-4678	-4628	-4636
Sub-002	-3159	-3775	-3806	-3767	-3766
Sub-003	-3733	-3747	-3740	-3717	-3736
Sub-004	-4144	-4098	-4091	-4095	-4089
Sub-005	-4270	-4321	-4315	-4313	-4203
Sub-006	-3447	-3751	-3755	-3740	-3725
Sub-007	-4003	-4074	-4070	-4073	-4022
Sub-008	*-2008*	*-2000*	*-1994*	*-1997*	*-1989*
Sub-009	-3930	-3979	-3974	-3969	-3955
Sub-010	-3912	-3946	-3940	-3938	-3833
Sub-011	-3910	-3987	-3981	-3979	-3977
Mean±SD	***-3732±683***	***-3850±671***	***-3849±672***	***-3838±666***	***-3812±659***
Mean±SD*	**-3904±394**	**-4035±287**	**-4035±285**	**-4022±281**	**-3994±276**

**with sub-008 removed*

5.4 Discussion

In this work we present a $PETCO_2$ ramp protocol that allows the assessment of non-linear features of CVR with TCD. All 11 participants completed the protocol without complications, however 3 participants noted that breathing the air with 10 % CO_2 made them feel breathless.

The timing of the ramp protocol components was determined experimentally with 4 trained volunteers with the aim to find a balance between the largest feasible range in $PETCO_2$ while maintaining the safety and comfort of participants. The 5 deep breaths were chosen to decrease and briefly maintain a $PETCO_2$ below baseline. After 30 s

of normal breathing on air, participants' $PETCO_2$ had returned to baseline, and after 40 s of breathing 5 % CO_2, the $PETCO_2$ values plateaued again at approximately 25 % above baseline. The 10 % CO_2 was maintained for the duration that all testing participants still found comfortable which resulted in a further increase in $PETCO_2$ to approximately 50 % above baseline.

The data showed minimal differences between the three ramp up segments with each acquisition except for in 1 participant (sub-008). The variation between the ramps in this participant is attributed to shallow breathing, resulting in $PETCO_2$ calculations from only partially expired breaths and significant differences in the $PETCO_2$ values between ramps. Due to potential inaccuracy of the $PETCO_2$ measurements, this participant was excluded from further statistical analysis. Noticeable differences between participant's MCA$\overline{v}$ responses to the ramp $PETCO_2$ protocol are that some participants show significantly more shouldering at the top and bottom of their response curve than others (such as sub-002, sub-010, and sub-006). The more linear responses (such as sub-003 and sub-004) could be due to not exceeding the linear regime for these participants. Furthermore, sub-002 with low resting blood flow measures had a large and fast increase in the normalised MCA$\overline{v}$ as $PETCO_2$ increased, but a minimal reduction in blood flow during the deep-breaths. These features will be important to explore in larger participant groups as well as between sessions of repeated measurements on the same subject.

Non-linear CVR features were observed in the TCD data of all subjects, however some illustrate greater plateauing than others at the top or bottom ranges of the stimuli. The 4p and 5p models showed much closer fits to the data compared to a

linear fit, based on significantly better BIC values for the non-linear models. Our results indicate that the linear regime in the CVR response is highly variable between subjects, as some individuals exhibit significant non-linear transitions or plateaus in the vascular response curve. These findings align with previous studies showing a sigmoidal CVR response as well as with literature showing that linear CVR metrics can be inconsistent due to variability in vascular reactivity across populations and experimental conditions [31][38][85][350][382][469]. The sigmoidal modelling approach used in this study addresses these limitations by providing parameters that capture the non-linear dynamics of vascular reactivity, such as the slope, response span, and inflection point while still allowing for a linear regime to exist, which are critical for understanding individualized vascular responses.

Both LSR and Bayesian methods were used to fit the non-linear models, with the greatest difference in methodology being the incorporation of priors into the Bayesian approach. The gaussian priors were based on the expected behaviour of the healthy physiology and were informed by existing but limited research. All priors were given wide gaussian standard deviations as not to over-bias the fitting based on expectations and allow for variation between subjects. While there is limited research that clearly defines the normal boundaries of blood flow parameters in the MCA, assumptions were made based on other CVR and physiology studies. CBF below 50 % of baseline has been shown to be a lower limit in the conscious brain and is very unlikely to occur, so while the absolute lower bounds of the sigmoid (parameter a) were set at 0, the priors for the Bayesian modelling of the lower bound were set at 30 % of baseline [84][477]. Furthermore, based on the results of non-linear CVR mapping by Fan et al.

and Ringelstein et al., it was assumed that the MCA$\overline{v}$ was unlikely to ever go above 300 % of baseline and the upper shoulder regime of the sigmoid occurred between 130 % to 160 % for most adults [117][350]. As a result, the maximum span of the sigmoids (parameter d) was set to reflect no more than a 4-fold increase in blood flow from hypocapnia and the priors for the Bayesian analysis were set to represent a 250 % increase with a wide standard deviation of ±50 %. The bounds for the slope of the linear regime (parameter b), inflection point (parameter c), and asymmetry parameter (parameter s), were all set to have wide bounds, with the slope assumed to be positive, and the priors of the inflection point set with a mean of 35 mmHg based on previous CVR research [31][38][85][117][284].

When assessed using the Bayesian fitting, the parameters values for the 4p and 5p models are very similar, however with the LSR fit, the values of the inflection point (parameter b) trades off significantly with the asymmetry parameter (parameter s) in the 5p model. The asymmetry parameter also showed significant variation between subjects when fit with the LSR method and despite resulting in the same BIC score (BIC = -4035 for both the LSR 4p and 5p methods), this suggests the model is over-fitting the data. When fitted with the Bayesian method, the asymmetry parameter stayed close to s = 1 for all subjects, suggesting that the sigmoids are quite symmetrical. With the minor asymmetry parameters, the 5p model still showed a slightly worse BIC score of -3994 compared to -4022 for the Bayes 4p model.

The Bayesian and LSR methods showed noticeable differences between the parameter values for some, but not all subjects, especially for the minimum blood velocity (parameter a), with more minor differences between the other parameters. When assessed

using both methods, the parameter 'c', representing the inflection point, aligns with previous literature where sigmoid midpoints typically sit between 36-46 mmHg, slightly above resting $PETCO_2$ levels [31][85][117]. Similarly, the response range ('a' and 'd') is consistent with reported spans, ranging from 90-150 % change in MCAv in TCD, but is more variable when assessed using the LSR method compared to the Bayesian method [85][117]. Our results suggest that the range of the linear regime is variable between participants, in some cases showing a linear regime above 10 mmHg which is higher than previously reported [31][38][117]. With the advantage of the priors, the Bayesian method more closely approaches the expected physiological ranges, while the LSR method hits the parameter limits for a number of participants in which cases it goes to unreasonable extremes to more closely fit all of the data, such as in the case of some very high asymmetry values with the 5p model. While the LSR method achieves a lower BIC score, this advantage is inherent to its optimization process, which explicitly minimizes the residual sum of squares error, a key component in BIC calculation. In contrast, the Bayesian approach is not directly optimized for this criterion, introducing a bias in favour of the LSR method when evaluated using the BIC. None-the-less, it is important to note that despite fitting the data as well as the physiological priors, the Bayesian method still results in a goodness of fit comparable to the LSR method, with a BIC of -4022 for the Bayesian 4p method and -4035 for the LSR 4p method.

It is important to note that neither method can be declared definitively more accurate or unbiased in the absence of a 'gold standard' or simulation-based validation. Instead, each approach offers unique advantages: the LSR method excels in computational simplicity and direct optimization of residuals, whereas the Bayesian approach

incorporates prior information and generates posterior distributions, enabling richer parameter estimation and uncertainty quantification.

5.4.1 Limitations and Future Work

With TCD allowing for high-temporal resolution blood velocity measures at a low cost, it is routinely used in clinical practice and research, however it is not without its limitations. The blood velocity measure can be affected by the angle of the probe with the blood vessel and a TCD's accuracy is highly dependent on the operator [337]. To mitigate these risks, the same trained operator helped with the acquisition of all TCD data, and MCA$\overline{v}$ values were normalised relative to the MCA$\overline{v}$ measured at baseline. Furthermore, since our CVR metrics were only based on blood velocity measured in the MCA it is not necessarily representative of blood flow in the rest of the brain as there may exist regional differences [31][214][440]. For example, integrating multimodal validation with BOLD fMRI would provide an opportunity to enrich our understanding of cerebrovascular dynamics across the brain. While TCD measures reflect blood velocity changes within the MCA, BOLD fMRI captures oxygenation-dependent signal changes that also incorporates cerebral perfusion and metabolism with high spatial resolution. Future assessment of this CVR ramp protocol in MRI will allow for measures of cerebral blood flow with high spatial resolution and the study of regional CVR across the brain.

One of the major assumptions in many CVR studies, including our own, is the reliance on $PETCO_2$ as a surrogate measure for $PaCO_2$. While $PETCO_2$ is a non-invasive and easily obtainable measure, it may not always accurately reflect $PaCO_2$ as it can be

influenced by variance in ventilation and perfusion [56][396][407][436]. Consequently, the use of $PETCO_2$ as a proxy for $PaCO_2$, while practical and frequently implemented in CVR studies, introduces a degree of uncertainty and potential error in the CVR values [298] Furthermore, other studies using programmable gas delivery systems can offer significant improvements in the stability of $PETCO_2$ values compared to fixed inspired CO_2 methods, and can therefore reduce the potential for error and enhance the precision of CVR mapping [41][125][352][443]. Moreover, direct arterial measurements, although more invasive, provide the most accurate assessment of $PaCO_2$. Our study utilises a fixed inhaled CO_2 system and breathing protocol, which, although less precise, is inexpensive and very easy to implement, making it a practical option for larger-scale or resource-limited studies.

Another limitation in our study is that continuous arterial blood pressure (ABP) measurements were not taken throughout the ramp protocol and only a baseline blood pressure measure was acquired while the participants were at rest using an arm cuff to rule out hypertension. Continuous ABP measurements could provide more insights into CVR by means of a conductance index which can somewhat account for the impact of changes in perfusion pressure on blood velocity and vasodilation [25][280]. Some studies have demonstrated that changes in ABP induced by vasoactive stimuli can impact the CBF response and therefore affect the CVR values in some adults [184][345][430][440]. Other studies have shown that when using up to 7 % inspired CO_2 gas mixtures, the increase in ABP has minimal effects on MCAv and CVR [445]. Further research by Battisti-Charbonney et al. showed that the MCAv response to CO_2 was unchanged by ABP considerations up to a threshold of $\sim$50 mmHg, above which both MCAv and

ABP demonstrated a linear increase with CO_2 tension [31]. A linear regime in MCA$\overline{v}$ was not noticeable at high $PETCO_2$ values in the results of our study, however the maximum $PETCO_2$ reached by most participants was only slightly above 50 mmHg (52 ± 2 mmHg on average) and was only maintained for a few seconds before participants returned to breathing air. It should also be noted that in patient groups, ABP could more significantly alter CVR [108], and accounting for ABP may become increasingly important when assessing older adults [280]. Future studies may benefit from measuring and accounting for continuous ABP changes especially when using hypercapnic stimuli that go significantly above 50 mmHg or when investigating patient groups.

It should also be noted that the model bounds and priors presented in our analysis of the CVR curves are based on a limited body of research on the physiological bounds of cerebral blood flow in nominally healthy humans. To mitigate this, large absolute bounds and wide standard deviations in the gaussian priors of the Bayesian models were defined to allow for subject variability and to not overly bias the model fits. Furthermore, the use of the BIC to compare models was presented as a means of assessing the distance of the model fits from the data, however it is not a fair direct comparison between the Bayesian and LSR modelling approaches since the BIC is based on the residual sum of squares error which the LSR method utilises to define its fit. Future analyses would benefit from including other statistical comparisons to assessment of model fits such as using separate datasets for model fitting and validation, or by leveraging simulations to benchmark the accuracy and bias of each approach under controlled conditions. Additionally, while this study focused on the dilation phase of

the CVR response, future research could investigate the constriction phase to provide a more comprehensive assessment of cerebrovascular dynamics. The potentially differing physiological mechanisms of dilation and constriction warrant further exploration.

While our ramp protocol and models provide valuable insights into the normal functioning of cerebrovascular mechanisms, it has limitations when applied to pathological conditions. Non-linear CVR is an emerging area of study that may offer a deeper understanding of cerebrovascular health and disease. However, the applicability of our findings to pathological states remains uncertain due to the lack of extensive research in this area, especially when using Bayesian priors based on physiology of healthy adults, as different models may be needed in diseased states. Studies have indicated that non-linear CVR measures can reveal important differences in patients with cerebrovascular diseases. For instance, research on patients with moyamoya disease has shown altered CVR patterns, suggesting potential diagnostic and prognostic utility [94][171][250][364]. Similarly, other studies have identified changes in CVR in conditions such as stroke, cognitive decline, and traumatic brain injury, highlighting its relevance in various pathologies [81][89][221][263][295][18] These findings imply that CVR measures could be useful in distinguishing and better understanding cerebrovascular pathology, and non-linear CVR may offer additional insights into the nature of the CVR impairment. Nevertheless, more research is needed to better understand how non-linear CVR changes in different diseases and to establish standardised protocols for its assessment in clinical settings. Expanding the study of non-linear CVR to pathological cohorts will be essential to validate its clinical applicability and enhance our understanding of cerebrovascular changes in disease.

Finally, our study presents the ramp protocol in only a small sample size of 11 healthy adults and requires more research in a larger cohort with a greater diversity of ages, backgrounds, and lifestyle factors to assess population variability, protocol tolerance, and repeatability. With the large dynamic range in blood flow, ease of implementation, high completion rate, and low equipment cost compared to other methods of assessing CVR, these methods and models could offer an accurate and convenient quantification of CBF dynamics useful for clinical adoption.

5.5 Conclusion

We developed a low-cost, clinically relevant method for assessing the non-linear features of CVR with TCD based on a $PETCO_2$ ramp protocol. This novel CVR protocol is designed as an accessible entryway into the study of non-linear CVR dynamics. The CVR responses to this protocol were better fit with 4- and 5-parameter sigmoids than a linear model and Bayesian model fitting allowed for prior physiological information to favour fitting the data within reasonable bounds. Future work includes extending the use of this cost-effective ramp protocol and non-linear CVR modelling in MRI in a larger participant group.

Data Availability

The materials used to support the findings of this research are available from the corresponding author upon reasonable request.

Acknowledgements

The authors would like to thank all the volunteers who participated in this study and Dr. Johannes Klein for training the team on transcranial Doppler ultrasound.

Funding Acknowledgements

This work was supported by Engineering and Physical Sciences Research Council UK through grant EP/S021507/1. GH was supported by Clarendon, and SS by the Rhodes Trust and the Canadian Institutes of Health Research (DSG-193252).

Declaration of Competing Interests

The authors declare that the research was conducted in the absence of any commercial or financial relationships that could be construed as a potential conflict of interest.

6 | Models of Cerebrovascular Reactivity in BOLD-fMRI and Transcranial Doppler Ultrasound

Preface

This chapter extends the multimodal investigation of cerebrovascular reactivity (CVR) by directly comparing measurements obtained via transcranial Doppler ultrasound (TCD) and BOLD-fMRI under a ramped hypercapnia stimulus. Through both linear and non-linear modelling strategies, the study evaluates the degree to which each modality captures dynamic vascular changes across a wide range of CO_2 levels. In doing so, it reveals that although linear CVR models produce consistent metrics, a simplified two-parameter sigmoid model may better account for non-linear aspects of vascular behaviour and improve inter-modality agreement. These findings contribute to a clearer understanding of how TCD and BOLD-fMRI measurements align and diverge, refining the methodological framework for future CVR research and clinical assessments.

This chapter was published as:

> **G. Hayes**, S. Sparks, J. Pinto, and D. P. Bulte, "Models of cerebrovascular reactivity in fMRI and transcranial doppler ultrasound," *J. Appl. Physiol.*, vol. 139, no. 1, pp. 219-230, 2025. doi: 10.1152/japplphysiol.00107.2025

A subset of these results was presented at the following conference:

G. Hayes, S. Sparks, J. Pinto, and D. P. Bulte, "Linear and sigmoidal cerebrovascular reactivity in fMRI and transcranial doppler ultrasound," *Organisation for Human Brain Mapping (OHBM)*, Jun. 2025, Brisbane, Australia.

By addressing the challenges of plateau effects and dynamic range variations, this work reinforces the importance of careful protocol design and choice of modelling parameters, paving the way for more robust cross-modal comparisons in the study of cerebrovascular physiology.

Author Contribution Statement

G. Hayes contributed to the study concept and design, recruitment, and led the data acquisition, analysis and interpretation, and writing of the manuscript. **S. Sparks** contributed to data acquisition, recruitment, and revision of the manuscript. **D. P. Bulte** developed the original study concept and design, and contributed to revision of the manuscript, and supervision. **J. Pinto** contributed to study design, ethics approvals, data acquisition, revision of the manuscript, and supervision. All authors read and approved the final manuscript.

Abstract

The ability of cerebrovasculature to adapt in order to meet tissue demands is vital for brain function and resilience. Cerebrovascular reactivity (CVR), a measure of the responsiveness of cerebrovasculature to vasoactive stimuli, is a valuable tool for evaluating cerebrovascular health. While CVR is commonly assessed using transcranial Doppler

ultrasound (TCD) or MRI-based techniques, direct comparisons between these two modalities remain limited, particularly when using stimuli that induce a large dynamic range. This study evaluates inter-modality correlations of CVR using TCD and blood oxygenation level-dependent functional MRI (BOLD-fMRI) during a ramped hypercapnic protocol and different modelling strategies. Linear correlations across broad $PETCO_2$ ranges validated the utility of linear CVR modelling in capturing repeatable metrics of the response using TCD and MRI. A four-parameter sigmoid model revealed significant inter-modality variability in span and bound parameters, improved by fixing these parameters and focusing on slope and inflection point, which enhanced the correlations between modalities. These results support the reliability of linear CVR modelling within narrow vasoactive response ranges in healthy subjects and propose a simplified two-parameter sigmoid model as an effective framework for characterising non-linear CVR dynamics. This work adds to the sparse literature on inter-modality CVR comparisons and indicates which CVR metrics are comparable between TCD and BOLD-fMRI, emphasising CVR as a useful tool for assessing cerebrovascular health in research and clinical contexts.

6.1 Introduction

The ability for brain vasculature to adapt to match tissue demands for blood flow is vital for neuronal function and resilience. Cerebrovascular reactivity (CVR) has become a common method of assessing the responsiveness of cerebrovasculature to vasoactive stimuli and has gained notoriety as a valuable tool for mapping cerebrovascular health in a broad range of cerebrovascular pathologies such as stroke [155], cerebral small

vessel disease [291][323], and dementia [72][349][422].

CVR is most commonly assessed using non-invasive transcranial Doppler ultrasound (TCD) and MRI-based techniques. In functional MRI (fMRI), blood-oxygen-level-dependent (BOLD) imaging provides an indirect measure of cerebrovascular changes by detecting variations in deoxyhaemoglobin concentrations, which are assumed to reflect changes in cerebral blood flow (CBF) under isometabolic conditions during CO_2 challenges [26][376]. This assumption, while widely accepted, may not always hold, particularly in pathological states where neurovascular coupling or metabolic activity may vary [474]. Arterial spin labelling (ASL), on the other hand, offers a more direct quantification of CBF by magnetically labelling arterial blood and using it as an endogenous tracer [438]. However, ASL has limitations in signal-to-noise ratio (SNR), and its accuracy during ramp stimuli is challenged by the changing transit times and bolus shapes that occur in response to altered $PaCO_2$ concentrations, potentially confounding CVR measurements [330][474].

In contrast, TCD measures blood flow velocity in large arteries, such as the middle cerebral artery (MCA), with high temporal resolution and minimal susceptibility to physiological noise [55][271]. Furthermore, it is a more cost-effective alternative to MRI, however it lacks spatial resolution and reflects macrovascular dynamics rather than the microvascular changes captured by MRI. Notably, changes that occur in cerebral haemodynamics throughout healthy ageing as well as in pathology are controversial and discrepancies between experimental techniques could be at fault. Understanding the relationship between TCD and BOLD-fMRI is crucial for establishing the reliability and complementarity of these modalities, particularly in clinical and research settings

where one method may be preferred due to accessibility or specific research goals. By harmonising findings across these techniques, researchers can ensure more robust and generalisable conclusions about cerebrovascular health and disease mechanisms.

The existing direct comparisons between TCD and fMRI have used steady-state or stepped hypercapnia with a fixed inspiration of air with up to 6 % CO_2 and calculated the CVR as a linear measure between the baseline and stimulus periods [55]. Using BOLD-derived measures of CVR using fixed inspiration of 5 % CO_2 in air, Burley et al. found no clear relationship between TCD and BOLD CVR measures, hypothesising that differences may be due to the vascular regions assessed by each method [55]. Conversely, Fico et al. reported good agreement between TCD and 4D flow MRI for middle cerebral artery velocity (MCAv) measurements, but noted that 4D flow MRI revealed additional age-related effects not apparent with TCD [120]. However, no studies to date have employed ramp stimuli with a large dynamics range to explore the relationship between non-linear CVR features between modalities, which may give more accurate and nuanced measures of the cerebrovascular response beyond the linear measure alone. Two-point, linear measures fail to capture the complex shape and orientation of the full CVR response, limiting their diagnostic and therapeutic utility. Linear models, while useful for capturing slope-based changes, rely on a single parameter to indicate dysfunction. This simplification overlooks critical features such as shifts in baseline CBF reserve, changes in the amplitude or speed of the response, and inflection points between lower and upper plateaus, which could reveal distinct pathological mechanisms. In contrast, non-linear models allow for a richer characterisation of CVR dynamics, incorporating multiple parameters that may provide deeper

insights into the nature of vascular dysfunction [31][38][85][117][284]. By providing a continuous and gradual increase in arterial CO_2, ramp stimuli can enable a detailed assessment of the full cerebrovascular response curve, including transitions between linear and plateau regions. In this context, we present an analysis of dynamic CVR to a ramp stimulus using TCD and BOLD-fMRI to compare both linear and non-linear CVR models between modalities.

6.2 Material and Methods

6.2.1 Participants

This study comprised two sessions 19 ± 18 days apart. Thirty-three healthy participants performed Session 1 that included assessing CVR with TCD. Twenty-five of these participants (13 females, aged 33 ± 11 years of age) came back for a 2nd session for CVR assessed using fMRI and were included for further analysis. Return participants were chosen based on representing both sexes and a broad range of age groups. Participants were excluded if they had any history of psychiatric or neurological disorders, hypertension, diabetes, or cardiovascular disease.

6.2.2 Data Acquisition

Dynamics of the cerebral blood flow response to a ramped breathing protocol were assessed in both TCD and BOLD-fMRI. An overview of the acquisition and analysis pipeline is presented in Figure 6.1. Participants completed two sessions. The first session included general physiological measurements, gas challenge feedback question-

naire, and TCD of the middle cerebral artery (MCA) with a gas protocol that causes a ramp increase in $PETCO_2$ ("ramp protocol"). Based on the gas challenge feedback answers, a subgroup of participants were asked to return for Session 2. In the second session, the same ramp protocol was repeated with BOLD-fMRI within 3 months.

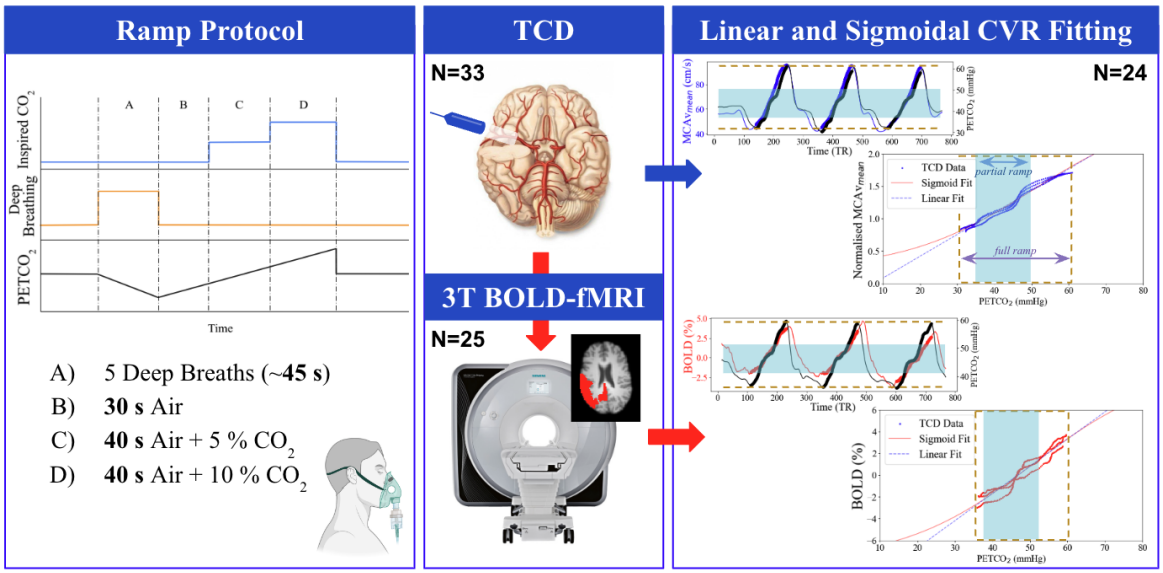

Figure 6.1: Diagram of the data acquisition and analysis pipeline. Participants took part in the ramp protocol (left), imaged using TCD (top-middle), and a subset repeated the protocol in BOLD-fMRI (bottom-middle). The ramp-up component of the TCD, MRI protocols (full and partial) were isolated and plotted as a function of their respective $PETCO_2$ traces with linear and sigmoidal CVR fits (right).

6.2.3 Ramp Protocol

Both modalities imaged the cerebrovascular response to a ramp protocol. A detailed description of the gas delivery apparatus is presented in [170], modified only by using an anaesthetic face mask (Intersurgical, Wokingham, Berkshire, UK) that allowed for gas sampling directly from the mask. The inspired gases were delivered using a custom gas delivery system built in-house at the University of Oxford where respiratory gas mixtures could be delivered one at a time at 15 L/min.

The ramp protocol consisted of 3 repetitions of 5 deep breaths, followed by 30 s of regular breathing on synthetic medical air (21 % O_2 / 79 % N_2), 40 s breathing a 5 % CO_2 balance air gas mixture (BOC Group, Linde, Surrey, UK), and 40 s breathing a 10 % CO_2 balance air gas mixture (BOC Group, Linde, Surrey, UK). Participants were trained prior to starting the ramp protocol to take full deep breaths without pauses and were allowed to test breathing each of the gases. This testing period was also used to check for leaks at the mask-face interface identified via the capnometry trace and the mask was adjusted as needed.

6.2.3.1 TCD Acquisition

The first method used to characterise the dynamics of the cerebral blood flow response to the ramp protocol was the blood flow velocity, measured in the left MCA continuously using a 2 MHz probe and clinical TCD (7760EN Doppler-BoxX Digital, Compumedics DWL). With the participant lying supine, the TCD probe was placed on the transtemporal window with transmission gel and was secured using an adjustable headset. The location and angle of the probe was changed until a consistent blood flow velocity profile was achieved. The deep breathing instructions were given verbally and the participants were notified when the gases were changed and for the last 10 s of breathing the 10 % CO_2 gas mixture.

6.2.3.2 MRI Acquisition

In the second session, participants completed the same ramp breathing protocol whilst BOLD-fMRI was acquired in a 3T Siemens Prisma scanner with a 32-channel head coil (GE-EPI sequence, TR/TE = 800/30 ms, MB = 6, 2.4 mm isotropic). A high-

resolution MPRAGE structural image was also acquired (1 mm isotropic, TR/TE = 1900 ms/3.97 ms).

The delivery of the gases in the ramp protocol was performed using an automated valve controller to switch between the gases and triggered directly by the MRI scanner, designed in-house [398]. This automated gas delivery was combined with timed visual cues to instruct participants when to take their deep breaths and providing a countdown for the last 10 s on the 10 % CO_2 gas mixture, mimicking what was done in Session 1.

6.2.4 Preprocessing

Data processing and analysis was performed using FSL 6.0 [196] and custom Python scripts. The end-tidal CO_2 ($PETCO_2$) peaks were selected automatically using peak detection from the SciPy package [426] and were used as a surrogate for arterial $PaCO_2$ [387].

For the TCD signal, a rolling mean of the MCAv was used to smooth the pulsatile signal (MCA$\overline{v}$). A low-pass filter was applied to the MCA$\overline{v}$ and $PETCO_2$ time courses with a window size of 50 samples (corresponding to 0.25 s), resulting in an effective cutoff frequency of 2 Hz. The filter was implemented using the rolling mean method in Python's Pandas library [405] to smooth high-frequency noise while preserving the physiological signal's key characteristics. MCA$\overline{v}$ was normalised relative to the baseline period to correct for probe angle variations. Only the three ramp-up, blood vessel dilation components of the protocol were isolated for further analysis to prioritise consistency in the modelling process and reduce potential variability as the dynamics for dilation and constriction may differ [472].

The BOLD-fMRI images underwent standard preprocessing that included motion correction, spatial smoothing (FWHM = 4 mm), fieldmap correction, and high pass filtering (275 s). The mean BOLD signal was calculated across active voxels of the right parietal lobe using the MNI152 brain atlas to ensure comparability with the MCA region evaluated with TCD [88][270]. Active voxels were determined by performing voxel-wise general linear modelling and selecting voxels with a z-score > 3.1.

To account for delays in both signals, a bulk shift was applied to each $PETCO_2$ trace to maximise its cross-correlation with the mean MCA$\overline{v}$ or BOLD signal (mean across subjects of -22 $\pm$ 4 s for the MCA$\overline{v}$ and -6 $\pm$ 5 s for the BOLD signal).

6.2.5 Data Analysis

To characterise CVR, both linear and sigmoidal models were fitted to the $PETCO_2$ vs. normalised MCA$\overline{v}$, and $PETCO_2$ vs. % BOLD signal. In the linear model the normalised signal response (MCA$\overline{v}$ or % BOLD), denoted by $\Delta S/S_0$, was fit with slope (m) and y-intercept (int), as shown in Equation (6.1).

$$\frac{\Delta S}{S_0} = m \cdot PETCO_2 \; + \; int \tag{6.1}$$

This linear model was applied to the full ramp data, as well as a partial ramp, segmented at 5 mmHg below baseline and 15 mmHg above baseline, to investigate the agreement between a more common CVR range induced by a 5 % CO_2 gas mixture alone. The partial range reflects the typical range used in many CVR studies employing up to 5 % CO_2, which is widely accessible and commonly used due to high

tolerability and ease of implementation [72][163][388][403]. By focusing on this partial range, our analysis clarifies how TCD- and BOLD-fMRI-derived CVR findings compare between those from previous studies, where CVR responses are often confined to a smaller hypercapnic range.

In the sigmoid model, the normalised signal response, $\Delta S/S_0$ was defined with 4 parameters: the minimum blood flow (a), the slope of the linear regime (1/b), the $PETCO_2$ value for the inflection point (c), and the blood flow span (d). Each parameter was fit to the data for each subject and modality independently. The sigmoid model is shown in Equation (6.2).

$$\frac{\Delta S}{S_0} = a \; + \; \frac{d}{1 + e^{\frac{1}{-b}(PETCO_2 - c)}} \tag{6.2}$$

Additionally, we also tested a 2-parameter sigmoid model, where the normalised signal response, $\Delta S/S_0$ was defined with fixed parameters minimum blood flow (a) and blood flow span (d) (normalised MCA$\overline{v}$: a = 0.2, d = 2.5; % BOLD: a = -8, d = 18) as these were more variable due to the low number of data points at the end ranges of the ramp protocol. In this case, only the slope of the linear regime (1/b), and the $PETCO_2$ value for the inflection point (c) were fit to the data for each subject and modality.

6.2.6 Statistics

Correlation between the modalities of each fitting parameter of interest was tested using the Pearson correlation coefficient ($p < 0.05$ significance). Additionally, the r-value correlation coefficient was used where $r < 0.4$ is attributed to weak correlation, $0.4 \leq r < 0.7$ indicates moderate correlation, and $r \geq 0.7$ indicates strong correlation [368].

A paired-samples t-test was performed to determine whether the baseline $PETCO_2$ values measured by TCD and MRI differed significantly.

6.3 Results

Thirty-three participants attended the first session (TCD), and 30 successfully completed the ramp protocol. Twenty-five participants came back for the second session (MRI) and all completed the ramp protocol. Data from 1 participant were not included in the analysis due to high noise levels. Across all subjects included in the analysis (N = 24), the mean change in $PETCO_2$ from the bottom of the ramp to peak hypercapnia was 27.5 ± 3.9 mmHg in TCD and 28.1 ± 4.8 mmHg in MRI (t-statistic = -0.509, p = 0.616). The mean baseline $PETCO_2$ during the TCD and MRI was 39.5 ± 3.9 mmHg and 43.2 ± 3.6 mmHg respectively (t-statistic = -6.115, p « 0.01). The average MCA$\overline{v}$ across subjects ranged from 79 ± 11 % to 170 ± 20 % of baseline and the average BOLD signal span was 7.1 ± 1.3 %. The TCD blood velocity measure and BOLD-fMRI signal, each with their corresponding CO_2 trace, for a representative subject is shown in Figure 6.2. The rolling mean blood velocity signal, MCA$\overline{v}$, is overlaid on the TCD signal, and the $PETCO_2$ points and interpolation are overlaid on the CO_2 signal. It should be noted that no significant trends between sexes or age groups were observed in the CVR parameters (see Table B.1 in Appendix B for a summary of the effects of sex and age on the CVR parameters).

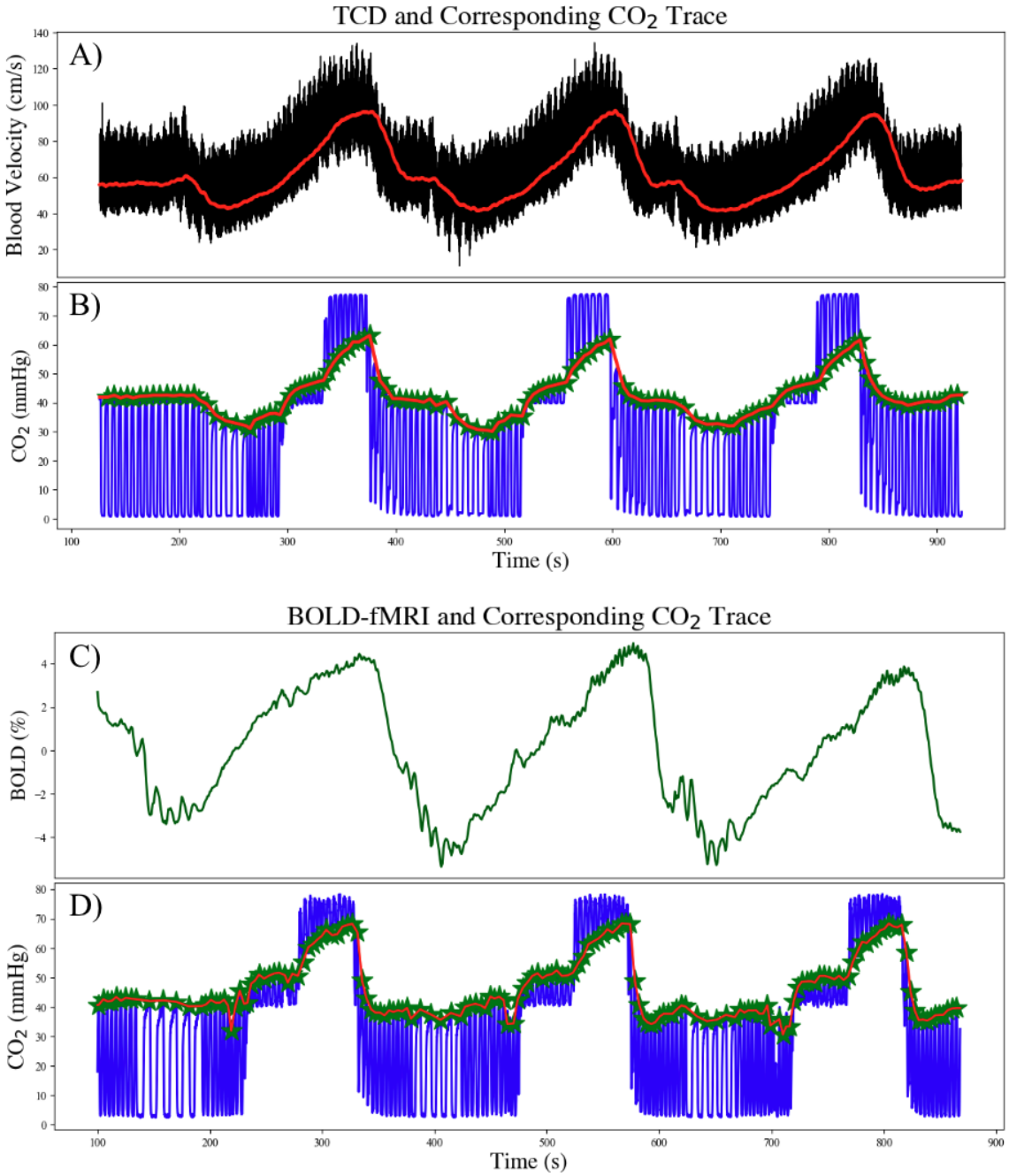

Figure 6.2: Signal traces during the ramp protocol of A) the TCD blood velocity (black) and rolling mean (red), B) the TCD CO_2 trace (black), $PETCO_2$ points (green stars) and interpolated $PETCO_2$ (red), C) percent BOLD-fMRI signal, and D) the MRI CO_2 trace (black), $PETCO_2$ points (green stars), and interpolated $PETCO_2$ (red). All plots are of a representative subject (MR-021).

Comparison plots between the slope of the linear fit (m) of the TCD ($PETCO_2$ vs. $MCA\overline{v}$) and BOLD-fMRI ($PETCO_2$ vs. % BOLD) CVR for the full ramp and partial

ramp are presented in Figure 6.3. The linear slopes both showed significant correlation between modalities for both the full ramp (p = 0.005, r = 0.559) and partial ramp (p = 0.001, r = 0.621).

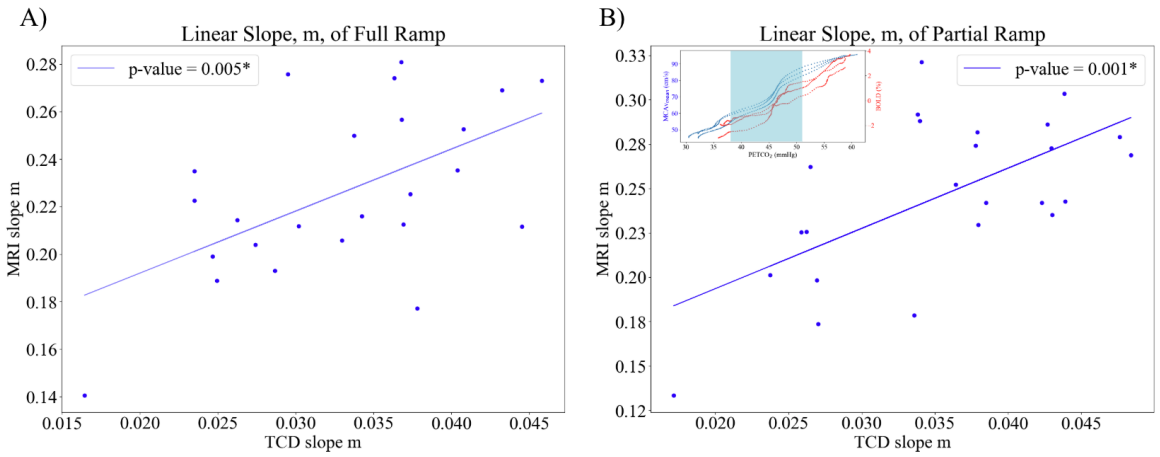

Figure 6.3: Parameter comparison plots between TCD and MRI of A) the linear slope parameter (m, signal$_{norm}$/mmHg) of the full ramp, and B) the linear slope parameter (m, signal$_{norm}$/mmHg) of the partial ramp.

Comparison plots between the 4-parameter sigmoidal fit of the TCD ($PETCO_2$ vs. $MCA\overline{v}$) and BOLD-fMRI ($PETCO_2$ vs. % BOLD) CVR for the full ramp are presented in Figure 6.4. Using all 4 parameters, extreme values for the span were obtained for many participants. No correlation was observed between modalities for the sigmoid minimum (p = 0.856, r = -0.039), slope (p = 0.633, r = -0.103), inflection point (p = 0.292, r = 0.224), and span (p = 0.685, r = 0.087).

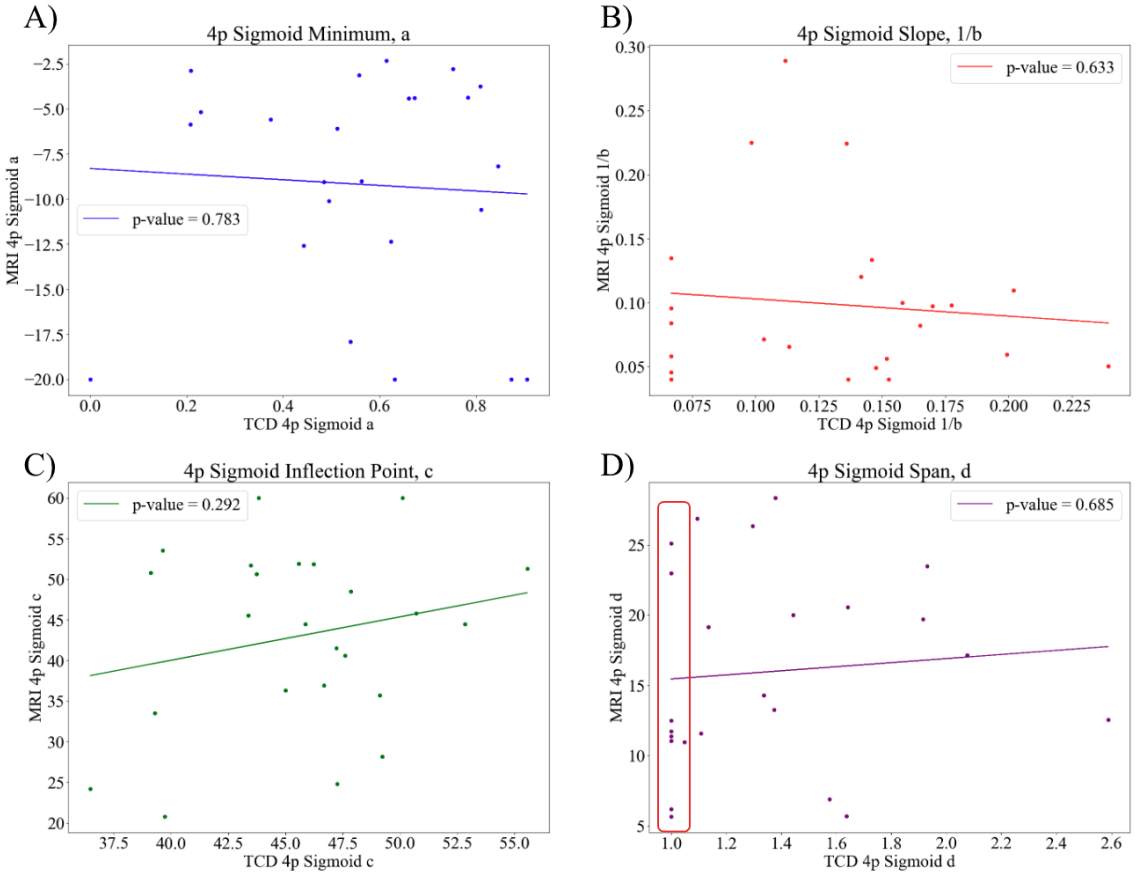

Figure 6.4: Parameter comparison plots between TCD and MRI of the 4-parameter sigmoid A) minimum signal parameter (a, signal_{norm}), B) slope parameter (1/b, signal_{norm}/mmHg), C) inflection point parameter (c, mmHg), and D) signal span parameter (d, signal_{norm}). A cluster of extreme values for the signal span (d) are circled in red.

Comparison plots between the 2-parameter sigmoidal fit of the TCD ($PETCO_2$ vs. MCA$\overline{v}$) and BOLD-fMRI ($PETCO_2$ vs. % BOLD) CVR for the full ramp are presented in Figure 6.5. In the 2-parameter fit, the minimum blood flow (a), and blood flow span (d) parameters were fixed and only the slope of the linear regime (1/b), and the $PETCO_2$ value for the inflection point (c) were fit. Significant correlation between modalities was found for the sigmoid slope ($p = 0.005$, $r = 0.557$) and the inflection point ($p = 0.016$, $r = 0.485$).

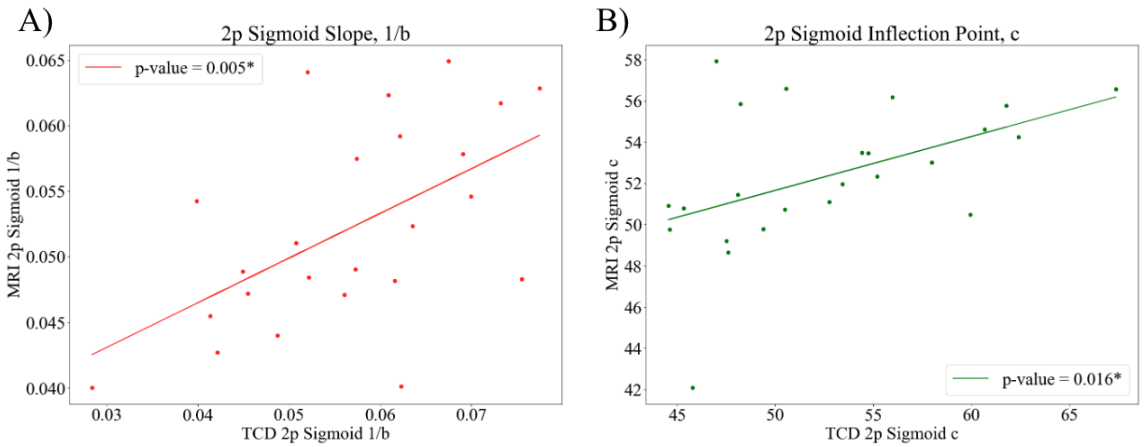

Figure 6.5: Parameter comparison plots between TCD and MRI of the 2-parameter sigmoid A) slope parameter (1/b, signal_{norm}/mmHg), and B) inflection point parameter (c, mmHg).

6.4 Discussion

This study compared CVR measured via TCD and BOLD-fMRI under a ramped hypercapnic stimulus. Our findings reveal significant correlations between modalities, particularly using linear CVR fitting and using a sigmoidal CVR fit with fixed minimum and maximum values for the response signal. Our results also highlight challenges with non-linear modelling of CVR using both TCD and BOLD-fMRI for characterising cerebrovascular dynamics.

6.4.1 Baseline Values and Response Magnitudes

The mean baseline $PETCO_2$ values of 39.5 ± 3.9 mmHg (TCD) and 43.2 ± 3.6 mmHg (MRI) align with the expected range of 35 - 45 mmHg for healthy adults [36][85][383]. The elevation in MRI baseline $PETCO_2$ compared to TCD was significant (t-statistic = -6.115, p « 0.01) and may reflect the enclosed environment of the MRI bore, which could

lead to reduced ventilation. Nevertheless, the $PETCO_2$ changes due to our ramp protocol in both tested methods (TCD and MRI) were not significantly different (t-statistic = -0.509, p = 0.616). Blood velocity changes ranging from 79 ± 11 % to 170 ± 20 % of baseline exceed those reported in previous ramp protocols by 20 - 50 % since other ramp protocols primarily employ lower concentrations of CO_2 [31][85][117][350]. The BOLD signal span of 7.1 ± 1.3 % BOLD is comparable to or exceeds values obtained using computerised $PETCO_2$ targeting methods at 3 T that target $PETCO_2$ between 46 and 60 mmHg (∼5 % BOLD signal) [38][383], with a slightly larger span (∼9 % BOLD signal) observed at 7 T [37]. These findings suggest that the ramp protocol employed here induced a robust cerebrovascular response.

6.4.2 Linear Relationships and Modality Agreement

Our results indicate significant linear correlations between TCD and BOLD-fMRI across ramp segments. For the partial ramp (spanning 20 mmHg), the linear fit demonstrated strong intermodal agreement (p = 0.001, r = 0.621). Similarly, the full ramp analysis revealed significant correlations (p = 0.005, r = 0.559). These findings support the utility of linear modelling in capturing consistent CVR responses, even across differing vascular territories assessed by TCD and BOLD-fMRI [120]. Importantly, this extends prior work showing linearity within smaller $PETCO_2$ spans (∼3 - 8 mmHg) to include larger ranges, such as up to the 20 mmHg used in this study [38][31][117]. Notably, this suggests that CVR values obtained using methods that employ a linear assessment of CVR are still comparable between BOLD-fMRI and TCD. This is the case with larger stimuli range up to 30 mmHg as shown by the linear fit of the full

ramp, as well as with a stimulus range of 20 mmHg as shown by the linear fit of the partial ramp, which approximates the upper bound of what is achieved using up to a 5 % CO_2 gas mixture [72][163][388][403].

However, a 2-point measure with a measurement taken at baseline and during hypercapnia may not always provide sufficient information for an accurate CVR as suggested by the lack of correlation between BOLD-fMRI and TCD found by Burley et al. [55]. Burley et al., observed no correlation between TCD and BOLD-derived CVR using fixed inspiration of 5 % CO_2 air in elderly and young adult participants [55]. Burley et al. employed a steady-state approach, where measurements were taken only at baseline and during a fixed hypercapnic plateau and may have missed transient or dynamic vascular responses that could contribute to intermodal agreement, especially with the smaller hypercapnic stimulus in achieved with 5 % CO_2 (∼15 - 20 mmHg).

Differences in vascular territories assessed by each modality may also play a role. TCD measures MCA flow velocity, predominantly reflecting large-vessel dynamics, whereas BOLD-fMRI integrates oxygenation changes across both macrovascular and microvascular territories. These differences could lead to reduced agreement in studies using steady-state methods, as vascular responses in microcirculatory regions may not align with large-vessel dynamics. Furthermore, Burley et al.'s participant cohort included elderly individuals, where vascular compliance and neurovascular coupling may be more variable or impaired compared to younger cohorts, potentially contributing to the lack of correlation. In contrast, our ramped protocol provides continuous measurements across a broader $PETCO_2$ range (∼30 mmHg), capturing both transient and sustained CVR responses, which may better account for intermodal differences and yield stronger

correlations between TCD and BOLD-fMRI.

Our results align closely with Fico et al., who demonstrated good agreement between CVR metrics derived from MCAv using TCD and 4D flow MRI with a stepped-hypercapnia protocol of 4 % and 6 % CO_2 [120]. Despite the significant differences between 4D flow MRI and BOLD-fMRI - where the former excels in quantifying blood flow dynamics and the latter only provides a proxy for CBF changes based on oxygen levels [277] - both studies underscore the potential for meaningful intermodal comparisons.

6.4.3 Non-linear Modelling and Parameter Variability

To the authors knowledge, this study is the first comparison between modalities for non-linear CVR mapping in the same subjects. The 4-parameter sigmoid modelling was employed to explore not only the linear response region, but also the inflection point and bounds of the response. However, extreme and variable fits for the minimum flow (a) and span (d) parameters were observed. These inconsistencies stem from limited data at the ends of the ramped response curve, making these parameters highly susceptible to noise, resulting in no correlation between any of the 4 parameters. Fixing the minimum flow (a) and span (d) parameters in the 2-parameter model significantly improved the correlation between modalities for the inflection point and slope with p = 0.005 and p = 0.016 respectively.

Interestingly, prior studies using non-linear modelling of CVR in TCD, MRI, and computational simulations have reported significant plateauing of the CVR response at $PETCO_2$ values above 45 - 50 mmHg [38][106][117][383]. However, based on our re-

sults there may be significant variability in those plateau regions which may impair the accuracy not only of the range of the response but also in the calculation of other parameters, such as the slope and the inflection point. The variability in the plateauing regions between modalities may stem from physiological factors, such as differences in vascular compliance, blood pressure, or autoregulation. Alternatively, the variability may be the result of noise at the end ranges of the ramp protocol where there is less data and a higher likelihood of motion due to participant discomfort.

6.4.4 Limitations

While this study demonstrates significant correlations between TCD and BOLD-fMRI CVR, several limitations should be acknowledged to contextualise the findings. A key limitation in this study is the absence of continuous mean arterial blood pressure monitoring, which restricts our ability to account for systemic blood pressure variations throughout the ramp protocol and between sessions that can influence cerebral blood flow and CVR. Variability in blood pressure between or during sessions introduces noise, potentially affecting measurements from both TCD and MRI [85][440]. To mitigate this, participants were screened for cardiovascular health conditions and a baseline blood pressure measure was acquired while the participants were at rest using an arm cuff to rule out hypertension.

TCD measures are inherently operator-dependent, with factors such as probe placement, insonation angle, and arterial diameter variability contributing to potential inconsistencies across sessions or participants [1][350]. This was mitigated by having the same trained operator acquire all of the TCD data and normalising the MCAv data

relative to baseline. Furthermore, the spatial resolution of TCD, which measures velocity in a single large artery such as the MCA, contrasts with the distributed signals captured by BOLD-fMRI. These inherent differences in spatial resolution and vascular territory coverage may limit the degree of intermodality agreement, particularly in regions influenced by local variations in neurovascular coupling [55][440].

The MRI data acquisition also presents limitations. The BOLD-fMRI signal is an indirect measure of CBF and is susceptible to confounding factors such as noise from physiological fluctuations, including cardiac and respiratory cycles [52]. In this study, we applied motion correction during preprocessing and used a consistent pipeline to extract BOLD responses from the parietal lobe, ensuring comparability with the vascular territory of the TCD measurements.

With the TCD and MRI acquisition sessions taking place on different days (19 $\pm$ 18 days apart), we could not control for all day-to-day differences in participants' physiological or environmental conditions, such as hydration, sleep quality, or stress, which may influence cerebrovascular dynamics, affecting the reproducibility of CVR results [55][249]. Within sessions, variations in the timing of CVR measurements relative to participant acclimation or fatigue could further introduce discrepancies, particularly in baseline $PETCO_2$ or respiratory patterns [468]. To reduce this impact, participants were scheduled for data collection during regular working hours and the ramp protocol was conducted with the participant in a supine position during both TCD and MRI data collection to minimise fluctuations in systemic factors.

A degree of demographic variability (such as in age, sex, and fitness level) was intention-

ally included in this study to assess modality agreement with a range of inter-individual differences. However, with only N = 24 included in this analysis, there is likely to be further variation in CVR responses not captured, affected by demographic, lifestyle, and health factors.

6.4.5 Implications and Future Directions

These results offer valuable insights into the complementary strengths of TCD and BOLD-fMRI. TCD's portability and high temporal resolution make it well-suited for dynamic or real-time monitoring, while BOLD-fMRI's superior spatial resolution provides a comprehensive view of regional vascular responses. The observed significant linear correlations across a wide range of $PETCO_2$ values suggest that these modalities, despite their inherent differences, can provide consistent and complementary measures of CVR.

Non-linear modelling results, particularly the variability observed in sigmoid parameter fits, highlight the methodological challenges in capturing the full complexity of CVR. The limited stability at the response curve's extrema underscores the need for hypercapnic protocols designed to extend the data range and improve reliability in estimating key parameters, such as the inflection point and plateau. Incorporating advanced imaging modalities like arterial spin labelling (ASL) or 4D flow MRI could further refine these analyses by contextualising findings within more detailed assessments of cerebrovascular dynamics, flow patterns, and oxygen metabolism.

Future studies should address systemic limitations, including continuous mean arterial blood pressure monitoring and simultaneous multimodal imaging, to improve in-

termodality comparisons. Additionally, implementing single-session assessments and standardised experimental protocols may help minimise day-to-day variability, such as changes in hydration, stress, or other physiological factors. Expanding participant demographics to include more varied age groups, health statuses, and fitness levels would also enhance the generalisability of findings.

Ultimately, advancing methodological approaches and integrating multimodal imaging strategies will help establish CVR as a reliable biomarker for cerebrovascular health, with potential applications ranging from early detection of vascular pathologies to monitoring treatment efficacy in conditions such as stroke, dementia, and traumatic brain injury. Understanding the relationship between TCD and BOLD-fMRI is crucial for aligning findings across these modalities, particularly given their inherent differences in vascular territories assessed, temporal and spatial resolution, and accessibility. Intermodal comparisons can resolve discrepancies observed in existing studies and ensure that CVR metrics derived from either method are robust and complementary. This is particularly relevant in clinical and research settings where one modality may be preferred due to practical constraints or research goals. By aligning TCD and BOLD-derived metrics, researchers can establish more reliable and generalisable conclusions about cerebrovascular health and disease mechanisms, bridging the gap between foundational research and clinical applications to ensure that CVR measures provide robust and actionable insights into brain health.

6.5 Conclusion

This study evaluated the agreement and challenges of assessing CVR using TCD and BOLD-fMRI during a ramped hypercapnic protocol. Significant linear correlations were observed between modalities across broad $PETCO_2$ ranges, affirming the utility of linear CVR modelling for capturing consistent responses using TCD and MRI. A four-parameter non-linear model demonstrated significant variability in span and bound parameters between modalities. This was improved by fixing these parameters and assessing only the sigmoid slope and inflection point, resulting in significantly better inter-modality correlation. These challenges underscore the importance of careful methodological design, particularly when interpreting the plateau and dynamic ranges of CVR responses. This work contributes to bridging the methodological gaps between which CVR metrics are reliable between TCD and BOLD-fMRI for assessing cerebrovascular physiology. Advancing multimodal CVR measurement techniques is crucial for leveraging CVR as a biomarker for cerebrovascular health, with potential applications in clinical diagnostics and therapeutic monitoring of brain health.

Data Availability

The materials used to support the findings of this research are available from the corresponding author upon reasonable request.

Acknowledgements

The authors would like to thank all the volunteers who participated in this study, the radiographers and professional staff at the Oxford Centre for Human Brain Activity, especially Juliet Semple, Nicola Aikin, David Parker, and Jon Campbell. We would also like to thank Dr. Johannes Klein for providing training on transcranial Doppler ultrasound, and Dr. Sebastian Rieger and Congxiyu Wang for their assistance during the MRI data acquisition.

Funding Acknowledgements

This work was supported by Engineering and Physical Sciences Research Council UK through grant EP/S021507/1. GH was supported by Clarendon, and SS by the Rhodes Trust and the Canadian Institutes of Health Research (DSG-193252).

Declaration of Competing Interests

The authors declare that the research was conducted in the absence of any commercial or financial relationships that could be construed as a potential conflict of interest.

7 | Transcranial Doppler Ultrasound Validation of BOLD-fMRI Cerebral Blood Flow Relationship

Preface

This chapter examines the relationship between transcranial Doppler ultrasound (TCD)-derived cerebral blood flow (CBF) velocity and BOLD-fMRI signals under a ramped CO_2 stimulus. By testing a simplified version of an existing haemodynamic model, the Davis Model, originally developed for BOLD calibration, the study provides the first validation of this framework using TCD. Twenty-five healthy participants underwent both TCD- and MRI-based sessions, revealing that linear fits and the Davis model can reliably capture the interplay between changes in the CBF velocity of the middle cerebral artery and the BOLD signal. These findings position TCD as a practical surrogate for CBF to evaluate BOLD calibration and pave the way for broader clinical and research applications involving TCD and BOLD-fMRI approaches.

This chapter was published as:

> **G. Hayes**, S. Sparks, J. Pinto, and D. P. Bulte, "Transcranial doppler ultrasound validation of BOLD-fMRI cerebral blood flow relationship," *Magn. Reson. Med.*, 2025. doi: 10.1002/mrm.70091.

A subset of these results was presented at the following conference:

> **G. Hayes**, S. Sparks, J. Pinto, and D. P. Bulte, "Transcranial doppler ultrasound

validation of BOLD-fMRI cerebral blood flow relationship," *British Neuroscience Association Festival of Neuroscience*, Apr. 2025, Liverpool, UK.

By affirming the consistency between TCD and BOLD-fMRI measurements, this work underscores the potential for integrating non-invasive ultrasound and MRI methods to advance cerebrovascular research and clinical implementation.

Author Contribution Statement

G. Hayes contributed to the study concept and design, recruitment, and led the data acquisition, analysis and interpretation, and writing of the manuscript. **J. Pinto** contributed to ethics approvals, study design, data acquisition, and critical revision of the manuscript. **S. Sparks** contributed to data acquisition, recruitment, and critical revision of the manuscript. **D. P. Bulte** contributed to the original study concept and design, critical revision of the manuscript, and supervision. All authors read and approved the final manuscript.

Abstract

Purpose: A precise understanding of the interplay between cerebral blood flow (CBF) and blood oxygen level-dependent (BOLD) fMRI signals is essential for advancing cerebrovascular research. This study is the first to evaluate whether an established haemodynamic model can characterise the relationship between BOLD signals and transcranial Doppler (TCD)-measured CBF velocity during a ramp CO_2 stimulus.

Methods: Twenty-five healthy participants underwent two sessions. In Session 1,

right middle cerebral artery velocity (MCAv) was acquired using clinical TCD. In Session 2, 3 T BOLD-fMRI data were collected. Both sessions used a ramp end-tidal CO_2 ($PETCO_2$) protocol with deep breaths followed by 5% and 10% CO_2. Data processing comprised motion correction, spatial smoothing, fieldmap correction, high-pass filtering, and time-shifting of $PETCO_2$ traces to align with respective MCAv or BOLD signals. A simplified haemodynamic model was fit using a range of parameters from the literature, and goodness of fit was assessed by the coefficient of determination (R^2).

Results: Final analysis included 21 participants. Consistent and "good" fits ($R^2 \geq 0.69$) were obtained for the values tested. Linear regression between MCAv and the BOLD signal indicated robust agreement ($R^2 = 0.720$). Our results align well with prior work on BOLD calibration and haemodynamic modelling of the CBF-BOLD relationship.

Conclusion: This research demonstrates that both a simplified haemodynamic model and linear models provide a robust framework for linking TCD-derived MCAv and BOLD-fMRI responses during hypercapnia in humans. These findings highlight TCD as a useful surrogate for CBF in BOLD calibration, providing a foundation for future cerebrovascular research.

7.1 Introduction

Understanding the relationship between cerebral blood flow (CBF) and the blood oxygen level-dependent (BOLD) functional magnetic resonance imaging (fMRI) signal is

critical for cerebrovascular research. Since pioneering work demonstrated the BOLD contrast mechanism, BOLD-fMRI has become a widely used tool for mapping brain function in both clinical and research settings [26][226][302][303]. However, although increases in metabolic activity (e.g., neuronal oxygen consumption) often accompany neural activation, interpreting changes in the BOLD signal solely in terms of these metabolic processes is difficult. This is because the BOLD signal itself arises from a complex interplay among CBF, cerebral blood volume (CBV), and the cerebral metabolic rate of oxygen consumption ($CMRO_2$) [57][130].

These parameters jointly determine the ratio of haemoglobin in the imaging voxel, a critical factor because haemoglobin can exist as paramagnetic deoxyhaemoglobin or diamagnetic oxyhaemoglobin [315]. Consequently, the concentration of deoxyhaemoglobin influences the magnetic susceptibility within and around blood vessels, modulating the MRI signal [302]. At rest, approximately 30-40 % of the oxygen is extracted across the capillary bed, creating a substantial level of deoxyhaemoglobin in venous and capillary vessels [230][320]. During neural activation, CBF increases more than $CMRO_2$, leading to a decrease in deoxyhaemoglobin concentration and an increase in the measured BOLD signal [57][130]. Meanwhile, CBV changes and volume exchange effects further complicate the relationship.

To facilitate the quantitative interpretation of this BOLD signal, the Davis model (also known as the deoxyhaemoglobin dilution model) was introduced, wherein calibrated fMRI methods can be employed to estimate underlying metabolic and haemodynamic parameters [92][182][326]. The classical Davis Model provides a relationship between changes in $CMRO_2$, CBF, and the BOLD signal in fMRI [92][182], as shown in Equa-

tion (7.1):

$$\frac{\Delta \mathrm{BOLD}}{\mathrm{BOLD}_0} = M\left[1 \; - \; \left(\frac{\mathrm{CBF}}{\mathrm{CBF}_0}\right)^{\alpha-\beta} \left(\frac{\mathrm{CMRO}_2}{\mathrm{CMRO}_{2|0}}\right)^{\beta}\right]. \tag{7.1}$$

where M is the scaling factor representing the maximum possible BOLD signal change under ideal conditions (dependent on field strength, baseline oxygenation, and vascular architecture, typically 8-12% in grey matter), α describes the relationship between CBF and venous CBV (typically 0.2-0.4), and β describes the coupling between CBF and $CMRO_2$ in terms of oxygen extraction fraction (typically 1.0-1.5 at 3 T) [54][73][74][92][150][152].

During a ramp hypercapnia protocol, CBF is changed while maintaining $CMRO_2$ relatively constant and therefore the last term of Equation (7.1) will be very close to 1. This has been approximated in Equation (7.2):

$$\frac{\Delta \mathrm{BOLD}}{\mathrm{BOLD}_0} = M\left[1 \; - \; \left(\frac{\mathrm{CBF}}{\mathrm{CBF}_0}\right)^{\gamma}\right]. \tag{7.2}$$

Where $\alpha - \beta$ describes the relationship between CBF, CBV, and $CMRO_2$, essentially characterising the contribution of CBF to the BOLD signal. This assumes an isometabolic response to hypercapnia, though it should be noted that this is still an area of controversy [455], with literature indicating reduced [73][104][454], unchanged [74][194], and increased [178] $CMRO_2$ with hypercapnia.

Typically, calibrated BOLD experiments use arterial spin labelling (ASL) to measure CBF [42][57][95]. ASL is a non-invasive technique that allows quantification of regional CBF by magnetically labelling arterial blood water as an endogenous tracer. Accurate measurement of CBF via ASL requires accounting for factors such as tagging efficiency,

blood T_1 changes, and transit delays [42][57]. Notably, these parameters may change during global vasoactive stimuli and must be measured or adjusted for, depending on the ASL method used, to ensure precise estimates of flow change.

Despite the wide adoption of ASL-based approaches, independent validation of the Davis model using alternative methods for measuring CBF is still missing. Transcranial Doppler (TCD) ultrasound, which measures blood flow velocity in the major cerebral arteries, might provide a promising non-invasive technique to complement and cross-check BOLD-fMRI findings. TCD has been extensively used to assess cerebrovascular reactivity, but to date, there has been no direct validation of the Davis model - or simplified variants thereof, assuming constant $CMRO_2$ - against TCD-derived flow velocity measures.

In this research, we present the first validation of the Davis model using TCD measurements of flow velocity in the middle cerebral artery (MCA), offering insights into the robustness of BOLD-fMRI quantification of CBF changes. By combining these two approaches, we seek to deepen our understanding of the BOLD signal's physiological underpinnings and enhance the interpretive power of fMRI in cerebrovascular research.

7.2 Methods

7.2.1 Data Acquisition

All procedures conformed to institutional research ethics standards and with the Declaration of Helsinki, as detailed in Hayes et al. 2025 [169]. Twenty-five healthy participants (13 Females, 33 ± 11 years) underwent two separate sessions (19 ± 18 days

apart). In the first session, TCD ultrasound (7760EN Doppler-BoxX Digital, Compumedics DWL) was used to measure blood velocity in the MCA, and in the second session, BOLD-fMRI data were acquired with a 3 T Siemens Prisma scanner (GE-EPI sequence, TR/TE = 800/30 ms, MB = 6, 2.4 mm isotropic. 32-channel head coil). A ramp $PETCO_2$ protocol [170] was used in both sessions. This protocol consisted of 3 cycles of deep breaths followed by exposure to air and air mixtures with increasing CO_2 contents (5% and 10% CO_2). End-tidal gases were collected through a face mask for accurate $PETCO_2$ measurement. Detailed descriptions of the participant demographics, ramp protocol, TCD/MRI acquisition parameters, and data preprocessing steps are provided in Hayes et al. 2025 [169].

7.2.2 Data Preprocessing

Data processing and analysis was performed using FSL 6.0 [196] and custom Python scripts. Smoothed TCD MCA blood velocity signals (MCA$\overline{v}$) were calculated using a rolling mean filter to reduce the pulsatile signals, then low-pass filtered to remove high-frequency noise above 2 Hz. MCA$\overline{v}$ was then normalised by dividing the smoothed blood velocity by the baseline blood velocity for each subject. The BOLD-fMRI data underwent standard corrections, including motion correction, spatial smoothing (FWHM = 4 mm), fieldmap correction, and high-pass filtering (275 s). A general linear approach was used to select active voxels with a Z-score > 3.1 and a corrected cluster significance threshold of $P = 0.05$ [446]. The mean BOLD signal was extracted from the right parietal region to align with the vascular territory of the MCA assessed by TCD. The BOLD signal was then shifted so that zero BOLD signal corresponded to

the baseline period. Finally, to account for respiratory delays in each modality, the corresponding $PETCO_2$ trace was time-shifted relative to the TCD or BOLD signal using cross-correlation. For a detailed account of these steps, see Hayes et al. 2025 [169].

7.2.3 Data Analysis

The aligned TCD MCA$\overline{v}$ vs. BOLD-fMRI data were fit with the simplified Davis model (Equation (7.2)) with fixed values of γ, solving only for the optimal M parameter using least squares regression. Values of γ = -1.2, -1.1, -1.0, and -0.9 were used based on values found in previous literature [73][74][92][150][152].

7.2.4 Statistics

Goodness of fit was assessed using the coefficient of determination, R^2, where $R^2 < 0.4$ indicates a poor fit, $0.4 \leq R^2 < 0.6$ indicates a moderate fit, $0.6 \leq R^2 < 0.8$ indicates a good fit, and $R^2 \geq 0.8$ indicates a very strong fit [77][448].

7.3 Results

Data from some participants were excluded due to significant noise or high signal variability. Across all subjects included in the analysis (N = 21), the mean change in $PETCO_2$ from the bottom of the ramp (minimum) to peak hypercapnia (maximum) was 27.8 ± 4.0 mmHg in TCD and 27.6 ± 4.9 mmHg in MRI (t-statistic = 0.175, $p = 0.863$). The mean baseline $PETCO_2$ during the TCD and MRI was 39.7 ± 3.7 mmHg and 43.3 ± 3.7 mmHg respectively (t-statistic = -6.299, $p \ll 0.01$). To align the

MRI and TCD signals, the overlapping $PETCO_2$ range was selected which, on average, ranged from 35.9 ± 4.1 mmHg to 59.6 ± 4.9 mmHg. Within this overlapping $PETCO_2$ range, the average MCA$\overline{v}$ across subjects ranged from 81 ± 7 % to 175 ± 19 % of baseline and the average BOLD signal ranged from -1.4 ± 1.1 % to 4.9 ± 1.0 %, with a maximum of 6.5 % BOLD.

The best fit curves of the linear regression and the Davis model with γ fixed at -1.2, -1.1, -1.0, and -0.9 on top of the combined subject data are presented in Figure 7.1. The optimal M for each γ is 0.080, 0.084, 0.091, and 0.099 respectively. The R^2 as a function of M for each fixed γ is presented in Figure 2. The R^2 of the best fits are 0.696, 0.701, 0.704, and 0.708 respectively, all corresponding to good fits to the data. The linear regression resulted in an R^2 of 0.720. All models were constrained to pass through the baseline point (1.0, 0.0).

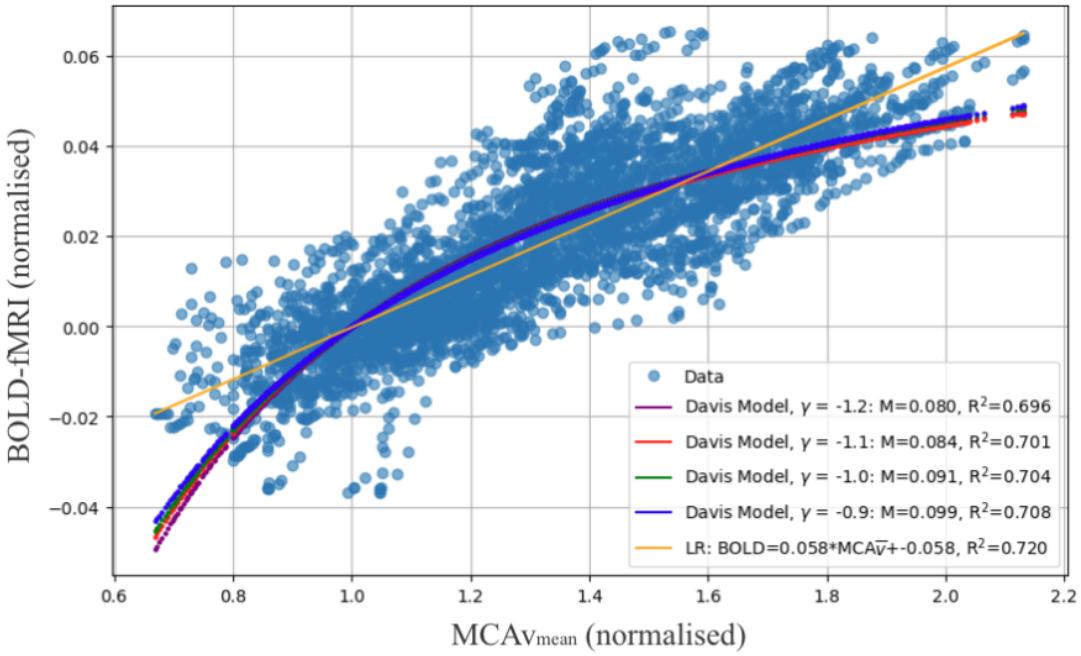

Figure 7.1: Group-level best fits of the Davis model with fixed parameters and corresponding M parameters optimised by least-squares regression. A linear regression (LR) of normalised BOLD signal as a function of normalised MCA$\overline{v}$ is also presented. The R^2 for each fit is presented in the legend.

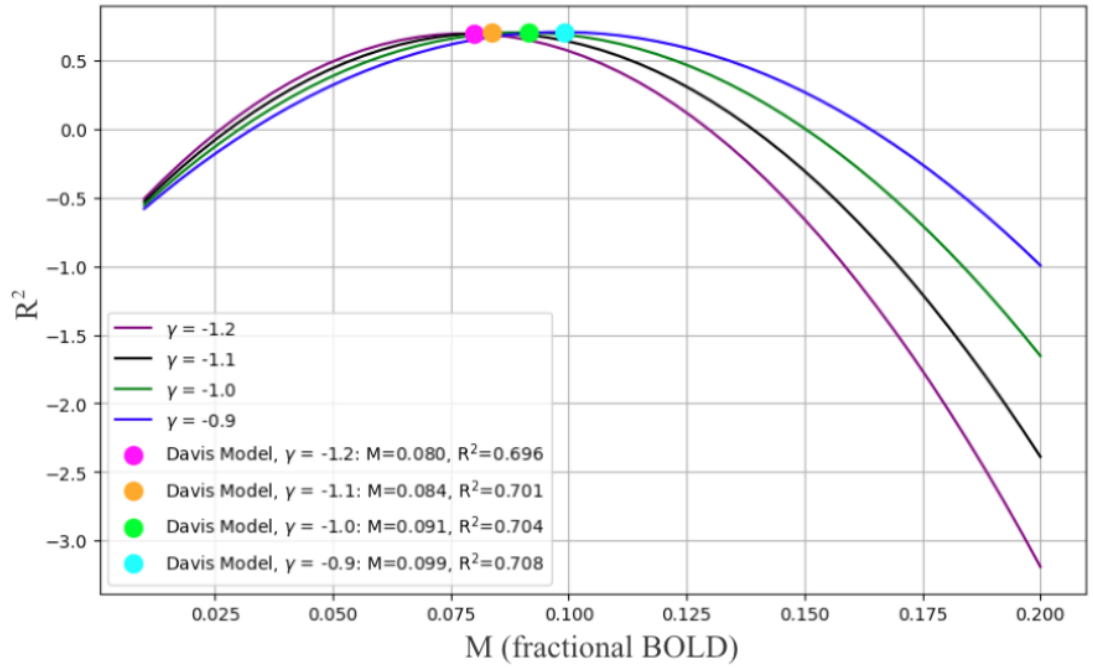

Figure 7.2: Coefficient of determination (R^2) as a function of the M parameter at fixed gammas of -1.2, -1.1, -1.0, and -0.9. The best fit M parameters are highlighted with their corresponding parameters in the legend.

7.4 Discussion

The principal finding of this study is that the simplified Davis model [92][182] provides a robust framework for characterising the relationship between BOLD-fMRI responses and changes in CBF, as proxied by TCD measures of blood velocity in the MCA. By investigating four different γ values (-1.2, -1.1, -1.0, and -0.9), drawn from previous literature [73][92][150][152], we obtained consistent and "good" fits ($R^2 \geq 0.69$). Furthermore, a simple linear regression between MCA$\overline{v}$ and the BOLD signal produced an R^2 of 0.720, indicating robust agreement and reinforcing the notion that BOLD can serve as a useful surrogate for assessing CBF velocity changes during isometabolic stimuli below 6.5 % BOLD signal change.

Our results align well with prior work on BOLD calibration and the Davis model. In the original formulation, Davis et al. (1998) suggested a method to quantify the interplay between the BOLD signal, CBF, and $CMRO_2$. Subsequent studies refined the model parameters, particularly the parameters that go into the γ exponent, highlighting its sensitivity to different field strengths and stimuli [54][73][103][150][162][182]. The γ values tested here span the range reported in these refined calibrations, and our findings support the validity of using these literature-derived values even when the assumption of constant $CMRO_2$ is employed.

Our approach also underscores the utility of TCD measurements as a rapid means of estimating flow changes in large intracranial arteries during hypercapnia challenges. While TCD-based velocity signals cannot directly capture local microvascular changes, prior research has demonstrated that MCAv correlates with more direct measures of

flow [439]. The present work contributes to this body of evidence by linking TCD responses to BOLD signal changes within the Davis model framework and using linear regression.

7.4.1 Impact of the Research

This study is, to our knowledge, the first to test the simplified Davis model using TCD-derived flow velocity measurements. By showing that the fitted M parameter (ranging from 0.080 to 0.099) remains stable across the tested γ values, we provide further support for the robustness and reliability of the Davis model in capturing hypercapnia-induced changes in BOLD signal. Our work indicates that for ramp CO_2 stimuli with an average change in $PETCO_2$ of 28 mmHg, both the simplified Davis model and a linear model can accurately describe BOLD responses, which will be of interest to researchers who require a less resource-intensive methodology than full ASL-based calibrated fMRI.

Moreover, these findings are directly relevant to clinical and translational cerebrovascular research. TCD is widely available in many clinical settings and provides a relatively inexpensive, bedside tool for assessing haemodynamic changes. Demonstrating that TCD can be coupled with BOLD-fMRI, even in separate sessions, to yield consistent physiological inferences, expands the potential for multi-modal validation of fMRI-based CBF measurements.

7.4.2 Limitations

Despite these promising results, several limitations must be acknowledged. TCD only quantifies blood flow velocity in a single large artery (the MCA in our case) rather than whole-brain or region-specific [439]. TCD and BOLD-fMRI data were also collected on different days with up to 83 days between sessions, potentially introducing intra-subject variability (e.g., as a result of sleep, stress levels, hydration status) [239][335]. Furthermore, future studies may benefit from replacing the assumption of isometabolic response to hypercapnia with additional direct measures [42][104]. Although the ramp CO_2 protocol elicited a range of responses that facilitated robust model fitting, variability between subjects in the CVR curve complicated the estimation of parameters such as M and γ without prior physiological constraints. A larger cohort would improve statistical power and the generalisability of the estimated parameters. The number of participants included in the analysis (N = 21) was modest and future research with larger cohorts is warranted to confirm these findings and to further explore physiological factors contributing to inter-individual variability in cerebrovascular responses.

7.5 Conclusion

Our findings demonstrate that the simplified Davis model, anchored by literature-based γ values, offers a strong fit to both BOLD and TCD velocity signals under a ramped hypercapnia protocol. The findings demonstrate reliable modelling of BOLD signal changes up to 6.5 % BOLD signal change, with the strong linear fit supporting BOLD-fMRI as a robust CBF estimate. This "proof-of-concept" technical validation

underscores the potential of integrating TCD as a complementary or surrogate method for quantifying haemodynamic changes in studies that aim to calibrate or interpret BOLD-fMRI data.

Data Availability

The materials used to support the findings of this research are available from the corresponding author upon reasonable request.

Acknowledgements

The authors would like to thank all the volunteers who participated in this study, the radiographers and professional staff at the Oxford Center for Human Brain Activity, especially Juliet Semple, Nicola Aikin, David Parker, and Jon Campbell. We would also like to thank Dr. Johannes Klein for providing training on transcranial Doppler ultrasound, and Dr. Sebastian Rieger and Congxiyu Wang for their assistance during MRI data acquisition.

Funding Acknowledgements

This work was supported by Engineering and Physical Sciences Research Council UK through grant EP/S021507/1. GH was supported by Clarendon, and SS by the Rhodes Trust and the Canadian Institutes of Health Research (DSG-193252).

Declaration of Competing Interests

The authors declare that the research was conducted in the absence of any commercial or financial relationships that could be construed as a potential conflict of interest.

8 | Conclusions and Future Work

8.1 Conclusions

One of the major challenges in cerebrovascular research is the accurate, accessible, and interpretable assessment of cerebrovascular reactivity (CVR). Traditional approaches often fail to capture the full complexity of vascular responses, limiting their clinical applicability and reliability as biomarkers for neurovascular diseases. This thesis set out to advance the field of CVR assessment by developing and validating novel acquisition and analysis methods that improve sensitivity, accessibility, and interpretability. Through the integration of multimodal imaging techniques-including transcranial Doppler ultrasound (TCD), blood oxygen level dependent functional MRI (BOLD-fMRI), and pupillary light response protocols - and the application of innovative modelling approaches such as Bayesian and non-linear frameworks, this work addresses longstanding challenges in capturing the full complexity of vascular responses. By demonstrating the feasibility and accessibility of new CVR protocols, the thesis not only enriches the methodological toolkit available to neurovascular researchers but also underscores the clinical potential of CVR as a biomarker for neurodegenerative disease and other pathologies. The sections that follow delve into the key findings, exploring how integrating vascular smooth muscle cell dynamics, validating complementary modalities, and refining computational models collectively inform the next generation of cerebrovascular research and clinical tools.

8.1.1 Integrating Vascular Physiology with Neurodegenerative Disease

In **Chapter 2**, we reviewed the critical role of vascular smooth muscle cells (VSMC) in neurodegenerative disorders and identified key mechanisms - such as altered VSMC phenotype, dysregulated signaling pathways, and oxidative stress interactions - that may underpin disease progression. The chapter underscored the potential of CVR and cerebral blood flow (CBF) measurements as tools to characterise VSMC dysfunction *in vivo*, highlighting the necessity for more targeted studies to isolate VSMC contributions within complex neurodegenerative pathologies.

8.1.2 Exploring Novel Relationships between Ocular and Cerebral Dynamics

Chapter 3 provided the first investigation into the relationship between pupillary light response (PLR) dynamics and CVR. The finding of a significant negative correlation between PLR latency in a dark flash protocol and CVR establishes an intriguing link between autonomic ocular responses and cerebrovascular health. This opens the door for further exploration of the PLR as a non-invasive biomarker that may complement existing CVR assessment techniques with very little added expense.

8.1.3 Advancements in CVR Mapping through Bayesian and Non-linear Modelling

Chapter 4 compared traditional linear General Linear Models with variational Bayesian (VB) approaches for CVR mapping using breath-hold BOLD-fMRI data. Both methodologies yielded robust amplitude and delay maps in grey matter that aligned with previous literature, with VB offering advantages such as continuous delay estimation and faster computation. These findings support the feasibility of Bayesian modelling to provide a more physiologically informed approach (via treating variables as probability distributions and incorporating prior knowledge into the model) and a computationally efficient framework for interpreting cerebrovascular dynamics.

In **Chapter 5**, a low-cost, TCD-based method for capturing the non-linear features of CVR was developed and validated using a $PETCO_2$ ramp protocol. The improved fit of non-linear sigmoid models over linear models, enhanced by Bayesian techniques incorporating physiological priors, demonstrates the protocol's potential as an accessible and low-cost entry point for studying complex CVR dynamics. In Chapter 6, these models were then refined by assessing CVR using the ramp protocol in a larger cohort imaged using both TCD and BOLD-fMRI.

8.1.4 Bridging Modalities and Validating Underlying Models

Chapter 6 addressed the challenges inherent in comparing CVR measurements obtained via TCD and BOLD-fMRI. The significant linear correlations between modalities across varying $PETCO_2$ levels validate the utility of linear CVR modelling; however,

they lack the range and inflection parameters from non-linear models. The refinement of non-linear modelling parameters improved inter-modality agreement, underscoring the importance of careful methodological design when interpreting the plateau and dynamic ranges of CVR responses.

Finally, **Chapter 7** validated the simplified Davis model for linking BOLD-fMRI signal changes with TCD-measured CBF. The strong linear relationship observed up to a 6.5 % BOLD signal change provides robust evidence that BOLD-fMRI can serve as a reliable proxy for CBF estimation, further solidifying the model's applicability in both research and clinical settings.

8.2 Limitations and Future Directions

Several limitations impacted the scope and timing of this research. Notably, a delay in data acquisition by one year - stemming from delays in the ethics approval processes and the constraints imposed by the COVID-19 pandemic-limited the early development of the methods presented. In addition, while this work explored non-linear CVR methods and PLR assessments, comparisons with more advanced computerised end-tidal forcing systems were not conducted due to their high cost and were not in the scope of the early development work presented in this thesis.

A further limitation apparent throughout the thesis is the absence of continuous arterial blood pressure (ABP) measurements. Although a baseline blood pressure measurement was taken using an arm cuff for all subjects in the Eye-Brain Studies, continuous ABP was not acquired. Some studies indicate that spontaneous or CO_2-driven ABP fluctua-

tions can influence CBF velocity and CVR [184][345][440], while others suggest minimal impact in healthy adults with intact cerebral autoregulation [108][31][445]. Future investigations, particularly in populations with potential autoregulatory impairments, would benefit from continuous ABP monitoring to capture subtle haemodynamic effects.

The Bayesian models employed in this work generally utilised wide priors, reflecting the current lack of detailed research on the physiological bounds of cerebrovascular dynamics. As further studies provide more robust data on these bounds, refining the Bayesian models will be essential to improve the personalisation and accuracy of CVR modelling. Such refinements must be balanced carefully to mitigate research-induced and population-based biases that could arise from over-constraining the models.

While the temporal features of CVR were primarily explored in Chapter 4 with the breath-hold BOLD-fMRI data, there is substantial promise in further investigating these features in both health and disease. A more in-depth temporal analysis could yield valuable insights into the dynamics of cerebrovascular regulation and its alterations under pathological conditions. For example, even if the amplitude in the CVR response is preserved, if there is a significant temporal delay for that response to take place, regionally or globally, it could indicate a risk factor or the presence of neurovascular pathology. This has been shown to be the case in Parkinson's disease [361], occlusion [334], Moyamoya disease [101], and sickle cell disease [236].

Another significant limitation is the relatively small sample sizes (10 - 25 healthy adults per study), which constrain the statistical power and generalisability of the physiolog-

ical findings and precluded a robust statistical exploration of differences related to sex, age, and lifestyle factors. These initial studies were designed primarily to prove method and model concepts rather than to provide definitive population-level statistics. There is a clear opportunity for future studies to investigate whether non-linear modelling approaches vary with these demographic and lifestyle variables. Moreover, the models and methods have not yet been tested in participants with pathological conditions. Future research should extend these protocols to larger and more diverse cohorts, including patient groups, to assess the clinical utility of these approaches.

Although our ramp protocol and associated models offer a cost-effective and accessible means to quantify CBF dynamics, their applicability in pathological conditions remains uncertain. Non-linear CVR is an emerging area that could provide deeper insights into cerebrovascular health and disease. However, our current findings are based on Bayesian priors derived from healthy adults, and different modelling approaches may be necessary for diseased states. Existing studies have shown altered CVR patterns in conditions such as moyamoya disease [94][171][250][364] and in other conditions including stroke [221][263][256], cognitive decline [61][349][18][422], and traumatic brain injury [81][89][295]. Expanding non-linear CVR assessments to include such pathological cohorts will be crucial for validating the clinical applicability of these methods and to identify if specific priors could be used to guide the diagnosis or treatment of pathology.

Collectively, these limitations provide clear directions for future research. Future studies should aim to refine model confidence metrics, optimise Bayesian priors based on emerging physiological data, and incorporate continuous arterial blood pressure mon-

itoring where feasible to further improve CVR measurement accuracy. Additionally, expanding research to larger, more diverse cohorts - including participants with cerebrovascular and neurodegenerative diseases - is essential for translating these methods into clinical practice. By addressing these challenges, future work can enhance the clinical utility of CVR as a biomarker, ultimately contributing to improved diagnostics and therapeutic monitoring in neurovascular health.

8.3 Final Remarks

Taken together, the research presented in this thesis highlights the potential of advanced cerebrovascular reactivity assessment methods in both research and clinical care. By bridging TCD and BOLD-fMRI approaches, integrating pupillometry for complementary measures, and employing robust Bayesian and non-linear modelling frameworks, this work demonstrates that CVR can be quantified with greater sensitivity, specificity, and accessibility than previously possible. The findings lay a critical foundation for detecting vascular dysfunction at earlier stages of neurodegenerative disease and for refining clinical decision making to support cerebrovascular health.

Beyond establishing a stronger methodological basis for CVR measurement, this thesis underscores the value of multimodal and non-invasive techniques as future mainstays of neurovascular assessment. The incorporation of ocular biomarkers, such as the PLR, opens additional avenues for uncovering new markers of cerebrovascular health. These approaches also show promise for resource-limited settings, where cost-effective diagnostics are essential. As technology advances and these methods become more

streamlined, it is conceivable that routine CVR assessment will play a pivotal role in personalising treatment and improving patient outcomes. Ultimately, by enhancing our ability to measure and interpret CVR in a range of contexts, the work presented here moves us closer to a future in which neurovascular diagnostics are more accurate, accessible, and responsive to the individual needs of patients.

Bibliography

[1] R. Aaslid, T. M. Markwalder, and H. Nornes, "Noninvasive transcranial doppler ultrasound recording of flow velocity in basal cerebral arteries," eng, *Journal of Neurosurgery*, vol. 57, no. 6, pp. 769–774, Dec. 1982, ISSN: 0022-3085. DOI: 10.3171/jns.1982.57.6.0769.

[2] S. AbdAlla, A. Langer, X. Fu, and U. Quitterer, "Ace inhibition with captopril retards the development of signs of neurodegeneration in an animal model of alzheimer's disease," en, *International Journal of Molecular Sciences*, vol. 14, no. 88, pp. 16 917–16 942, Aug. 2013, ISSN: 1422-0067. DOI: 10.3390/ijms140816917.

[3] J. A. Aguilar-Pineda, K. J. Vera-Lopez, P. Shrivastava, *et al.*, "Dysfunctional vascular smooth muscle cells mediate early and late-stage neuroinflammation and tau hyperphosphorylation," en, p. 2021.04.13.439741, Apr. 2021. DOI: 10.1101/2021.04.13.439741.

[4] J. A. Aguilar-Pineda, K. J. Vera-Lopez, P. Shrivastava, *et al.*, "Vascular smooth muscle cell dysfunction contribute to neuroinflammation and tau hyperphosphorylation in alzheimer disease," *iScience*, vol. 24, no. 9, p. 102 993, 2021. DOI: 10.1016/j.isci.2021.102993.

[5] P. N. Ainslie and J. Duffin, "Integration of cerebrovascular co2 reactivity and chemoreflex control of breathing: Mechanisms of regulation, measurement, and interpretation," *American Journal of Physiology-Regulatory, Integrative and Comparative Physiology*, vol. 296, no. 5, R1473–R1495, May 2009, ISSN: 0363-6119. DOI: 10.1152/ajpregu.91008.2008.

[6] O. Aktas, P. Küry, B. Kieseier, and H.-P. Hartung, "Fingolimod is a potential novel therapy for multiple sclerosis," en, *Nature Reviews Neurology*, vol. 6, no. 77, pp. 373–382, Jul. 2010, ISSN: 1759-4766. DOI: 10.1038/nrneurol.2010.76.

[7] S. Al-Bachari, L. M. Parkes, R. Vidyasagar, *et al.*, "Arterial spin labelling reveals prolonged arterial arrival time in idiopathic parkinson's disease," en, *NeuroImage: Clinical*, vol. 6, pp. 1–8, Jan. 2014, ISSN: 2213-1582. DOI: 10.1016/j.nicl.2014.07.014.

[8] R. Aldea, R. O. Weller, D. M. Wilcock, R. O. Carare, and G. Richardson, "Cerebrovascular smooth muscle cells as the drivers of intramural periarterial drainage of the brain," *Frontiers in Aging Neuroscience*, vol. 11, p. 1, 2019, ISSN: 1663-4365. DOI: 10.3389/fnagi.2019.00001.

[9] P. W. Alford, B. E. Dabiri, J. A. Goss, M. A. Hemphill, M. D. Brigham, and K. K. Parker, "Blast-induced phenotypic switching in cerebral vasospasm," *Proceedings of the National Academy of Sciences*, vol. 108, no. 31, pp. 12 705–12 710, Aug. 2011. DOI: 10.1073/pnas.1105860108.

[10] N. C. Alonzo, B. T. Hyman, G. W. Rebeck, and S. M. Greenberg, "Progression of cerebral amyloid angiopathy: Accumulation of amyloid-β40 in Affected Vessels," *Journal of Neuropathology & Experimental Neurology*, vol. 57, no. 4, pp. 353–359, Apr. 1998, ISSN: 0022-3069. DOI: 10.1097/00005072-199804000-00008.

[11] M. Alwatban, D. L. Murman, and G. Bashford, "Cerebrovascular reactivity impairment in preclinical alzheimer's disease," eng, *Journal of Neuroimaging: Official Journal of the American Society of Neuroimaging*, vol. 29, no. 4, pp. 493–498, Jul. 2019, ISSN: 1552-6569. DOI: 10.1111/jon.12606.

[12] F. Amyot, C. Davis, M. Sangobowale, *et al.*, "Cerebrovascular reactivity measurement with functional near infrared spectroscopy," eng, *Journal of Visualized Experiments: JoVE*, no. 184, Jun. 2022, ISSN: 1940-087X. DOI: 10.3791/61284.

[13] K. Andrade, O. Pontes-Neto, J. Leite, A. Santos, O. Baffa, and D. Araujo, "Quantitative aspects of brain perfusion dynamic induced by bold fmri," gd, *Arq. Neuropsiquiatr*, vol. 64, pp. 895–898, 2006. DOI: 10.1590/S0004-282X2006000600001.

[14] L. G. Apostolova, L. Mosconi, P. M. Thompson, *et al.*, "Subregional hippocampal atrophy predicts alzheimer's dementia in the cognitively normal," *Neurobiology of Aging*, vol. 31, no. 7, pp. 1077–1088, Jul. 2010, ISSN: 0197-4580. DOI: 10.1016/j.neurobiolaging.2008.08.008.

[15] M. T. Armentero, A. Pinna, S. Ferré, J. L. Lanciego, C. E. Müller, and R. Franco, "Past, present and future of a2a adenosine receptor antagonists in the therapy of parkinson's disease," en, *Pharmacology & Therapeutics*, vol. 132, no. 3, pp. 280–299, Dec. 2011, ISSN: 0163-7258. DOI: 10.1016/j.pharmthera.2011.07.004.

[16] A. Aron, M. Gluck, and R. Poldrack, "Long-term test-retest reliability of functional mri in a classification learning task," en, *NeuroImage*, vol. 29, pp. 1000–1006, 2006. DOI: 10.1016/j.neuroimage.2005.08.010.

[17] D. Arteaga, M. Strother, C. Faraco, *et al.*, "The vascular steal phenomenon is an incomplete contributor to negative cerebrovascular reactivity in patients with symptomatic intracranial stenosis," en, *J. Cereb. Blood Flow Metab*, vol. 34, pp. 1453–1462, 2014. DOI: 10.1038/jcbfm.2014.106.

[18] V. Aslanyan, W. J. Mack, N. E. Ortega, *et al.*, "Cerebrovascular reactivity in alzheimer's disease signature regions is associated with mild cognitive impairment in adults with hypertension," en, *Alzheimer's & Dementia*, vol. 20, no. 3, pp. 1784–1796, 2024, ISSN: 1552-5279. DOI: 10.1002/alz.13572.

[19] K. Asraf, N. Torika, R. N. Apte, and S. Fleisher-Berkovich, "Microglial activation is modulated by captopril: In vitro and in vivo studies," *Frontiers in Cellular Neuroscience*, vol. 12, 2018, ISSN: 1662-5102. DOI: 10.3389/fncel.2018.00116.

[20] H. Attias, "A variational bayesian framework for graphical models," en, in *Proceedings of the 12th International Conference on Neural Information Processing Systems, NIPS'99*, Cambridge, MA, USA: MIT Press, 1999, pp. 209–215.

[21] D. Attwell, A. M. Buchan, S. Charpak, M. Lauritzen, B. A. MacVicar, and E. A. Newman, "Glial and neuronal control of brain blood flow," en, *Nature*, vol. 468, no. 73217321, pp. 232–243, Nov. 2010, ISSN: 1476-4687. DOI: 10.1038/nature09613.

[22] S. Atwi, H. Shao, D. E. Crane, *et al.*, "Bold-based cerebrovascular reactivity vascular transfer function isolates amplitude and timing responses to better characterize cerebral small vessel disease," en, *NMR in Biomedicine*, vol. 32, no. 3, e4064, 2019, ISSN: 1099-1492. DOI: 10.1002/nbm.4064.

[23] J. T. Baeten, A. R. Jackson, K. M. McHugh, and B. Lilly, "Loss of notch2 and notch3 in vascular smooth muscle causes patent ductus arteriosus," en, *genesis*, vol. 53, no. 12, pp. 738–748, 2015, ISSN: 1526-968X. DOI: 10.1002/dvg.22904.

[24] J. Baeten and B. Lilly, "Notch signaling in vascular smooth muscle cells," *Advances in pharmacology (San Diego, Calif.)*, vol. 78, pp. 351–382, 2017, ISSN: 1054-3589. DOI: 10.1016/bs.apha.2016.07.002.

[25] T. G. Bailey, T. Klein, A. L. Meneses, *et al.*, "Cerebrovascular function and its association with systemic artery function and stiffness in older adults with and without mild cognitive impairment," *European Journal of Applied Physiology*, vol. 122, no. 8, pp. 1843–1856, 2022, ISSN: 1439-6319. DOI: 10.1007/s00421-022-04956-w.

[26] P. A. Bandettini, E. C. Wong, R. S. Hinks, R. S. Tikofsky, and J. S. Hyde, "Time course epi of human brain function during task activation," en, *Magnetic Resonance in Medicine*, vol. 25, no. 2, pp. 390–397, 1992, ISSN: 1522-2594. DOI: 10.1002/mrm.1910250220.

[27] R. Bandopadhyay, A. E. Kingsbury, M. R. Cookson, *et al.*, "The expression of dj-1 (park7) in normal human cns and idiopathic parkinson's disease," eng, *Brain: A Journal of Neurology*, vol. 127, no. Pt 2, pp. 420–430, Feb. 2004, ISSN: 0006-8950. DOI: 10.1093/brain/awh054.

[28] J. N. Barnes, R. E. Harvey, K. B. Miller, *et al.*, "Cerebrovascular reactivity and vascular activation in postmenopausal women with histories of preeclampsia," *Hypertension*, vol. 71, no. 1, pp. 110–117, 2018, ISSN: 0194-911X. DOI: 10.1161/hypertensionaha.117.10248.

[29] R. T. Bartus, T. L. Baumann, J. Siffert, *et al.*, "Safety/feasibility of targeting the substantia nigra with aav2-neurturin in parkinson patients," en, *Neurology*, vol. 80, no. 18, pp. 1698–1701, Apr. 2013, ISSN: 0028-3878, 1526-632X. DOI: 10.1212/WNL.0b013e3182904faa.

[30] L. Bathala, M. M. Mehndiratta, and V. K. Sharma, "Transcranial doppler: Technique and common findings (part 1)," *Annals of Indian Academy of Neurology*, vol. 16, no. 2, pp. 174–179, 2013, ISSN: 0972-2327. DOI: 10.4103/0972-2327.112460.

[31] A. Battisti-Charbonney, J. Fisher, and J. Duffin, "The cerebrovascular response to carbon dioxide in humans," en, *The Journal of Physiology*, vol. 589, no. 12, pp. 3039–3048, 2011, ISSN: 1469-7793. DOI: 10.1113/jphysiol.2011.206052.

[32] R. D. Bell, R. Deane, N. Chow, *et al.*, "Srf and myocardin regulate lrp-mediated amyloid-β clearance in brain vascular cells," *Nature Cell Biology*, vol. 11, no. 2, pp. 143–153, 2009, ISSN: 1465-7392. DOI: 10.1038/ncb1819.

[33] Y. Benjamini and Y. Hochberg, "Controlling the false discovery rate: A practical and powerful approach to multiple testing," en, *J. R. Stat. Soc. Ser. B Methodol*, vol. 57, pp. 289–300, 1995. DOI: 10.1111/j.2517-6161.1995.tb02031.x.

[34] G. Berman, D. Muttuvelu, D. Berman, *et al.*, "Decreased retinal sensitivity in depressive disorder: A controlled study," en, *Acta Psychiatrica Scandinavica*, vol. 137, no. 3, pp. 231–240, 2018, ISSN: 1600-0447. DOI: 10.1111/acps.12851.

[35] L. Bertram, M. B. McQueen, K. Mullin, D. Blacker, and R. E. Tanzi, "Systematic meta-analyses of alzheimer disease genetic association studies: The alzgene database," en, *Nature Genetics*, vol. 39, no. 11, pp. 17–23, Jan. 2007, ISSN: 1546-1718. DOI: 10.1038/ng1934.

[36] A. A. Bhogal, J. B. De Vis, J. C. W. Siero, *et al.*, "The bold cerebrovascular reactivity response to progressive hypercapnia in young and elderly," en, *NeuroImage*, vol. 139, pp. 94–102, Oct. 2016, ISSN: 1053-8119. DOI: 10.1016/j.neuroimage.2016.06.010.

[37] A. A. Bhogal, M. E. P. Philippens, J. C. W. Siero, *et al.*, "Examining the regional and cerebral depth-dependent bold cerebrovascular reactivity response at 7t," eng, *NeuroImage*, vol. 114, pp. 239–248, Jul. 2015, ISSN: 1095-9572. DOI: 10.1016/j.neuroimage.2015.04.014.

[38] A. A. Bhogal, J. C. Siero, J. A. Fisher, *et al.*, "Investigating the non-linearity of the bold cerebrovascular reactivity response to targeted hypo/hypercapnia at 7t," *NeuroImage*, vol. 98, pp. 296–305, 2014, ISSN: 1053-8119. DOI: 10.1016/j.neuroimage.2014.05.006.

[39] S. Bista Karki, K. J. Coppell, L. V. Mitchell, and K. C. Ogbuehi, "Dynamic pupillometry in type 2 diabetes: Pupillary autonomic dysfunction and the severity of diabetic retinopathy," eng, *Clinical Ophthalmology (Auckland, N.Z.)*, vol. 14, pp. 3923–3930, 2020, ISSN: 1177-5467. DOI: 10.2147/OPTH.S279872.

[40] G. W. Blair, M. J. Thrippleton, Y. Shi, *et al.*, "Intracranial hemodynamic relationships in patients with cerebral small vessel disease," en, *Neurology*, vol. 94, no. 21, e2258–e2269, May 2020, ISSN: 0028-3878, 1526-632X. DOI: 10.1212/WNL.0000000000009483.

[41] N. P. Blockley, I. D. Driver, S. T. Francis, J. A. Fisher, and P. A. Gowland, "An improved method for acquiring cerebrovascular reactivity maps," en, *Magnetic Resonance in Medicine*, vol. 65, no. 5, pp. 1278–1286, 2011, ISSN: 1522-2594. DOI: 10.1002/mrm.22719.

[42] N. P. Blockley, V. E. M. Griffeth, A. B. Simon, and R. B. Buxton, "A review of calibrated blood oxygenation level-dependent (bold) methods for the measurement of task-induced changes in brain oxygen metabolism," *NMR in biomedicine*, vol. 26, no. 8, 987â1003, Aug. 2013, ISSN: 0952-3480. DOI: 10.1002/nbm.2847.

[43] R. Bobe, L. Hadri, J. J. Lopez, *et al.*, "Serca2a controls the mode of agonist-induced intracellular ca2+ signal, transcription factor nfat and proliferation in human vascular smooth muscle cells," en, *Journal of Molecular and Cellular Cardiology*, vol. 50, no. 4, pp. 621–633, Apr. 2011, ISSN: 0022-2828. DOI: 10.1016/j.yjmcc.2010.12.016.

[44] V. Bonifati, P. Rizzu, M. J. van Baren, *et al.*, "Mutations in the dj-1 gene associated with autosomal recessive early-onset parkinsonism," eng, *Science (New York, N.Y.)*, vol. 299, no. 5604, pp. 256–259, Jan. 2003, ISSN: 1095-9203. DOI: 10.1126/science.1077209.

[45] R. van den Boom, S. A. L. Oberstein, A. Spilt, *et al.*, "Cerebral hemodynamics and white matter hyperintensities in cadasil," en, *Journal of Cerebral Blood Flow & Metabolism*, vol. 23, no. 5, pp. 599–604, May 2003, ISSN: 0271-678X. DOI: 10.1097/01.WCB.0000062341.61367.D3.

[46] O. Bracko, B. N. Njiru, M. Swallow, M. Ali, M. Haft-Javaherian, and C. B. Schaffer, "Increasing cerebral blood flow improves cognition into late stages in alzheimer's disease mice," en, *Journal of Cerebral Blood Flow & Metabolism*, vol. 40, no. 7, pp. 1441–1452, Jul. 2020, ISSN: 0271-678X. DOI: 10.1177/0271678X19873658.

[47] J. C. Bradley, K. C. Bentley, A. I. Mughal, H. Bodhireddy, and S. M. Brown, "Dark-adapted pupil diameter as a function of age measured with the neuroptics

pupillometer," *Journal of Refractive Surgery*, vol. 27, no. 3, pp. 202–207, Mar. 2011. DOI: 10.3928/1081597X-20100511-01.

[48] J. E. Brayden, "Potassium channels in vascular smooth muscle," en, *Clinical and Experimental Pharmacology and Physiology*, vol. 23, no. 12, pp. 1069–1076, 1996, ISSN: 1440-1681. DOI: 10.1111/j.1440-1681.1996.tb01172.x.

[49] T. S. Breusch and A. R. Pagan, "A simple test for heteroscedasticity and random coefficient variation," *Econometrica*, vol. 47, no. 5, pp. 1287–1294, 1979, ISSN: 0012-9682. DOI: 10.2307/1911963.

[50] J. E. Brian, "Carbon dioxide and the cerebral circulation," *Anesthesiology*, vol. 88, no. 5, pp. 1365–1386, May 1998, ISSN: 0003-3022. DOI: 10.1097/00000542-199805000-00029.

[51] M. Bright, D. Bulte, P. Jezzard, and J. Duyn, "Characterization of regional heterogeneity in cerebrovascular reactivity dynamics using novel hypocapnia task and bold fmri," mg, *NeuroImage*, vol. 48, pp. 166–175, 2009. DOI: 10.1016/j.neuroimage.2009.05.026.

[52] M. Bright and K. Murphy, "Reliable quantification of bold fmri cerebrovascular reactivity despite poor breath-hold performance," en, *NeuroImage*, vol. 83, pp. 559–568, 2013. DOI: 10.1016/j.neuroimage.2013.07.007.

[53] A. Britzolaki, J. Saurine, B. Klocke, and P. M. Pitychoutis, "A role for serca pumps in the neurobiology of neuropsychiatric and neurodegenerative disorders," eng, *Advances in Experimental Medicine and Biology*, vol. 1131, pp. 131–161, 2020, ISSN: 0065-2598. DOI: 10.1007/978-3-030-12457-1_6.

[54] D. P. Bulte, K. Drescher, and P. Jezzard, "Comparison of hypercapnia-based calibration techniques for measurement of cerebral oxygen metabolism with mri," en, *Magnetic Resonance in Medicine*, vol. 61, no. 2, 391â398, 2009, ISSN: 1522-2594. DOI: 10.1002/mrm.21862.

[55] C. V. Burley, S. T. Francis, K. N. Thomas, A. C. Whittaker, S. J. E. Lucas, and K. J. Mullinger, "Contrasting measures of cerebrovascular reactivity between mri and doppler: A cross-sectional study of younger and older healthy individuals," *Frontiers in Physiology*, vol. 12, 2021, ISSN: 1664-042X. DOI: 10.3389/fphys.2021.656746.

[56] M. Bussotti, D. MagrÃ¬, E. Previtali, *et al.*, "End-tidal pressure of co2 and exercise performance in healthy subjects," en, *European Journal of Applied Physiology*, vol. 103, no. 6, pp. 727–732, Aug. 2008, ISSN: 1439-6319, 1439-6327. DOI: 10.1007/s00421-008-0773-z.

[57] R. B. Buxton, L. R. Frank, E. C. Wong, B. Siewert, S. Warach, and R. R. Edelman, "A general kinetic model for quantitative perfusion imaging with arterial spin labeling," en, *Magnetic Resonance in Medicine*, vol. 40, no. 3, 383â396, 1998, ISSN: 1522-2594. DOI: 10.1002/mrm.1910400308.

[58] L. Calvier, P. Chouvarine, E. Legchenko, *et al.*, "Pparγ Links BMP2 and TGFβ1 Pathways in Vascular Smooth Muscle Cells, Regulating Cell Proliferation and Glucose Metabolism," eng, *Cell Metabolism*, vol. 25, no. 5, 1118–1134.e7, May 2017, ISSN: 1932-7420. DOI: 10.1016/j.cmet.2017.03.011.

[59] C. Camargo, E. Martins, M. Lange, *et al.*, "Abnormal cerebrovascular reactivity in patients with parkinson's disease," en, *Park. Dis*, p. 523 041, 2015. DOI: 10.1155/2015/523041.

[60] R. J. Cannistraro, M. Badi, B. H. Eidelman, D. W. Dickson, E. H. Middlebrooks, and J. F. Meschia, "Cns small vessel disease: A clinical review," en, *Neurology*, vol. 92, no. 24, pp. 1146–1156, Jun. 2019, ISSN: 0028-3878, 1526-632X. DOI: 10.1212/WNL.0000000000007654.

[61] S. Cantin, M. Villien, O. Moreaud, *et al.*, "Impaired cerebral vasoreactivity to co2 in alzheimer's disease using bold fmri," en, *NeuroImage*, vol. 58, no. 2, pp. 579–587, Sep. 2011, ISSN: 1053-8119. DOI: 10.1016/j.neuroimage.2011.06.070.

[62] J. M. J. R. Carr, H. G. Caldwell, and P. N. Ainslie, "Cerebral blood flow, cerebrovascular reactivity and their influence on ventilatory sensitivity," en, *Experimental Physiology*, vol. 106, no. 7, pp. 1425–1448, 2021, ISSN: 1469-445X. DOI: 10.1113/EP089446.

[63] J. K. Cataldo, J. J. Prochaska, and S. A. Glantz, "Cigarette smoking is a risk factor for alzheimer's disease: An analysis controlling for tobacco industry affiliation," *Journal of Alzheimer's Disease*, vol. 19, no. 2, pp. 465–480, 2010, ISSN: 1387-2877. DOI: 10.3233/jad-2010-1240.

[64] S. J. Catchlove, A. Pipingas, M. E. Hughes, and H. Macpherson, "Magnetic resonance imaging for assessment of cerebrovascular reactivity and its relationship to cognition: A systematic review," *BMC Neuroscience*, vol. 19, no. 1, p. 21, Apr. 2018, ISSN: 1471-2202. DOI: 10.1186/s12868-018-0421-4.

[65] F. Cerza, M. Renzi, C. Gariazzo, *et al.*, "Long-term exposure to air pollution and hospitalization for dementia in the rome longitudinal study," *Environmental Health*, vol. 18, no. 1, p. 72, Aug. 2019, ISSN: 1476-069X. DOI: 10.1186/s12940-019-0511-5.

[66] H. Chabriat, S. Pappata, L. Ostergaard, *et al.*, "Cerebral hemodynamics in cadasil before and after acetazolamide challenge assessed with mri bolus tracking," *Stroke*, vol. 31, no. 8, pp. 1904–1912, Aug. 2000. DOI: 10.1161/01.STR.31.8.1904.

[67] C.-P. Chang, K.-C. Wu, C.-Y. Lin, and Y. Chern, "Emerging roles of dysregulated adenosine homeostasis in brain disorders with a specific focus on neurodegenerative diseases," *Journal of Biomedical Science*, vol. 28, no. 1, p. 70, Oct. 2021, ISSN: 1423-0127. DOI: 10.1186/s12929-021-00766-y.

[68] T.-Y. Chang, H.-L. Liu, T.-H. Lee, *et al.*, "Change in cerebral perfusion after carotid angioplasty with stenting is related to cerebral vasoreactivity: A study using dynamic susceptibility-weighted contrast-enhanced mr imaging and functional mr imaging with a breath-holding paradigm," en, *AJNR Am. J. Neuroradiol*, vol. 30, pp. 1330–1336, 2009. DOI: 10.3174/ajnr.A1589.

[69] M. Chappell, A. Groves, B. Whitcher, and M. Woolrich, "Variational bayesian inference for a nonlinear forward model," en, *IEEE Trans. Signal Process*, vol. 57, pp. 223–236, 2009. DOI: 10.1109/TSP.2008.2005752.

[70] G. Chen, Z. Saad, J. Britton, D. Pine, and R. Cox, "Linear mixed-effects modeling approach to fmri group analysis," en, *NeuroImage*, vol. 73, pp. 176–190, 2013. DOI: 10.1016/j.neuroimage.2013.01.047.

[71] G. Chen, P. Taylor, and R. Cox, "Is the statistic value all we should care about in neuroimaging?" en, *NeuroImage*, vol. 147, pp. 952–959, 2017. DOI: 10.1016/j.neuroimage.2016.09.066.

[72] G. Chen, P. Taylor, S. Haller, *et al.*, "Intraclass correlation: Improved modeling approaches and applications for neuroimaging," en, *Hum. Brain Mapp*, vol. 39, pp. 1187–1206, 2018. DOI: 10.1002/hbm.23909.

[73] J. J. Chen and G. B. Pike, "Bold-specific cerebral blood volume and blood flow changes during neuronal activation in humans," en, *NMR in Biomedicine*, vol. 22, no. 10, 1054â1062, 2009, ISSN: 1099-1492. DOI: 10.1002/nbm.1411.

[74] J. J. Chen and G. B. Pike, "Global cerebral oxidative metabolism during hypercapnia and hypocapnia in humans: Implications for bold fmri," en, *Journal of Cerebral Blood Flow Metabolism*, vol. 30, no. 6, 1094â1099, Jun. 2010, ISSN: 0271-678X. DOI: 10.1038/jcbfm.2010.42.

[75] J. W. Chen, Z. J. Gombart, S. Rogers, S. K. Gardiner, S. Cecil, and R. M. Bullock, "Pupillary reactivity as an early indicator of increased intracranial pressure: The introduction of the neurological pupil index," *Surgical Neurology International*, vol. 2, p. 82, Jun. 2011, ISSN: 2229-5097. DOI: 10.4103/2152-7806.82248.

[76] Y.-L. Chen, Z. Daneva, M. Kuppusamy, *et al.*, "Novel smooth muscle ca2+-signaling nanodomains in blood pressure regulation," *Circulation*, vol. 146, no. 7, pp. 548–564, Aug. 2022. DOI: 10.1161/CIRCULATIONAHA.121.058607.

[77] D. Chicco, M. J. Warrens, and G. Jurman, "The coefficient of determination r-squared is more informative than smape, mae, mape, mse and rmse in regression analysis evaluation," en, *PeerJ Computer Science*, vol. 7, e623, Jul. 2021. DOI: 10.7717/peerj-cs.623.

[78] K.-H. Cho, H.-S. Nam, D.-J. Kang, M.-H. Park, and J.-H. Kim, "Long-term alcohol consumption caused a significant decrease in serum high-density lipoprotein (hdl)-cholesterol and apolipoprotein a-i with the atherogenic changes of hdl in middle-aged korean women," en, *International Journal of Molecular Sciences*, vol. 23, no. 1515, p. 8623, Jan. 2022, ISSN: 1422-0067. DOI: 10.3390/ijms23158623.

[79] P. S. Chougule, R. P. Najjar, M. T. Finkelstein, N. Kandiah, and D. Milea, "Light-induced pupillary responses in alzheimer's disease," *Frontiers in Neurology*, vol. 10, p. 360, Apr. 2019, ISSN: 1664-2295. DOI: 10.3389/fneur.2019.00360.

[80] N. Chow, R. D. Bell, R. Deane, *et al.*, "Serum response factor and myocardin mediate arterial hypercontractility and cerebral blood flow dysregulation in alzheimer's phenotype," *Proceedings of the National Academy of Sciences*, vol. 104, no. 3, pp. 823–828, 2007, ISSN: 0027-8424. DOI: 10.1073/pnas.0608251104.

[81] N. Churchill, M. Hutchison, S. Graham, and T. Schweizer, "Cerebrovascular reactivity after sport concussion: From acute injury to 1 year after medical clearance," en, *Front. Neurol*, vol. 11, 2020.

[82] D. Cicchetti, "Methodological commentary the precision of reliability and validity estimates re-visited: Distinguishing between clinical and statistical significance of sample size requirements," en, *J. Clin. Exp. Neuropsychol*, vol. 23, pp. 695–700, 2001. DOI: 10.1076/jcen.23.5.695.1249.

[83] M. J. Cipolla, *Control of Cerebral Blood Flow*, en. Morgan & Claypool Life Sciences, 2009. [Online]. Available: https://www.ncbi.nlm.nih.gov/books/NBK53082/.

[84] J. A. H. R. Claassen, D. H. J. Thijssen, R. B. Panerai, and F. M. Faraci, "Regulation of cerebral blood flow in humans: Physiology and clinical implications of autoregulation," *Physiological Reviews*, vol. 101, no. 4, pp. 1487–1559, Oct. 2021, ISSN: 0031-9333. DOI: 10.1152/physrev.00022.2020.

[85] J. A. H. R. Claassen, R. Zhang, Q. Fu, S. Witkowski, and B. D. Levine, "Transcranial doppler estimation of cerebral blood flow and cerebrovascular conductance during modified rebreathing," *Journal of Applied Physiology*, vol. 102, no. 3, pp. 870–877, Mar. 2007, ISSN: 8750-7587. DOI: 10.1152/japplphysiol.00906.2006.

[86] C. M. Clements, R. S. McNally, B. J. Conti, T. W. Mak, and J. P.-Y. Ting, "Dj-1, a cancer- and parkinson's disease-associated protein, stabilizes the antioxidant transcriptional master regulator nrf2," eng, *Proceedings of the National Academy of Sciences of the United States of America*, vol. 103, no. 41, pp. 15 091–15 096, Oct. 2006, ISSN: 0027-8424. DOI: 10.1073/pnas.0607260103.

[87] A. Cohen and Y. Wang, "Improving the assessment of breath-holding induced cerebral vascular reactivity using a multiband multi-echo asl/bold sequence," en, *Sci. Rep*, vol. 9, p. 5079, 2019. DOI: 10.1038/s41598-019-41199-w.

[88] D. Collins, C. Holmes, T. Peters, and A. Evans, "Automatic 3-d model-based neuroanatomical segmentation," ny, *Hum. Brain Mapp*, vol. 3, pp. 190–208, 1995. DOI: 10.1002/hbm.460030304.

[89] L. Costa, C. Niftrik, D. Crane, J. Fierstra, and A. Bethune, "Temporal profile of cerebrovascular reactivity impairment, gray matter volumes, and persistent symptoms after mild traumatic head injury," en, *Front. Neurol*, vol. 7, p. 70, 2016. DOI: 10.3389/fneur.2016.00070.

[90] M. Coucha, M. Abdelsaid, R. Ward, Y. Abdul, and A. Ergul, "Impact of metabolic diseases on cerebral circulation: Structural and functional consequences," en, in *Comprehensive Physiology*. John Wiley & Sons, Ltd, 2018, pp. 773–799, ISBN: 978-0-470-65071-4. DOI: 10.1002/cphy.c170019. [Online]. Available: https://onlinelibrary.wiley.com/doi/abs/10.1002/cphy.c170019.

[91] R. W. Cox, "AFNI: Software for Analysis and Visualization of Functional Magnetic Resonance Neuroimages," *Computers and Biomedical Research*, vol. 29, no. 3, pp. 162–173, Jun. 1996, ISSN: 0010-4809. DOI: 10.1006/cbmr.1996.0014. [Online]. Available: https://www.sciencedirect.com/science/article/pii/S0010480996900142 (visited on 01/24/2024).

[92] T. L. Davis, K. K. Kwong, R. M. Weisskoff, and B. R. Rosen, "The coefficient of determination r-squared is more informative than smape, mae, mape, mse and rmse in regression analysis evaluation," *Proceedings of the National Academy of Sciences*, vol. 7, no. 4, 1834â1839, Feb. 1998. DOI: 10.7717/peerj-cs.623.

[93] B. N. Davis-Dusenbery, C. Wu, A. Hata, and W. C. Sessa, "Micromanaging vascular smooth muscle cell differentiation and phenotypic modulation," *Arteriosclerosis, Thrombosis, and Vascular Biology*, vol. 31, no. 11, pp. 2370–2377, Nov. 2011. DOI: 10.1161/ATVBAHA.111.226670.

[94] P. T. Deckers, W. van Hoek, A. Kronenburg, *et al.*, "Contralateral improvement of cerebrovascular reactivity and tia frequency after unilateral revascularization surgery in moyamoya vasculopathy," en, *NeuroImage: Clinical*, vol. 30, p. 102 684, Jan. 2021, ISSN: 2213-1582. DOI: 10.1016/j.nicl.2021.102684.

[95] J. A. Detre, J. S. Leigh, D. S. Williams, and A. P. Koretsky, "Perfusion imaging," en, *Magnetic Resonance in Medicine*, vol. 23, no. 1, 37â45, 1992, ISSN: 1522-2594. DOI: 10.1002/mrm.1910230106.

[96] J. A. Detre and J. Wang, "Technical aspects and utility of fmri using bold and asl," eng, *Clinical Neurophysiology: Official Journal of the International Federation of Clinical Neurophysiology*, vol. 113, no. 5, pp. 621–634, May 2002, ISSN: 1388-2457. DOI: 10.1016/s1388-2457(02)00038-x.

[97] N. D. DiProspero, S. Kim, and M. A. Yassa, "Chapter 8 - magnetic resonance imaging biomarkers for cognitive decline in down syndrome," en, in *The Neurobiology of Aging and Alzheimer Disease in Down Syndrome*, E. Head and I. Lott, Eds. Academic Press, Jan. 2022, pp. 149–172, ISBN: 978-0-12-818845-3. DOI: 10.1016/B978-0-12-818845-3.00014-1.

[98] U. Dirnagl, B. Kaplan, M. Jacewicz, and W. Pulsinelli, "Continuous measurement of cerebral cortical blood flow by laser—doppler flowmetry in a rat stroke model," en, *Journal of Cerebral Blood Flow & Metabolism*, vol. 9, no. 5, pp. 589–596, Oct. 1989, ISSN: 0271-678X. DOI: 10.1038/jcbfm.1989.84.

[99] S. Dohgu, F. Takata, J. Matsumoto, I. Kimura, A. Yamauchi, and Y. Kataoka, "Monomeric α-synuclein induces blood-brain barrier dysfunction through activated brain pericytes releasing inflammatory mediators in vitro," eng, *Microvascular Research*, vol. 124, pp. 61–66, Jul. 2019, ISSN: 1095-9319. DOI: 10.1016/j.mvr.2019.03.005.

[100] C. Domingos, I. Esteves, A. R. Fouto, A. Ruiz-Tagle, G. Caetano, and P. Figueiredo, "Cerebrovascular reactivity mapping using breath-hold bold-fmri: Comparison of signal models combined with voxelwise lag optimization," en, p. 2024.03.22.586319, Mar. 2024. DOI: 10.1101/2024.03.22.586319.

[101] M. J. Donahue, M. K. Strother, K. P. Lindsey, L. M. Hocke, Y. Tong, and B. d. Frederick, "Time delay processing of hypercapnic fmri allows quantitative parameterization of cerebrovascular reactivity and blood flow delays," en, *Journal of Cerebral Blood Flow & Metabolism*, vol. 36, no. 10, pp. 1767–1779, 2016, ISSN: 0271-678X. DOI: 10.1177/0271678X15608643.

[102] M. Donahue, P. Laar, P. Zijl, R. Stevens, and J. Hendrikse, "Vascular space occupancy (vaso) cerebral blood volume-weighted mri identifies hemodynamic impairment in patients with carotid artery disease," en, *J. Magn. Reson. Imaging JMRI*, vol. 29, pp. 718–724, 2009. DOI: 10.1002/jmri.21667.

[103] I. D. Driver, E. L. Hall, S. J. Wharton, S. E. Pritchard, S. T. Francis, and P. A. Gowland, "Calibrated bold using direct measurement of changes in venous oxygenation," *NeuroImage*, vol. 63, no. 3, 1178â1187, Nov. 2012, ISSN: 1053-8119. DOI: 10.1016/j.neuroimage.2012.08.045.

[104] I. D. Driver, R. G. Wise, and K. Murphy, "Graded hypercapnia-calibrated bold: Beyond the iso-metabolic hypercapnic assumption," English, *Frontiers in Neuroscience*, vol. 11, May 2017, ISSN: 1662-453X. DOI: 10.3389/fnins.2017.00276. [Online]. Available: https://www.frontiersin.org/journals/neuroscience/articles/10.3389/fnins.2017.00276/full.

[105] R. K. Dubey, D. G. Gillespie, K. Osaka, F. Suzuki, and E. K. Jackson, "Adenosine inhibits growth of rat aortic smooth muscle cells," *Hypertension*, vol. 27, no. 3, pp. 786–793, Mar. 1996. DOI: 10.1161/01.HYP.27.3.786.

[106] J. Duffin, D. J. Mikulis, and J. A. Fisher, "Control of cerebral blood flow by blood gases," *Frontiers in Physiology*, vol. 12, 2021, ISSN: 1664-042X. DOI: 10.3389/fphys.2021.640075.

[107] J. Duffin, O. Sobczyk, A. Crawley, *et al.*, "The role of vascular resistance in bold responses to progressive hypercapnia," en, *Human Brain Mapping*, vol. 38, no. 11, pp. 5590–5602, 2017, ISSN: 1097-0193. DOI: 10.1002/hbm.23751.

[108] J. Dumville, R. B. Panerai, N. S. Lennard, A. R. Naylor, and D. H. Evans, "Can cerebrovascular reactivity be assessed without measuring blood pressure in patients with carotid artery disease?" *Stroke*, vol. 29, no. 5, pp. 968–974, May 1998. DOI: 10.1161/01.STR.29.5.968.

[109] E. DuPre, T. Salo, R. Markello, P. Kundu, K. Whitaker, and D. Handwerker, mi, 2019. DOI: 10.5281/zenodo.2558498. [Online]. Available: https://doi.org/10.5281/zenodo.2558498.

[110] J. Durbin and G. S. Watson, "Testing for serial correlation in least squares regression. i," eng, *Biometrika*, vol. 37, no. 3–4, pp. 409–428, Dec. 1950, ISSN: 0006-3444.

[111] K. Eaton, J. Szaflarski, M. Altaye, *et al.*, "Reliability of fmri for studies of language in post-stroke aphasia subjects," en, *NeuroImage*, vol. 41, pp. 311–322, 2008. DOI: 10.1016/j.neuroimage.2008.02.033.

[112] M. K. Eckstein, B. Guerra-Carrillo, A. T. Miller Singley, and S. A. Bunge, "Beyond eye gaze: What else can eyetracking reveal about cognition and cognitive development?" *Developmental Cognitive Neuroscience*, Sensitive periods across development, vol. 25, pp. 69–91, Jun. 2017, ISSN: 1878-9293. DOI: 10.1016/j.dcn.2016.11.001.

[113] EODG, *Oxford physics: Atmospheric, oceanic and planetary physics: Weather*. [Online]. Available: https://eodg.atm.ox.ac.uk/eodg/weather/weather_nocol.html.

[114] J. F. Ervin, C. Pannell, M. Szymanski, K. Welsh-Bohmer, D. E. Schmechel, and C. M. Hulette, "Vascular smooth muscle actin is reduced in alzheimer disease brain: A quantitative analysis," *Journal of Neuropathology & Experimental Neurology*, vol. 63, no. 7, pp. 735–741, 2004, ISSN: 0022-3069. DOI: 10.1093/jnen/63.7.735.

[115] A. V. Espinosa, M. Shinohara, L. M. Porchia, *et al.*, "Regulator of calcineurin 1 modulates cancer cell migration in vitro," en, *Clinical & Experimental Metastasis*, vol. 26, no. 6, pp. 517–526, Aug. 2009, ISSN: 1573-7276. DOI: 10.1007/s10585-009-9251-1.

[116] V. Esteban, N. Méndez-Barbero, L. Jiménez-Borreguero, *et al.*, "Regulator of calcineurin 1 mediates pathological vascular wall remodeling," en, *J. Exp. Med*, vol. 208, pp. 2125–2139, 2011. DOI: 10.1084/jem.20110503.

[117] J.-L. Fan, A. W. Subudhi, J. Duffin, A. T. Lovering, R. C. Roach, and B. Kayser, "Altitudeomics: Resetting of cerebrovascular co2 reactivity following acclimatization to high altitude," *Frontiers in Physiology*, vol. 6, 2016, ISSN: 1664-042X. [Online]. Available: https://www.frontiersin.org/journals/physiology/articles/10.3389/fphys.2015.00394.

[118] S. Favaretto, U. Walter, C. Baracchini, and A. Cagnin, "Transcranial sonography in neurodegenerative diseases with cognitive decline," eng, *Journal of*

Alzheimer's disease: JAD, vol. 61, no. 1, pp. 29–40, 2018, ISSN: 1875-8908. DOI: 10.3233/JAD-170382.

[119] R. Feinberg, E. Podolak, and G. C. R. Institute, *Latency of pupillary reflex to light stimulation and its relationship to aging*. English. Sep. 1965. [Online]. Available: https://rosap.ntl.bts.gov/view/dot/20753.

[120] B. Fico, K. Miller, L. Rivera-Rivera, *et al.*, "Cerebral hemodynamics comparison between transcranial doppler ultrasound and 4d flow mri," *Physiology*, vol. 38, no. S1, p. 5 731 124, May 2023, ISSN: 1548-9213. DOI: 10.1152/physiol.2023.38.S1.5731124.

[121] C. R. Fields, N. Bengoa-Vergniory, and R. Wade-Martins, "Targeting alpha-synuclein as a therapy for parkinson's disease," *Frontiers in Molecular Neuroscience*, vol. 12, 2019, ISSN: 1662-5099. DOI: 10.3389/fnmol.2019.00299.

[122] J. Fierstra, C. Niftrik, M. Piccirelli, *et al.*, "Diffuse gliomas exhibit whole brain impaired cerebrovascular reactivity," it, *Magn. Reson. Imaging*, vol. 45, pp. 78–83, 2018. DOI: 10.1016/j.mri.2017.09.017.

[123] J Fierstra, O Sobczyk, A Battisti-Charbonney, *et al.*, "Measuring cerebrovascular reactivity: What stimulus to use?" *The Journal of Physiology*, vol. 591, no. Pt 23, pp. 5809–5821, Dec. 2013, ISSN: 0022-3751. DOI: 10.1113/jphysiol.2013.259150.

[124] J. A. Filosa and J. A. Iddings, "Astrocyte regulation of cerebral vascular tone," *American Journal of Physiology - Heart and Circulatory Physiology*, vol. 305, no. 5, H609–H619, Sep. 2013, ISSN: 0363-6135. DOI: 10.1152/ajpheart.00359.2013.

[125] J. A. Fisher, S. Iscoe, and J. Duffin, "Sequential gas delivery provides precise control of alveolar gas exchange," *Respiratory Physiology & Neurobiology*, vol. 225, pp. 60–69, May 2016, ISSN: 1569-9048. DOI: 10.1016/j.resp.2016.01.004.

[126] J. A. Fisher, O. Sobczyk, A. Crawley, *et al.*, "Assessing cerebrovascular reactivity by the pattern of response to progressive hypercapnia," *Human Brain Mapping*, vol. 38, no. 7, pp. 3415–3427, Apr. 2017, ISSN: 1065-9471. DOI: 10.1002/hbm.23598.

[127] M. Flanagan, E. B. Larson, C. S. Latimer, *et al.*, "Clinical-pathologic correlations in vascular cognitive impairment and dementia," en, *Biochimica et Biophysica Acta (BBA) - Molecular Basis of Disease*, Vascular contributions to cognitive impairment and dementia (VCID), vol. 1862, no. 5, pp. 945–951, May 2016, ISSN: 0925-4439. DOI: 10.1016/j.bbadis.2015.08.019.

[128] F. Fotiou, K. N. Fountoulakis, M. Tsolaki, A. Goulas, and A. Palikaras, "Changes in pupil reaction to light in alzheimer's disease patients: A preliminary report," en, *International Journal of Psychophysiology*, vol. 37, no. 1, pp. 111–120, Jul. 2000, ISSN: 0167-8760. DOI: 10.1016/S0167-8760(00)00099-4.

[129] K. Fountoulakis, F. Fotiou, A. Iacovides, *et al.*, "Changes in pupil reaction to light in melancholic patients," eng, *International Journal of Psychophysiology: Official Journal of the International Organization of Psychophysiology*, vol. 31, no. 2, pp. 121–128, Jan. 1999, ISSN: 0167-8760. DOI: 10.1016/s0167-8760(98)00046-4.

[130] P. T. Fox and M. E. Raichle, "Focal physiological uncoupling of cerebral blood flow and oxidative metabolism during somatosensory stimulation in human subjects.," *Proceedings of the National Academy of Sciences*, vol. 83, no. 4, 1140â1144, Feb. 1986. DOI: 10.1073/pnas.83.4.1140.

[131] A. Frismantiene, M. Philippova, P. Erne, and T. J. Resink, "Smooth muscle cell-driven vascular diseases and molecular mechanisms of vsmc plasticity," *Cellular Signalling*, vol. 52, pp. 48–64, 2018, ISSN: 0898-6568. DOI: 10.1016/j.cellsig.2018.08.019.

[132] S. Frost, L. Robinson, C. C. Rowe, *et al.*, "Evaluation of cholinergic deficiency in preclinical alzheimer's disease using pupillometry," en, *Journal of Ophthalmology*, vol. 2017, e7935406, Aug. 2017, ISSN: 2090-004X. DOI: 10.1155/2017/7935406.

[133] J. J. Fuster and V. Andrés, "Telomere biology and cardiovascular disease," *Circulation Research*, vol. 99, no. 11, pp. 1167–1180, Nov. 2006. DOI: 10.1161/01.RES.0000251281.00845.18.

[134] Z. S. Galis and J. J. Khatri, "Matrix metalloproteinases in vascular remodeling and atherogenesis," *Circulation Research*, vol. 90, no. 3, pp. 251–262, Feb. 2002. DOI: 10.1161/res.90.3.251.

[135] J. Gallego, A. Pedraza, S. Lopez, *et al.*, "Glomerulus classification and detection based on convolutional neural networks," en, *Journal of Imaging*, vol. 4, no. 11, p. 20, Jan. 2018. DOI: 10.3390/jimaging4010020.

[136] S. Gan, S. Qiu, Y. Feng, *et al.*, "Identification of genes associated with the effect of inflammation on the neurotransmission of vascular smooth muscle cell," *Experimental and Therapeutic Medicine*, vol. 13, no. 4, pp. 1303–1312, 2017, ISSN: 1792-0981. DOI: 10.3892/etm.2017.4138.

[137] J.-H. Gao, I. Miller, S. Lai, J. Xiong, and P. T. Fox, "Quantitative assessment of blood inflow effects in functional mri signals," en, *Magnetic Resonance in Medicine*, vol. 36, no. 2, pp. 314–319, 1996, ISSN: 1522-2594. DOI: 10.1002/mrm.1910360219.

[138] U. C. Garg and A. Hassid, "Nitric oxide-generating vasodilators and 8-bromo-cyclic guanosine monophosphate inhibit mitogenesis and proliferation of cultured rat vascular smooth muscle cells.," en, *The Journal of Clinical Investigation*, vol. 83, no. 5, pp. 1774–1777, May 1989, ISSN: 0021-9738. DOI: 10.1172/JCI114081.

[139] S. Giannopoulos, A. H. Katsanos, G. Tsivgoulis, and R. S. Marshall, "Statins and cerebral hemodynamics," *Journal of Cerebral Blood Flow & Metabolism*, vol. 32, no. 11, pp. 1973–1976, Nov. 2012, ISSN: 0271-678X. DOI: 10.1038/jcbfm.2012.122.

[140] J. S. Gill, A. V. Zezulka, M. J. Shipley, S. K. Gill, and D. G. Beevers, "Stroke and alcohol consumption," *New England Journal of Medicine*, vol. 315, no. 17, pp. 1041–1046, Oct. 1986, ISSN: 0028-4793. DOI: 10.1056/NEJM198610233151701.

[141] P. Giulia, L. Michele, F. Andrea, *et al.*, "Brain atrophy, anti-smooth muscle antibody and cognitive impairment: An association study," *Aging and Disease*, vol. 7, no. 4, pp. 318–325, Nov. 2015, ISSN: 2152-5250. DOI: 10.14336/AD.2015.1124.

[142] L. Glodzik, C. Randall, H. Rusinek, and M. J. d. Leon, "Cerebrovascular reactivity to carbon dioxide in alzheimer's disease," *Journal of Alzheimer's Disease*, vol. 35, no. 3, pp. 427–440, 2013, ISSN: 1387-2877. DOI: 10.3233/jad-122011.

[143] L. Glodzik, H. Rusinek, M. Brys, *et al.*, "Framingham cardiovascular risk profile correlates with impaired hippocampal and cortical vasoreactivity to hypercapnia," eng, *Journal of Cerebral Blood Flow and Metabolism: Official Journal of the International Society of Cerebral Blood Flow and Metabolism*, vol. 31, no. 2, pp. 671–679, Feb. 2011, ISSN: 1559-7016. DOI: 10.1038/jcbfm.2010.145.

[144] S. D. Goode, S. Krishan, C. Alexakis, R. Mahajan, and D. P. Auer, "Precision of cerebrovascular reactivity assessment with use of different quantification methods for hypercapnia functional mr imaging," en, *American Journal of Neuroradiology*, vol. 30, no. 5, pp. 972–977, May 2009, ISSN: 0195-6108, 1936-959X. DOI: 10.3174/ajnr.A1496.

[145] R. Grabner, A. Neubauer, and E. Stern, "Superior performance and neural efficiency: The impact of intelligence and expertise," en, *Brain Res. Bull*, vol. 69, pp. 422–439, 2006. DOI: 10.1016/j.brainresbull.2006.02.009.

[146] N. S. Graham and D. J. Sharp, "Understanding neurodegeneration after traumatic brain injury: From mechanisms to clinical trials in dementia," en, *Journal of Neurology, Neurosurgery & Psychiatry*, vol. 90, no. 11, pp. 1221–1233, Nov. 2019, ISSN: 0022-3050, 1468-330X. DOI: 10.1136/jnnp-2017-317557.

[147] K. N. Green, A. Demuro, Y. Akbari, *et al.*, "Serca pump activity is physiologically regulated by presenilin and regulates amyloid î^2*production*," *The Journal of Cell Biology*, vol. 181, no. 7, pp. 1107–1116, Jun. 2008, ISSN: 0021-9525. DOI: 10.1083/jcb.200706171.

[148] K. K. Griendling, C. A. Minieri, J. D. Ollerenshaw, and R. W. Alexander, "Angiotensin ii stimulates nadh and nadph oxidase activity in cultured vascular smooth muscle cells," eng, *Circulation Research*, vol. 74, no. 6, pp. 1141–1148, Jun. 1994, ISSN: 0009-7330. DOI: 10.1161/01.res.74.6.1141.

[149] K. K. Griendling, M. Ushio-Fukai, B. Lassègue, and R. W. Alexander, "Angiotensin ii signaling in vascular smooth muscle," *Hypertension*, vol. 29, no. 1, pp. 366–370, 1997, ISSN: 0194-911X. DOI: 10.1161/01.hyp.29.1.366.

[150] V. E. Griffeth and R. B. Buxton, "A theoretical framework for estimating cerebral oxygen metabolism changes using the calibrated-bold method: Modeling the effects of blood volume distribution, hematocrit, oxygen extraction fraction, and tissue signal properties on the bold signal," *NeuroImage*, vol. 58, no. 1, 198â212, Sep. 2011, ISSN: 1053-8119. DOI: 10.1016/j.neuroimage.2011.05.077.

[151] W. M. Grossmann and B. Koeberle, "The dose-response relationship of acetazolamide on the cerebral blood flow in normal subjects," *Cerebrovascular Diseases*, vol. 10, no. 1, pp. 65–69, 2000, ISSN: 1015-9770, 1421-9786. DOI: 10.1159/000016027.

[152] R. L. Grubb, M. E. Raichle, J. O. Eichling, and M. M. Ter-Pogossian, "The effects of changes in paco2 on cerebral blood volume, blood flow, and vascular mean transit time," eng, *Stroke*, vol. 5, no. 5, 630â639, 1974, ISSN: 0039-2499. DOI: 10.1161/01.str.5.5.630.

[153] C. Guibert, T. Ducret, and J.-P. Savineau, "Expression and physiological roles of trp channels in smooth muscle cells," en, in *Transient Receptor Potential*

Channels (Advances in Experimental Medicine and Biology), M. S. Islam, Ed., Advances in Experimental Medicine and Biology. Dordrecht: Springer Netherlands, 2011, pp. 687–706, ISBN: 978-94-007-0265-3. DOI: 10.1007/978-94-007-0265-3_36.

[154] D.-C. Guo, C. L. Papke, V. Tran-Fadulu, *et al.*, "Mutations in smooth muscle alpha-actin (acta2) cause coronary artery disease, stroke, and moyamoya disease, along with thoracic aortic disease," eng, *American Journal of Human Genetics*, vol. 84, no. 5, pp. 617–627, May 2009, ISSN: 1537-6605. DOI: 10.1016/j.ajhg.2009.04.007.

[155] A. Gupta, J. L. Chazen, M. Hartman, *et al.*, "Cerebrovascular reserve and stroke risk in patients with carotid stenosis or occlusion," *Stroke*, vol. 43, no. 11, pp. 2884–2891, Nov. 2012. DOI: 10.1161/STROKEAHA.112.663716.

[156] T. J. Guzik, N. E. Hoch, K. A. Brown, *et al.*, "Role of the t cell in the genesis of angiotensin ii induced hypertension and vascular dysfunction," eng, *The Journal of Experimental Medicine*, vol. 204, no. 10, pp. 2449–2460, Oct. 2007, ISSN: 0022-1007. DOI: 10.1084/jem.20070657.

[157] J. H. Haga, Y.-S. J. Li, and S. Chien, "Molecular basis of the effects of mechanical stretch on vascular smooth muscle cells," en, *Journal of Biomechanics*, vol. 40, no. 5, pp. 947–960, Jan. 2007, ISSN: 0021-9290. DOI: 10.1016/j.jbiomech.2006.04.011.

[158] J. N. Haidey, G. Peringod, A. Institoris, *et al.*, "Astrocytes regulate ultra-slow arteriole oscillations via stretch-mediated trpv4-cox-1 feedback," en, *Cell Reports*, vol. 36, no. 5, p. 109 405, Aug. 2021, ISSN: 2211-1247. DOI: 10.1016/j.celrep.2021.109405.

[159] C. N. Hall, C. Reynell, B. Gesslein, *et al.*, "Capillary pericytes regulate cerebral blood flow in health and disease," eng, *Nature*, vol. 508, no. 7494, pp. 55–60, Apr. 2014, ISSN: 1476-4687. DOI: 10.1038/nature13165.

[160] C. A. Hall and R. P. Chilcott, "Eyeing up the future of the pupillary light reflex in neurodiagnostics," en, *Diagnostics*, vol. 8, no. 11, p. 19, Mar. 2018, ISSN: 2075-4418. DOI: 10.3390/diagnostics8010019.

[161] M. R. Halliday, S. V. Rege, Q. Ma, *et al.*, "Accelerated pericyte degeneration and blood–brain barrier breakdown in apolipoprotein e4 carriers with alzheimer's disease," en, *Journal of Cerebral Blood Flow & Metabolism*, vol. 36, no. 1, pp. 216–227, Jan. 2016, ISSN: 0271-678X. DOI: 10.1038/jcbfm.2015.44.

[162] H. V. Hare, N. P. Blockley, A. G. Gardener, S. Clare, and D. P. Bulte, "Investigating the field-dependence of the davis model: Calibrated fmri at 1.5, 3 and 7 t," *Neuroimage*, vol. 112, 189â196, May 2015, ISSN: 1053-8119. DOI: 10.1016/j.neuroimage.2015.02.068.

[163] H. V. Hare, M. Germuska, M. E. Kelly, and D. P. Bulte, "Comparison of co2 in air versus carbogen for the measurement of cerebrovascular reactivity with magnetic resonance imaging," *Journal of Cerebral Blood Flow Metabolism*, vol. 33, no. 11, pp. 1799–1805, Nov. 2013, ISSN: 0271-678X. DOI: 10.1038/jcbfm.2013.131.

[164] D. A. Hartmann, A.-A. Berthiaume, R. I. Grant, *et al.*, "Brain capillary pericytes exert a substantial but slow influence on blood flow," en, *Nature Neuroscience*,

vol. 24, no. 55, pp. 633–645, May 2021, ISSN: 1546-1726. DOI: 10.1038/s41593-020-00793-2.

[165] D. A. Hartmann, V. Coelho-Santos, and A. Y. Shih, "Pericyte control of blood flow across microvascular zones in the central nervous system," eng, *Annual Review of Physiology*, vol. 84, pp. 331–354, Feb. 2022, ISSN: 1545-1585. DOI: 10.1146/annurev-physiol-061121-040127.

[166] T.-K. Hauser, A. Seeger, B. Bender, *et al.*, "Hypercapnic bold mri compared to h215o pet/ct for the hemodynamic evaluation of patients with moyamoya disease," en, *NeuroImage: Clinical*, vol. 22, p. 101 713, Jan. 2019, ISSN: 2213-1582. DOI: 10.1016/j.nicl.2019.101713.

[167] C. A. Hawkes, P. M. Sullivan, S. Hands, R. O. Weller, J. A. R. Nicoll, and R. O. Carare, "Disruption of arterial perivascular drainage of amyloid-β from the brains of mice expressing the human APOE ϵ4 allele," eng, *PloS One*, vol. 7, no. 7, e41636, 2012, ISSN: 1932-6203. DOI: 10.1371/journal.pone.0041636.

[168] G. Hayes, J. Pinto, S. Sparks, C. Wang, S. Suri, and D. Bulte, "Vascular smooth muscle cell dysfunction in neurodegeneration," en, *Front. Neurosci*, vol. 16, 2022.

[169] G. Hayes, S. Sparks, D. P. Bulte, and J. Pinto, "Models of cerebrovascular reactivity in bold-fmri and transcranial doppler ultrasound," Feb. 2025.

[170] G. Hayes, S. Sparks, J. Pinto, and D. P. Bulte, "Ramp protocol for non-linear cerebrovascular reactivity with transcranial doppler ultrasound," *Journal of Neuroscience Methods*, vol. 416, p. 110 381, Apr. 2025, ISSN: 0165-0270. DOI: 10.1016/j.jneumeth.2025.110381.

[171] S. He, X. Wang, H. Niu, *et al.*, "Evaluation of cerebrovascular reactivity in moyamoya disease using oxygen-dependent magnetic resonance imaging," *iScience*, vol. 27, no. 2, p. 108 923, Jan. 2024, ISSN: 2589-0042. DOI: 10.1016/j.isci.2024.108923.

[172] D. F. R. Heijtel, H. J. M. M. Mutsaerts, E. Bakker, *et al.*, "Accuracy and precision of pseudo-continuous arterial spin labeling perfusion during baseline and hypercapnia: A head-to-head comparison with 15o h2o positron emission tomography," en, *NeuroImage*, vol. 92, pp. 182–192, May 2014, ISSN: 1053-8119. DOI: 10.1016/j.neuroimage.2014.02.011.

[173] R. J. Hendrickson, P. A. Cahill, I. H. McKillop, J. V. Sitzmann, and E. M. Redmond, "Ethanol inhibits mitogen activated protein kinase activity and growth of vascular smooth muscle cells in vitro," en, *European Journal of Pharmacology*, vol. 362, no. 2, pp. 251–259, Dec. 1998, ISSN: 0014-2999. DOI: 10.1016/S0014-2999(98)00771-7.

[174] T. L. Henshall, A. Keller, L. He, *et al.*, "Notch3 is necessary for blood vessel integrity in the central nervous system," *Arteriosclerosis, Thrombosis, and Vascular Biology*, vol. 35, no. 2, pp. 409–420, Feb. 2015. DOI: 10.1161/ATVBAHA.114.304849.

[175] A. L. Hernandez, K. C. O'Connor, and D. A. Hafler, "Chapter 52 - multiple sclerosis," en, in *The Autoimmune Diseases (Fifth Edition)*, N. R. Rose and I. R. Mackay, Eds. Boston: Academic Press, Jan. 2014, pp. 735–756, ISBN: 978-0-12-384929-8. DOI: 10.1016/B978-0-12-384929-8.00052-6.

[176] W. Herrington, B. Lacey, P. Sherliker, J. Armitage, and S. Lewington, "Epidemiology of atherosclerosis and the potential to reduce the global burden of

atherothrombotic disease," *Circulation Research*, vol. 118, no. 4, pp. 535–546, Feb. 2016. DOI: 10.1161/CIRCRESAHA.115.307611.

[177] C. Heyn, J. Poublanc, A. Crawley, *et al.*, "Quantification of cerebrovascular reactivity by blood oxygen level–dependent mr imaging and correlation with conventional angiography in patients with moyamoya disease," en, *American Journal of Neuroradiology*, vol. 31, no. 5, pp. 862–867, May 2010, ISSN: 0195-6108, 1936-959X. DOI: 10.3174/ajnr.A1922.

[178] D. Highton, M. Caldwell, I. Tachtsidis, C. E. Elwell, M. Smith, and C. E. Cooper, "The influence of carbon dioxide on cerebral metabolism and oxygen consumption: Combining multimodal monitoring with dynamic systems modelling," *Biology Open*, vol. 13, no. 1, bio060087, Jan. 2024, ISSN: 2046-6390. DOI: 10.1242/bio.060087.

[179] R. H. P. Hilgers and R. C. Webb, "Molecular aspects of arterial smooth muscle contraction: Focus on rho," en, *Experimental Biology and Medicine*, vol. 230, no. 11, pp. 829–835, Dec. 2005, ISSN: 1535-3702. DOI: 10.1177/153537020523001107.

[180] R. A. Hill, L. Tong, P. Yuan, S. Murikinati, S. Gupta, and J. Grutzendler, "Regional blood flow in the normal and ischemic brain is controlled by arteriolar smooth muscle cell contractility and not by capillary pericytes," eng, *Neuron*, vol. 87, no. 1, pp. 95–110, Jul. 2015, ISSN: 1097-4199. DOI: 10.1016/j.neuron.2015.06.001.

[181] C.-C. Ho, Y.-C. Chen, M.-H. Tsai, *et al.*, "Ambient particulate matter induces vascular smooth muscle cell phenotypic changes via nox1/ros/nf-κB Dependent and Independent Pathways: Protective effects of polyphenols," en, *Antioxidants*, vol. 10, no. 55, p. 782, May 2021, ISSN: 2076-3921. DOI: 10.3390/antiox10050782.

[182] R. D. Hoge, J. Atkinson, B. Gill, G. R. Crelier, S. Marrett, and G. B. Pike, "Investigation of bold signal dependence on cerebral blood flow and oxygen consumption: The deoxyhemoglobin dilution model," eng, *Magnetic Resonance in Medicine*, vol. 42, no. 5, 849â863, Nov. 1999, ISSN: 0740-3194. DOI: 10.1002/(sici)1522-2594(199911)42:5<849::aid-mrm4>3.0.co;2-z.

[183] R. L. Hoiland, H. G. Caldwell, J. M. J. R. Carr, *et al.*, "Nitric oxide contributes to cerebrovascular shear-mediated dilatation but not steady-state cerebrovascular reactivity to carbon dioxide," eng, *The Journal of Physiology*, vol. 600, no. 6, pp. 1385–1403, Mar. 2022, ISSN: 1469-7793. DOI: 10.1113/JP282427.

[184] C. A. Howe, H. G. Caldwell, J. Carr, D. Nowak-Flück, P. N. Ainslie, and R. L. Hoiland, "Cerebrovascular reactivity to carbon dioxide is not influenced by variability in the ventilatory sensitivity to carbon dioxide," en, *Experimental Physiology*, vol. 105, no. 5, pp. 904–915, 2020, ISSN: 1469-445X. DOI: 10.1113/EP088192.

[185] C. Iadecola, "Neurovascular regulation in the normal brain and in alzheimer's disease," en, *Nature Reviews Neuroscience*, vol. 5, no. 55, pp. 347–360, May 2004, ISSN: 1471-0048. DOI: 10.1038/nrn1387.

[186] C. Iadecola, "The pathobiology of vascular dementia," eng, *Neuron*, vol. 80, no. 4, pp. 844–866, Nov. 2013, ISSN: 1097-4199. DOI: 10.1016/j.neuron.2013.10.008.

[187] K. Ide, M. Worthley, T. Anderson, and M. J. Poulin, "Effects of the nitric oxide synthase inhibitor l-nmma on cerebrovascular and cardiovascular responses to hypoxia and hypercapnia in humans," *The Journal of Physiology*, vol. 584, no. Pt 1, pp. 321–332, Oct. 2007, ISSN: 0022-3751. DOI: 10.1113/jphysiol.2007.138206.

[188] S. Ihalainen, R. Soliymani, E. Iivanainen, *et al.*, "Proteome analysis of cultivated vascular smooth muscle cells from a cadasil patient," *Molecular Medicine*, vol. 13, no. 5–6, pp. 305–314, 2007, ISSN: 1076-1551. DOI: 10.2119/2006-00069.ihalainen.

[189] I. Ikegaki, T. Hattori, T. Yamaguchi, *et al.*, "Involvement of rho-kinase in vascular remodeling caused by long-term inhibition of nitric oxide synthesis in rats," en, *European Journal of Pharmacology*, vol. 427, no. 1, pp. 69–75, Sep. 2001, ISSN: 0014-2999. DOI: 10.1016/S0014-2999(01)01181-5.

[190] N. Ishizaka, M. Noda, S. Yokoyama, K. Kawasaki, M. Yamamoto, and H. Higashida, "Muscarinic acetylcholine receptor subtypes in the human iris," *Brain Research*, vol. 787, no. 2, pp. 344–347, Mar. 1998, ISSN: 0006-8993. DOI: 10.1016/S0006-8993(97)01554-0.

[191] Y. Iturria-Medina, R. C. Sotero, P. J. Toussaint, *et al.*, "Early role of vascular dysregulation on late-onset alzheimer's disease based on multifactorial data-driven analysis," *Nature Communications*, vol. 7, no. 1, p. 11 934, 2016. DOI: 10.1038/ncomms11934.

[192] W. J. Jagust, J. L. Eberling, B. R. Reed, C. A. Mathis, and T. F. Budinger, "Clinical studies of cerebral blood flow in alzheimer's disease," eng, *Annals of the New York Academy of Sciences*, vol. 826, pp. 254–262, Sep. 1997, ISSN: 0077-8923. DOI: 10.1111/j.1749-6632.1997.tb48477.x.

[193] F.-P. Jahns, J. P. Miroz, M. Messerer, *et al.*, "Quantitative pupillometry for the monitoring of intracranial hypertension in patients with severe traumatic brain injury," en, *Critical Care*, vol. 23, no. 1, p. 155, May 2019, ISSN: 1364-8535. DOI: 10.1186/s13054-019-2436-3.

[194] V. Jain, M. C. Langham, T. F. Floyd, G. Jain, J. F. Magland, and F. W. Wehrli, "Rapid magnetic resonance measurement of global cerebral metabolic rate of oxygen consumption in humans during rest and hypercapnia," eng, *Journal of Cerebral Blood Flow and Metabolism: Official Journal of the International Society of Cerebral Blood Flow and Metabolism*, vol. 31, no. 7, 1504â1512, Jul. 2011, ISSN: 1559-7016. DOI: 10.1038/jcbfm.2011.34.

[195] M. Jankowska-Kieltyka, A. Roman, and I. Nalepa, "The air we breathe: Air pollution as a prevalent proinflammatory stimulus contributing to neurodegeneration," *Frontiers in Cellular Neuroscience*, vol. 15, Jun. 2021, ISSN: 1662-5102. DOI: 10.3389/fncel.2021.647643.

[196] M. Jenkinson, C. Beckmann, T. Behrens, M. Woolrich, and S. Smith, "Fsl," fy, *YEARS OF fMRI*, vol. 20, pp. 782–790, 2012. DOI: 10.1016/j.neuroimage.2011.09.015.

[197] H. T. Jeong, D. S. Kim, K. W. Kang, Y. T. Nam, J. E. Oh, and E. K. Cho, "Factors affecting basilar artery pulsatility index on transcranial doppler," en, *Korean Journal of Clinical Laboratory Science*, vol. 50, no. 4, pp. 477–483, Dec. 2018, ISSN: 1738-3544. DOI: 10.15324/kjcls.2018.50.4.477.

[198] M. Jessup, B. Greenberg, D. Mancini, *et al.*, "Calcium upregulation by percutaneous administration of gene therapy in cardiac disease (cupid)," *Circulation*, vol. 124, no. 3, pp. 304–313, Jul. 2011. DOI: 10.1161/CIRCULATIONAHA.111.022889.

[199] L. Jin, Z. Ying, and R. C. Webb, "Activation of rho/rho kinase signaling pathway by reactive oxygen species in rat aorta," *American Journal of Physiology-Heart and Circulatory Physiology*, vol. 287, no. 4, H1495–H1500, Oct. 2004, ISSN: 0363-6135. DOI: 10.1152/ajpheart.01006.2003.

[200] H. Jo, S. Gotts, R. Reynolds, *et al.*, "Effective preprocessing procedures virtually eliminate distance-dependent motion artifacts in resting state fmri," en, *J. Appl. Math*, p. 935 154, 2013. DOI: 10.1155/2013/935154.

[201] A. Joutel, F. Andreux, S. Gaulis, *et al.*, "The ectodomain of the notch3 receptor accumulates within the cerebrovasculature of cadasil patients," eng, *The Journal of Clinical Investigation*, vol. 105, no. 5, pp. 597–605, Mar. 2000, ISSN: 0021-9738. DOI: 10.1172/JCI8047.

[202] A. Joutel, K. Vahedi, C. Corpechot, *et al.*, "Strong clustering and stereotyped nature of notch3 mutations in cadasil patients," eng, *Lancet (London, England)*, vol. 350, no. 9090, pp. 1511–1515, Nov. 1997, ISSN: 0140-6736. DOI: 10.1016/S0140-6736(97)08083-5.

[203] A. Joutel, C. Corpechot, A. Ducros, *et al.*, "Notch3 mutations in cadasil, a hereditary adult-onset condition causing stroke and dementia," en, *Nature*, vol. 383, no. 66026602, pp. 707–710, Oct. 1996, ISSN: 1476-4687. DOI: 10.1038/383707a0.

[204] S. Ju, L. Lim, Y.-J. Ki, D.-H. Choi, and H. Song, "Oxidative stress generated by polycyclic aromatic hydrocarbons from ambient particulate matter enhance vascular smooth muscle cell migration through mmp upregulation and actin reorganization," *Particle and Fibre Toxicology*, vol. 19, no. 1, p. 29, Apr. 2022, ISSN: 1743-8977. DOI: 10.1186/s12989-022-00472-z.

[205] A. D. Kane, Y. Niu, E. A. Herrera, A. J. Morton, and D. A. Giussani, "Impaired nitric oxide mediated vasodilation in the peripheral circulation in the r6/2 mouse model of huntington's disease.," *Scientific reports*, vol. 6, no. 1, p. 25 979, 2016. DOI: 10.1038/srep25979.

[206] H.-S. Kang, Y.-J. Moon, Y.-Y. Kim, *et al.*, "Smooth-muscle progenitor cells isolated from patients with moyamoya disease: Novel experimental cell model: Laboratory investigation," en$_U$S, *Journal of Neurosurgery*, vol. 120, no. 2, pp. 415–425, Feb. 2014, ISSN: 1933-0693, 0022-3085. DOI: 10.3171/2013.9.JNS131000.

[207] S. Kang, H.-H. Woo, K. Kim, *et al.*, "Dysfunction of vascular smooth muscle and vascular remodeling by simvastatin," *Toxicological Sciences*, vol. 138, no. 2, pp. 446–556, 2014, ISSN: 1096-6080. DOI: 10.1093/toxsci/kfu011.

[208] K. Karavanaki, A. G. Davies, L. P. Hunt, M. H. Morgan, and J. D. Baum, "Pupil size in diabetes.," en, *Archives of Disease in Childhood*, vol. 71, no. 6, pp. 511–515, Dec. 1994, ISSN: 0003-9888, 1468-2044. DOI: 10.1136/adc.71.6.511.

[209] V. Karoor, M. Oka, S. J. Walchak, L. B. Hersh, Y. E. Miller, and E. C. Dempsey, "Neprilysin regulates pulmonary artery smooth muscle cell phenotype through a platelet-derived growth factor receptor–dependent mechanism," *Hypertension*, vol. 61, no. 4, pp. 921–930, Apr. 2013. DOI: 10.1161/HYPERTENSIONAHA.111.199588.

[210] A. Kastrup, C. Thomas, C. Hartmann, and M. Schabet, "Sex dependency of cerebrovascular co2 reactivity in normal subjects," *Stroke*, vol. 28, no. 12, pp. 2353–2356, Dec. 1997. DOI: 10.1161/01.STR.28.12.2353.

[211] M. Kawajiri, M. Mogi, N. Higaki, *et al.*, "Reduced angiotensin ii levels in the cerebrospinal fluid of patients with amyotrophic lateral sclerosis," en, *Acta Neurologica Scandinavica*, vol. 119, no. 5, pp. 341–344, 2009, ISSN: 1600-0404. DOI: 10.1111/j.1600-0404.2008.01099.x.

[212] T. Kawakubo, R. Mori, K. Shirotani, N. Iwata, and M. Asai, "Neprilysin is suppressed by dual-specificity tyrosine-phosphorylation regulated kinase 1a (dyrk1a) in down-syndrome-derived fibroblasts," *Biological and Pharmaceutical Bulletin*, vol. 40, no. 3, pp. 327–333, 2017, ISSN: 0918-6158. DOI: 10.1248/bpb.b16-00825.

[213] D. Kester and M. Mueller, "Bayesicfitting, a python toolbox for bayesian fitting and evidence calculation.: Including a nested sampling implementation.," *Astronomy and Computing*, vol. 37, p. 100 503, Oct. 2021, ISSN: 2213-1337. DOI: 10.1016/j.ascom.2021.100503.

[214] S. S. Kety and C. F. Schmidt, "The effects of altered arterial tensions of carbon dioxide and oxygen on cerebral blood flow and cerebral oxygen consumption of normal young men 1," *Journal of Clinical Investigation*, vol. 27, no. 4, pp. 484–492, Jul. 1948, ISSN: 0021-9738.

[215] R. Khalil, "Vascular smooth muscle dysfunction and vascular disease," en, in *Regulation of Vascular Smooth Muscle Function*, Morgan & Claypool Life Sciences, 2010.

[216] N. Kiaie, A. M. Gorabi, Å. Reiner, T. Jamialahmadi, M. Ruscica, and A. Sahebkar, "Effects of statins on renin–angiotensin system," *Journal of Cardiovascular Development and Disease*, vol. 8, no. 7, p. 80, Jul. 2021, ISSN: 2308-3425. DOI: 10.3390/jcdd8070080.

[217] D. Kim, T. M. Hughes, M. E. Lipford, *et al.*, "Relationship between cerebrovascular reactivity and cognition among people with risk of cognitive decline," *Frontiers in Physiology*, vol. 12, p. 645 342, May 2021, ISSN: 1664-042X. DOI: 10.3389/fphys.2021.645342.

[218] F. J. Kirkham, T. S. Padayachee, S. Parsons, L. S. Seargeant, F. R. House, and R. G. Gosling, "Transcranial measurement of blood velocities in the basal cerebral arteries using pulsed doppler ultrasound: Velocity as an index of flow," *Ultrasound in Medicine & Biology*, vol. 12, no. 1, pp. 15–21, Jan. 1986, ISSN: 0301-5629. DOI: 10.1016/0301-5629(86)90139-0.

[219] D. Kleinfeld, P. P. Mitra, F. Helmchen, and W. Denk, "Fluctuations and stimulus-induced changes in blood flow observed in individual capillaries in layers 2 through 4 of rat neocortex," *Proceedings of the National Academy of Sciences*, vol. 95, no. 26, pp. 15 741–15 746, Dec. 1998. DOI: 10.1073/pnas.95.26.15741.

[220] T. Koo and M. Li, "A guideline of selecting and reporting intraclass correlation coefficients for reliability research," en, *J. Chiropr. Med*, vol. 15, pp. 155–163, 2016. DOI: 10.1016/j.jcm.2016.02.012.

[221] A. Krainik, M. Hund-Georgiadis, S. Zysset, and D. Cramon, "Regional impairment of cerebrovascular reactivity and bold signal in adults after stroke," en,

Stroke, vol. 36, pp. 1146–1152, 2005. DOI: 10.1161/01.STR.0000166178.40973.a7.

[222] A. Krettek, G. Fager, P. Jernberg, G. Ãstergren Lundén, and F. Lustig, "Quantitation of platelet-derived growth factor receptors in human arterial smooth muscle cells in vitro," *Arteriosclerosis, Thrombosis, and Vascular Biology*, vol. 17, no. 11, pp. 2395–2404, Nov. 1997. DOI: 10.1161/01.ATV.17.11.2395.

[223] A. Kumar, Ekavali, J. Mishra, K. Chopra, and D. K. Dhull, "Possible role of p-glycoprotein in the neuroprotective mechanism of berberine in intracerebroventricular streptozotocin-induced cognitive dysfunction," en, *Psychopharmacology*, vol. 233, no. 1, pp. 137–152, Jan. 2016, ISSN: 1432-2072. DOI: 10.1007/s00213-015-4095-7.

[224] V. Kumar, K. Bishayee, S. Park, U. Lee, and J. Kim, "Oxidative stress in cerebrovascular disease and associated diseases," *Frontiers in Endocrinology*, vol. 14, p. 1 124 419, Feb. 2023, ISSN: 1664-2392. DOI: 10.3389/fendo.2023.1124419.

[225] S. Kuroda and K. Houkin, "Moyamoya disease: Current concepts and future perspectives," eng, *The Lancet. Neurology*, vol. 7, no. 11, pp. 1056–1066, Nov. 2008, ISSN: 1474-4422. DOI: 10.1016/S1474-4422(08)70240-0.

[226] K. K. Kwong, J. W. Belliveau, D. A. Chesler, *et al.*, "Dynamic magnetic resonance imaging of human brain activity during primary sensory stimulation," eng, *Proceedings of the National Academy of Sciences of the United States of America*, vol. 89, no. 12, 5675â5679, Jun. 1992, ISSN: 0027-8424. DOI: 10.1073/pnas.89.12.5675.

[227] P. Lanting, R. L. Strijers, J. E. Bos, T. J. Faes, and J. J. Heimans, "The cause of increased pupillary light reflex latencies in diabetic patients: The relationship between pupillary light reflex and visual evoked potential latencies," eng, *Electroencephalography and Clinical Neurophysiology*, vol. 78, no. 2, pp. 111–115, Feb. 1991, ISSN: 0013-4694. DOI: 10.1016/0013-4694(91)90110-p.

[228] S. Lavi, D. Gaitini, V. Milloul, and G. Jacob, "Impaired cerebral co2 vasoreactivity: Association with endothelial dysfunction," eng, *American Journal of Physiology. Heart and Circulatory Physiology*, vol. 291, no. 4, H1856–1861, Oct. 2006, ISSN: 0363-6135. DOI: 10.1152/ajpheart.00014.2006.

[229] R. E. Law, S. Goetze, X.-P. Xi, *et al.*, "Expression and function of pparγ in Rat and Human Vascular Smooth Muscle Cells," *Circulation*, vol. 101, no. 11, pp. 1311–1318, Mar. 2000. DOI: 10.1161/01.CIR.101.11.1311.

[230] L. N. N. Le, G. J. Wheeler, E. N. Holy, *et al.*, "Cortical oxygen extraction fraction using quantitative bold mri and cerebral blood flow during vasodilation," English, *Frontiers in Physiology*, vol. 14, Oct. 2023, ISSN: 1664-042X. DOI: 10.3389/fphys.2023.1231793. [Online]. Available: https://www.frontiersin.org/journals/physiology/articles/10.3389/fphys.2023.1231793/full.

[231] B.-C. Lee, H.-H. Tsai, A. P.-H. Huang, *et al.*, "Arterial spin labeling imaging assessment of cerebrovascular reactivity in hypertensive small vessel disease," *Frontiers in Neurology*, vol. 12, 2021, ISSN: 1664-2295. DOI: 10.3389/fneur.2021.640069.

[232] C.-f. Lee and Y. Chern, "Chapter ten - adenosine receptors and huntington's disease," en, in *International Review of Neurobiology* (Adenosine Receptors in Neurology and Psychiatry), A. Mori, Ed., Adenosine Receptors in Neurology

and Psychiatry. Academic Press, Jan. 2014, vol. 119, pp. 195–232. DOI: 10.1016/B978-0-12-801022-8.00010-6.

[233] S.-H. Lee, S. M. Gomes, J. Ghalayini, K. G. Iliadi, and G. L. Boulianne, "Angiotensin converting enzyme inhibitors and angiotensin receptor blockers rescue memory defects indrosophila-expressing alzheimerâs disease-related transgenes independently of the canonical renin angiotensin system," English, *eneuro*, vol. 7, no. 6, ENEURO.0235–20.2020, Oct. 2020, ISSN: 2373-2822. DOI: 10.1523/eneuro.0235-20.2020.

[234] R. Leoni, K. Mazzeto-Betti, K. Andrade, and D. Araujo, "Quantitative evaluation of hemodynamic response after hypercapnia among different brain territories by fmri," en, *NeuroImage*, vol. 41, pp. 1192–1198, 2008. DOI: 10.1016/j.neuroimage.2008.03.035.

[235] A. G. Lerner, A. Bernabé-Ortiz, R. Ticse, *et al.*, "Type 2 diabetes and cardiac autonomic neuropathy screening using dynamic pupillometry," eng, *Diabetic Medicine: A Journal of the British Diabetic Association*, vol. 32, no. 11, pp. 1470–1478, Nov. 2015, ISSN: 1464-5491. DOI: 10.1111/dme.12752.

[236] J. Leung, P. D. Kosinski, P. L. Croal, and A. Kassner, "Developmental trajectories of cerebrovascular reactivity in healthy children and young adults assessed with magnetic resonance imaging," *The Journal of Physiology*, vol. 594, no. 10, pp. 2681–2689, 2016, ISSN: 1469-7793. DOI: 10.1113/jp271056.

[237] D. Leys, H. Hénon, M.-A. Mackowiak-Cordoliani, and F. Pasquier, "Poststroke dementia," English, *The Lancet Neurology*, vol. 4, no. 11, 752â759, Nov. 2005, ISSN: 1474-4422. DOI: 10.1016/s1474-4422(05)70221-0.

[238] J.-M. Li, T.-X. Cui, T. Shiuchi, *et al.*, "Nicotine enhances angiotensin ii-induced mitogenic response in vascular smooth muscle cells and fibroblasts," *Arteriosclerosis, Thrombosis, and Vascular Biology*, vol. 24, no. 1, pp. 80–84, Jan. 2004. DOI: 10.1161/01.ATV.0000104007.17365.1c.

[239] R. Li, Z. Zhuo, Y. Hong, *et al.*, "Effects of the fasting-postprandial state on arterial spin labeling mri-based cerebral perfusion quantification in alzheimerâs disease," en, *Journal of Magnetic Resonance Imaging*, vol. 60, no. 5, 2173â2183, 2024, ISSN: 1522-2586. DOI: 10.1002/jmri.29348.

[240] W. Li, J. Li, W. Liu, B. T. Altura, and B. M. Altura, "Alcohol-induced apoptosis of canine cerebral vascular smooth muscle cells: Role of extracellular and intracellular calcium ions," eng, *Neuroscience Letters*, vol. 354, no. 3, pp. 221–224, Jan. 2004, ISSN: 0304-3940. DOI: 10.1016/j.neulet.2003.10.047.

[241] K.-W. Liang, C.-T. Ting, S.-C. Yin, *et al.*, "Berberine suppresses mek/erk-dependent egr-1 signaling pathway and inhibits vascular smooth muscle cell regrowth after in vitro mechanical injury," en, *Biochemical Pharmacology*, vol. 71, no. 6, pp. 806–817, Mar. 2006, ISSN: 0006-2952. DOI: 10.1016/j.bcp.2005.12.028.

[242] M. K. Liem, S. A. J. L. Oberstein, J. Haan, *et al.*, "Cerebrovascular reactivity is a main determinant of white matter hyperintensity progression in cadasil," en, *American Journal of Neuroradiology*, vol. 30, no. 6, pp. 1244–1247, Jun. 2009, ISSN: 0195-6108, 1936-959X. DOI: 10.3174/ajnr.A1533.

[243] A. Lin, N. J. Peiris, H. Dhaliwal, *et al.*, "Mural cells: Potential therapeutic targets to bridge cardiovascular disease and neurodegeneration," *Cells*, vol. 10, no. 3, p. 593, 2021. DOI: 10.3390/cells10030593.

[244] R. Lin, Z. Xie, J. Zhang, *et al.*, "Clinical and immunopathological features of moyamoya disease," en, *PLOS ONE*, vol. 7, no. 4, e36386, Apr. 2012, ISSN: 1932-6203. DOI: 10.1371/journal.pone.0036386.

[245] V. Lindner, C. Booth, I. Prudovsky, D. Small, T. Maciag, and L. Liaw, "Members of the jagged/notch gene families are expressed in injured arteries and regulate cell phenotype via alterations in cell matrix and cell-cell interaction," en, *The American Journal of Pathology*, vol. 159, no. 3, pp. 875–883, Sep. 2001, ISSN: 0002-9440. DOI: 10.1016/S0002-9440(10)61763-4.

[246] M. Lindquist, S. Geuter, T. Wager, and B. Caffo, "Modular preprocessing pipelines can reintroduce artifacts into fmri data," en, *Hum. Brain Mapp*, vol. 40, pp. 2358–2376, 2019. DOI: 10.1002/hbm.24528.

[247] I. Lipp, K. Murphy, X. Caseras, and R. Wise, "Agreement and repeatability of vascular reactivity estimates based on a breath-hold task and a resting state scan," en, *NeuroImage*, vol. 113, pp. 387–396, 2015. DOI: 10.1016/j.neuroimage.2015.03.004.

[248] L. A. Lipsitz, S. Mukai, J. Hamner, M. Gagnon, and V. Babikian, "Dynamic regulation of middle cerebral artery blood flow velocity in aging and hypertension," *Stroke*, vol. 31, no. 8, pp. 1897–1903, Aug. 2000. DOI: 10.1161/01.STR.31.8.1897.

[249] P. Liu, J. De Vis, and H. Lu, "Cerebrovascular reactivity (cvr) mri with co2 challenge: A technical review," *NeuroImage*, vol. 187, pp. 104–115, Feb. 2019, ISSN: 1053-8119. DOI: 10.1016/j.neuroimage.2018.03.047.

[250] P. Liu, G. Liu, M. C. Pinho, *et al.*, "Cerebrovascular reactivity mapping using resting-state bold functional mri in healthy adults and patients with moyamoya disease," eng, *Radiology*, vol. 299, no. 2, pp. 419–425, May 2021, ISSN: 1527-1315. DOI: 10.1148/radiol.2021203568.

[251] P. Liu, B. G. Welch, Y. Li, *et al.*, "Multiparametric imaging of brain hemodynamics and function using gas-inhalation mri," en, *NeuroImage*, vol. 146, pp. 715–723, Feb. 2017, ISSN: 1053-8119. DOI: 10.1016/j.neuroimage.2016.09.063.

[252] P. Liu, C. Xu, Z. Lin, *et al.*, "Cerebrovascular reactivity mapping using intermittent breath modulation," *NeuroImage*, vol. 215, p. 116 787, Jul. 2020, ISSN: 1053-8119. DOI: 10.1016/j.neuroimage.2020.116787.

[253] S. Liu and Z. Lin, "Vascular smooth muscle cells mechanosensitive regulators and vascular remodeling," *Journal of Vascular Research*, vol. 59, no. 2, pp. 90–113, 2022, ISSN: 1018-1172, 1423-0135. DOI: 10.1159/000519845.

[254] G. Livingston, J. Huntley, A. Sommerlad, *et al.*, "Dementia prevention, intervention, and care: 2020 report of the lancet commission," *The Lancet*, vol. 396, no. Dement Geriatr Cogn Dis 37 2014, pp. 413–446, 2020, ISSN: 0140-6736. DOI: 10.1016/s0140-6736(20)30367-6.

[255] T. G. von Lueder, D. Atar, and H. Krum, "Current role of neprilysin inhibitors in hypertension and heart failure," eng, *Pharmacology & Therapeutics*, vol. 144,

no. 1, pp. 41–49, Oct. 2014, ISSN: 1879-016X. DOI: 10.1016/j.pharmthera.2014.05.002.

[256] C. Lugnan, P. Caruso, L. Rossi, G. Furlanis, M. Naccarato, and P. Manganotti, "Changes in cerebrovascular reactivity as a marker of cognitive impairment risk: A transcranial doppler study," en, *Journal of Ultrasound*, Jan. 2025, ISSN: 1876-7931. DOI: 10.1007/s40477-025-00986-0.

[257] X. Ma, Y. Wang, and N. L. Stephens, "Serum deprivation induces a unique hypercontractile phenotype of cultured smooth muscle cells," *American Journal of Physiology-Cell Physiology*, vol. 274, no. 5, pp. C1206–C1214, 1998, ISSN: 0363-6143. DOI: 10.1152/ajpcell.1998.274.5.c1206.

[258] Y.-G. Ma, Y.-B. Zhang, Y.-G. Bai, *et al.*, "Berberine alleviates the cerebrovascular contractility in streptozotocin-induced diabetic rats through modulation of intracellular ca2+ handling in smooth muscle cells," *Cardiovascular Diabetology*, vol. 15, no. 1, p. 63, Apr. 2016, ISSN: 1475-2840. DOI: 10.1186/s12933-016-0382-9.

[259] C. P. Mack, "Signaling mechanisms that regulate smooth muscle cell differentiation," *Arteriosclerosis, Thrombosis, and Vascular Biology*, vol. 31, no. 7, pp. 1495–1505, Jul. 2011. DOI: 10.1161/ATVBAHA.110.221135.

[260] B. A. MacVicar and E. A. Newman, "Astrocyte regulation of blood flow in the brain," *Cold Spring Harbor Perspectives in Biology*, vol. 7, no. 5, a020388, May 2015, ISSN: 1943-0264. DOI: 10.1101/cshperspect.a020388.

[261] S. Magon, G. Basso, P. Farace, G. Ricciardi, A. Beltramello, and A. Sbarbati, "Reproducibility of bold signal change induced by breath holding," en, *NeuroImage*, vol. 45, pp. 702–712, 2009. DOI: 10.1016/j.neuroimage.2008.12.059.

[262] R. Markello and E. DuPre, *Physiopy/peakdet: A toolbox for physiological peak detection analyses*, en, 2020. DOI: 10.5281/zenodo.7244954. [Online]. Available: https://doi.org/10.5281/zenodo.7244954.

[263] H. Markus and M. Cullinane, "Severely impaired cerebrovascular reactivity predicts stroke and tia risk in patients with carotid artery stenosis and occlusion," en, *Brain J. Neurol*, vol. 124, pp. 457–467, 2001. DOI: 10.1093/brain/124.3.457.

[264] G. Marsboom and S. L. Archer, "Pathways of proliferation: New targets to inhibit the growth of vascular smooth muscle cells," *Circulation research*, vol. 103, no. 10, pp. 1047–1049, Nov. 2008, ISSN: 0009-7330. DOI: 10.1161/CIRCRESAHA.108.188003.

[265] O. Marshall, H. Lu, J.-C. Brisset, *et al.*, "Impaired cerebrovascular reactivity in multiple sclerosis," *JAMA Neurology*, vol. 71, no. 10, pp. 1275–1281, 2014, ISSN: 2168-6149. DOI: 10.1001/jamaneurol.2014.1668.

[266] R. Martier and P. Konstantinova, "Gene therapy for neurodegenerative diseases: Slowing down the ticking clock," *Frontiers in Neuroscience*, vol. 14, 2020, ISSN: 1662-453X. DOI: 10.3389/fnins.2020.580179.

[267] J. T. Martin, J. Pinto, D. Bulte, and M. Spitschan, "Pyplr: A versatile, integrated system of hardware and software for researching the human pupillary light reflex," en, *Behavior Research Methods*, vol. 54, no. 6, pp. 2720–2739, Dec. 2022, ISSN: 1554-3528. DOI: 10.3758/s13428-021-01759-3.

[268] D. C. Mash, Q. Ouyang, J. Pablo, *et al.*, "Cocaine abusers have an overexpression of î± − *synucleinindopamineneurons*," *The Journal of Neuroscience*, vol. 23, no. 7, pp. 2564–2571, Apr. 2003, ISSN: 0270-6474. DOI: 10.1523/JNEUROSCI.23-07-02564.2003.

[269] T. Matsushita, N. Isobe, M. Kawajiri, *et al.*, "Csf angiotensin ii and angiotensin-converting enzyme levels in anti-aquaporin-4 autoimmunity," eng, *Journal of the Neurological Sciences*, vol. 295, no. 1–2, pp. 41–45, Aug. 2010, ISSN: 1878-5883. DOI: 10.1016/j.jns.2010.05.014.

[270] J. Mazziotta, A. Toga, A. Evans, *et al.*, "A probabilistic atlas and reference system for the human brain: International consortium for brain mapping (icbm," en, *Philos. Trans. R. Soc. Lond. Ser. B*, vol. 356, pp. 1293–1322, 2001. DOI: 10.1098/rstb.2001.0915.

[271] M. N. McDonnell, N. M. Berry, M. A. Cutting, H. A. Keage, J. D. Buckley, and P. R. Howe, "Transcranial doppler ultrasound to assess cerebrovascular reactivity: Reliability, reproducibility and effect of posture," *PeerJ*, vol. 1, e65, Apr. 2013, ISSN: 2167-8359. DOI: 10.7717/peerj.65.

[272] S. McSwain, D. Hamel, P. Smith, *et al.*, "End-tidal and arterial carbon dioxide measurements correlate across all levels of physiologic dead space," en, *Respir. Care*, vol. 55, pp. 288–293, 2010. DOI: 10.4187/respcare.10550288.

[273] M. Meki, A. El-Baz, P. Sethu, and G. Giridharan, "Effects of pulsatility on arterial endothelial and smooth muscle cells," eng, *Cells, Tissues, Organs*, Mar. 2022, ISSN: 1422-6421. DOI: 10.1159/000524317.

[274] H. Meng, L. Fan, C.-J. Zhang, *et al.*, "Synthetic vsmcs induce bbb disruption mediated by mypt1 in ischemic stroke.," *iScience*, vol. 24, no. 9, p. 103 047, 2021, ISSN: 2589-0042. DOI: 10.1016/j.isci.2021.103047.

[275] E. Merlet, L. Lipskaia, A. Marchand, *et al.*, "A calcium-sensitive promoter construct for gene therapy," en, *Gene Therapy*, vol. 20, no. 33, pp. 248–254, Mar. 2013, ISSN: 1476-5462. DOI: 10.1038/gt.2012.30.

[276] A. Mestanikova, I. Ondrejka, M. Mestanik, *et al.*, "Pupillary light reflex is altered in adolescent depression," en, *Physiological Research*, S277–S284, Aug. 2017, ISSN: 1802-9973, 0862-8408. DOI: 10.33549/physiolres.933683.

[277] J. Mikhail Kellawan, J. W. Harrell, E. M. Schrauben, *et al.*, "Quantitative cerebrovascular 4d flow mri at rest and during hypercapnia challenge," *Magnetic Resonance Imaging*, vol. 34, no. 4, pp. 422–428, May 2016, ISSN: 0730-725X. DOI: 10.1016/j.mri.2015.12.016.

[278] A. Milanlioglu, A. Yaman, M. Kolukisa, and T. Asil, "Evaluation of cerebral hemodynamic status in patients with unilateral symptomatic carotid artery stenosis during motor tasks, through use of transcranial doppler sonography," eng, *Arquivos De Neuro-Psiquiatria*, vol. 80, no. 4, pp. 339–343, Apr. 2022, ISSN: 1678-4227. DOI: 10.1590/0004-282X-ANP-2020-0571.

[279] B. J. Miller, S. Sareddy, P. B. Rosenquist, and W. V. McCall, "Pupillary light reflex markers of suicide risk in a trans-diagnostic sample," en, *Schizophrenia Research*, vol. 235, pp. 1–2, Sep. 2021, ISSN: 0920-9964. DOI: 10.1016/j.schres.2021.06.027.

[280] K. B. Miller, A. J. Howery, R. E. Harvey, M. W. Eldridge, and J. N. Barnes, "Cerebrovascular reactivity and central arterial stiffness in habitually exercising

healthy adults," English, *Frontiers in Physiology*, vol. 9, Aug. 2018, ISSN: 1664-042X. DOI: 10.3389/fphys.2018.01096. [Online]. Available: https://www.frontiersin.org/journals/physiology/articles/10.3389/fphys.2018.01096/full.

[281] T. Minamino, S. A. Mitsialis, and S. Kourembanas, "Hypoxia extends the life span of vascular smooth muscle cells through telomerase activation," *Molecular and Cellular Biology*, vol. 21, no. 10, pp. 3336–3342, May 2001. DOI: 10.1128/MCB.21.10.3336-3342.2001.

[282] J. S. Miners, S. Morris, S. Love, and P. G. Kehoe, "Accumulation of insoluble amyloid-β in Down's Syndrome is Associated with Increased BACE-1 and Neprilysin Activities," *Journal of Alzheimer's Disease*, vol. 23, no. 1, pp. 101–108, 2011, ISSN: 1387-2877. DOI: 10.3233/jad-2010-101395.

[283] S. Miners, H. Moulding, R. Silva, and S. Love, "Reduced vascular endothelial growth factor and capillary density in the occipital cortex in dementia with lewy bodies," *Brain Pathology*, vol. 24, no. 4, pp. 334–343, 2014, ISSN: 1750-3639. DOI: 10.1111/bpa.12130.

[284] J. S. Minhas, R. B. Panerai, and T. G. Robinson, "Modelling the cerebral haemodynamic response in the physiological range of paco2," eng, *Physiological Measurement*, vol. 39, no. 6, p. 065 001, Jun. 2018, ISSN: 1361-6579. DOI: 10.1088/1361-6579/aac76b.

[285] L. M. Minter, D. M. Turley, P. Das, *et al.*, "Inhibitors of γ-secretase block in vivo and in vitro T helper type 1 polarization by preventing Notch upregulation of Tbx21," en, *Nature Immunology*, vol. 6, no. 77, pp. 680–688, Jul. 2005, ISSN: 1529-2916. DOI: 10.1038/ni1209x.

[286] G. D. Mitsis, P. N. Ainslie, M. J. Poulin, P. A. Robbins, and V. Z. Marmarelis, "Nonlinear modeling of the dynamic effects of arterial pressure and blood gas variations on cerebral blood flow in healthy humans," en, in *Post-Genomic Perspectives in Modeling and Control of Breathing*, J. Champagnat, M. Denavit-Saubié', G. Fortin, A. S. Foutz, and M. Thoby-Brisson, Eds., ser. Advances in Experimental Medicine and Biology, Boston, MA: Springer US, 2005, pp. 259–265, ISBN: 978-0-387-27023-4. DOI: 10.1007/0-387-27023-X_39.

[287] S. Moia, *Smoia/euskalibur_dataproc.* en, 2022.

[288] S. Moia, R. Stickland, A. Ayyagari, M. Termenon, C. Caballero-Gaudes, and M. Bright, "Voxelwise optimization of hemodynamic lags to improve regional cvr estimates in breath-hold fmri," en, *Annu. Int. Conf. IEEE Eng. Med. Biol. Soc. IEEE Eng. Med. Biol. Soc. Annu. Int. Conf*, pp. 1489–1492, 2020. DOI: 10.1109/EMBC44109.2020.9176225.

[289] S. Moia, M. Termenon, E. Uruñuela, *et al.*, "Ica-based denoising strategies in breath-hold induced cerebrovascular reactivity mapping with multi echo bold fmri," en, *NeuroImage*, vol. 233, p. 117 914, 2021. DOI: 10.1016/j.neuroimage.2021.117914.

[290] T. L. Montagnoli, J. S. da Silva, S. Z. Sudo, *et al.*, "Rock inhibition as potential target for treatment of pulmonary hypertension," en, *Cells*, vol. 10, no. 77, p. 1648, Jul. 2021, ISSN: 2073-4409. DOI: 10.3390/cells10071648.

[291] F. C. Moreton, B. Cullen, C. Delles, *et al.*, "Vasoreactivity in cadasil: Comparison to structural mri and neuropsychology," en, *Journal of Cerebral Blood Flow*

& Metabolism, vol. 38, no. 6, pp. 1085–1095, Jun. 2018, ISSN: 0271-678X. DOI: 10.1177/0271678X17710375.

[292] D. Morrow, J. P. Cullen, W. Liu, P. A. Cahill, and E. M. Redmond, "Alcohol inhibits smooth muscle cell proliferation via regulation of the notch signaling pathway," *Arteriosclerosis, Thrombosis, and Vascular Biology*, vol. 30, no. 12, pp. 2597–2603, Dec. 2010. DOI: 10.1161/ATVBAHA.110.215681.

[293] J. C. Murdoch, J. C. Rodger, S. S. Rao, C. D. Fletcher, and M. G. Dunnigan, "Down's syndrome: An atheroma-free model?" en, *Br Med J*, vol. 2, no. 6081, pp. 226–228, Jul. 1977, ISSN: 0007-1447, 1468-5833. DOI: 10.1136/bmj.2.6081.226.

[294] K. Murphy, A. D. Harris, and R. G. Wise, "Robustly measuring vascular reactivity differences with breath-hold: Normalising stimulus-evoked and resting state bold fmri data," *NeuroImage*, vol. 54, no. 1, 369â379, Jan. 2011, ISSN: 1053-8119. DOI: 10.1016/j.neuroimage.2010.07.059.

[295] W. A. C. Mutch, M. J. Ellis, L. N. Ryner, *et al.*, "Brain magnetic resonance imaging co2 stress testing in adolescent postconcussion syndrome," en, *Journal of Neurosurgery*, vol. 125, no. 3, pp. 648–660, Sep. 2016, ISSN: 1933-0693. DOI: 10.3171/2015.6.jns15972.

[296] S. Na, O. Collin, F. Chowdhury, *et al.*, "Rapid signal transduction in living cells is a unique feature of mechanotransduction," *Proceedings of the National Academy of Sciences*, vol. 105, no. 18, pp. 6626–6631, May 2008. DOI: 10.1073/pnas.0711704105.

[297] K. L. Narayanan, V. Chopra, H. D. Rosas, K. Malarick, and S. Hersch, "Rho kinase pathway alterations in the brain and leukocytes in huntington's disease," en, *Molecular Neurobiology*, vol. 53, no. 4, pp. 2132–2140, May 2016, ISSN: 1559-1182. DOI: 10.1007/s12035-015-9147-9.

[298] B. S. Nassar and G. A. Schmidt, "Estimating arterial partial pressure of carbon dioxide in ventilated patients: How valid are surrogate measures?" eng, *Annals of the American Thoracic Society*, vol. 14, no. 6, pp. 1005–1014, Jun. 2017, ISSN: 2325-6621. DOI: 10.1513/AnnalsATS.201701-034FR.

[299] C. H. G. Neutel, G. Corradin, P. Puylaert, G. R. Y. De Meyer, W. Martinet, and P.-J. Guns, "High pulsatile load decreases arterial stiffness: An ex vivo study," *Frontiers in Physiology*, vol. 12, 2021, ISSN: 1664-042X. DOI: 10.3389/fphys.2021.741346.

[300] K. Niwa, L. Younkin, C. Ebeling, *et al.*, "Aβ1–40-related reduction in functional hyperemia in mouse neocortex during somatosensory activation," *Proceedings of the National Academy of Sciences*, vol. 97, no. 17, pp. 9735–9740, Aug. 2000. DOI: 10.1073/pnas.97.17.9735.

[301] J. M. Oakes, R. M. Fuchs, J. D. Gardner, E. Lazartigues, and X. Yue, "Nicotine and the renin-angiotensin system," *American Journal of Physiology-Regulatory, Integrative and Comparative Physiology*, vol. 315, no. 5, R895–R906, Nov. 2018, ISSN: 0363-6119. DOI: 10.1152/ajpregu.00099.2018.

[302] S Ogawa, T. M. Lee, A. R. Kay, and D. W. Tank, "Brain magnetic resonance imaging with contrast dependent on blood oxygenation.," *Proceedings of the National Academy of Sciences*, vol. 87, no. 24, 9868â9872, Dec. 1990. DOI: 10.1073/pnas.87.24.9868.

[303] S Ogawa, D. W. Tank, R Menon, *et al.*, "Intrinsic signal changes accompanying sensory stimulation: Functional brain mapping with magnetic resonance imaging.," *Proceedings of the National Academy of Sciences*, vol. 89, no. 13, 5951â5955, Jul. 1992. DOI: 10.1073/pnas.89.13.5951.

[304] A. H. Ohlrogge, L. Frost, and R. B. Schnabel, "Harmful impact of tobacco smoking and alcohol consumption on the atrial myocardium," en, *Cells*, vol. 11, no. 1616, p. 2576, Jan. 2022, ISSN: 2073-4409. DOI: 10.3390/cells11162576.

[305] A. Oshorov, E. Alexandrova, K. Muradyan, O. Sosnovskaya, E. Sokolova, and I. Savin, "Pupillometry as a method for monitoring of pupillary light reflex in icu patients," en, *Voprosy neirokhirurgii imeni N.N. Burdenko*, vol. 85, no. 3, p. 117, 2021, ISSN: 0042-8817. DOI: 10.17116/neiro202185031117.

[306] A. Ovsenik, M. Podbregar, and A. Fabjan, "Cerebral blood flow impairment and cognitive decline in heart failure," *Brain and Behavior*, vol. 11, Jun. 2021. DOI: 10.1002/brb3.2176.

[307] G. K. Owens, M. S. Kumar, and B. R. Wamhoff, "Molecular regulation of vascular smooth muscle cell differentiation in development and disease," *Physiological Reviews*, vol. 84, no. 3, pp. 767–801, Jul. 2004, ISSN: 0031-9333. DOI: 10.1152/physrev.00041.2003.

[308] S. Palfi, J. M. Gurruchaga, G. S. Ralph, *et al.*, "Long-term safety and tolerability of prosavin, a lentiviral vector-based gene therapy for parkinson's disease: A dose escalation, open-label, phase 1/2 trial," en, *The Lancet*, vol. 383, no. 9923, pp. 1138–1146, Mar. 2014, ISSN: 0140-6736. DOI: 10.1016/S0140-6736(13)61939-X.

[309] M. Panahi, N. Yousefi Mesri, E.-B. Samuelsson, *et al.*, "Differences in proliferation rate between cadasil and control vascular smooth muscle cells are related to increased tgfβ expression," *Journal of Cellular and Molecular Medicine*, vol. 22, no. 6, pp. 3016–3024, Jun. 2018, ISSN: 1582-1838. DOI: 10.1111/jcmm.13534.

[310] J. C. Park, H. E. Moss, and J. J. McAnany, "The pupillary light reflex in idiopathic intracranial hypertension," eng, *Investigative Ophthalmology & Visual Science*, vol. 57, no. 1, pp. 23–29, Jan. 2016, ISSN: 1552-5783. DOI: 10.1167/iovs.15-18181.

[311] J. G. Park, C. T. Moon, D. S. Park, and S. W. Song, "Clinical utility of an automated pupillometer in patients with acute brain lesion," *Journal of Korean Neurosurgical Society*, vol. 58, no. 4, pp. 363–367, Oct. 2015. DOI: 10.3340/jkns.2015.58.4.363.

[312] P. Parra, R. Costa, D. R. de Asúa, F. Moldenhauer, and C. Suárez, "Atherosclerotic surrogate markers in adults with down syndrome: A case-control study," en, *The Journal of Clinical Hypertension*, vol. 19, no. 2, pp. 205–211, 2017, ISSN: 1751-7176. DOI: 10.1111/jch.12890.

[313] M. P. Parsons and L. A. Raymond, "Chapter 20 - huntington disease," en, in *Neurobiology of Brain Disorders*, M. J. Zigmond, L. P. Rowland, and J. T. Coyle, Eds. San Diego: Academic Press, Jan. 2015, pp. 303–320, ISBN: 978-0-12-398270-4. DOI: 10.1016/B978-0-12-398270-4.00020-3.

[314] M. P. Pase, A. Beiser, J. J. Himali, *et al.*, "Aortic stiffness and the risk of incident mild cognitive impairment and dementia," *Stroke*, vol. 47, no. 9, pp. 2256–2261, Sep. 2016. DOI: 10.1161/STROKEAHA.116.013508.

[315] L. Pauling and C. D. Coryell, "The magnetic properties and structure of the hemochromogens and related substances," *Proceedings of the National Academy of Sciences*, vol. 22, no. 3, 159â163, Mar. 1936. DOI: 10.1073/pnas.22.3.159.

[316] J. D. Pearson, J. S. Carleton, and J. L. Gordon, "Metabolism of adenine nucleotides by ectoenzymes of vascular endothelial and smooth-muscle cells in culture," *Biochemical Journal*, vol. 190, no. 2, pp. 421–429, Aug. 1980, ISSN: 0264-6021. DOI: 10.1042/bj1900421.

[317] K. Peebles, L. Celi, K. McGrattan, C. Murrell, K. Thomas, and P. N. Ainslie, "Human cerebrovascular and ventilatory co2 reactivity to end-tidal, arterial and internal jugular vein pco2," en, *The Journal of Physiology*, vol. 584, no. 1, pp. 347–357, 2007, ISSN: 1469-7793. DOI: 10.1113/jphysiol.2007.137075.

[318] L. Pelizzari, M. M. Laganà, F. Rossetto, *et al.*, "Cerebral blood flow and cerebrovascular reactivity correlate with severity of motor symptoms in parkinson's disease," *Therapeutic Advances in Neurological Disorders*, vol. 12, p. 1 756 286 419 838 354, Mar. 2019, ISSN: 1756-2856. DOI: 10.1177/1756286419838354.

[319] S.-L. Peng, X. Chen, Y. Li, K. M. Rodrigue, D. C. Park, and H. Lu, "Age-related changes in cerebrovascular reactivity and their relationship to cognition: A four-year longitudinal study," *NeuroImage*, vol. 174, pp. 257–262, Jul. 2018, ISSN: 1053-8119. DOI: 10.1016/j.neuroimage.2018.03.033.

[320] J. S. Perlmutter, W. J. Powers, P. Herscovitch, P. T. Fox, and M. E. Raichle, "Regional asymmetries of cerebral blood flow, blood volume, and oxygen utilization and extraction in normal subjects," en, *Journal of Cerebral Blood Flow Metabolism*, vol. 7, no. 1, 64â67, Feb. 1987, ISSN: 0271-678X. DOI: 10.1038/jcbfm.1987.9.

[321] O. M. Peters and R. H. Brown, "Chapter 18 - amyotrophic lateral sclerosis," en, in *Neurobiology of Brain Disorders*, M. J. Zigmond, L. P. Rowland, and J. T. Coyle, Eds. San Diego: Academic Press, Jan. 2015, pp. 262–280, ISBN: 978-0-12-398270-4. DOI: 10.1016/B978-0-12-398270-4.00018-5.

[322] R. Peters, N. Ee, J. Peters, A. Booth, I. Mudway, and K. J. Anstey, "Air pollution and dementia: A systematic review," eng, *Journal of Alzheimer's disease: JAD*, vol. 70, no. s1, S145–S163, 2019, ISSN: 1875-8908. DOI: 10.3233/JAD-180631.

[323] T. Pfefferkorn, S. v. Stuckrad-Barre, J. Herzog, T. Gasser, G. F. Hamann, and M. Dichgans, "Reduced cerebrovascular co2 reactivity in cadasil," *Stroke*, vol. 32, no. 1, pp. 17–21, 2001, ISSN: 0039-2499. DOI: 10.1161/01.str.32.1.17.

[324] Y. Pi, L.-l. Zhang, B.-h. Li, *et al.*, "Inhibition of reactive oxygen species generation attenuates tlr4-mediated proinflammatory and proliferative phenotype of vascular smooth muscle cells," en, *Laboratory Investigation*, vol. 93, no. 88, pp. 880–887, Aug. 2013, ISSN: 1530-0307. DOI: 10.1038/labinvest.2013.79.

[325] F. Piguet, S. Alves, and N. Cartier, "Clinical gene therapy for neurodegenerative diseases: Past, present, and future," *Human Gene Therapy*, vol. 28, no. 11, pp. 988–1003, Nov. 2017, ISSN: 1043-0342. DOI: 10.1089/hum.2017.160.

[326] G. B. Pike, "Quantitative functional mri: Concepts, issues and future challenges," *NeuroImage*, 20 YEARS OF fMRI, vol. 62, no. 2, 1234â1240, Aug. 2012, ISSN: 1053-8119. DOI: 10.1016/j.neuroimage.2011.10.046.

[327] J. Pillai and D. Zacá, "Clinical utility of cerebrovascular reactivity mapping in patients with low grade gliomas," en, *World J. Clin. Oncol*, vol. 2, pp. 397–403, 2011. DOI: 10.5306/wjco.v2.i12.397.

[328] J. Pinto, M. Bright, D. Bulte, and P. Figueiredo, "Cerebrovascular reactivity mapping without gas challenges: A methodological guide," en, *Front. Physiol*, vol. 11, 2021. DOI: https://doi.org/10.3389/fphys.2020.608475.

[329] J. Pinto, J. Jorge, I. Sousa, P. Vilela, and P. Figueiredo, "Fourier modeling of the bold response to a breath-hold task: Optimization and reproducibility," en, *NeuroImage*, vol. 135, pp. 223–231, 2016. DOI: 10.1016/j.neuroimage.2016.02.037.

[330] J. Pinto, N. P. Blockley, J. W. Harkin, and D. P. Bulte, "Modelling spatiotemporal dynamics of cerebral blood flow using multiple-timepoint arterial spin labelling mri," eng, *Frontiers in Physiology*, vol. 14, 2023, ISSN: 1664-042X. DOI: 10.3389/fphys.2023.1142359.

[331] M. Platten, S. Youssef, E. M. Hur, *et al.*, "Blocking angiotensin-converting enzyme induces potent regulatory t cells and modulates th1- and th17-mediated autoimmunity," eng, *Proceedings of the National Academy of Sciences of the United States of America*, vol. 106, no. 35, pp. 14 948–14 953, Sep. 2009, ISSN: 1091-6490. DOI: 10.1073/pnas.0903958106.

[332] M. Poittevin, P. Lozeron, R. Hilal, B. I. Levy, T. Merkulova-Rainon, and N. Kubis, "Smooth muscle cell phenotypic switching in stroke," *Translational Stroke Research*, vol. 5, no. 3, pp. 377–384, 2014, ISSN: 1868-4483. DOI: 10.1007/s12975-013-0306-x.

[333] J. Poublanc, J. Han, D. Mandell, *et al.*, "Vascular steal explains early paradoxical blood oxygen level-dependent cerebrovascular response in brain regions with delayed arterial transit times," en, *Cerebrovasc. Dis. Extra*, vol. 3, pp. 55–64, 2013. DOI: 10.1159/000348841.

[334] J. Poublanc, A. P. Crawley, O. Sobczyk, *et al.*, "Measuring cerebrovascular reactivity: The dynamic response to a step hypercapnic stimulus," eng, *Journal of Cerebral Blood Flow and Metabolism: Official Journal of the International Society of Cerebral Blood Flow and Metabolism*, vol. 35, no. 11, pp. 1746–1756, 2015, ISSN: 1559-7016. DOI: 10.1038/jcbfm.2015.114.

[335] G. R. Poudel, C. R. H. Innes, and R. D. Jones, "Cerebral perfusion differences between drowsy and nondrowsy individuals after acute sleep restriction," *Sleep*, vol. 35, no. 8, 1085â1096, Aug. 2012, ISSN: 0161-8105. DOI: 10.5665/sleep.1994.

[336] M. J. Poulin, P. J. Liang, and P. A. Robbins, "Dynamics of the cerebral blood flow response to step changes in end-tidal pco2 and po2 in humans," en, *Journal of Applied Physiology*, vol. 81, no. 3, pp. 1084–1095, Sep. 1996, ISSN: 8750-7587, 1522-1601. DOI: 10.1152/jappl.1996.81.3.1084.

[337] S. Purkayastha and F. Sorond, "Transcranial doppler ultrasound: Technique and application," en, *Seminars in Neurology*, vol. 32, pp. 411–420, Jan. 2013, ISSN: 0271-8235. DOI: 10.1055/s-0032-1331812.

[338] H. Qiu, Y. Wu, Q. Wang, *et al.*, "Effect of berberine on pparα-NO signalling pathway in vascular smooth muscle cell proliferation induced by angiotensin

IV," eng, *Pharmaceutical Biology*, vol. 55, no. 1, pp. 227–232, Dec. 2017, ISSN: 1744-5116. DOI: 10.1080/13880209.2016.1257642.

[339] J. Qiu, Y. Zheng, J. Hu, *et al.*, "Biomechanical regulation of vascular smooth muscle cell functions: From in vitro to in vivo understanding," *Journal of The Royal Society Interface*, vol. 11, no. 90, p. 20 130 852, Jan. 2014. DOI: 10.1098/rsif.2013.0852.

[340] Quantiphyse, 2023.

[341] A. Rahman, M. Ekman, Y. Shakirova, *et al.*, "Late onset vascular dysfunction in the r6/1 model of huntington's disease," *European Journal of Pharmacology*, vol. 698, no. 1–3, pp. 345–353, 2013, ISSN: 0014-2999. DOI: 10.1016/j.ejphar.2012.10.026.

[342] G. N. Rao and B. C. Berk, "Active oxygen species stimulate vascular smooth muscle cell growth and proto-oncogene expression.," *Circulation Research*, vol. 70, no. 3, pp. 593–599, Mar. 1992. DOI: 10.1161/01.RES.70.3.593.

[343] A. Rayshubskiy, T. J. Wojtasiewicz, C. B. Mikell, *et al.*, "Direct, intraoperative observation of ∼0.1 Hz hemodynamic oscillations in awake human cortex: Implications for fmri," *NeuroImage*, vol. 87, pp. 323–331, Feb. 2014, ISSN: 1053-8119. DOI: 10.1016/j.neuroimage.2013.10.044.

[344] L. Raz, J. Knoefel, and K. Bhaskar, "The neuropathology and cerebrovascular mechanisms of dementia," *Journal of Cerebral Blood Flow & Metabolism*, vol. 36, no. 1, pp. 172–186, 2015, ISSN: 0271-678X. DOI: 10.1038/jcbfm.2015.164.

[345] R. E. Regan, J. A. Fisher, and J. Duffin, "Factors affecting the determination of cerebrovascular reactivity," *Brain and Behavior*, vol. 4, no. 5, pp. 775–788, 2014, ISSN: 2162-3279. DOI: 10.1002/brb3.275.

[346] S. S. M. Rensen, P. A. F. M. Doevendans, and G. J. J. M. v. Eys, "Regulation and characteristics of vascular smooth muscle cell phenotypic diversity," *Netherlands Heart Journal*, vol. 15, no. 3, pp. 100–108, 2007, ISSN: 1568-5888. DOI: 10.1007/bf03085963.

[347] A. A. M. Rensink, R. M. W. de Waal, B. Kremer, and M. M. Verbeek, "Pathogenesis of cerebral amyloid angiopathy," en, *Brain Research Reviews*, vol. 43, no. 2, pp. 207–223, Oct. 2003, ISSN: 0165-0173. DOI: 10.1016/j.brainresrev.2003.08.001.

[348] J. D. Reuck, V. Deramecourt, F. Auger, *et al.*, "Post-mortem 7.0-tesla magnetic resonance study of cortical microinfarcts in neurodegenerative diseases and vascular dementia with neuropathological correlates," *Journal of the Neurological Sciences*, vol. 346, no. 1–2, pp. 85–89, 2014, ISSN: 0022-510X. DOI: 10.1016/j.jns.2014.07.061.

[349] J. Richiardi, A. U. Monsch, T. Haas, *et al.*, "Altered cerebrovascular reactivity velocity in mild cognitive impairment and alzheimer's disease," *Neurobiology of Aging*, vol. 36, no. 1, pp. 33–41, 2015, ISSN: 0197-4580. DOI: 10.1016/j.neurobiolaging.2014.07.020.

[350] E. B. Ringelstein, C Sievers, S Ecker, P. A. Schneider, and S. M. Otis, "Noninvasive assessment of co2-induced cerebral vasomotor response in normal individuals and patients with internal carotid artery occlusions.," *Stroke*, vol. 19, no. 8, pp. 963–969, Aug. 1988. DOI: 10.1161/01.STR.19.8.963.

[351] E. B. Ringelstein, S. Van Eyck, and I. Mertens, "Evaluation of cerebral vasomotor reactivity by various vasodilating stimuli: Comparison of co2 to acetazolamide," en, *Journal of Cerebral Blood Flow & Metabolism*, vol. 12, no. 1, pp. 162–168, Jan. 1992, ISSN: 0271-678X. DOI: 10.1038/jcbfm.1992.20.

[352] P. A. Robbins, G. D. Swanson, and M. G. Howson, "A prediction-correction scheme for forcing alveolar gases along certain time courses," eng, *Journal of Applied Physiology: Respiratory, Environmental and Exercise Physiology*, vol. 52, no. 5, pp. 1353–1357, May 1982, ISSN: 0161-7567. DOI: 10.1152/jappl.1982.52.5.1353.

[353] A. Rodell, J. Aanerud, H. Braendgaard, and A. Gjedde, "Low residual cbf variability in alzheimer's disease after correction for co2 effect," *Frontiers in Neuroenergetics*, vol. 4, 2012, ISSN: 1662-6427. DOI: 10.3389/fnene.2012.00008.

[354] M. Roerecke, J. Kaczorowski, S. W. Tobe, G. Gmel, O. S. M. Hasan, and J. Rehm, "The effect of a reduction in alcohol consumption on blood pressure: A systematic review and meta-analysis," English, *The Lancet Public Health*, vol. 2, no. 2, e108–e120, Feb. 2017, ISSN: 2468-2667. DOI: 10.1016/S2468-2667(17)30003-8.

[355] A. E. Roher, Z. Garami, S. L. Tyas, *et al.*, "Transcranial doppler ultrasound blood flow velocity and pulsatility index as systemic indicators for alzheimer's disease," eng, *Alzheimer's & Dementia: The Journal of the Alzheimer's Association*, vol. 7, no. 4, pp. 445–455, Jul. 2011, ISSN: 1552-5279. DOI: 10.1016/j.jalz.2010.09.002.

[356] F. Romagnosi, F. Bongiovanni, and M. Oddo, "Eyeing up the injured brain: Automated pupillometry and optic nerve sheath diameter," eng, *Current Opinion in Critical Care*, vol. 26, no. 2, pp. 115–121, Apr. 2020, ISSN: 1531-7072. DOI: 10.1097/MCC.0000000000000710.

[357] E. Roy-Vallejo, J. M. Galván-Román, F. Moldenhauer, and D. R. d. Asúa, "Adults with down syndrome challenge another paradigm: When aging no longer entails arterial hypertension," *The Journal of Clinical Hypertension*, vol. 22, no. 7, pp. 1127–1133, 2020, ISSN: 1524-6175. DOI: 10.1111/jch.13930.

[358] J. Royea, M. Lacalle-Aurioles, L. J. Trigiani, A. Fermigier, and E. Hamel, "At2r's (angiotensin ii type 2 receptor's) role in cognitive and cerebrovascular deficits in a mouse model of alzheimer disease," *Hypertension*, vol. 75, no. 6, pp. 1464–1474, Jun. 2020. DOI: 10.1161/HYPERTENSIONAHA.119.14431.

[359] Q. Rui, H. Ni, D. Li, R. Gao, and G. Chen, "The role of lrrk2 in neurodegeneration of parkinson disease," *Current Neuropharmacology*, vol. 16, no. 9, pp. 1348–1357, Nov. 2018, ISSN: 1570-159X. DOI: 10.2174/1570159X16666180222165418.

[360] A. Ruitenberg, T. den Heijer, S. L. M. Bakker, *et al.*, "Cerebral hypoperfusion and clinical onset of dementia: The rotterdam study," en, *Annals of Neurology*, vol. 57, no. 6, pp. 789–794, 2005, ISSN: 1531-8249. DOI: 10.1002/ana.20493.

[361] S. G. Ryman, N. Shaff, A. Dodd, *et al.*, "Reduced and delayed cerebrovascular reactivity in patients with parkinson's disease," en, *Movement Disorders*, vol. 38, no. 7, pp. 1262–1272, 2023, ISSN: 1531-8257. DOI: 10.1002/mds.29429.

[362] S. Sabia, A. Fayosse, J. Dumurgier, *et al.*, "Alcohol consumption and risk of dementia: 23 year follow-up of whitehall ii cohort study," *BMJ*, vol. 362, k2927, 2018, ISSN: 0959-8138. DOI: 10.1136/bmj.k2927.

[363] K. Sam, A. P. Crawley, J. Conklin, *et al.*, "Development of white matter hyperintensity is preceded by reduced cerebrovascular reactivity," *Annals of Neurology*, vol. 80, no. 2, pp. 277–285, Aug. 2016, ISSN: 0364-5134. DOI: 10.1002/ana.24712.

[364] K. Sam, J. Poublanc, O. Sobczyk, *et al.*, "Assessing the effect of unilateral cerebral revascularisation on the vascular reactivity of the non-intervened hemisphere: A retrospective observational study," en, *BMJ Open*, vol. 5, no. 2, e006014, Feb. 2015, ISSN: 2044-6055, 2044-6055. DOI: 10.1136/bmjopen-2014-006014.

[365] A. R. Sandy, J. Stoolman, K. Malott, P. Pongtornpipat, B. M. Segal, and I. Maillard, "Notch signaling regulates t cell accumulation and function in the central nervous system during experimental autoimmune encephalomyelitis," en, *The Journal of Immunology*, vol. 191, no. 4, pp. 1606–1613, Aug. 2013, ISSN: 0022-1767, 1550-6606. DOI: 10.4049/jimmunol.1301116.

[366] P. A. Sarafidis, A. I. Kanaki, and A. N. Lasaridis, "Statins and blood pressure: Is there an effect or not?" *The Journal of Clinical Hypertension*, vol. 9, no. 6, pp. 460–467, May 2007, ISSN: 1524-6175. DOI: 10.1111/j.1524-6175.2007.06625.x.

[367] T. Sawma, A. Shaito, N. Najm, *et al.*, "Role of rhoa and rho-associated kinase in phenotypic switching of vascular smooth muscle cells: Implications for vascular function," en, *Atherosclerosis*, vol. 358, pp. 12–28, Oct. 2022, ISSN: 0021-9150. DOI: 10.1016/j.atherosclerosis.2022.08.012.

[368] P. Schober, C. Boer, and L. A. Schwarte, "Correlation coefficients: Appropriate use and interpretation," en-US, *Anesthesia Analgesia*, vol. 126, no. 5, p. 1763, May 2018, ISSN: 0003-2999. DOI: 10.1213/ANE.0000000000002864.

[369] B. G. Schultz, D. K. Patten, and D. J. Berlau, "The role of statins in both cognitive impairment and protection against dementia: A tale of two mechanisms," *Translational Neurodegeneration*, vol. 7, no. 1, p. 5, Feb. 2018, ISSN: 2047-9158. DOI: 10.1186/s40035-018-0110-3.

[370] G. Schwarz, "Estimating the dimension of a model," *The Annals of Statistics*, vol. 6, no. 2, pp. 461–464, Mar. 1978, ISSN: 0090-5364, 2168-8966. DOI: 10.1214/aos/1176344136.

[371] A. Scuteri, M. Tesauro, S. Appolloni, F. Preziosi, A. M. Brancati, and M. Volpe, "Arterial stiffness as an independent predictor of longitudinal changes in cognitive function in the older individual," en-US, *Journal of Hypertension*, vol. 25, no. 5, pp. 1035–1040, May 2007, ISSN: 0263-6352. DOI: 10.1097/HJH.0b013e3280895b55.

[372] J. M. Serrador, P. A. Picot, B. K. Rutt, J. K. Shoemaker, and R. L. Bondar, "Mri measures of middle cerebral artery diameter in conscious humans during simulated orthostasis," *Stroke*, vol. 31, no. 7, pp. 1672–1678, Jul. 2000. DOI: 10.1161/01.STR.31.7.1672.

[373] S. S. Shapiro and M. B. Wilk, "An analysis of variance test for normality (complete samples)," *Biometrika*, vol. 52, no. 3/4, pp. 591–611, 1965, ISSN: 0006-3444. DOI: 10.2307/2333709.

[374] Y. Shi, M. J. Thrippleton, S. D. Makin, *et al.*, "Cerebral blood flow in small vessel disease: A systematic review and meta-analysis," en, *Journal of Cerebral*

Blood Flow & Metabolism, vol. 36, no. 10, pp. 1653–1667, Oct. 2016, ISSN: 0271-678X. DOI: 10.1177/0271678X16662891.

[375] Z.-D. Shi and J. M. Tarbell, "Fluid flow mechanotransduction in vascular smooth muscle cells and fibroblasts," en, *Annals of Biomedical Engineering*, vol. 39, no. 6, pp. 1608–1619, Jun. 2011, ISSN: 1573-9686. DOI: 10.1007/s10439-011-0309-2.

[376] A. Shiino, Y. Morita, A. Tsuji, *et al.*, "Estimation of cerebral perfusion reserve by blood oxygenation level–dependent imaging: Comparison with single-photon emission computed tomography," *Journal of Cerebral Blood Flow Metabolism*, vol. 23, no. 1, pp. 121–135, Jan. 2003, ISSN: 0271-678X. DOI: 10.1097/01.WCB.0000037546.46809.CA.

[377] H. Shimokawa, "Reactive oxygen species promote vascular smooth muscle cell proliferation," *Circulation Research*, vol. 113, no. 9, pp. 1040–1042, Oct. 2013. DOI: 10.1161/CIRCRESAHA.113.302049.

[378] P. Shrout and J. Fleiss, "Intraclass correlations: Uses in assessing rater reliability," en, *Psychol. Bull*, vol. 86, pp. 420–428, 1979. DOI: 10.1037//0033-2909.86.2.420.

[379] S. Singhal and H. S. Markus, "Cerebrovascular reactivity and dynamic autoregulation in nondemented patients with cadasil (cerebral autosomal dominant arteriopathy with subcortical infarcts and leukoencephalopathy)," en, *Journal of Neurology*, vol. 252, no. 2, pp. 163–167, Feb. 2005, ISSN: 1432-1459. DOI: 10.1007/s00415-005-0624-3.

[380] B. D. Skinner, S. R. C. Weaver, S. J. E. Lucas, and R. A. I. Lucas, "Menstrual phase influences cerebrovascular responsiveness in females but may not affect sex differences," *Frontiers in Physiology*, vol. 13, p. 1 035 452, Jan. 2023, ISSN: 1664-042X. DOI: 10.3389/fphys.2022.1035452.

[381] E. Sleight, M. Stringer, I. Marshall, J. Wardlaw, and M. Thrippleton, "Cerebrovascular reactivity measurement using magnetic resonance imaging: A systematic review," en, *Front. Physiol*, vol. 12, p. 643 468, 2021. DOI: 10.3389/fphys.2021.643468.

[382] M. Slessarev, "Experimental protocols in cvr," en, in *Cerebrovascular Reactivity: Methodological Advances and Clinical Applications* (Neuromethods), J. Chen and J. Fierstra, Eds., Neuromethods. New York, NY: Springer US, 2022, pp. 19–32, ISBN: 978-1-07-161763-2. DOI: 10.1007/978-1-0716-1763-2_2. [Online]. Available: https://doi.org/10.1007/978-1-0716-1763-2_2.

[383] O. Sobczyk, A. Battisti-Charbonney, J. Fierstra, *et al.*, "A conceptual model for co2-induced redistribution of cerebral blood flow with experimental confirmation using bold mri," *NeuroImage*, vol. 92, pp. 56–68, 2014, ISSN: 1053-8119. DOI: 10.1016/j.neuroimage.2014.01.051.

[384] C. G. Sobey, C. P. Judkins, V. Sundararajan, T. G. Phan, G. R. Drummond, and V. K. Srikanth, "Risk of major cardiovascular events in people with down syndrome," en, *PLOS ONE*, vol. 10, no. 9, e0137093, Sep. 2015, ISSN: 1932-6203. DOI: 10.1371/journal.pone.0137093.

[385] S. Solis-Barquero, R. Echeverria-Chasco, M. Calvo-Imirizaldu, *et al.*, "Breath-hold induced cerebrovascular reactivity measurements using optimized pseudo-

continuous arterial spin labeling," en, *Front. Physiol*, vol. 12, p. 621 720, 2021. DOI: 10.3389/fphys.2021.621720.

[386] S. Sorrentino, A. Polini, V. Arima, *et al.*, "Neurovascular signals in amyotrophic lateral sclerosis," *Current Opinion in Biotechnology*, vol. 74, pp. 75–83, 2022, ISSN: 0958-1669. DOI: 10.1016/j.copbio.2021.10.021.

[387] V. R. Spano, D. M. Mandell, J. Poublanc, *et al.*, "Co2 blood oxygen level–dependent mr mapping of cerebrovascular reserve in a clinical population: Safety, tolerability, and technical feasibility," *Radiology*, vol. 266, no. 2, pp. 592–598, Feb. 2013, ISSN: 0033-8419. DOI: 10.1148/radiol.12112795.

[388] S. Sparks, G. Hayes, J. Pinto, and D. Bulte, "Characterising cerebrovascular reactivity and the pupillary light response-a comparative study," English, *Frontiers in Physiology*, vol. 15, Aug. 2024, ISSN: 1664-042X. DOI: 10.3389/fphys.2024.1384113. [Online]. Available: https://www.frontiersin.org/journals/physiology/articles/10.3389/fphys.2024.1384113/full.

[389] S. Sparks, J. Pinto, G. Hayes, M. Spitschan, and D. P. Bulte, "The impact of alzheimer's disease risk factors on the pupillary light response," eng, *Frontiers in Neuroscience*, vol. 17, 2023, ISSN: 1662-4548. DOI: 10.3389/fnins.2023.1248640.

[390] R. E. Speer and R. R. Ratan, "Drug treatment for neurodegenerative disorders among the elderly: Re-engaging homeostatic programs," *Aging Health*, vol. 5, no. 2, pp. 133–136, Apr. 2009, ISSN: 1745-509X. DOI: 10.2217/ahe.09.11.

[391] A. St. Paul, C. B. Corbett, R. Okune, and M. V. Autieri, "Angiotensin ii, hypercholesterolemia, and vascular smooth muscle cells: A perfect trio for vascular pathology," *International Journal of Molecular Sciences*, vol. 21, no. 12, p. 4525, Jun. 2020, ISSN: 1422-0067. DOI: 10.3390/ijms21124525.

[392] R. M. Starke, M. S. Ali, P. M. Jabbour, *et al.*, "Cigarette smoke modulates vascular smooth muscle phenotype: Implications for carotid and cerebrovascular disease," en, *PLOS ONE*, vol. 8, no. 8, e71954, Aug. 2013, ISSN: 1932-6203. DOI: 10.1371/journal.pone.0071954.

[393] R. Stickland, K. Zvolanek, S. Moia, A. Ayyagari, C. Caballero-Gaudes, and M. Bright, "A practical modification to a resting state fmri protocol for improved characterization of cerebrovascular function," en, *NeuroImage*, vol. 239, p. 118 306, 2021. DOI: 10.1016/j.neuroimage.2021.118306.

[394] R. Stickland, K. Zvolanek, S. Moia, C. Caballero-Gaudes, and M. Bright, *Lag-optimized bold cerebrovascular reactivity derived from breathing task data has a stronger relationship with baseline cerebral blood flow*, en, 2022. DOI: 10.1101/2022.03.08.483492. [Online]. Available: https://doi.org/10.1101/2022.03.08.483492.

[395] J. Su, J. Li, W. Li, B. T. Altura, and B. M. Altura, "Cocaine induces apoptosis in cerebral vascular muscle cells: Potential roles in strokes and brain damage," eng, *European Journal of Pharmacology*, vol. 482, no. 1–3, pp. 61–66, Dec. 2003, ISSN: 0014-2999. DOI: 10.1016/j.ejphar.2003.09.056.

[396] X. Sun, X. Shi, Y. Cao, *et al.*, "Variation of petco2 during incremental exercise and severity of ipah and cteph," *BMC Pulmonary Medicine*, vol. 22, p. 249, Jun. 2022, ISSN: 1471-2466. DOI: 10.1186/s12890-022-02045-4.

[397] S. Suri, C. Mackay, M. Kelly, *et al.*, "Reduced cerebrovascular reactivity in young adults carrying the apoe ϵ4 allele," en, *Alzheimers Dement. J. Alzheimers Assoc*, vol. 11, pp. 648–657 1, 2015. DOI: 10.1016/j.jalz.2014.05.1755.

[398] S. Suri, D. Bulte, S. T. Chiesa, *et al.*, "Study protocol: The heart and brain study," *Frontiers in Physiology*, vol. 12, 2021, ISSN: 1664-042X. DOI: 10.3389/fphys.2021.643725.

[399] N. Szarka, M. R. Pabbidi, K. Amrein, *et al.*, "Traumatic brain injury impairs myogenic constriction of cerebral arteries: Role of mitochondria-derived h2o2 and trpv4-dependent activation of bkca channels," *Journal of Neurotrauma*, vol. 35, no. 7, pp. 930–939, Apr. 2018, ISSN: 0897-7151. DOI: 10.1089/neu.2017.5056.

[400] Y. Takano, O. Sakamoto, C. Kiyofuji, and K. Ito, "A comparison of the end-tidal co2 measured by portable capnometer and the arterial p co2 in spontaneously breathing patients," en, *Respir. Med*, vol. 97, pp. 476–481, 2003. DOI: 10.1053/rmed.2002.1468.

[401] C. M. Tallon, A. R. Barker, D. Nowak-FlÃ¼ck, P. N. Ainslie, and A. M. McManus, "The influence of age and sex on cerebrovascular reactivity and ventilatory response to hypercapnia in children and adults," eng, *Experimental Physiology*, vol. 105, no. 7, pp. 1090–1101, Jul. 2020, ISSN: 1469-445X. DOI: 10.1113/EP088293.

[402] W. Tamo, T. Imaizumi, K. Tanji, *et al.*, "Expression of α-synuclein in vascular endothelial and smooth muscle cells," en, *International Congress Series*, Advances in Brain Research. Cerebrovascular Disorders and Neurodegeneration. Proceedings of the 6th Hirosaki International Forum of Medical Science, vol. 1251, pp. 173–179, Jun. 2003, ISSN: 0531-5131. DOI: 10.1016/S0531-5131(03)00120-1.

[403] F. B. Tancredi and R. D. Hoge, "Comparison of cerebral vascular reactivity measures obtained using breath-holding and co2 inhalation," *Journal of Cerebral Blood Flow Metabolism*, vol. 33, no. 7, pp. 1066–1074, Jul. 2013, ISSN: 0271-678X. DOI: 10.1038/jcbfm.2013.48.

[404] W. R. Taylor, J. W. Chen, H. Meltzer, *et al.*, "Quantitative pupillometry, a new technology: Normative data and preliminary observations in patients with acute head injury: Technical note," en$_U$*S*, *Journal of Neurosurgery*, vol. 98, no. 1, pp. 205–213, Jan. 2003. DOI: 10.3171/jns.2003.98.1.0205.

[405] T. pandas development team, *Pandas-dev/pandas: Pandas*, Sep. 2024. DOI: 10.5281/zenodo.13819579. [Online]. Available: https://zenodo.org/records/13819579.

[406] S. Thalman, K. L. Van Pelt, A.-L. Lin, *et al.*, "A preliminary study of cerebral blood flow, aging and dementia in people with down syndrome," eng, *Journal of intellectual disability research: JIDR*, vol. 64, no. 12, pp. 934–945, Dec. 2020, ISSN: 1365-2788. DOI: 10.1111/jir.12784.

[407] W. Thirapatarapong, H. F. Armstrong, B. M. Thomashow, and M. N. Bartels, "Differences in gas exchange between severities of chronic obstructive pulmonary disease," *Respiratory Physiology & Neurobiology*, vol. 186, no. 1, pp. 81–86, Mar. 2013, ISSN: 1569-9048. DOI: 10.1016/j.resp.2012.12.013.

[408] N. Thorin-Trescases, O. de Montgolfier, A. Pinçon, *et al.*, "Impact of pulse pressure on cerebrovascular events leading to age-related cognitive decline," *American Journal of Physiology-Heart and Circulatory Physiology*, vol. 314, no. 6, H1214–H1224, Jun. 2018, ISSN: 0363-6135. DOI: 10.1152/ajpheart.00637.2017.

[409] K. Tokairin, S. Hamauchi, M. Ito, *et al.*, "Vascular smooth muscle cell derived from ips cell of moyamoya disease - comparative characterization with endothelial cell transcriptome," eng, *Journal of Stroke and Cerebrovascular Diseases: The Official Journal of National Stroke Association*, vol. 29, no. 12, p. 105 305, Dec. 2020, ISSN: 1532-8511. DOI: 10.1016/j.jstrokecerebrovasdis.2020.105305.

[410] Y. Tong, L. M. Hocke, and B. B. Frederick, "Low frequency systemic hemodynamic "noise" in resting state bold fmri: Characteristics, causes, implications, mitigation strategies, and applications," English, *Frontiers in Neuroscience*, vol. 13, Aug. 2019, ISSN: 1662-453X. DOI: 10.3389/fnins.2019.00787.

[411] A. Topiwala, C. Wang, K. P. Ebmeier, *et al.*, "Associations between moderate alcohol consumption, brain iron, and cognition in uk biobank participants: Observational and mendelian randomization analyses," en, *PLOS Medicine*, vol. 19, no. 7, e1004039, Jul. 2022, ISSN: 1549-1676. DOI: 10.1371/journal.pmed.1004039.

[412] R. M. Touyz, R. Alves-Lopes, F. J. Rios, *et al.*, "Vascular smooth muscle contraction in hypertension," *Cardiovascular Research*, vol. 114, no. 4, pp. 529–539, Mar. 2018, ISSN: 0008-6363. DOI: 10.1093/cvr/cvy023.

[413] J. Q. Truong and K. J. Ciuffreda, "Quantifying pupillary asymmetry through objective binocular pupillometry in the normal and mild traumatic brain injury (mtbi) populations," *Brain Injury*, vol. 30, no. 11, pp. 1372–1377, Sep. 2016, ISSN: 0269-9052. DOI: 10.1080/02699052.2016.1192220.

[414] J.-C. Tsai, M. Jain, C.-M. Hsieh, *et al.*, "Induction of apoptosis by pyrrolidinedithiocarbamate and n-acetylcysteine in vascular smooth muscle cells (â)," English, *Journal of Biological Chemistry*, vol. 271, no. 7, pp. 3667–3670, Feb. 1996, ISSN: 0021-9258, 1083-351X. DOI: 10.1074/jbc.271.7.3667.

[415] M. Tsuji, A. Duplessis, G. Taylor, R. Crocker, and J. J. Volpe, "Near infrared spectroscopy detects cerebral ischemia during hypotension in piglets," en, *Pediatric Research*, vol. 44, no. 44, pp. 591–595, Oct. 1998, ISSN: 1530-0447. DOI: 10.1203/00006450-199810000-00020.

[416] T. Tuon, S. Valvassori, J. Lopes-Borges, *et al.*, "Physical training exerts neuroprotective effects in the regulation of neurochemical factors in an animal model of parkinson's disease," en, *Neuroscience*, vol. 227, pp. 305–312, Dec. 2012, ISSN: 03064522. DOI: 10.1016/j.neuroscience.2012.09.063.

[417] P. R. K. Turnbull, N. Irani, N. Lim, and J. R. Phillips, "Origins of pupillary hippus in the autonomic nervous system," *Investigative Ophthalmology & Visual Science*, vol. 58, no. 1, pp. 197–203, Jan. 2017, ISSN: 1552-5783. DOI: 10.1167/iovs.16-20785.

[418] N. Tustison, P. Cook, A. Klein, *et al.*, "Large-scale evaluation of ants and freesurfer cortical thickness measurements," en, *NeuroImage*, vol. 99, pp. 166–179, 2014. DOI: 10.1016/j.neuroimage.2014.05.044.

[419] M. H. Tuszynski, J. H. Yang, D. Barba, *et al.*, "Nerve growth factor gene therapy: Activation of neuronal responses in alzheimer disease," *JAMA Neurology*, vol. 72, no. 10, pp. 1139–1147, Oct. 2015, ISSN: 2168-6149. DOI: 10.1001/jamaneurol.2015.1807.

[420] A. H. M. Van Mil, A. Spilt, M. A. Van Buchem, *et al.*, "Nitric oxide mediates hypoxia-induced cerebral vasodilation in humans," *Journal of Applied Physiology*, vol. 92, no. 3, pp. 962–966, Mar. 2002, ISSN: 8750-7587. DOI: 10.1152/japplphysiol.00616.2001.

[421] M. Vanlandewijck, L. He, M. A. Mäe, *et al.*, "A molecular atlas of cell types and zonation in the brain vasculature," eng, *Nature*, vol. 554, no. 7693, pp. 475–480, Feb. 2018, ISSN: 1476-4687. DOI: 10.1038/nature25739.

[422] E. Vicenzini, M. C. Ricciardi, M. Altieri, *et al.*, "Cerebrovascular reactivity in degenerative and vascular dementia: A transcranial doppler study," *European Neurology*, vol. 58, no. 2, pp. 84–89, 2007, ISSN: 0014-3022, 1421-9913. DOI: 10.1159/000103642.

[423] M. Viitanen, E. Sundström, M. Baumann, M. Poyhonen, S. Tikka, and H. Behbahani, "Experimental studies of mitochondrial function in cadasil vascular smooth muscle cells," en, *Experimental Cell Research*, vol. 319, no. 3, pp. 134–143, Feb. 2013, ISSN: 0014-4827. DOI: 10.1016/j.yexcr.2012.09.015.

[424] N. Villalba, S. K. Sonkusare, T. A. Longden, *et al.*, "Traumatic brain injury disrupts cerebrovascular tone through endothelial inducible nitric oxide synthase expression and nitric oxide gain of function," *Journal of the American Heart Association*, vol. 3, no. 6, e001474, Dec. 2014. DOI: 10.1161/JAHA.114.001474.

[425] A. Virdis, M. F. Neves, F. Amiri, R. M. Touyz, and E. L. Schiffrin, "Role of nad(p)h oxidase on vascular alterations in angiotensin ii-infused mice," en-US, *Journal of Hypertension*, vol. 22, no. 3, pp. 535–542, Mar. 2004, ISSN: 0263-6352.

[426] P. Virtanen, R. Gommers, T. E. Oliphant, *et al.*, "Scipy 1.0: Fundamental algorithms for scientific computing in python," en, *Nature Methods*, vol. 17, no. 33, pp. 261–272, Mar. 2020, ISSN: 1548-7105. DOI: 10.1038/s41592-019-0686-2.

[427] N. Vodovar, C. Paquet, A. Mebazaa, J.-M. Launay, J. Hugon, and A. Cohen-Solal, "Neprilysin, cardiovascular, and alzheimer's diseases: The therapeutic split?" *European Heart Journal*, vol. 36, no. 15, pp. 902–905, Apr. 2015, ISSN: 0195-668X. DOI: 10.1093/eurheartj/ehv015.

[428] A. Vromman, N. Trabelsi, C. Rouxel, G. Bériziat, I. Limon, and R. Blaise, "β-amyloid context intensifies vascular smooth muscle cells induced inflammatory response and de-differentiation," *Aging Cell*, vol. 12, no. 3, pp. 358–369, 2013, ISSN: 1474-9718. DOI: 10.1111/acel.12056.

[429] S. Wakino, U. Kintscher, S. Kim, F. Yin, W. A. Hsueh, and R. E. Law, "Peroxisome proliferator-activated receptor γ Ligands Inhibit Retinoblastoma Phosphorylation and G1 $\rightarrow$s transition in vascular smooth muscle cells *," English, *Journal of Biological Chemistry*, vol. 275, no. 29, pp. 22 435–22 441, Jul. 2000, ISSN: 0021-9258, 1083-351X. DOI: 10.1074/jbc.M910452199.

[430] H. J. Walsh, R. T. Junejo, G. Y. H. Lip, and J. P. Fisher, "The effect of hypertension on cerebrovascular carbon dioxide reactivity in atrial fibrillation patients," en, *Hypertension Research*, vol. 47, no. 6, pp. 1678–1687, Jun. 2024, ISSN: 1348-4214. DOI: 10.1038/s41440-024-01662-2.

[431] C. Wang, G. Reid, C. E. Mackay, G. Hayes, D. P. Bulte, and S. Suri, "A systematic review of the association between dementia risk factors and cerebrovascular reactivity," en, *Neuroscience & Biobehavioral Reviews*, vol. 148, p. 105 140, May 2023, ISSN: 0149-7634. DOI: 10.1016/j.neubiorev.2023.105140.

[432] H. Wang, the GBD 2015 Mortality, and C. of Death Collaborators, "Global, regional, and national life expectancy, all-cause mortality, and cause-specific mortality for 249 causes of death, 1980–2015: A systematic analysis for the global burden of disease study 2015," English, *The Lancet*, vol. 388, no. 10053, pp. 1459–1544, Oct. 2016, ISSN: 0140-6736, 1474-547X. DOI: 10.1016/S0140-6736(16)31012-1.

[433] S. Wang and C. Jia, "Trpv1 inhibits smooth muscle cell phenotype switching in a mouse model of abdominal aortic aneurysm," *Channels*, vol. 14, no. 1, pp. 59–68, Feb. 2020, ISSN: 1933-6950. DOI: 10.1080/19336950.2020.1730020.

[434] Y. Wang, A. A. Zekveld, G. Naylor, *et al.*, "Parasympathetic nervous system dysfunction, as identified by pupil light reflex, and its possible connection to hearing impairment," en, *PLOS ONE*, vol. 11, no. 4, e0153566, Apr. 2016, ISSN: 1932-6203. DOI: 10.1371/journal.pone.0153566.

[435] Y. Wang, L. Pan, C. B. Moens, and B. Appel, "Notch3 establishes brain vascular integrity by regulating pericyte number," *Development*, vol. 141, no. 2, pp. 307–317, Jan. 2014, ISSN: 0950-1991. DOI: 10.1242/dev.096107.

[436] K. Wasserman, A. L. Van Kessel, and G. G. Burton, "Interaction of physiological mechanisms during exercise," eng, *Journal of Applied Physiology*, vol. 22, no. 1, pp. 71–85, Jan. 1967, ISSN: 0021-8987. DOI: 10.1152/jappl.1967.22.1.71.

[437] M. Webster, M. Makaroun, D. Steed, H. Smith, D. Johnson, and H. Yonas, "Compromised cerebral blood flow reactivity is a predictor of stroke in patients with symptomatic carotid artery occlusive disease," en, *J. Vasc. Surg*, vol. 21, pp. 338–345, 1995. DOI: 10.1016/S0741-5214(95)70274-1.

[438] D. S. Williams, J. A. Detre, J. S. Leigh, and A. P. Koretsky, "Magnetic resonance imaging of perfusion using spin inversion of arterial water.," *Proceedings of the National Academy of Sciences*, vol. 89, no. 1, pp. 212–216, Jan. 1992. DOI: 10.1073/pnas.89.1.212.

[439] C. K. Willie, F. L. Colino, D. M. Bailey, *et al.*, "Utility of transcranial doppler ultrasound for the integrative assessment of cerebrovascular function," *Journal of Neuroscience Methods*, vol. 196, no. 2, 221â237, Mar. 2011, ISSN: 0165-0270. DOI: 10.1016/j.jneumeth.2011.01.011.

[440] C. K. Willie, D. B. Macleod, A. D. Shaw, *et al.*, "Regional brain blood flow in man during acute changes in arterial blood gases," en, *The Journal of Physiology*, vol. 590, no. 14, pp. 3261–3275, 2012, ISSN: 1469-7793. DOI: 10.1113/jphysiol.2012.228551.

[441] E. A. Winkler, J. D. Sengillo, J. S. Sullivan, J. S. Henkel, S. H. Appel, and B. V. Zlokovic, "Blood-spinal cord barrier breakdown and pericyte reductions in amyotrophic lateral sclerosis," eng, *Acta Neuropathologica*, vol. 125, no. 1, pp. 111–120, Jan. 2013, ISSN: 1432-0533. DOI: 10.1007/s00401-012-1039-8.

[442] B. Winn, D. Whitaker, D. B. Elliott, and N. J. Phillips, "Factors affecting light-adapted pupil size in normal human subjects," eng, *Investigative Ophthalmology & Visual Science*, vol. 35, no. 3, pp. 1132–1137, Mar. 1994, ISSN: 0146-0404.

[443] R. G. Wise, K. T. S. Pattinson, D. P. Bulte, *et al.*, "Dynamic forcing of end-tidal carbon dioxide and oxygen applied to functional magnetic resonance imaging," eng, *Journal of Cerebral Blood Flow and Metabolism: Official Journal of the International Society of Cerebral Blood Flow and Metabolism*, vol. 27, no. 8, pp. 1521–1532, Aug. 2007, ISSN: 0271-678X. DOI: 10.1038/sj.jcbfm.9600465.

[444] K. J. Won, S. H. Jung, C.-K. Lee, *et al.*, "Dj-1/park7 protects against neointimal formation via the inhibition of vascular smooth muscle cell growth," *Cardiovascular Research*, vol. 97, no. 3, pp. 553–561, Mar. 2013, ISSN: 0008-6363. DOI: 10.1093/cvr/cvs363.

[445] M. L. Worley, E. L. Reed, N. Klaes, Z. J. Schlader, and B. D. Johnson, "Cool head-out water immersion does not alter cerebrovascular reactivity to hypercapnia despite elevated middle cerebral artery blood velocity: A pilot study," en, *PLOS ONE*, vol. 19, no. 3, e0298587, Mar. 2024, ISSN: 1932-6203. DOI: 10.1371/journal.pone.0298587.

[446] K. J. Worsley, "Statistical analysis of activation images," in *Functional Magnetic Resonance Imaging: An Introduction to Methods*, P. Jezzard, P. M. Matthews, and S. M. Smith, Eds. Oxford University Press, Nov. 2001, p. 0, ISBN: 978-0-19-263071-1. DOI: 10.1093/acprof:oso/9780192630711.003.0014. [Online]. Available: https://doi.org/10.1093/acprof:oso/9780192630711.003.0014.

[447] M. D. Worssam and H. F. Jørgensen, "Mechanisms of vascular smooth muscle cell investment and phenotypic diversification in vascular diseases," eng, *Biochemical Society Transactions*, vol. 49, no. 5, pp. 2101–2111, Nov. 2021, ISSN: 1470-8752. DOI: 10.1042/BST20210138.

[448] S. Wright, *Correlation and causation*, 1921. [Online]. Available: https://cir.nii.ac.jp/crid/1370567187556110595.

[449] S. Z. Wu, A. V. Masurkar, and L. J. Balcer, "Afferent and efferent visual markers of alzheimer's disease: A review and update in early stage disease," eng, *Frontiers in Aging Neuroscience*, vol. 12, p. 572 337, 2020, ISSN: 1663-4365. DOI: 10.3389/fnagi.2020.572337.

[450] B. M. Wynne, C.-W. Chiao, and R. C. Webb, "Vascular smooth muscle cell signaling mechanisms for contraction to angiotensin ii and endothelin-1," *Journal of the American Society of Hypertension: JASH*, vol. 3, no. 2, pp. 84–95, Mar. 2009, ISSN: 1933-1711. DOI: 10.1016/j.jash.2008.09.002.

[451] A. Xie, J. B. Skatrud, R. Khayat, J. A. Dempsey, B. Morgan, and D. Russell, "Cerebrovascular response to carbon dioxide in patients with congestive heart failure," *American Journal of Respiratory and Critical Care Medicine*, vol. 172, no. 3, pp. 371–378, Aug. 2005, ISSN: 1073-449X. DOI: 10.1164/rccm.200406-807OC.

[452] A. Xie, J. B. Skatrud, B. Morgan, *et al.*, "Influence of cerebrovascular function on the hypercapnic ventilatory response in healthy humans," eng, *The Journal of Physiology*, vol. 577, no. Pt 1, pp. 319–329, Nov. 2006, ISSN: 0022-3751. DOI: 10.1113/jphysiol.2006.110627.

[453] A. Xie, J. B. Skatrud, D. S. Puleo, P. S. Rahko, and J. A. Dempsey, "Apnea-hypopnea threshold for co2 in patients with congestive heart failure," *American*

Journal of Respiratory and Critical Care Medicine, vol. 165, no. 9, pp. 1245–1250, May 2002, ISSN: 1073-449X. DOI: 10.1164/rccm.200110-022OC.

[454] F. Xu, J. Uh, M. R. Brier, *et al.*, "The influence of carbon dioxide on brain activity and metabolism in conscious humans," eng, *Journal of Cerebral Blood Flow and Metabolism: Official Journal of the International Society of Cerebral Blood Flow and Metabolism*, vol. 31, no. 1, 58â67, Jan. 2011, ISSN: 1559-7016. DOI: 10.1038/jcbfm.2010.153.

[455] D. A. Yablonskiy, "Cerebral metabolic rate in hypercapnia: Controversy continues," en, *Journal of Cerebral Blood Flow Metabolism*, vol. 31, no. 7, 1502â1503, Jul. 2011, ISSN: 0271-678X. DOI: 10.1038/jcbfm.2011.32.

[456] H.-M. Yang, B.-K. Kim, J.-Y. Kim, *et al.*, "Pparγ modulates vascular smooth muscle cell phenotype via a protein kinase G-dependent pathway and reduces neointimal hyperplasia after vascular injury," en, *Experimental & Molecular Medicine*, vol. 45, no. 1111, e65–e65, Nov. 2013, ISSN: 2092-6413. DOI: 10.1038/emm.2013.112.

[457] Y. Yang, Y. Yu, and K. Yao, "Pupillary dysfunction in type 2 diabetes mellitus to refine the early diagnosis of diabetic autonomic neuropathy," *Neuro-Ophthalmology*, vol. 30, no. 1, pp. 17–21, Jan. 2006, ISSN: 0165-8107. DOI: 10.1080/01658100600599527.

[458] T. Yasuda and H. Mochizuki, "The regulatory role of α-synuclein and parkin in neuronal cell apoptosis; possible implications for the pathogenesis of Parkinson's disease," en, *Apoptosis*, vol. 15, no. 11, pp. 1312–1321, Nov. 2010, ISSN: 1573-675X. DOI: 10.1007/s10495-010-0486-8.

[459] C. Ye, Y. Liang, Y. Chen, *et al.*, "Berberine improves cognitive impairment by simultaneously impacting cerebral blood flow and β-Amyloid Accumulation in an APP/tau/PS1 Mouse Model of Alzheimer's Disease," en, *Cells*, vol. 10, no. 55, p. 1161, May 2021, ISSN: 2073-4409. DOI: 10.3390/cells10051161.

[460] Y. Ye, X. Liu, N. Wu, *et al.*, "Efficacy and safety of berberine alone for several metabolic disorders: A systematic review and meta-analysis of randomized clinical trials," *Frontiers in Pharmacology*, vol. 12, 2021, ISSN: 1663-9812. DOI: 10.3389/fphar.2021.653887.

[461] M. Yemisci, Y. Gursoy-Ozdemir, A. Vural, A. Can, K. Topalkara, and T. Dalkara, "Pericyte contraction induced by oxidative-nitrative stress impairs capillary reflow despite successful opening of an occluded cerebral artery," eng, *Nature Medicine*, vol. 15, no. 9, pp. 1031–1037, Sep. 2009, ISSN: 1546-170X. DOI: 10.1038/nm.2022.

[462] U. S. Yezhuvath, J. Uh, Y. Cheng, *et al.*, "Forebrain-dominant deficit in cerebrovascular reactivity in alzheimer's disease," en, *Neurobiology of Aging*, vol. 33, no. 1, pp. 75–82, Jan. 2012, ISSN: 0197-4580. DOI: 10.1016/j.neurobiolaging.2010.02.005.

[463] Y. Yoshida, F. Une, Y. Utatsu, *et al.*, "Adenosine and neopterin levels in cerebrospinal fluid of patients with neurological disorders," *Internal Medicine*, vol. 38, no. 2, pp. 133–139, 1999. DOI: 10.2169/internalmedicine.38.133.

[464] G.-X. Yu, M. Mueller, B. E. Hawkins, *et al.*, "Traumatic brain injury in vivo and in vitro contributes to cerebral vascular dysfunction through impaired gap junction communication between vascular smooth muscle cells," eng, *Journal*

of Neurotrauma, vol. 31, no. 8, pp. 739–748, Apr. 2014, ISSN: 1557-9042. DOI: 10.1089/neu.2013.3187.

[465] A. Zacharek, J. Chen, X. Cui, Y. Yang, and M. Chopp, "Simvastatin increases notch signaling activity and promotes arteriogenesis after stroke," *Stroke*, vol. 40, no. 1, pp. 254–260, Jan. 2009. DOI: 10.1161/STROKEAHA.108.524116.

[466] F. H. R. van der Zande, P. a. M. Hofman, and W. H. Backes, "Mapping hypercapnia-induced cerebrovascular reactivity using bold mri," eng, *Neuroradiology*, vol. 47, no. 2, pp. 114–120, Feb. 2005, ISSN: 0028-3940. DOI: 10.1007/s00234-004-1274-3.

[467] V. Zerbi, M. Wiesmann, T. L. Emmerzaal, *et al.*, "Resting-state functional connectivity changes in aging apoe4 and apoe-ko mice," en, *Journal of Neuroscience*, vol. 34, no. 42, pp. 13 963–13 975, Oct. 2014, ISSN: 0270-6474, 1529-2401. DOI: 10.1523/JNEUROSCI.0684-14.2014.

[468] M. Y. Zhao, A. P. Fan, D. Y.-T. Chen, *et al.*, "Using arterial spin labeling to measure cerebrovascular reactivity in moyamoya disease: Insights from simultaneous pet/mri," eng, *Journal of Cerebral Blood Flow and Metabolism: Official Journal of the International Society of Cerebral Blood Flow and Metabolism*, p. 271678X221083471, Mar. 2022, ISSN: 1559-7016. DOI: 10.1177/0271678X221083471.

[469] M. Y. Zhao, A. Woodward, A. P. Fan, *et al.*, "Reproducibility of cerebrovascular reactivity measurements: A systematic review of neuroimaging techniques*," *Journal of Cerebral Blood Flow & Metabolism*, vol. 42, no. 5, pp. 700–717, May 2022, ISSN: 0271-678X. DOI: 10.1177/0271678X211056702.

[470] Y. Zhao, S. K. Biswas, P. H. McNulty, M. Kozak, J. Y. Jun, and L. Segar, "Pdgf-induced vascular smooth muscle cell proliferation is associated with dysregulation of insulin receptor substrates," eng, *American Journal of Physiology. Cell Physiology*, vol. 300, no. 6, pp. C1375–1385, Jun. 2011, ISSN: 1522-1563. DOI: 10.1152/ajpcell.00670.2008.

[471] Y. Zhao, P. M. Vanhoutte, and S. W. S. Leung, "Vascular nitric oxide: Beyond enos," en, *Journal of Pharmacological Sciences*, vol. 129, no. 2, pp. 83–94, Oct. 2015, ISSN: 1347-8613. DOI: 10.1016/j.jphs.2015.09.002.

[472] Y. Zheng, Y. Pan, S. Harris, *et al.*, "A dynamic model of neurovascular coupling: Implications for blood vessel dilation and constriction," *NeuroImage*, Computational Models of the Brain, vol. 52, no. 3, pp. 1135–1147, Sep. 2010, ISSN: 1053-8119. DOI: 10.1016/j.neuroimage.2010.01.102.

[473] Y. Zhou, X. Wang, L. Guo, *et al.*, "Trpv1 activation inhibits phenotypic switching and oxidative stress in vascular smooth muscle cells by upregulating pparα," en, *Biochemical and Biophysical Research Communications*, vol. 545, pp. 157–163, Mar. 2021, ISSN: 0006-291X. DOI: 10.1016/j.bbrc.2021.01.072.

[474] Y. Zhou, Z. B. Rodgers, and A. H. Kuo, "Cerebrovascular reactivity measured with arterial spin labeling and blood oxygen level dependent techniques," *Magnetic Resonance Imaging*, vol. 33, no. 5, pp. 566–576, Jun. 2015, ISSN: 0730-725X. DOI: 10.1016/j.mri.2015.02.018.

[475] B. V. Zlokovic, "New therapeutic targets in the neurovascular pathway in alzheimer's disease," *Neurotherapeutics*, vol. 5, no. 3, pp. 409–414, Jul. 2008, ISSN: 1933-7213. DOI: 10.1016/j.nurt.2008.05.011.

[476] B. V. Zlokovic, "Neurovascular pathways to neurodegeneration in alzheimer's disease and other disorders," *Nature Reviews Neuroscience*, vol. 12, no. 12, pp. 723–738, 2011, ISSN: 1471-003X. DOI: 10.1038/nrn3114.

[477] G. J. del Zoppo, F. R. Sharp, W.-D. Heiss, and G. W. Albers, "Heterogeneity in the penumbra," en, *Journal of Cerebral Blood Flow & Metabolism*, vol. 31, no. 9, pp. 1836–1851, Sep. 2011, ISSN: 0271-678X. DOI: 10.1038/jcbfm.2011.93.

[478] K. Zvolanek, S. Moia, J. Dean, R. Stickland, C. Caballero-Gaudes, and M. Bright, "Comparing end-tidal co2, respiration volume per time (rvt), and average gray matter signal for mapping cerebrovascular reactivity amplitude and delay with breath-hold task bold fmri," en, *NeuroImage*, vol. 272, p. 120 038, 2023. DOI: 10.1016/j.neuroimage.2023.120038.

A | Appendix - Bayesian Modelling Approaches for Breath-Hold Induced Cerebrovascular Reactivity

A.0.1 Cerebrovascular Reactivity and Delay Maps Across Sessions

All sessions for one representative subject are presented in Figure A.1 and Figure A.2, respectively, for both the variational Bayesian (VB) and lagged general linear model (lGLM) methods.

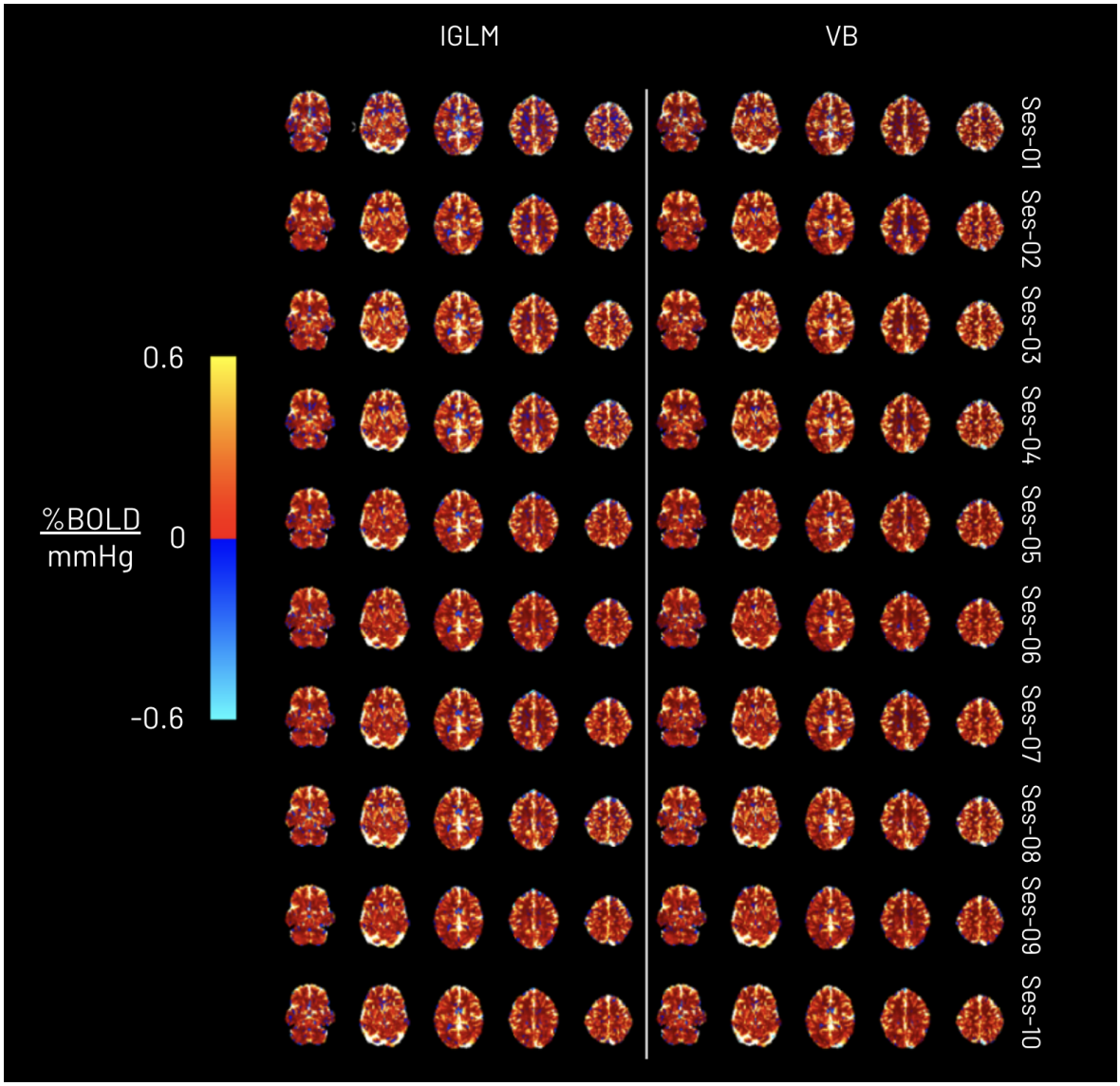

Figure A.1: CVR amplitude maps obtained using the lagged-GLM (lGLM) and variational Bayesian (VB) analyses for all the sessions of a representative subject (subject 002). Each row represents a session.

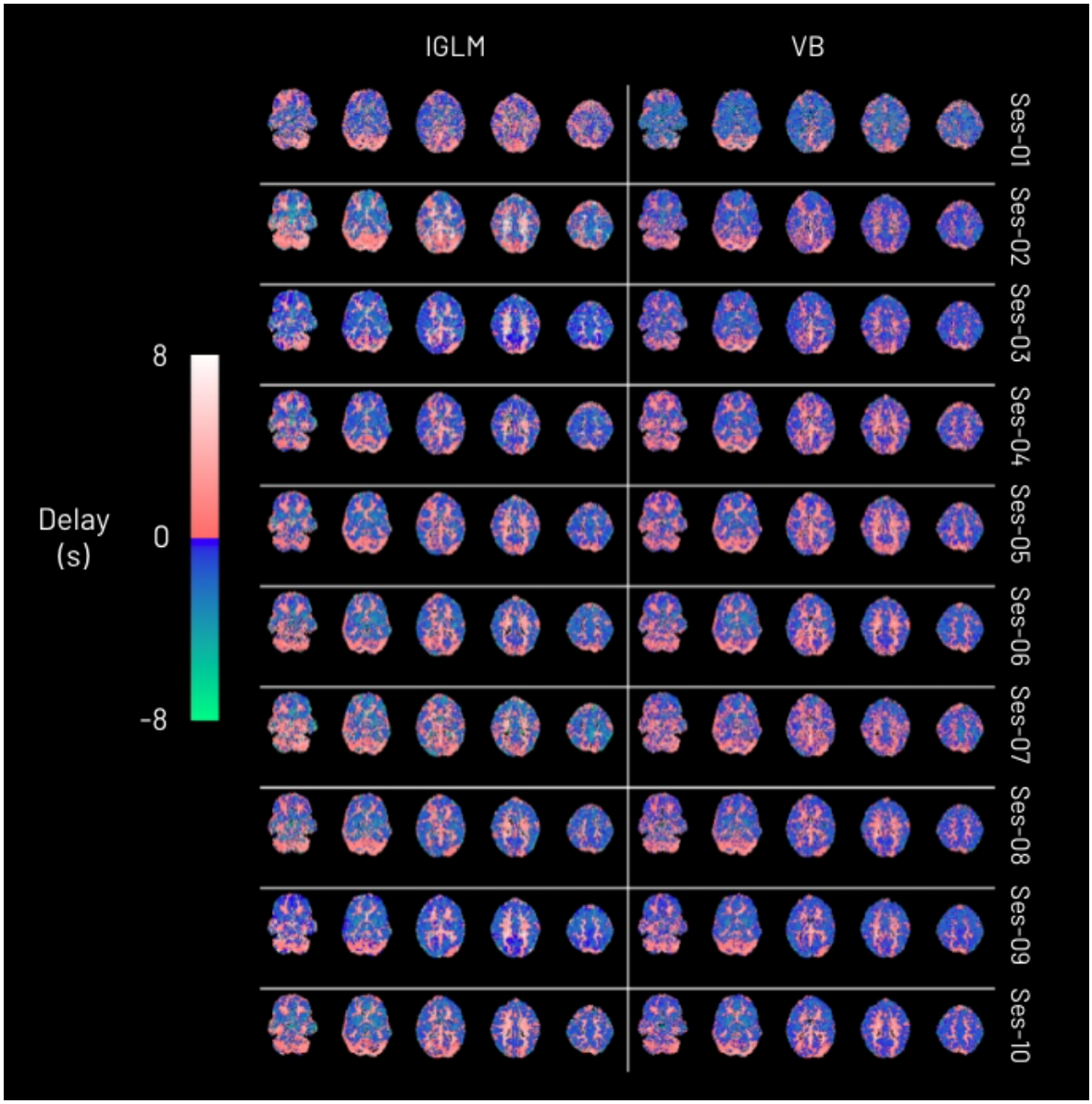

Figure A.2: CVR haemodynamic delay maps obtained using the lagged-GLM (lGLM) and variational Bayesian (VB) analyses for all the sessions of a representative subject (subject 002). Each row represents a session.

A.0.2 Revised Linear Mixed Effects Z-Scores

The thresholded z-score maps for the CVR and delay LMEr comparison are presented Figure A.3. The absolute value of the z-score is thresholded at 2.63 for the CVR map and 2.60 for delay map, corresponding to a cluster-corrected p-value of 0.01.

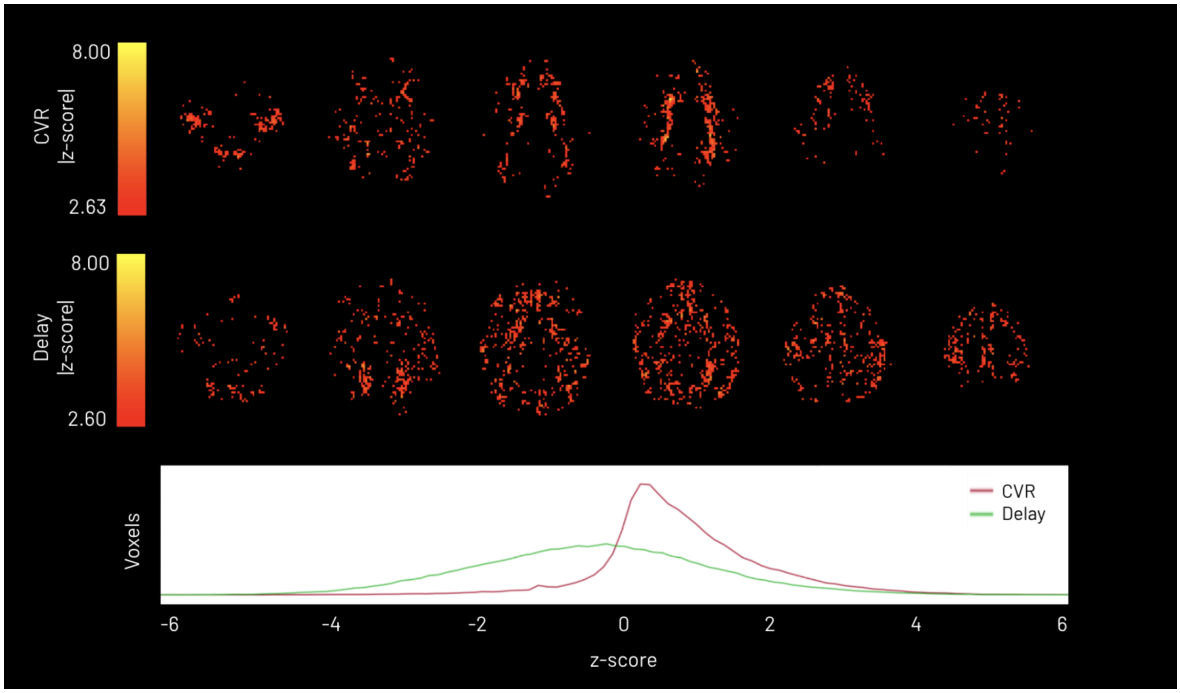

Figure A.3: CVR and delay z-score maps from the revised linear mixed effects (LMEr) pairwise comparison between the lagged-GLM (lGLM) and variational Bayesian (VB) analyses. The absolute value of the z-score is thresholded at 2.63 for the CVR map and 2.60 for delay map, corresponding to a cluster-corrected p-value of 0.01.

Group-Level Mean and Median CVR and Delay Values

The CVR and delay values within each of the 8 regions of the MNI brain atlas (MNI-maxprob-thr25 brain atlas at 2.5mm in FSL) are shown in Table A.1.

Table A.1: Regional CVR amplitude and delay values for lGLM and VB methods in 8 MNI-atlas regions of the brain.

	CVR (% BOLD/mmHg)				Delay Values (s)			
	lGLM		VB		lGLM		VB	
Regions	**Mean**	**Median**	**Mean**	**Median**	**Mean**	**Median**	**Mean**	**Median**
Caudate	0.104	0.127	0.094	0.103	-0.128	-1.104	-0.110	-0.524
Cerebellum	0.153	0.132	0.174	0.112	1.397	1.692	0.958	0.862
Frontal Lobe	0.199	0.161	0.200	0.144	-0.848	-1.667	-0.601	-0.597
Insula	0.172	0.184	0.162	0.172	-1.004	-1.596	-0.757	-1.01
Occipital Lobe	0.237	0.155	0.220	0.141	-0.268	-0.633	-0.101	-0.212
Parietal Lobe	0.189	0.157	0.197	0.141	-0.727	-1.183	-0.468	-0.530
Putamen	0.143	0.152	0.129	0.133	-1.483	-2.254	-0.989	-1.276
Temporal Lobe	0.170	0.120	0.175	0.096	-0.280	-0.667	-0.153	-0.299
Thalamus	0.191	0.152	0.177	0.132	-0.396	-1.229	-0.276	-0.631

A.0.3 Variance and Coefficients of Variation

The VB method computes variance maps for each model parameter, detailing an uncertainty metric in the posterior outputs. Since the variance scales with the amplitude of the parameter, a parameter known as the coefficient of variation (CoV) was calculated by dividing the variance by the parameter of interest as shown in Figure A.4 for the CVR and delay CoV. The CoV histograms in Figure A.4 illustrate the mean and variability in the parameter estimates in white matter, grey matter, and cerebral spinal fluid.

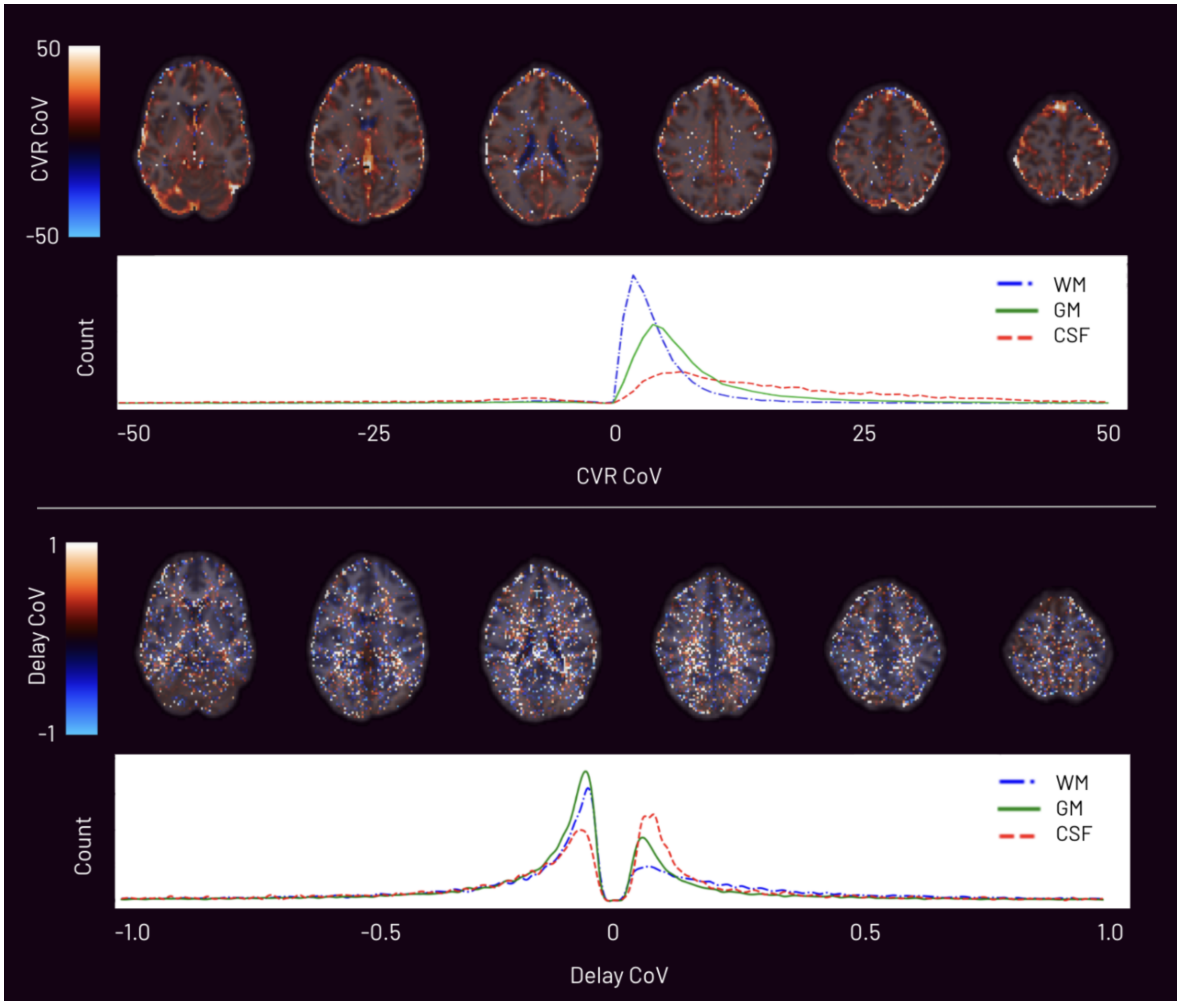

Figure A.4: Coefficient of variation (CoV) map of variational Bayesian-derived CVR (top) and delay (bottom) for a representative subject and session. The respective CoV histogram distributions are plotted of white matter (blue, dashed), grey matter (green, solid), and cerebral spinal fluid (red, long-dashed)

B | Appendix - Models of Cerebrovascular Reactivity in BOLD-fMRI and Transcranial Doppler Ultrasound

B.0.1 Summary of Age and Sex Effects on TCD and MRI-Derived CVR Parameters

A summary of multiple linear regression results assessing the effect of age and sex on the CVR parameters are presented in Table B.1. Notably, sex and age had no statistically significant impact on any of the CVR parameters. The Shapiro-Wilk test was used to examine whether the regression residuals are normally distributed and if they are normally distributed, the ordinary least squares (OLS) model was used, if not, the robust linear model (RLM) was used [373]. The Breusch-Pagan test confirmed that all parameters maintain constant variance (homoscedasticity) [49]. The Durbin-Watson statistic was used to confirm the presence of autocorrelation among the residuals (independence) [110]. Together, these checks verify that the key assumptions of linear regression are sufficiently met.

Table B.1: Summary of multiple linear regression results examining the effect of age and sex on TCD and MRI-based CVR parameters. Each row lists a specific parameter and the model type used (ordinary least squares (OLS) for normally distributed parameters and robust linear model (RLM) for non-normally distributed parameters, determined by the Shapiro-Wilk test). The estimated regression coefficients (and p-values) for age and sex, the model R^2, and p-values/statistics for residual diagnostics: Breusch-Pagan test (homoscedasticity), and Durbin-Watson statistic (independence). Statistically significant was taken as p-values < 0.05.

Modality	Parameter	Model used	Shapiro-Wilk p-value	Age regression coefficient	Age p-value	Sex regression coefficient	Sex p-value	R^2	Breusch-Pagan statistic	Breusch-Pagan p-value	Durbin-Watson statistic
TCD	Linear slope	OLS	0.785	0.0002	**0.327**	0.0000	**0.989**	0.047	1.744	0.418	1.453
	4p Model 'a'	OLS	0.418	0.0031	**0.519**	0.0538	**0.593**	0.038	3.145	0.208	1.884
	4p Model 'b'	RLM	0.001	-0.0044	**0.951**	-0.8640	**0.563**	-	-	-	-
	4p Model 'c'	OLS	0.617	0.0946	**0.304**	-2.4582	**0.206**	0.106	0.083	0.959	1.816
	4p Model 'd'	RLM	0.010	0.0035	**0.680**	-0.0829	**0.637**	-	-	-	-
	2p Model 'b'	RLM	0.003	-0.0589	**0.498**	-0.5911	**0.746**	-	-	-	-
	2p Model 'c'	OLS	0.097	-0.0860	**0.514**	-0.9926	**0.719**	0.030	3.024	0.221	1.209
MRI	Linear slope	OLS	0.630	-0.0006	**0.409**	0.0028	**0.856**	0.033	0.384	0.825	1.410
	4p Model 'a'	RLM	0.010	-0.0675	**0.642**	1.4495	**0.635**	-	-	-	-
	4p Model 'b'	OLS	0.251	0.0184	**0.894**	0.9167	**0.753**	0.006	1.579	0.454	2.474
	4p Model 'c'	OLS	0.626	-0.1001	**0.659**	2.6819	**0.574**	0.022	2.429	0.297	2.810
	4p Model 'd'	OLS	0.114	0.0261	**0.860**	0.1196	**0.969**	0.002	4.770	0.092	2.611
	2p Model 'b'	OLS	0.764	0.0572	**0.332**	-0.5542	**0.651**	0.049	0.041	0.980	1.449
	2p Model 'c'	OLS	0.130	0.1053	**0.120**	-1.8117	**0.199**	0.156	1.839	0.399	1.879